

## INFORMATION TO USERS

This was produced from a copy of a document sent to us for microfilming. While the most advanced technological means to photograph and reproduce this document have been used, the quality is heavily dependent upon the quality of the material submitted.

The following explanation of techniques is provided to help you understand markings or notations which may appear on this reproduction.

1. The sign or "target" for pages apparently lacking from the document photographed is "Missing Page(s)". If it was possible to obtain the missing page(s) or section, they are spliced into the film along with adjacent pages. This may have necessitated cutting through an image and duplicating adjacent pages to assure you of complete continuity.
2. When an image on the film is obliterated with a round black mark it is an indication that the film inspector noticed either blurred copy because of movement during exposure, or duplicate copy. Unless we meant to delete copyrighted materials that should not have been filmed, you will find a good image of the page in the adjacent frame.
3. When a map, drawing or chart, etc., is part of the material being photographed the photographer has followed a definite method in "sectioning" the material. It is customary to begin filming at the upper left hand corner of a large sheet and to continue from left to right in equal sections with small overlaps. If necessary, sectioning is continued again—beginning below the first row and continuing on until complete.
4. For any illustrations that cannot be reproduced satisfactorily by xerography, photographic prints can be purchased at additional cost and tipped into your xerographic copy. Requests can be made to our Dissertations Customer Services Department.
5. Some pages in any document may have indistinct print. In all cases we have filmed the best available copy.

**University  
Microfilms  
International**

300 N. ZEEB ROAD, ANN ARBOR, MI 48106  
18 BEDFORD ROW, LONDON WC1R 4EJ, ENGLAND

8012286

KIM, MYUNG HOON

I. EFFECT OF PH ON THE INTERFACIAL BEHAVIOR OF URACIL.  
II. INTERFACIAL BEHAVIOR OF ADENINE AND ITS NUCLEOSIDES AND  
ITS NUCLEOTIDES. III. A PRELIMINARY STUDY OF  
ELECTROCHEMICAL OXIDATION OF 5-METHYLTETRAHYDROPTERIN

The University of Oklahoma

PH.D.

1979

University  
Microfilms  
International

300 N. Zeeb Road, Ann Arbor, MI 48106

18 Bedford Row, London WC1R 4EJ, England

Copyright 1980

by

KIM, MYUNG HOON

All Rights Reserved

PLEASE NOTE:

In all cases this material has been filmed in the best possible way from the available copy. Problems encountered with this document have been identified here with a check mark .

1. Glossy photographs \_\_\_\_\_
2. Colored illustrations \_\_\_\_\_
3. Photographs with dark background \_\_\_\_\_
4. Illustrations are poor copy \_\_\_\_\_
5. Print shows through as there is text on both sides of page \_\_\_\_\_
6. Indistinct, broken or small print on several pages \_\_\_\_\_ throughout  
\_\_\_\_\_
7. Tightly bound copy with print lost in spine \_\_\_\_\_
8. Computer printout pages with indistinct print  \_\_\_\_\_
9. Page(s) \_\_\_\_\_ lacking when material received, and not available from school or author \_\_\_\_\_
10. Page(s) \_\_\_\_\_ seem to be missing in numbering only as text follows \_\_\_\_\_
11. Poor carbon copy \_\_\_\_\_
12. Not original copy, several pages with blurred type \_\_\_\_\_
13. Appendix pages are poor copy \_\_\_\_\_
14. Original copy with light type \_\_\_\_\_
15. Curling and wrinkled pages \_\_\_\_\_
16. Other \_\_\_\_\_

THE UNIVERSITY OF OKLAHOMA

GRADUATE COLLEGE

- I. EFFECT OF pH ON THE INTERFACIAL BEHAVIOR OF URACIL
- II. INTERFACIAL BEHAVIOR OF ADENINE AND ITS NUCLEOSIDES AND ITS NUCLEOTIDES
- III. A PRELIMINARY STUDY OF ELECTROCHEMICAL OXIDATION OF 5-METHYLTETRAHYDROPTERIN

A DISSERTATION

SUBMITTED TO THE GRADUATE FACULTY

in partial fulfillment of the requirements for the

degree of

DOCTOR OF PHILOSOPHY

BY

MYUNG HOON KIM

Norman, Oklahoma

1979

- I. EFFECT OF pH ON THE INTERFACIAL BEHAVIOR OF URACIL
- II. INTERFACIAL BEHAVIOR OF ADENINE AND ITS NUCLEOSIDES AND ITS NUCLEOTIDES
- III. A PRELIMINARY STUDY OF ELECTROCHEMICAL OXIDATION OF 5-METHYLTETRAHYDROPTERIN

APPROVED BY

*John Daykin*  
*E. LeRoy Blair*  
*Simon H. Wender*  
*Robert W. Taylor*  
*Donald S. Perkins*

DISSERTATION COMMITTEE

DEDICATION

To my parents

## ACKNOWLEDGEMENT

The author wishes to express his deepest appreciation to Dr. Glenn Dryhurst, who suggested these interesting problems and introduced me to electrochemical approaches to the biochemical systems, and gave me excellent opportunity to work with him so that I could get acquainted with various electrochemical methods. The career of a graduate student, which culminates in a work such as presented here is not just a period of acquisition of knowledge, but more importantly of personal growth and development in the arts of thinking. The primary responsibility of a research director to a graduate student is to help him in paths of self-discovery. It is in these qualities that Dr. Dryhurst excels, not only in imparting his knowledge and experience in the field, but in creating the atmosphere in which a student can learn responsibility, self-instruction, and determination to complete a task once started.

Thanks also extends to Dr. Sherril Christian, who was a co-principle investigator of the project, for his warm personality and very kind help with various theoretical aspects of this work, Dr. LeRoy Blank for many helpful discussions, and Dr. Richard Taylor, Dr. Simon Wender and Dr. Donald Perkins for serving in the research advisory committee.

My parents deserve a special thanks for not only their financial aid, but more importantly for their faith, encouragement, tireless patience and love. The long journey of my education has been a burden on them and I hope they can share in the fulfillment of the goals which this manuscript represents.

The author also wishes to thank Mr. Ron Stermer for his preparation of many fine electrocapillary, Dr. Eric Enwall for kind consultations about computer programs, The University of Oklahoma Computer Center for making available hours of computer time, Dr. Viktor Brabec for his help with numerous experimental works, and all his fellow graduate students and other postdoctoral fellows for the various discussions about research and teaching and their help, and Ms. Nancy Nielsen for her help in the final typing.

## TABLE OF CONTENTS

	Page
LIST OF TABLES . . . . .	ix
LIST OF FIGURES . . . . .	x
ABSTRACTS . . . . .	xiv
 Chapter	
I. INTRODUCTION . . . . .	1
Interfacial Phenomena . . . . .	1
Interfacial Adsorption Effects in Biological Systems . .	3
Electrical Double Layer and Surface Potential . . . . .	9
Review of Adsorption of Nucleobases, Nucleosides, Nucleotides, DNA and Polynucleotides . . . . .	14
Research Objectives . . . . .	21
II. THEORY . . . . .	22
The Significance of Adsorption Isotherm . . . . .	24
Gibbs Adsorption Equation . . . . .	27
Lippman Equation . . . . .	31
Generalized Frumkin Isotherm for Charged Surface . . . .	32
Congruence of the Electrosorption Isotherms . . . . .	34
III. EXPERIMENTAL. . . . .	37
Chemicals . . . . .	37
Differential Capacitance Measurement . . . . .	39
Direct Surface Tension Measurements Using Capillary Electrometers . . . . .	49

TABLE OF CONTENTS (continued)

Chapter	Page
IV. EFFECT OF pH ON THE INTERFACIAL BEHAVIOR OF URACIL . . .	58
Results . . . . .	59
Dilute Adsorption Region at pH 3, 5 and 8 . . . . .	62
Dilute Adsorption Region at pH 11 . . . . .	71
Capacitance Pit Region . . . . .	77
Discussion . . . . .	81
V. INTERFACIAL BEHAVIOR OF ADENINE AND ITS NUCLEOSIDES AND NUCLEOTIDES . . . . .	89
Results and Discussion . . . . .	91
Dilute Adsorption Region . . . . .	96
Capacitance Pit Region . . . . .	102
Surface Orientation . . . . .	107
Adenine . . . . .	107
Adenosine . . . . .	113
Adenosine-5'-monophosphate . . . . .	122
Conclusions . . . . .	123
VI. A PRELIMINARY STUDY OF ELECTROCHEMICAL OXIDATION OF 5-METHYLTETRAHYDROPTERIN AT THE PYROLYTIC GRAPHITE ELECTRODE . . . . .	126
INTRODUCTION . . . . .	126
EXPERIMENTAL . . . . .	129
Chemicals . . . . .	129
Voltammetric Procedure . . . . .	130
Coulometric Electrolysis Procedure . . . . .	132

TABLE OF CONTENTS (continued)

Chapter	Page
Thin-layer Spectroelectrochemistry Experiments . . .	133
Isolation of Electrolysis Products . . . . .	134
 RESULTS	
Stability of 5-Methyltetrahydropterin in Aqueous Media . . . . .	137
Linear and Cyclic Voltammetry at the PGE . . . . .	137
pH Study . . . . .	143
<i>E<sub>p</sub></i> vs. pH Plot . . . . .	143
<i>i<sub>p</sub></i> vs. pH Plot . . . . .	145
Scan Rate Study . . . . .	145
Concentration Study . . . . .	145
Controlled Potential Coulometry . . . . .	148
Spectroelectrochemical Study . . . . .	151
Isolation of Products . . . . .	154
Possible Reaction Scheme . . . . .	158
 APPENDIX . . . . .	 160
 REFERENCES . . . . .	 195

## LIST OF TABLES

Table	Page
1. Fundamental types of isotherms . . . . .	25
2. Parameters of the generalized Frumkin isotherm for uracil determined from differential capacitance methods at various pH values in the dilute adsorption region . .	70
3. Area occupied by one uracil molecule at maximum surface coverage in the dilute and capacitance pit region between pH 3 and 8 . . . . .	80
4. Parameters of the generalized Frumkin equation for adenine, adenosine and AMP determined by analysis of capacitance and maximum bubble pressure data in the dilute adsorption region . . . . .	101
5. Area occupied per molecule at maximum surface coverage in the dilute and capacitance pit adsorption regions for adenine and adenosine . . . . .	112
6. UV spectrophotometric study of the stability of 5-methyl-tetrahydropterin in aqueous solution . . . . .	137
7. Coulometric determination of the number of electrons involved in the oxidation of 5-methyltetrahydropterin. .	148

## LIST OF FIGURES

Figure	Page
1. A model of the electrical double layer <sup>38</sup> and potential-distance profile . . . . .	10
2. A model of a membrane and potential-distance profiles . .	11
3. Schematic representation of the variation of concentration of species <i>i</i> with distance from an interface . . . . .	28
4A. Test of a.c. adsorption equilibrium on uracil (30.00 mM) in pH 8 phosphate buffer . . . . .	44
4B. Test of a.c. adsorption on 6-methyladenosine (1.0 mM) in pH 8 fluoride buffer . . . . .	45
5A. Test for d.c. adsorption equilibrium on uracil in pH 8 phosphate buffer. . . . .	46
5B. Test for d.c. adsorption equilibrium on 6-dimethyladenosine in pH 8 fluoride buffer (0.5 M NaF plus 0.01 M Na <sub>2</sub> HPO <sub>4</sub> ) .	47
6. Apparatus for direct measurement of interfacial (or surface) tension at the mercury/solution interface . . . . .	50
7. Interfacial tension <u>vs.</u> potential curves for 0.5 M NaF plus 0.01 M Na <sub>2</sub> HPO <sub>4</sub> buffer pH 8 . . . . .	53
8. Charge <u>vs.</u> potential curves for 0.5 M NaF plus 0.01 M Na <sub>2</sub> HPO <sub>4</sub> buffer pH 8 . . . . .	55
9. Differential capacitance <u>vs.</u> potential curve for fluoride pH 8 buffer solution (0.5 M NaF plus 0.01 M Na <sub>2</sub> HPO <sub>4</sub> ) . .	57
10. Differential capacitance <u>versus</u> potential curves for uracil at (A) pH 3.0, (B) pH 5.0, (C) pH 8.0 and (D) pH 11.0 in phosphate buffers having an ionic strength of 0.5 M . . . . .	60,61

LIST OF FIGURES (continued)

Figure	Page
11. Composite $\pi$ <u>versus</u> $\ln a$ plots for uracil at (A) pH 3.0, (B) pH 5.0 and (C) pH 8.0 in phosphate buffers having an ionic strength of 0.5 M . . . . .	63
12. Test of congruence of the electrosorption isotherms of uracil at pH 3.0 with respect to potential . . . . .	66
13. Charge <u>versus</u> potential plots for uracil in phosphate buffer pH 3.0 having an ionic strength of 0.5 M . . . . .	67
14. Reduced adsorption isotherms for uracil at (A) pH 3.0, (B) pH 5.0 and (C) pH 8.0 in phosphate buffers, ionic strength 0.5 M . . . . .	69
15. Composite $\pi$ <u>versus</u> $\ln a$ plots for uracil at pH 11.0 in phosphate buffer, ionic strength 0.5 M at various charge values (indicated in the figure) . . . . .	72
16. Test of congruence of electrosorption isotherms with respect to charge for uracil in phosphate buffer pH 11.0, ionic strength 0.5 M. . . . .	73
17. Reduced adsorption isotherm for uracil in phosphate buffer pH 11.0, ionic strength 0.5 M. . . . .	76
18. Surface spreading pressure, $\gamma$ , <u>versus</u> $\ln a$ plots for uracil at (A) pH 3.0, (B) pH 5.0 and (C) pH 8.0 in phosphate buffers, ionic strength 0.5 M . . . . .	78
19. Real and projected areas of uracil. . . . .	83
20. Possible mode of binding of uracil and its derivatives to the electrode surface when in a perpendicular surface orientation . . . . .	84
21. (A) Free energy of adsorption <u>versus</u> potential curve for uracil in phosphate buffer pH 3.0 and (B) free energy <u>versus</u> electrode charge curve for uracil in phosphate buffer pH 11.0 . . . . .	88
22. Differential capacitance <u>vs.</u> potential curves for (A) adenine, (B) adenosine, (C) 6-methyladenosine, (D) 6-dimethyladenosine and (E) adenosine-5'-monophosphate in 0.5 M NaF plus 0.01 M Na <sub>2</sub> HPO <sub>4</sub> buffer pH 8.0 . . . . .	92,93

LIST OF FIGURES (continued)

Figure	Page
23. Composite $\pi$ vs. $\ln a$ plots for (A) adenine, (B) adenosine and (C) adenosine-5'-monophosphate in 0.5 M NaF plus 0.01 M Na <sub>2</sub> HPO <sub>4</sub> pH 8.0 . . . . .	97
24. Reduced electrosorption isotherms for (A) adenine, (B) adenosine and (C) AMP in 0.5 M NaF plus 0.01 M Na <sub>2</sub> HPO <sub>4</sub> buffer pH 8.0 . . . . .	99
Isotherm (D) is for adenine in borate buffer pH 9.0 . . . . .	100
25. Surface spreading pressure, $\pi$ , vs. $\ln a$ plots for adenine in 0.5 M NaF plus 0.01 M Na <sub>2</sub> HPO <sub>4</sub> pH 8.0 . . . . .	104
26. Projected areas for adenine . . . . .	108
27. Proposed surface orientations for (A) adenine in the capacitance pit centered at -0.5 V, (B) adenosine, methyl- and dimethyladenosine in the capacitance pit centered at <u>ca.</u> -0.4 V and (C) adenosine and methyladenosine in the capacitance pit centered at <u>ca.</u> -1.25 V. . . . .	110,111
28. Schematic illustration of the torsion angle, CN, in purine nucleosides. . . . .	115
29. Permanent dipole moments for adenine, <sup>157,158</sup> adenosine <sup>159</sup> and their methylated derivatives . . . . .	118
30. Cyclic voltammogram of 1.0 mM 5-methyltetrahydropterin in pH 3.0 phosphate buffer at the PGE . . . . .	138
31A. Cyclic voltammogram of 1.00 mM 5-methyltetrahydropterin in pH 8.0 phosphate buffer at the PGE . . . . .	139
31B. Cyclic voltammogram of 1.00 mM 5-methyltetrahydropterin in pH 8.0 phosphate buffer at the PGE . . . . .	140
32. Variation of the peak current ratio, $i_{PR}^I / i_{PR}^{II}$ , with the scan rate for 5-methyltetrahydropterin in pH 3.0 (O) and in pH 8.0 (□) phosphate buffer at the PGE . . . . .	142
33. Variation of peak potentials ( $E_p$ ) with pH for 1.0 mM 5-methyltetrahydropterin at the PGE . . . . .	144
34. Variation of peak currents ( $i_p$ ) with pH for peak P <sub>O</sub> <sup>I</sup> of 1.00 mM 5-methyltetrahydropterin at the PGE in phosphate buffers . . . . .	146

LIST OF FIGURES (continued)

Figure	Page
35. Variation of $i_p/V^{1/2}$ with the scan rate for 1.00 mM 5-methyltetrahydropterin at the PGE at pH 3.0 (O) and pH 8.0 (□) phosphate buffers . . . . .	147
36. Variation of $i_p/C$ with concentration (C) at the PGE for peak $P_0^I$ of 5-methyltetrahydropterin in pH 3.0 (O, 5 mV/sec; ●, 20 mV/sec) and in pH 8.0 (□, 5 mV/sec) phosphate buffer . . . . .	149
37. UV spectrum of 5-methyltetrahydropterin in pH 3.0 phosphate buffer before (A) and after (B) the controlled potential electrolysis at +0.45 V . . . . .	150
38. UV spectrum of 10.0 mM 5-methyltetrahydropterin solution electrolyzing at +0.50 V in pH 3.0 phosphate buffer at a graphite electrode in a thin layer spectroelectrochemical cell . . . . .	152
39. UV spectrum of 10.0 mM 5-methyltetrahydropterin solution electrolyzing at +0.15 V in pH 8.0 phosphate buffer at a graphite electrode in a thin layer spectroelectrochemical cell . . . . .	153
40. Liquid chromatogram of the oxidation products of 10.0 mg of 5-methyltetrahydropterin in pH 3.0 phosphate buffer electrolyzing at +0.45 V (vs. SCE) and separated in a dual column, single system of Sephadex G-10 which was eluted with doubly distilled water . . .	155
41. Mass spectrum (direct insertion, 70 eV) of electrolysis product of 5-methyltetrahydropterin in pH 3.0 phosphate buffer . . . . .	156
42. Mass spectrum (GC/MS) of the silylated electrolysis product of 5-methyltetrahydropterin in pH 3.0 phosphate buffer . . . . .	157

## ABSTRACTS

### I. Effect of pH on the Interfacial Behavior of Uracil

The adsorption of uracil at the mercury electrode-solution interface has been studied by differential capacitance and maximum bubble pressure methods as a function of pH. At pH 8.0 and below uracil exhibits an initial, dilute adsorption region where the area occupied by one adsorbed uracil molecule,  $69 \pm 5 \text{ \AA}^2$ , is close to that expected if the pyrimidine molecule is adsorbed flat on the electrode surface, *i.e.* with the plane of the ring atoms parallel to the electrode surface. At a bulk solution concentration of about 21 mM and at potentials centered at *ca.* -0.5 V the uracil molecule undergoes an abrupt surface reorientation and adopts a perpendicular stance on the electrode. The area occupied by one uracil molecule in the perpendicular orientation is  $39 \pm 3 \text{ \AA}^2$ . At pH 11.0 uracil exists as a monoanion and in this form is significantly less strongly adsorbed in the initial flat surface orientation. The reorientation of adsorbed uracil monoanions from the flat to perpendicular stance is not observed at pH 11.0 until the bulk solution concentration of uracil reaches *ca.* 65 mM.

### II. Interfacial Behavior of Adenine and Its Nucleosides and Nucleotides

The adsorption of adenine, adenosine and AMP has been studied by surface electrochemical methods at pH 8.0. All compounds exhibit an initial or dilute adsorption region where they are probably adsorbed with the base flat on the electrode surface. It is proposed that adenosine and AMP adopt the *syn* conformation so that the sugar or sugar phosphate moiety, respectively, is largely rotated out of the plane of the electrode and the base residues can pack together almost as closely as the free bases. At potentials centered at -0.5 V and bulk solution concentrations  $\geq$  *ca.* 3 mM adenine appears to undergo a surface reorientation and adopts a perpendicular stance. In this new orientation it is proposed that adenine is bound to the electrode through its amino group hydrogen atoms forming a  $\text{N} \begin{array}{l} \text{H} \cdots \text{H} \\ \text{H} \cdots \text{H} \end{array} \text{---} \text{electrode}$  electrode hydrogen bond. Adenosine appears to form two types of perpendicular layers. At small positive electrode charges it is suggested that it adopts an *anti* conformation and is adsorbed with the negative end of its permanent dipole directed towards the electrode. At more negative potentials it is proposed that adenosine retains the *anti* conformation but is adsorbed with the positive end of its dipole directed towards the electrode.

### III. A Preliminary Study of Electrochemical Oxidation of 5-methyltetrahydropterin

The oxidation of 5-methyltetrahydropterin has been studied at the pyrolytic graphite electrode and a reticulated vitreous carbon electrode by a variety of techniques including cyclic voltammetry, linear sweep voltammetry, controlled potential coulometry and rapid-scan thin-layer

spectroelectrochemistry. 5-Methyltetrahydropterin undergoes a two electron/two proton electrochemical oxidation at the PGE with a peak potential( $E_p$ ) of + 0.33 V (vs. SCE) in pH 3.0 phosphate buffer. The reactant appears to be adsorbed on the electrode surface prior to the electron transfer to the electrode. It is proposed that the immediate product is a quinonoid ion. This quinonoid ion intermediate is very unstable in solution and rapidly undergoes a rearrangement to 5-methyl-5,6-dihydropterin which is more difficult to reduce than the quinonoid ion. The product of this short term electrolysis product appears to be different from the product of long term electrolysis in the controlled potential coulometric cell as evidenced by the UV spectra.

## CHAPTER I

### INTRODUCTION

#### Interfacial Phenomena

The behavior of molecules at interfaces (solid/liquid, liquid/liquid, and solid/gas, etc.), or adsorption, has been a center of interest for many scientists for the last several decades. This is because various important chemical and physical processes occur at such interfacial regions. Several of the numerous examples<sup>1</sup> of the interfacial processes are given below;

1) One of the most well known adsorbents is charcoal used in gas masks and industrial purifications processes. With its surface area of about  $1100 \text{ m}^2/\text{g}$ , it is capable of adsorbing and holding large quantities of poisons or impurities that one might wish to remove from a stream of air or solution mixtures.

2) Many chemical reactions occur in the presence of certain surfaces that do not proceed at all, or do so only very slowly, in the absence of such surfaces.<sup>2</sup> Heterogeneous catalysis, which has been employed in various processes is a typical reaction at an interface. Examples of such catalysts are Pt black for hydrogenation reactions and silica-alumina gel for cracking of heavy petroleum fractions. It is easily seen that adsorbed molecules or ions may enter into a

reaction quite different from that which occurs in bulk, homogeneous solution. In kinetic terms, the molecules on the surface are such that they may react through a state of much lower activation energy than can the normal molecules. It follows that heterogeneous catalysis can be understood in detail only when the nature of the adsorbed species is so understood.<sup>2</sup>

3) A surfactant is an organic compound consisting of two parts, a hydrophobic portion of a long hydrocarbon chain and a hydrophilic or polar group. The combined hydrophobic and hydrophilic moieties render the compound surface active and thus able to concentrate at the interface between a surfactant solution and another phase such as air, soil, textile or other substrate to be cleaned.<sup>3</sup>

4) In adsorption chromatography, especially in gas-solid chromatography, physical adsorption is responsible for the separation of various compounds of a mixture, which capitalizes on different adsorption characteristics of the component molecules.

5) Most electrochemical reactions involve a transfer of electrons which occurs at a charged electrode/electrolyte solution interface. Sometimes the reactant adsorbs on the electrode surface prior to the electron transfer. Therefore, the adsorption behavior (i.e., orientation or possible structural modification on the surface) of the reactant molecules may have significant effects in the reaction mechanism.

6) The interfacial behavior of molecules is also extremely important in biological reactions. Body fluids such as blood, lymph, and extracellular fluids, etc., are all colloidal systems, containing

a great variety of molecular species in the form of particles, sometimes charged, of colloidal size, in addition to a large number of dissolved molecules and ions which are much smaller in size than colloids. The existence of these surface charges is responsible for the electric potential hence electric fields around such particles, and is of prime importance for the stability of such solutions and in determining the interaction of these particles either among themselves or the surfaces of the vessels or membranes which are themselves charged.<sup>4</sup>

Detailed examples of these biological aspects of the surface charge will be given in the following section.

#### Interfacial Adsorption Effects in Biological Systems

A large number of chemical and physical mechanisms in biological systems appear to depend to a great extent upon the interaction of biodynamic molecules with an electrically charged membrane. However, the chemistry and physics of these molecules adsorbed at the membrane-fluid interface are not well understood. Basic studies of interfacial phenomena in vivo are rendered difficult by the multitudes of surface active compounds which exist in biological fluids and the virtual impossibility of identifying specific interactions between a given adsorbate molecule and active site on a biological interface.

It is well documented<sup>5,6,7</sup> that clotting of blood is a process which involves the effect of surface charge in its initial stages. The initiation of clotting starts with the activation of the coagulation factor XII (Hageman Factor). Factor XII exists in a precursor form in the endothelial blood vessel lining but, on exposure to subendothelial

collagen or many other foreign surfaces such as skin or glass, it is converted into an active form, F XII<sub>a</sub>.<sup>8</sup> The molecular details of this conversion are largely unknown. Most activators of the F XII → F XII<sub>a</sub> conversion share the property of being negatively charged, furthermore certain topological arrangement of these negative charges appears to be essential.<sup>9,10</sup> Polycations such as spermine or polylysine interfere with the F XII activating ability of negatively charged surfaces. Negatively charged material such as heparin do not inhibit the activation. It has been suggested that activation of F XII after adsorption on the surface involves unfolding of the molecule (a protein with M.W. 95,000) with resultant exposure of reactive or catalytic sites that are normally masked within the native protein. These studies are of particular relevance to the properties of prosthetic devices in the circulatory system.

One clear indication that emerges from the studies referred to above is that the properties of proteins, and therefore also probably other important macromolecules such as nucleic acids and lipids can be altered upon contact with certain charged surfaces. It would appear that among the various possibilities the structure of surface adsorbed macromolecules is intrinsically different from the unbound molecule. Thus, an adsorbed macromolecule could be bound at a specific site at the biological interface thus preventing the normal reaction of this site. Alternatively, the altered molecular structure could result in exposure of otherwise shielded sites within the macromolecule to the contacting medium, hence activating or repressing the biological function of the molecule. In particular, it

would seem highly likely that partial or complete denaturation or unwinding of polypeptide chains or nucleic acid helices could be a very likely effect at charged interfaces.<sup>11</sup> In other words, the conformation of biomolecules at surfaces may be dependent on the charge on the surface (hence electric potential and electric fields around the surface) to modify its behavior or functions.

Some studies have suggested biological roles of interfacial processes occurring in vivo. For example, electric fields have been known for some time to influence the conformation of various natural and biosynthetic polynucleotides in solution. Hill<sup>12</sup> has calculated that high electric fields could bring about separation of the two molecular chains of nucleotides in DNA. Based on birefringence measurements, it has been demonstrated<sup>13</sup> that in a high intensity electric field ( $> 10^4$  V/cm) DNA first aggregates and then undergoes a structural transition in which the angles of the purine and the pyrimidine bases with respect to the helix axis are altered. In an electric field of about  $2 \times 10^4$  V/cm ribosomal RNA and polynucleotides such as poly(A) and poly(U) appear to undergo a transient opening of base pairs followed by only partial reassociation of the unfolded regions.<sup>14</sup>

The potentials that exist at certain biological membranes such as a cell membrane are thought to be on the order of 0.1 V. In a biological fluid having an ionic strength of 0.1 to 0.2 M, this potential would extend over distances of 10-100 Å.<sup>15</sup> This corresponds to electric fields of  $10^5$ - $10^6$  V/cm. Clearly, if a biopolymer such as DNA or RNA is present in close proximity to such a biosurface then

it seems quite reasonable to suggest that macromolecular structural transitions might occur. In fact, in living organisms DNA, for example, is partially associated with the nuclear or cytoplasmic membrane, or with the interface of the nucleolus.<sup>16-19</sup> A theory has been advanced that replication could begin at the level of the nuclear or cellular wall.<sup>18-20</sup> Indeed, Hill<sup>12</sup> has suggested that the electric fields and their variations at biological interfaces might act as the trigger for division of genetic material in the cell prior to self-duplication.<sup>20</sup>

An especially interesting aspect of electrical activity associated with biological processes is the existence of the potential of injury at a trauma site. It has been observed that this potential which is measured between the limb shaft and the outer layer of muscle at the site, follows a different time course in the healing of, for example, a limb amputation in a species which can regenerate the limb as opposed to one which exhibits only scar tissue formation.<sup>21,22</sup> It has been shown that implantation of small electrodes across this injury site in a non-regenerating species causes partial limb regeneration even in a complex organism such as the rat.<sup>23,24,25</sup> This implies that fundamental biological processes (ultimately at the genetic level) may be controlled by the natural or artificially applied electrical environment at a tissue repair site. It has been noted<sup>26</sup> that the cellular process of fracture healing in amphibians is in some way related to the electrical phenomena produced by the fractured bone. In an effort to make clinical use of this "animal electricity", attempts have been made to stimulate fracture repair utilizing surgically implanted electrodes.<sup>22</sup> Recently an alternate method of

influencing the electrical environment of a fracture site, which uses an external pulsed electromagnetic field to induce a potential in the bone, has been demonstrated.<sup>27</sup> This method uses a coil located outside of the body, and requires no surgical procedure. It has been successful as a method for stimulation of healing of bone fractures in human patients.

At physiological bulk-phase pH value of 7.2 all mammalian cells so far examined carry a net negative charge at their surfaces. However, the surface potential of a cell is not constant but can undergo some rather dramatic changes. For example, cells isolated from the regenerating livers of rats some days after partial hepatectomy and cells from neonates have significantly higher electrophoretic mobilities than liver cells from normal adults,<sup>28</sup> i.e., cell proliferation is associated with increased net surface negativity. Similarly, the electrophoretic mobilities of certain tumor cells increase with growth rate.<sup>29</sup> At the time of mitosis a very significant increase in net surface negativity has been observed in various types of cultured tumor cells.<sup>30,31</sup> Indeed, Ambrose et al.<sup>32,33</sup> have noted a correlation between malignancy and increased cell surface negativity, although this is certainly not thought to be a universal correlation.<sup>34</sup>

A substantial amount of evidence is being developed which indicates that interaction with biological interfaces is a prerequisite for the manifestation of the biological effects of polynucleotides in mammalian cell systems in vivo and in vitro. Thus, Field et al.<sup>35</sup> have reported that RNA double strands, and particularly poly(I)-poly(C) induce interferon formation in mammalian cells. Subsequently, Schell<sup>36</sup>

has shown that poly(I)-poly(C) is adsorbed to the outside of the cell followed by strand separation and ultimately by interferon formation. It has further been suggested<sup>37</sup> that other biological effects of polynucleotides, such as adjuvant effects and enzyme inhibition/activation requires interaction of the polynucleotides with the charged cell surface.

### Electrical Double Layer and Surface Potential

Because of the existence of the charge on the electrode surface, an electrode/solution interface is generally characterized by a well-defined electrical double layer bounded on one side by the electrode surface and on the other side by an ionic layer across which a relatively high electric field develops (up to ca.  $10^6$  V/cm) due to the large potential difference extending over a very small distance (Fig. 1). This constitutes the so-called inner or compact double layer, the width of which is only a few atomic diameters, and it is well known that the dielectric constant of solvent molecules in this region is decreased.<sup>39</sup> On the boundary between the inner and the diffuse layer the field strength has only about 1/10 of its original value, and it then decreases in the diffuse layer to virtually zero as shown in the figure. In a medium of ionic strength of ca. 0.1-0.2 M, which is a typical of biological fluids, the depth of the diffuse layer is about 100 Å.<sup>40</sup> Extensive discussion on the double layer can be found in several review articles.<sup>40,41</sup>

The surface potential of cell membrane/biological fluid interface arises from the charge on the surface since the cell surface and cellular membrane have ionizable groups on them such as the carboxyl group of sialic acid and phosphate groups of phospholipids to give negative surface charges.<sup>42</sup> Hence, there is an electrical double layer set up correspondingly bounded on one side by the membrane surface and the other side by an ionic layer across which most of the potential drop occurs<sup>43,44</sup> as shown in Fig. 2. Cope has presented some convincing arguments that a cell surface/biological fluid interface

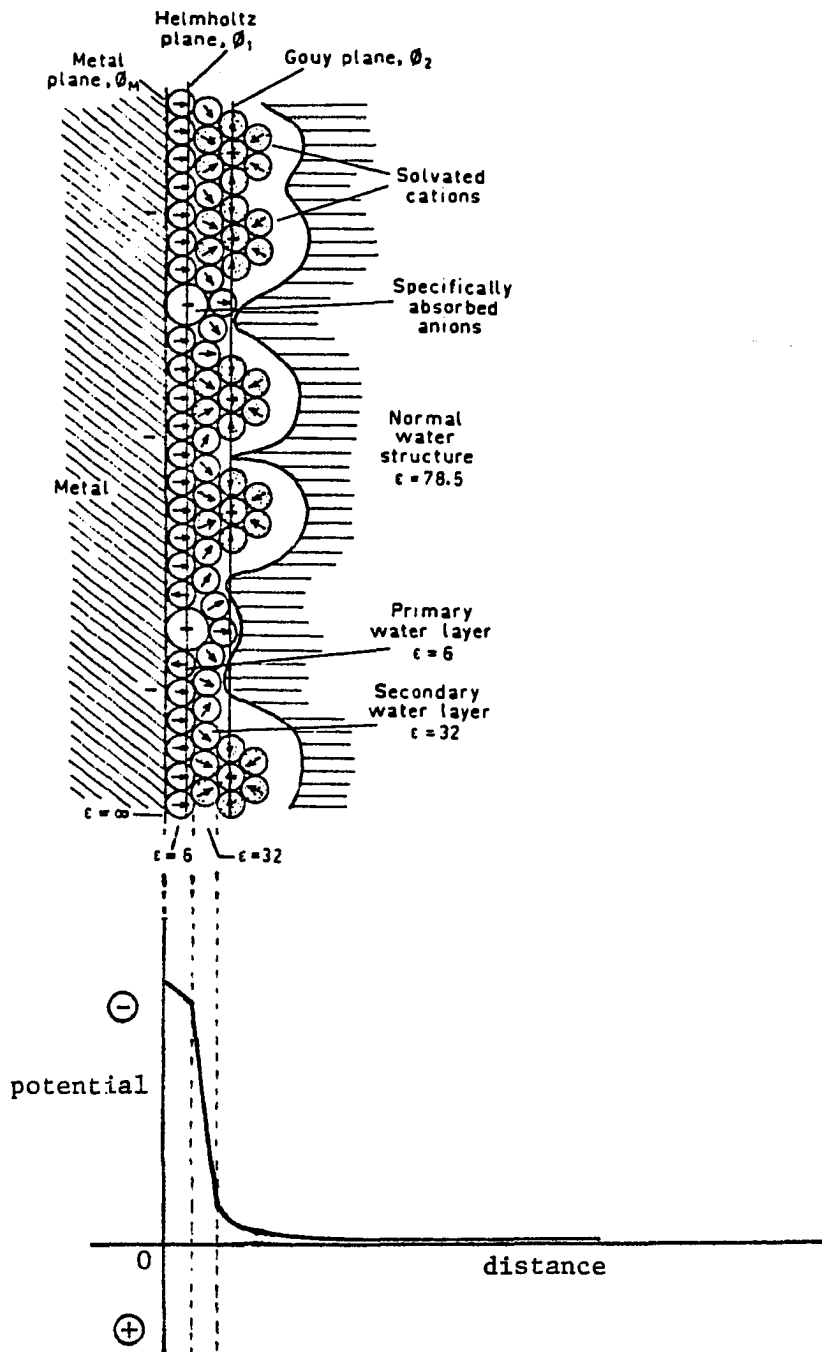


Fig. 1

A model of the electrical double layer<sup>38</sup> and potential-distance profile .

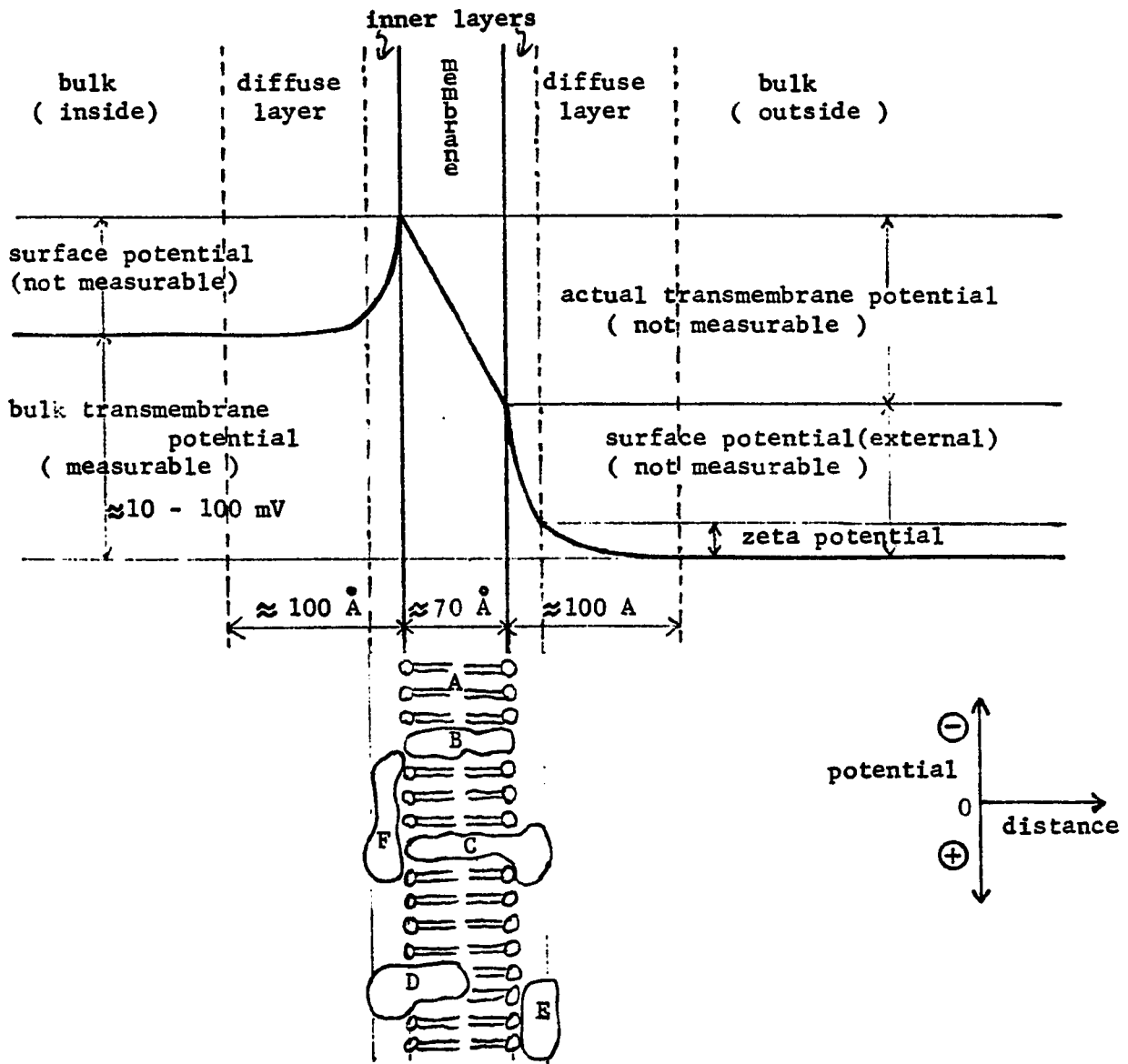


Fig. 2

A model of a membrane and potential-distance profiles. This profile was originally adapted from reference (45), and modified for the double layers. The basic structural feature is a phospho-lipid bilayer region(A) with various functional and structural protein complexes embedded(B, C, D, E and F ).

may be regarded as being very similar to a liquid/solid interface which exhibits electrical behavior analogous to that occurring at an electrode/solution interface.<sup>44,46-53</sup> It should be noted that the slope of the potential-distance curve in Fig. 2 is equal to the electric field strength (Volt/cm). Since there is a very strong electric field (typically  $10^5$  V/cm) in the membrane and interfacial region, the behavior of molecules or ions in this region is expected to be significantly different from that in the bulk medium.

The nature of the material comprising the charged surface, the decrease of dielectric constant and the electric field through the double layer may be important in controlling biological and other reactions in, for example, the following fashion.<sup>53</sup>

- 1) Adsorption may occur at the surface resulting in structural changes of the adsorbed species hence controlling its reactivity.
- 2) Concentration of the specific reactants at the surface might be quite different from that in the bulk solution. Increased surface concentrations through adsorption could facilitate intermolecular association, chemical reactions, etc.
- 3) Adsorption might occur with the adsorbed material oriented toward the solution, and hence to potential reactants, in a very specific fashion facilitating or hindering various chemical processes. The orientation phenomena could be surface-potential controlled.
- 4) The intense electrostatic field at the interfacial region could facilitate stabilization or destabilization of the ground state, intermediates or transition state in a reaction.
- 5) The  $pK_a$  values, for example, of species that pass into the electrical

double layer may be altered hence again influencing the course of chemical reactions.

Because a charged cell surface-biological fluid interface is similar to a charged electrode-electrolyte solution interface, it seems reasonable that an understanding of the interfacial behavior of biomolecules at the latter interface might reveal significant information regarding the interactions of these molecules at biological interfaces.

It would seem to be self-evident, however, that interfacial studies of nucleic acids and other polynucleotides, and interpretation of the data so collected, must rely on a fundamental knowledge of the interfacial behaviors of the monomeric units, i.e., the nucleobases, nucleosides and nucleotides. Several investigators have reported that various monomeric purine and pyrimidine derivatives are adsorbed at mercury electrode.<sup>55-62,65</sup> Such studies, however, have generally been very qualitative; they have revealed virtually nothing about the surface areas occupied by the adsorbed molecules and hence their probably surface orientations, the nature of the adsorption isotherms and the effects of potential on the adsorption processes, the intermolecular interaction between adsorbed molecules and the electrode surface. A brief review of the qualitative adsorption studies, so far reported, of such molecules will be given in the following section.

Review of Adsorption of Nucleobases, Nucleosides, Nucleotides, DNA  
and Polynucleotides

A number of reports have indicated that many purines, pyrimidines, their nucleosides and nucleotides are adsorbed at the dropping mercury electrode (DME),<sup>55-57,63-65</sup> principally at the potential of zero charge (pzc) or electrocapillary maximum potential (ECM). Such studies have been based primarily on alternating current polarography and differential capacitance measurements of the electrical double layer. Dryhurst and his coworkers in this laboratory have already reported a considerable amount of quantitative work on the adsorption of thymine, uracil and adenine and their derivatives.<sup>110,138,145,146</sup> It is particularly relevant to note that those purines and pyrimidines adsorbed at the DME that are normal components of nucleic acids (e.g., adenine, guanine, thymine, cytosine and uracil), exhibit pronounced depressions or pits in the differential capacitance vs. potential curves above certain bulk concentrations,<sup>64-67</sup> although such a behavior has been also found with several other aromatic organic compounds.<sup>67</sup> Such pits have been interpreted as indicative of strong intermolecular association between the adsorbed molecules. 6-Hydroxypteridine exhibits a similar phenomenon.<sup>67</sup> Adsorption-association effects have also been noted for nucleosides, deoxyribonucleosides, and deoxyribonucleotides of cytosine,<sup>63,65</sup> thymine, adenine, and guanine. Surprisingly however, Janik and Sommer<sup>68</sup> found that uridine monophosphate adsorbed at DME but gave no evidence for association on the electrode apparently because of electrostatic repulsion between negatively charged phosphate groups. However, since other nucleotides particularly those found

naturally in nucleic acids do adsorb and associate, there must be some fundamental difference between surface interactions of various nucleotides.

Elving et al.<sup>65</sup> have proposed that the principal mode of association of the cytosine nucleosides, nucleotides and oligonucleotides is a vertical overlapping or stacking of bases. Adenosine and deoxyguanosine<sup>63</sup> show two regions of potential where pits occur suggesting changes in orientation of the adsorbed and associated species at the electrode. Many other purine and pyrimidine derivatives show evidence for reorientation of the adsorbed species with change in potential.<sup>65</sup> The adsorption of nicotinamide adenine dinucleotide ( $\text{NAD}^+$ ,  $\text{NADH}$ ) at a glassy carbon electrode has also been studied recently by Elving et al.<sup>160-162</sup> It is proposed that  $\text{NAD}^+$  produced by anodic oxidation of the  $\text{NADH}$  is first rapidly adsorbed in a planar configuration relative to the electrode surface and probably bound to the surface through the adenine moiety. There is then a relatively slow reorientation of the adsorbed  $\text{NADH}$  molecules to a perpendicular orientation relative to the electrode surface; the perpendicularly oriented adsorbate, which likely involves interaction between parallel adenine and pyridinium rings, is more tightly bound to the surface than the planar oriented adsorbate.

Krznaric, Valenta and Nürnberg<sup>155,169,170</sup> reported several quantitative studies on the adsorption of nucleotides at the hanging mercury drop electrode (HMDE). It is shown that adenine oligonucleotides and poly (A) adsorb at the HMDE via the adenine base residues of the nucleotide chain according to their voltammetric studies, and that cytidine (at pH 3.24) follows a Frumkin type isotherm at lower concen-

tration.

Although many studies have been reported on the adsorption of nucleobases, nucleosides and nucleotides, the nature of the interaction between electrode and adsorbate molecules in the capacitance pit region are not well understood. Dryhurst et al.<sup>110</sup> proposed that hydrogen bonding between the hydrogen atom of the amino group of the bases and the electrode surface is a primary interaction for the molecular orientation in the capacitance pit, while Vetterl<sup>144,171</sup> suggested that it could be interpreted in terms of the interaction of electric fields with the charges and the dipole moments of the adsorbate molecules.

Reports have appeared regarding electrochemical studies of the adsorption of DNA and polynucleotides. Miller<sup>69</sup> used a differential capacity method to study the adsorption of DNA at the DME. At pH 6 he found that DNA is apparently adsorbed at potentials more positive than -1.2 V (vs. SCE) and desorbed at ca. -1.3 V. Miller also proposed that a negatively charged electrode double helical DNA unfolds. Such behavior is of considerable biological and electrochemical interest. However, more recently Flemming<sup>70</sup> has reexamined the behavior of DNA at the DME by a.c. polarography and could not confirm the unfolding of DNA at positive potentials. Palaček and coworkers<sup>71,72,73</sup> have reviewed the extensive d.c. and a.c., pulse and oscillopolarographic studies on DNA and polynucleotides. A number of peaks and waves for native and denatured DNA and polynucleotides are clearly of a non-faradaic nature, i.e., due to adsorption-desorption phenomena. Recent studies by Paleček et al.<sup>163,164</sup> demonstrate the conformational changes which

can be induced as a function of electrode potential. The influence of adsorption of double-stranded (ds) DNA, ds RNA and homopolymeric pairs at a mercury electrode on conformation of these polynucleotides was studied. Changes in the polarographic reducibility of polynucleotides, which were followed by means of normal pulse polarography and linear sweep voltammetry at the dropping mercury electrode were exploited to indicate conformational changes. It was found that, as a consequence of adsorption of ds polynucleotides on the negatively charged electrode, conformational changes similar to denaturation take place in a narrow potential region around  $-1.2$  V. After sufficiently long time of contact with the electrode (10 sec) these changes reach limiting values which can approach total denaturation. Upon adsorption of ds polynucleotides on the electrode charged to more positive potentials than  $-1.2$  V no conformational changes occur or only a small part of the polynucleotide is very quickly denatured--the remainder of the molecule preserves its ds structure. Conformational changes of adsorbed ds polynucleotides are influenced by factors which change the stability of ds polynucleotides in solution. It is supposed that denaturation of ds polynucleotides in the region (around  $-1.2$  V) might result from the strains connected with the repulsion of certain segments of the molecule anchored on the electrode from the negatively charged surface. Thus, Valenta and Grahmann<sup>74</sup> have concluded that protonated molecules of DNA are adsorbed via  $\pi$ -bonding of their pyrimidine and purine residues while the other parts of the DNA molecule, including the sugar and phosphate group, are oriented toward the solution. The data of Elving et al.,<sup>65</sup> however, seems to implicate the phosphate-

ribose residues in a much more important role in the interfacial properties, at least in the case of simple nucleosides and nucleotides. In addition, Valenta and Grahmann<sup>74</sup> seem to suggest that the macromolecular DNA even in its denatured form lies flat on the electrode. This is extremely unlikely, indeed there is considerable evidence, both theoretical and experimental (see, for example, references 75 and 76), that adsorption of flexible macromolecules to a plane interface results in the molecule adopting a structure consisting of adsorbed segment trains alternating with free loops extending out into the solution. If this is the case for DNA and polynucleotides, considerably more detailed and quantitative data is required before their behavior, conformation and structure at the electrode interface is sensibly characterized. Janik and Sommer<sup>68</sup> reported the first effort to investigate semi-quantitatively the adsorption of a polynucleotide (poly(U)) at the DME. They found considerable looping of the polynucleotide out into the solution.

Nürnberg and his coworkers<sup>165,166</sup> have also studied the adsorption and interfacial behavior of DNA and related biosynthetic polynucleotides in moderately acid solution (pH 5.6) over the whole extended potential range of adsorption up to -1.6 V (vs. SCE) at the HMDE by a potentiostatic double-step sweep method. Three potential ranges corresponding to different interfacial situations could be distinguished for the investigated polynucleotides. In the first range between -0.4 and -1.2 V the biopolymer is adsorbed. If the biopolymer has initially a double stranded form progressive irreversible deconformation occurs as well in this potential range. In the second range

between -1.2 and -1.6 V biopolymers are adsorbed and adenine and cytosine moieties undergo a totally irreversible reduction forming, according to the nature of the polynucleotide, a more or less completely blocking film of strongly adsorbed reduced biopolymer. In the third range beyond -1.6 V no adsorption and thus reduction occurs.

Brabec and Dryhurst<sup>167,168</sup> studied the electrochemical oxidation and adsorption of polyriboadenylic acid (poly(A)) by differential pulse voltammetry and a.c. voltammetry. Poly(A) is adsorbed at graphite electrodes between at least 0.2 V and 1.4 V. Single-stranded poly(A) is relatively flexible and, when adsorbed at a graphite electrode surface, conforms to a large extent to the contours of the rough electrode surface so that many adenine residues are accessible to the electrode and a relatively large voltammetric peak current is observed. However, double stranded poly(A) has a more rigid structure such that when adsorbed on a graphite electrode it cannot conform so readily to the contours of the electrode surface, hence fewer adenine residues are accessible to the electrode and a smaller voltammetric peak current is observed.

According to the differential pulse voltammetric studies by Dryhurst et al.<sup>167,168</sup> DNA is adsorbed at the surface of the graphite electrodes in a broad range of potentials including the potentials of electrochemical oxidation of DNA. Both native and denatured DNAs yield two single, well defined and separated peaks on the differential pulse voltammograms. The more negative peak corresponds to electrochemical oxidation of guanine residues, whereas the more positive peak corresponds to electrochemical oxidation of adenine residues.

Both peaks of native DNA occur at the same potential as peaks of denatured DNA. However, electrochemical oxidation of adenine and guanine residues at graphite electrodes is markedly suppressed in native DNA. The heights of the two peaks represent a sensitive indicator of the helix-coil transition of DNA. It is suggested that the decreased differential pulse-voltammetric activity of native DNA is connected with its decreased flexibility.

### Research Objectives

The main objective of this investigation was to characterize the behavior of several nucleobases, nucleosides and nucleotides at a charged mercury electrode/electrolyte solution interface. As revealed in the previous section, many of these compounds exhibit two regions of adsorption. The first or dilute adsorption region is where gradual changes are observed in the capacitance (C) vs. potential (E) curves in the low concentration range, typically less than 5 mM. The second or compact adsorption region where a sudden depression in the C vs. E curves (i.e., capacitance pit) is observed in the relatively high concentration range.

In the first part of this dissertation, adsorption of uracil, especially the effect of pH of the electrolyte solution, was investigated and the adsorption parameters were evaluated and the mode of adsorption was proposed.

In the second part, the adsorption of adenine, adenosine and its methylated derivatives, and adenosine monophosphate is characterized to evaluate the adsorption parameters and to propose possible molecular orientations of these compounds at the electrode surface and to elucidate the nature of interaction between the electrode and the adsorbate molecules.

## CHAPTER II

### THEORY

Although the study of the adsorption of organic substances at electrodes was already at a high experimental level with Gouy's electrocapillary work at the beginning of this century,<sup>77</sup> the first quantitative theory of the effect of the electric field on adsorption was formulated by Frumkin in two papers published in 1925<sup>78</sup> and 1926.<sup>79</sup> These works laid the basis of the thermodynamic (according to its own author) theory, which though extended and improved,<sup>80,81</sup> has since then fundamentally remained the same. Its broad validity is at present generally recognized.<sup>97</sup>

A new theory, which can be referred to as a molecular theory, was developed by Butler<sup>82</sup> in 1929. The main difference between the two theories resides in the size of the background model. Frumkin's theory is based on a macroscopic model of condensers in parallel, whereas Butler's theory focuses on microscopic (molecular) structures, although macroscopic values of properties are in fact used. Butler's theory appears rather attractive from a physical point of view, yet it encounters tremendous theoretical difficulties so that it is less practically useful than Frumkin's.<sup>97</sup>

Later, other authors followed the two main lines above. A

theory on molecular grounds was advanced by Bockris et al. in 1963<sup>83</sup> and 1967,<sup>84</sup> while conceptual retouches to the thermodynamic approach were suggested by Hansen et al.<sup>85</sup> and Parsons<sup>86</sup> in the sixties. Although the two kinds of approach are not contrasting in principle, there has been, however, much discussion<sup>86-92</sup> up to now about the model of the double layer in the presence of organic adsorbate.

As a matter of fact, 50 years after the development of the first theory, there does not appear to be at our disposal a fully satisfactory quantitative theory capable of predicting a priori the interfacial behavior of any neutral substance in detail. For these reasons, systematic experimental studies of organic adsorption are still welcome because that way the number of possible cases will be enlarged and further insight will be gained into the matter. A number of reviews,<sup>81,87,93-97</sup> have appeared on this topic over the last several years. A paper by Trasatti<sup>97</sup> provides a concise and plain description of the line to follow in the experimental acquisition and subsequent interpretative analysis on a molecular basis of parameters essential for the diagnosis of the kind of adsorption.

Experimental study for adsorption phenomena were carried out only on Hg electrodes<sup>98</sup> which allow the use of particularly suitable techniques. Practically all developments and improvements in this field have been made with the aid of experimental results using Hg electrodes. The experimental situation for other electrodes is rather complex.<sup>81,93,99</sup>

### The Significance of Adsorption Isotherm

Adsorption isotherm equations are equilibrium relationships between the concentration of adsorbate on the surface and in the bulk of solution at a constant temperature. Various types of isotherms have been proposed.<sup>100</sup> They differ in the way the state of the organic substance on the surface is described.<sup>86,101,102</sup> However, a survey of the literature reveals that adsorption phenomena can be described by three fundamental types of isotherm which in practice reduce to just one (Table 1).

Different states of the adsorbate molecule on the surface may be possible. The simplest state for a molecule on a surface is the ideal condition in which no adsorbate-adsorbate interactions are effective, either for reasons of molecular size or for reasons of intermolecular forces. In this respect, the adsorbate may be considered as a non-interacting point particle. The related equation of state is that for a two dimensional ideal gas model, where the surface pressure ( $\pi$ ) is substituted for pressure (P) and the surface concentration ( $\Gamma$ ) for the volume concentration (C). The resulting isotherm is called the Henry's law isotherm where the surface concentration and the surface coverage are directly proportional to the bulk concentration (eqn. (1a) and (1b)), and the surface pressure is directly proportional to the surface concentration (eqn. (2)). The proportionality constant (k), which is directly related to the adsorption coefficient (B), straightforwardly represents the equilibrium constant for the adsorption.

TABLE 1

## Fundamental Types of Isotherms

Model	Henry	Isotherm	Equation of State
Two-dimensional ideal gas	Henry	$\theta = Bc$	$\pi = \Gamma RT$
Correction for Molecular Size	Langmuir	$\frac{\theta}{1 - \theta} = Bc$	$\pi = \frac{\Gamma}{m} RT(1 - \theta)$
Correction for particle-particle interaction	Frumkin	$\frac{\theta}{1 - \theta} e^{2\alpha\theta} = Bc$	$\pi = -\frac{\Gamma}{m} RT[\ln(1 - \theta) + \alpha\theta^2]$

$c$  = bulk concentration of the adsorbate

$\Gamma$  = surface concentration of the adsorbate

$\theta$  = fraction of the surface covered by the adsorbate

$B$  = adsorption coefficient

$\pi$  = surface pressure

$\alpha$  = intermolecular adsorption coefficient

$R$  = Boltzman constant ( $1.38054 \times 10^{-16}$  erg deg<sup>-1</sup>)

$T$  = absolute temperature

$e$  = 2.71828

$$\Gamma = k C \quad (1a)$$

$$\theta = B C \quad (1b)$$

$$\pi = \Gamma R T \quad (2)$$

In a real system, a molecule of adsorbate will occupy a volume equal to its own size. Account for this in the equation of state leads to the Langmuir isotherm (eqn. (3)) which originally, however, was derived from kinetic considerations.<sup>103</sup> This isotherm describes the localized adsorption of particles which interact not because of intermolecular forces but for reasons of size. In this case, if a fraction  $\theta$  of surface is occupied by the adsorbate, further adsorption can only take place on the free part  $(1-\theta)$ . The surface concentration and the surface pressure can be expressed by eqns. (3) and (4), respectively.

$$\frac{\theta}{1-\theta} = BC \quad (3)$$

$$\pi = -\Gamma_m RT(1-\theta) \quad (4)$$

If adsorbate-adsorbate surface repulsion or attraction is present, this can be introduced into the equation of state by means of a quadratic term. Various corrections along these lines have been proposed by different authors.<sup>86</sup> Frumkin<sup>78</sup> has suggested the introduction of the quadratic term into the Langmuir equation of state. Thus, the resulting Frumkin isotherm is in practice a Langmuir isotherm multiplied by an exponential term containing a molecular interaction parameter (eqn. (5)), and the surface pressure can be given by eqn. (6).

$$\pi = \Gamma_m RT[\ln(1-\theta) + \alpha\theta^2] \quad (5)$$

$$\frac{\theta}{1-\theta} = BCe^{+2\alpha\theta} \quad (6)$$

where,  $\Gamma_m$  is the surface concentration at full monolayer surface

coverage. For  $\alpha = 0$ , the Frumkin isotherm (eqn. (6)) reduces to the Langmuir isotherm (eqn. (3)). A value of  $\alpha > 1$  indicates intermolecular attraction between adjacent adsorbate molecules, while  $\alpha < 1$  means repulsion. It should be also noted that the Frumkin isotherm reduces to the Henry isotherm when  $\alpha = 0$  and  $C \ll 1$ .

### Gibbs Adsorption Equation

#### The Relationship Between Surface Concentration and Surface Pressure

Gibbs<sup>104</sup> conceived the idea of measuring adsorption as the integral of perturbation in concentration with distance. His integral is shown schematically in Figure 3.<sup>105</sup> It represents the total of the concentration perturbation from the electrode surface to the bulk solution, at which point the change in concentration with distance approaches zero. The result of this summation is known as the Gibbs surface excess (or commonly surface concentration),  $\Gamma$ , and is given by the equation

$$\Gamma_i = \int_0^{\infty} C_i(x) dx \quad (7)$$

where  $C_i(x)$  is the perturbation in concentration of species  $i$  at a

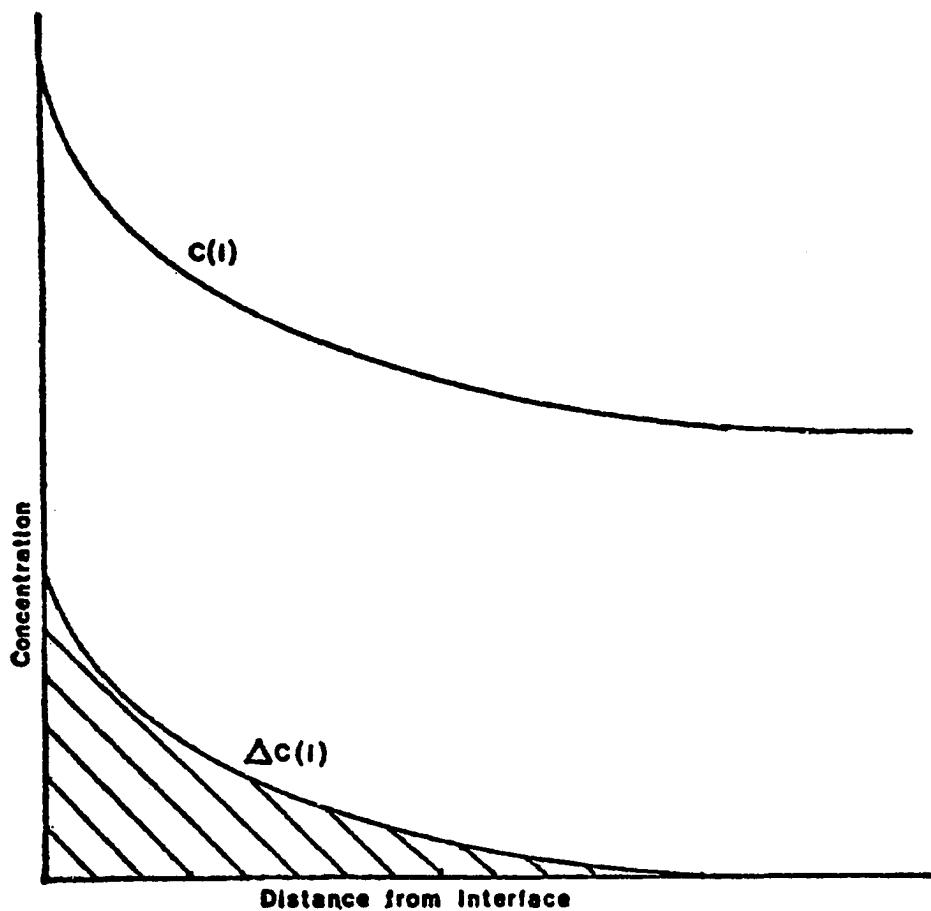


Fig. 3  
Schematic representation of the variation of concentration of species  $i$  with distance from an interface. Both the actual concentration,  $C_i$ , and the concentration perturbation,  $\Delta C_i$ , are shown. The shaded area represents the Gibbs surface excess,  $\Gamma_i$  (reference 105).

distance  $x$  from the electrode surface. Often the surface excess of a particular species is assumed to be approximately equal to the quantity of that species adsorbed on the surface.

Although it is not possible to directly measure the variation in concentration of a species with distance from the electrode, the surface excess or surface concentration can be evaluated indirectly by determining a measurable quantity such as surface tension. Surface tension (or surface free energy) is related to the surface excess according to the Gibbs adsorption equation:<sup>106</sup>

$$d\gamma = -\sum_i \Gamma_i d\mu_i \quad (8)$$

$$d\gamma = -RT \sum_i \Gamma_i d \ln a_i \quad (9)$$

where,  $\mu_i$  is chemical potential of a species  $i$  and  $a_i$  is the activity of the species.

If the surface has an electrical charge, an additional term  $qdE$ , which is simply the work done by the charge as the electric potential changes, must be introduced:<sup>107,108</sup>

$$-d\gamma = qdE + RT \sum_i \Gamma_i d\mu_i \quad (10)$$

$$\text{or } \Gamma_i = -\frac{1}{RT} \left( \frac{\partial \gamma}{\partial \ln a_i} \right)_{E, T, \mu_j (j \neq i)} \quad (11)$$

Surface pressure,  $\pi$ , is defined as the difference in the surface tension with and without adsorbate:<sup>108</sup>

$$\pi = -(\gamma_{\text{org}} - \gamma_w) = -\Delta\gamma \quad (12)$$

where,  $\gamma_w$  is the surface tension in the absence of organic adsorbate

$\gamma_{\text{org}}$  is the surface tension in the presence of organic adsorbate.

$$d\pi = -d\gamma \quad (12a)$$

therefore, for a dilute solution

$$\Gamma_i = \frac{1}{RT} \left( \frac{\partial \pi}{\partial \ln c_i} \right)_{E, T, \mu_j (j=1)} \quad (13)$$

where  $c_i$  is the concentration of the adsorbate species  $i$ .

The significance of eqn. (13) is that the surface excess can be evaluated if surface pressure is determined as a function of concentration. The slope of  $\pi$  vs.  $\ln c_i$  curve at any point would yield the surface excess at that particular concentration, and from the limiting slope where  $c_i$  approaches infinity the maximum surface excess (*i.e.*, the surface excess at full monolayer surface coverage,  $\Gamma_m$ ) can be found.

$$\lim_{c_i \rightarrow \infty} \left( \frac{\partial \pi}{\partial \ln c_i} \right)_{E, T, \mu_j (j=1)} = \Gamma_m RT \quad (14)$$

The molecular area, which is the area occupied by one molecule (or ion) of adsorbate on the electrode surface, can be readily obtained from  $\Gamma_m$  calculated from the limiting slope, *i.e.*, eqn. (14);

$$\begin{aligned} \text{Molecular Area} &= \frac{1}{(\text{Avogadro's Number}) \times \Gamma_m} \text{ (cm}^2\text{)} \\ &= \frac{10^{16}}{(6.022 \times 10^{23}) \times \Gamma_m} \text{ (\AA}^2\text{)} \end{aligned}$$

Lippman Equation

Relationship Between Surface Tension, Surface Charge  
and Potential and Double Layer Capacitance

For the charged electrode/electrolyte solution interface, the surface tension is also dependent on the surface electrical potential as described by the Lippman eqn. (15),<sup>109</sup> which is really a differential form of the Gibbs adsorption equation (10) for a charged surface.

$$\left(\frac{\partial \gamma}{\partial E}\right)_{T,P,a} = -q \quad (15)$$

$$C = \frac{dq}{dE} \quad (16)$$

where C is the capacitance of the electrical double layer

$$\text{therefore, } \left(\frac{\partial^2 \gamma}{\partial E^2}\right)_{T,P,a} = -C \quad (17)$$

In other words, if the capacitance is determined as a function of potential, the surface charge and surface tension can be obtained respectively by a single and double integration of the capacitance with respect to potential:<sup>110</sup>

$$q = \int_{E^*}^E C dE + q^* \quad (18)$$

$$\gamma = \int_{E^*}^E q dE + \gamma^* \quad (19)$$

where, E\* is the starting potential of the integration

q\* is the integration constant which corresponds to the charge  
at E\*

$\gamma^*$  is the surface tension at E\*.

Generalized Frumkin Isotherm for Charged Surface

For electrified surface-adsorbate interactions, it has been shown<sup>80</sup> that the adsorption coefficient,  $B$ , is no longer constant since the adsorption equilibrium is dependent on the electric field (hence the potential or the surface charge) according to eqn. (20).

$$B = B_0 e^{-\phi/\Gamma_m RT} \quad (20)$$

Here  $B_0$  is the adsorption coefficient at the electrocapillary maximum potential (i.e., at  $q=0$ ) for the electrolyte solution without the adsorbate. Combining equations (6) and (20), an equation referred to as the generalized Frumkin isotherm<sup>111</sup> is obtained:

$$\frac{\theta}{1-\theta} = B_0 c e^{-\phi/\Gamma_m RT} e^{2\alpha\theta} \quad (21)$$

In this equation the electric field dependent function,  $\phi$ , can be expressed as a function of the potential:<sup>111</sup>

$$\phi = \int_0^E q_w dE + C'E(E_N - \frac{1}{2}E) \quad (22)$$

where  $q_w$  is charge at a potential  $E$  for the background electrolyte solution

$C'$  is the capacitance of the double layer for the electrode completely covered with adsorbate monolayer (assumed constant), i.e., at  $\theta=1$ .

$E_N$  is the electrocapillary maximum potential at  $\theta=1$ .

The potential,  $E$ , in equation (22) is also relative to the ECM for the background electrolyte solution. Integration of eqn. (22) gives

$$\phi = G(E) + C'EE_N - \frac{1}{2} C'E^2 \quad (23)$$

where  $G(E) = \int_0^E q_w dE = \gamma_w(0) - \gamma_w(E) \quad (24)$

$\gamma_w(0)$  is the surface tension of the background electrolyte

solution at  $E=0$ .

$\gamma_w(E)$  is the surface tension of the background electrolyte at potential  $E$ .

Hence  $G(E)$  can be determined experimentally from the difference between the interfacial tension at the ECM and the value at any potential  $E$  in the absence of an organic adsorbate. Eqn. (22) which essentially relates the fractional surface coverage ( $\theta$ ) as a function of concentration ( $c$ ) and potential ( $E$ ) can be rewritten as follows:

$$\frac{\theta}{1-\theta} = B_o c e^{2\alpha\theta[G(E)-C'EE_M - \frac{1}{2}C'E^2] / \Gamma_m RT} \quad (25)$$

The surface pressure ( $\pi$ ) for the Frumkin isotherm is expressed as a function of the fractional surface coverage ( $\theta$ ) by eqn. (5)

$$\pi = - \Gamma_m RT [\ln(1-\theta) + \alpha\theta^2] \quad (5)$$

A nonlinear least square computer program was used to fit  $\pi$  values at various concentrations and potentials to give the best values of  $\alpha$ ,  $B_o$ ,  $\Gamma_m$ ,  $C'$ , and  $E_N$ .<sup>112</sup> This is done by first taking trial values of the latter 5 parameters and calculating values of  $\theta_i$  from eqn. (25) for each pair of concentration  $c_i$  and potential  $E_i$  values by an iterative numerical method. This set of calculated  $\theta_i$  values was then used to predict a set of  $\pi_i$  values using eqn. (5). For a given set of parameters, a value of the sum of squares of the residuals (i.e., errors),  $s = \sum (\pi_i^{\text{experimental}} - \pi_i^{\text{calculated}})^2$ , is then obtained. The value of  $s$  is minimized with respect to variation of all five parameters, and standard errors in all the parameters and the root mean square deviation in  $\pi$  are also calculated. For most of the systems, convergence was obtained within 5 to 20 iteration cycles provided

reasonably good initial estimates of the parameter values were made. In those systems where electrocapillary and capacitance data were available, it was often useful to fix  $E_N$  values, which is determined readily from the electrocapillary curves for large concentrations of the organic adsorbate (i.e., at  $\theta \rightarrow 1$ ). In addition,  $C'$  may generally be estimated by measuring the capacitance of nearly saturated solution of the organic compound at a potential at, or very close to, the potential of maximum adsorption (this is easily recognized as the potential at which  $\pi$  reaches its maximum value in  $\pi$  vs.  $E$  plots particularly in solutions where  $\theta \rightarrow 1$ ). The latter approach has also been used by Hansen and coworkers.<sup>111</sup>

#### Congruence of the Electrosorption Isotherms

When  $\pi$  vs  $\ln a$  curves at various constant potentials are superimposable by simply shifting the entire graph horizontally along the  $\ln a$  axis it generally means that interactions between molecules of the adsorbate are independent of potential (or that the constant  $\alpha$  is invariant with potential); namely, the adsorption isotherms are congruent with respect to potential. Such behavior is typical of many organic compounds such as thiourea,<sup>130,192</sup> n-butanol,<sup>173</sup> acetanilide<sup>174</sup> and thymine.<sup>146</sup> However, in the case of phenol<sup>91,122</sup> the  $\pi$  vs.  $\ln a$  curves are not superimposable at different potentials. This has been interpreted as indicating that the phenol molecules are adsorbed parallel to the electrode surface at a positively charged electrode and perpendicular to the electrode at a negatively charged electrode.

The fact that  $\pi$  vs.  $\ln a$  plots are superimposable by abscissa

translation has been widely used to prove that the adsorption isotherms are congruent with respect to potential. However, Parsons<sup>173</sup> has shown that superimposability of  $\pi$  vs.  $\ln a$  plots is not sufficiently sensitive to provide adequate proof of the congruence of electrosorption isotherms with respect to potential. Accordingly, the first step in interpretation of the interfacial behavior of a molecule was to decide by a more sensitive method whether the adsorption isotherms were congruent with respect to potential or charge. If the adsorption isotherm is congruent with respect to potential, it follows from Parson's proof<sup>176</sup> that at any fixed value of electrode potential the charge density,  $q$ , in the presence of the adsorbed organic molecules should be a linear function of the fractional surface coverage,  $\theta$ , i.e.,

$$q = q_w(1+\theta)+q'\theta \quad (26)$$

Here,  $q_w$  and  $q'$  denote the values of charge at the same electrode potential in the presence of pure supporting electrolyte and when the surface is saturated ( $\theta=1$ ), respectively. If the adsorption is congruent with respect to charge, it follows<sup>176</sup> that at any constant value of  $q$ , the electrode potential in the presence of adsorbed organic molecules should be a linear function of  $\theta$ , i.e.,

$$E = E_w(1-\theta) + E'\theta \quad (27)$$

Here  $E_w$  and  $E'$  are the values of electrode potential at the same  $q$  in the presence of pure supporting electrolyte and when the surface is saturated ( $\theta=1$ ), respectively.

Isotherms ( $\theta$  vs. concentration or activity) may be obtained by using eqn. (26) at fixed potentials or eqn. (27) at fixed charges

to calculate  $\theta$ . If the isotherms at different potentials with  $\theta$  values calculated from eqn. (26) have the same geometrical shape, i.e., they may be superimposed by abscissa translation, then the isotherms are congruent with respect to potential. Alternatively, if the isotherms at different charges with  $\theta$  values calculated from eqn. (27) have identical geometrical shapes, then the isotherms are congruent with respect to charge. These tests were first proposed by Damaskin<sup>88</sup> and coworkers<sup>89</sup> and recently have been slightly modified by Mohilner et al.<sup>177</sup> Both of these tests, however, rely on a fairly precise knowledge of  $C'$ , the capacitance of a completely monolayer covered electrode surface ( $\theta=1$ ) which is normally assumed to be constant and independent of charge and potential.<sup>178</sup> Accordingly, tests for congruence of the adsorption isotherms have been carried out by preparing plots of  $q$  vs.  $\Gamma RT$  at fixed potentials as a test of eqn. (26) and plots of  $E$  vs.  $\Gamma RT$  at fixed charges as a test of eqn. (27).

## CHAPTER III

### EXPERIMENTAL

#### Chemicals

Uracil was obtained from Sigma and, after drying in an oven for three hrs at 100°C, was used without further purification.

Adenine, N<sup>6</sup>-methyladenine(6-methyladenine), N<sup>6</sup>,N<sup>6</sup>-dimethyladenine(6-dimethyladenine), adenosine, and adenosine-5'-monophosphate (AMP) were obtained from Calbiochem.

N<sup>6</sup>-methylaminopurine-9-ribose(6-methyladenosine) and N<sup>6</sup>,N<sup>6</sup>-dimethyl aminopurine-9-ribose (or 6-dimethyladenosine) were obtained from Sigma.

The borate pH 9 buffer system was constituted as follows: 17.5 g Na<sub>2</sub>B<sub>4</sub>O<sub>7</sub>·10 H<sub>2</sub>O, 67.7 g KCl and 16.85 ml 1M HCl diluted to 1 liter with deionized water. Upon dilution with an equal volume of water the latter buffer has an ionic strength of 0.5 M.

The fluoride pH 8 buffer consisted of 0.5 M sodium fluoride which was made 0.01 M in Na<sub>2</sub>HPO<sub>4</sub>.

The phosphate buffer systems (pH 3.0, 5.0, 8.0, 11.0) were prepared from appropriate mixtures of H<sub>3</sub>PO<sub>4</sub>, NaH<sub>2</sub>PO<sub>4</sub>·7H<sub>2</sub>O, and Na<sub>3</sub>PO<sub>4</sub>·12H<sub>2</sub>O (Fisher Scientific Co., reagent grade). All buffer solution had an ionic strength of 0.5 M.

Although commercial, triply distilled mercury (Bethlehem Apparatus Co., Hellertown, Pa.) could be used satisfactorily with the dropping mercury electrode (DME) for differential capacitance measurements, the mercury was further purified for use in the maximum bubble pressure measurement experiments. This was accomplished by washing the mercury at least three times with dilute (1 M)  $\text{HNO}_3$ , then washed three times with deionized water. After careful drying the mercury was distilled.

### Differential Capacitance Measurement

Differential capacitance measurements were obtained by a phase selective alternating current polarographic method. This a.c. polarographic method was employed in preference to the more conventional impedance bridge method<sup>113,116</sup> because of its relative ease of use. In addition, Jehring<sup>114,115</sup> has convincingly demonstrated that a.c. polarography is a very suitable method for measurement of differential capacitance and provides data that may be used for quantitative interpretation of adsorption phenomena at electrodes.

In a.c. polarography a slow, linear potential sweep is applied (which is the same as in d.c. polarography), and in addition a small, sinusoidal potential is superimposed on the d.c. ramp potential. Typically, the alternating potential has a frequency of 100 Hz and an amplitude of 10 mV. The potential the electrode actually sees is an alternating potential oscillating around the value of the linear potential. The utility of a.c. polarography in measuring differential capacitance stems from the fact that the current which is used to charge the electrical double layer, called the charging current, is directly proportional to the differential capacitance of the double layer at the interface. A.c. polarography can be used to measure this charging current by taking advantage of the fact that it is 90° out of phase with the applied alternating potential. Phase-selective amplifiers are used to select only that current which is 90° out of phase with the applied potential. A Princeton Applied Research Corporation (PAR) Model 121 Lock-in Amplifier/Phase Detector was employed for this purpose. It was used in conjunction with a PAR Model 174

Polarographic Analyzer and a PAR Model 174/50 A.C. Polarographic Analyzer Interface.

The usual polarographic dropping mercury electrode (DME) was used following siliconization.<sup>118</sup> This procedure involved, first, cleaning the capillary by pulling through it a small volume of water, then dilute nitric acid. Then, several milliliters of water were pulled through, followed by a large enough volume of acetone to thoroughly dry the capillary. Water vapor was pulled through the capillary by hanging it over a boiling water bath for 5 minutes. It was then immediately dipped into dichlorodimethylsilane so that this, too, was pulled into the capillary. After the capillary was completely wetted with the silane, it was again suspended over boiling water, and the siliconization procedure was repeated. The capillary was dried with air for three hours, and about 2 cm of the tip was removed before use. The DME was equipped with a mechanical drop dislodger.

A pool of mercury inserted at the bottom of a thermostatted 5 ml-capacity cell served as the counter electrode. A saturated calomel reference electrode (SCE) was positioned close to the DME using a fine Luggin capillary. (All potentials are referred to the SCE at 25°C.) The d.c. potential was scanned at a sweep rate of 0.005 V/sec. All a.c. polarograms and alternating current vs. time curves were recorded on a Hewlett Packard Model 7001A X-Y recorder.

The polarographic cell may be considered as an electric circuit consisting of a capacity (C) of the double layer and resistance (R) of the solution in series. The current can be given<sup>119</sup> by the equation

$$I = \frac{\Delta E}{\sqrt{R^2 + \frac{1}{C\omega^2}}} \quad (28)$$

where  $\Delta E$  is potential applied

$\omega$  is the angular velocity of the a.c. potential ( $\omega = 2\pi f$ )

$f$  is the frequency of the a.c. potential

From eqn. (28),

$$I = \frac{\omega C \Delta E}{\sqrt{R^2 C^2 \omega^2 + 1}} \quad (29)$$

For small values of  $R$  (less than 1 K  $\Omega$ ) and relatively low frequency ( $f \leq 100$  Hz), eqn. (29) reduces to

$$I = 2\pi f C \Delta E \quad (30)$$

$$\text{or } C = \frac{I}{2\pi f A \Delta E} \quad (31)$$

where  $C$  is the differential capacity ( $\mu\text{F}/\text{cm}^2$ )

$I$  is the charging current ( $\mu\text{A}$ )

$\Delta E$  is the amplitude of the applied alternating potential (mV)

$A$  is the surface area of the DME at the time current is sampled ( $\text{cm}^2$ ).

This equation is valid as long as the resistance of the test solution is small and the frequency of the applied alternating potential is low.<sup>119</sup> The PAR instrumentation required calibration to this equation prior to making measurement on test solution. For calibration purposes, a 1.00 + 0.01  $\mu\text{F}$  capacitor (Southern Electronic) was used in place of the polarographic cell. Because the capacitance of the precision capacitor was known, the value of the charging current given by the PAR instrumentation could be compared with the expected value. Any

discrepancy in the two values was compensated by a calibration factor,  $F_c$ , which is the ratio of the charging current calculated to that given by the PAR instrumentation.

If the formation time of the double layer is less than the half-period of the applied alternating potential, the differential capacitance must be independent of frequency.<sup>119</sup> Alternatively, if the frequency of the applied potential is so large that any adsorbed uracil derivative cannot adsorb or desorb as fast as the potential oscillates, then a.c. equilibrium does not exist. Variation of the differential capacitance with a change in frequency of the applied a.c. potential is often observed, particularly with solid electrodes.<sup>120</sup> Usually this variation is linear, and in many instances differential capacitance is reported as the value extrapolated to zero frequency.

For all of the compounds in this study measurements of differential capacitance between 10 and 200 Hz indicated no dependence on frequency at any potential. This was tested by measuring the charging current of two solutions of varying concentrations for each compound at frequencies of 20, 100, and 200 Hz. The differential capacitance was then calculated from equation (31). It was not possible to measure differential capacitance at frequencies greater than 200 Hz because the a.c. polarographic method is restricted to relatively low frequencies.<sup>121</sup> However, because of the absence of any significant frequency dispersion over the frequency range observed, all differential capacitance data in this study were measured at 100 Hz and with a modulating potential of 10 mV peak-to-peak. Most of the compounds investigated in this study showed frequency independence

of the double layer capacitance below 500 Hz. However, certain methyl derivatives of adenosine exhibit frequency dependence of the capacitance. In Figure 4, typical examples of such a test for a.c. equilibrium tests are shown.

Sometimes, particularly with very high molecular weight organic species, the time required for the interfacial region to come to equilibrium at a given d.c. potential can be very long. However, for the compounds used in this study, the value of the differential capacitance per unit area of electrode at a fixed frequency of 100 Hz (where a.c. equilibrium was known to exist) was found to be constant at times greater than one second after application of potential. This was true over the entire range of potentials studied. The same solutions used in the a.c. equilibrium study were used to record current versus time curves over the entire drop life of the DME at -0.5 V, -1.0 V and -1.5 V. A similar curve was recorded for the pH buffer solution alone. Ratios of charging current for test solutions containing organic compound to charging current for the background solution taken at one-second intervals over the drop lifetime were constant, indicating d.c. equilibrium after one second. Typical examples of such a d.c. equilibrium test are shown in Figure 5.

For convenience, all subsequent measurements were made with a controlled drop time of two seconds, and the current was sampled shortly ( $\frac{1}{16}$  second) before the end of the drop life time (namely,  $1 \frac{15}{16}$  sec after the dislodging of the drop). The siliconized DME had a flow rate of 1.1415 mg/sec at open circuit. The drop area at the time of sampling was  $0.01669 \text{ cm}^2$ . The a.c. polarograms were normally recorded between -0.2 V and -1.8 V.

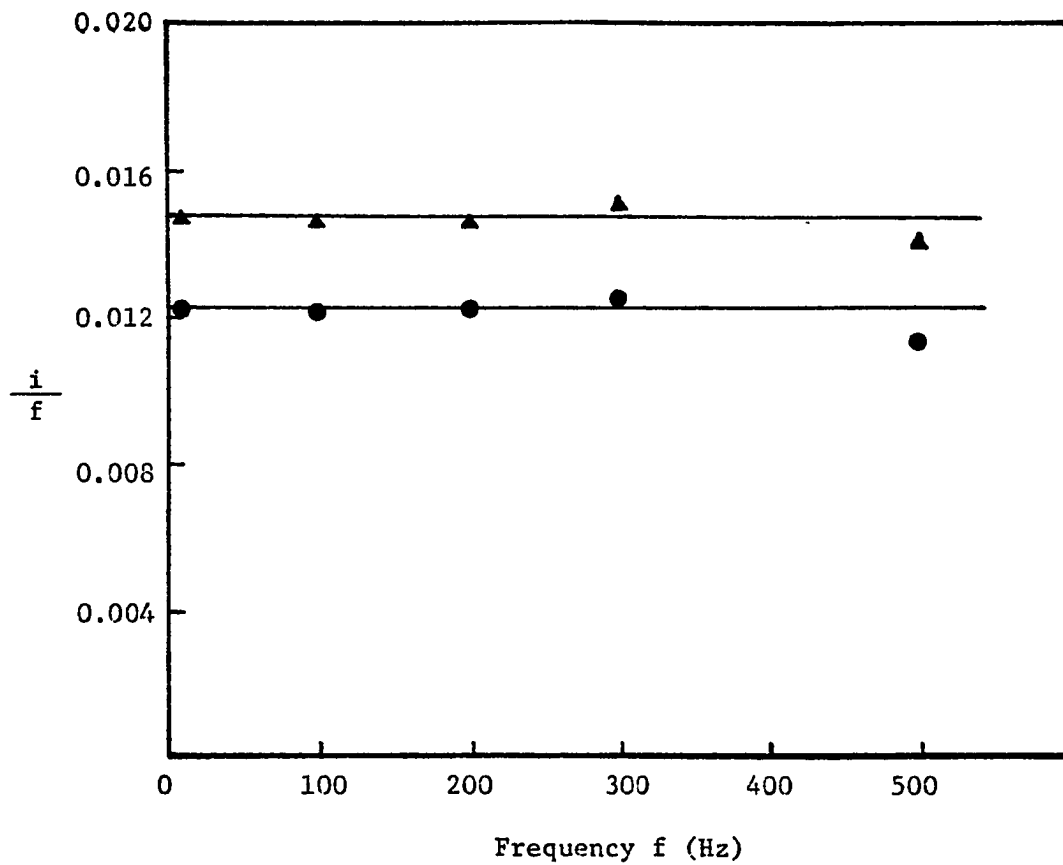


Fig. 4 A

Test of a.c. adsorption equilibrium on uracil (30.00 mM) in pH 11 phosphate buffer. The constancy of the current-to-frequency ratio implies that the capacitance is independent of frequency.

● at - 0.4 V,     ▲ at - 1.0 V.

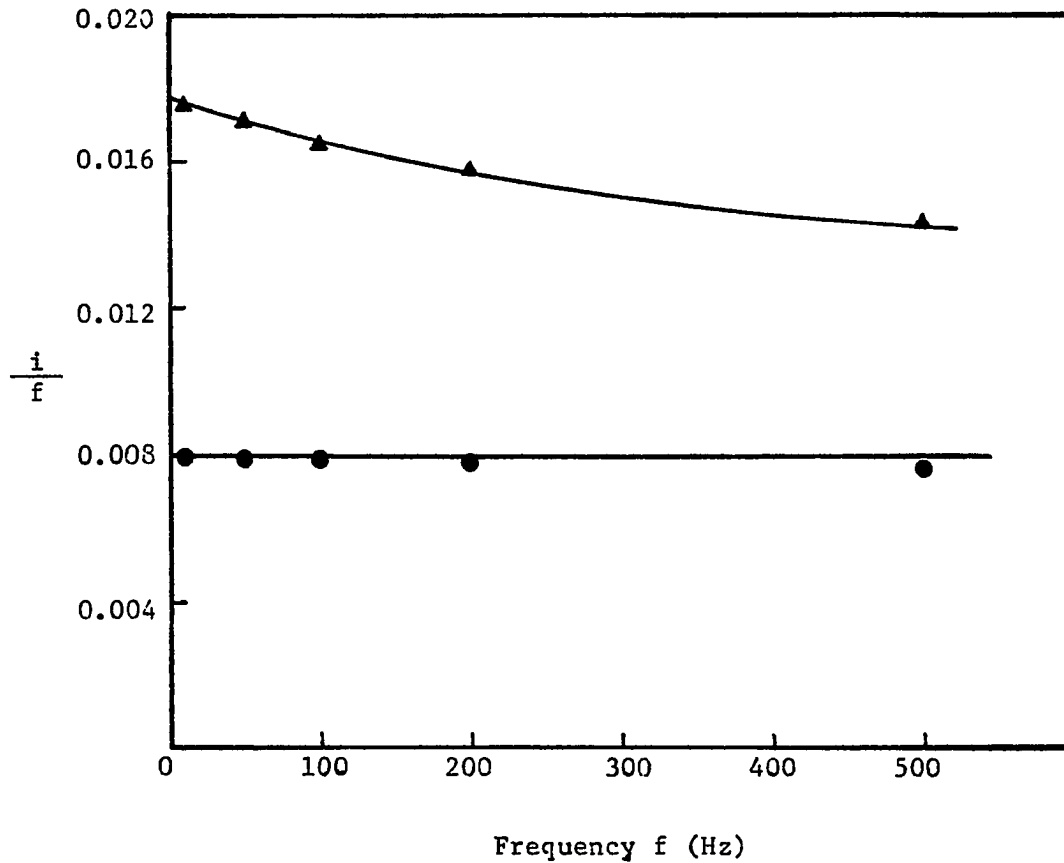


Fig. 4 B

Test of a.c. adsorption equilibrium on 6-methyladenosine (1.0 mM) in pH 8 fluoride buffer. The capacitance is independent of frequency at - 0.4 V (●), however it decreases significantly as frequency increases at - 1.2 V (▲). 6-dimethyladenosine exhibits similar frequency dependence of capacitance.

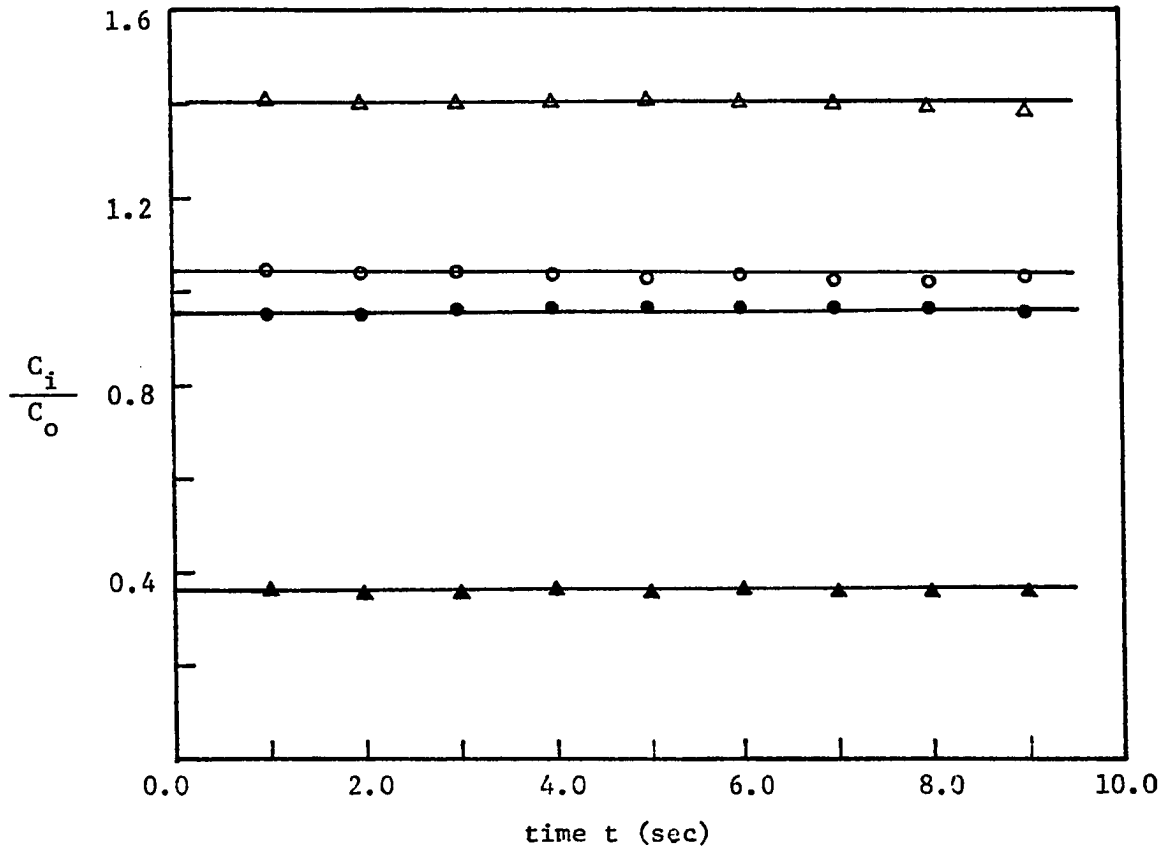


Fig. 5 A

Test for d.c. adsorption equilibrium on uracil in pH 8 phosphate buffer. The time independence of the capacitance ratio,  $C_i/C_o$ , indicates a rapid (at least within 1 sec) establishment of  $i^0$  adsorption equilibria, where  $C_i$  is capacitance of the background electrolyte solution without uracil and  $C_o$  is capacitance of the electrolyte solution with the organic adsorbate.

1.00 mM solution (●), 30.00 mM (▲) at - 0.5 V (vs. SCE)

1.00 mM solution (○), 30.00 mM (△) at - 1.0 V.

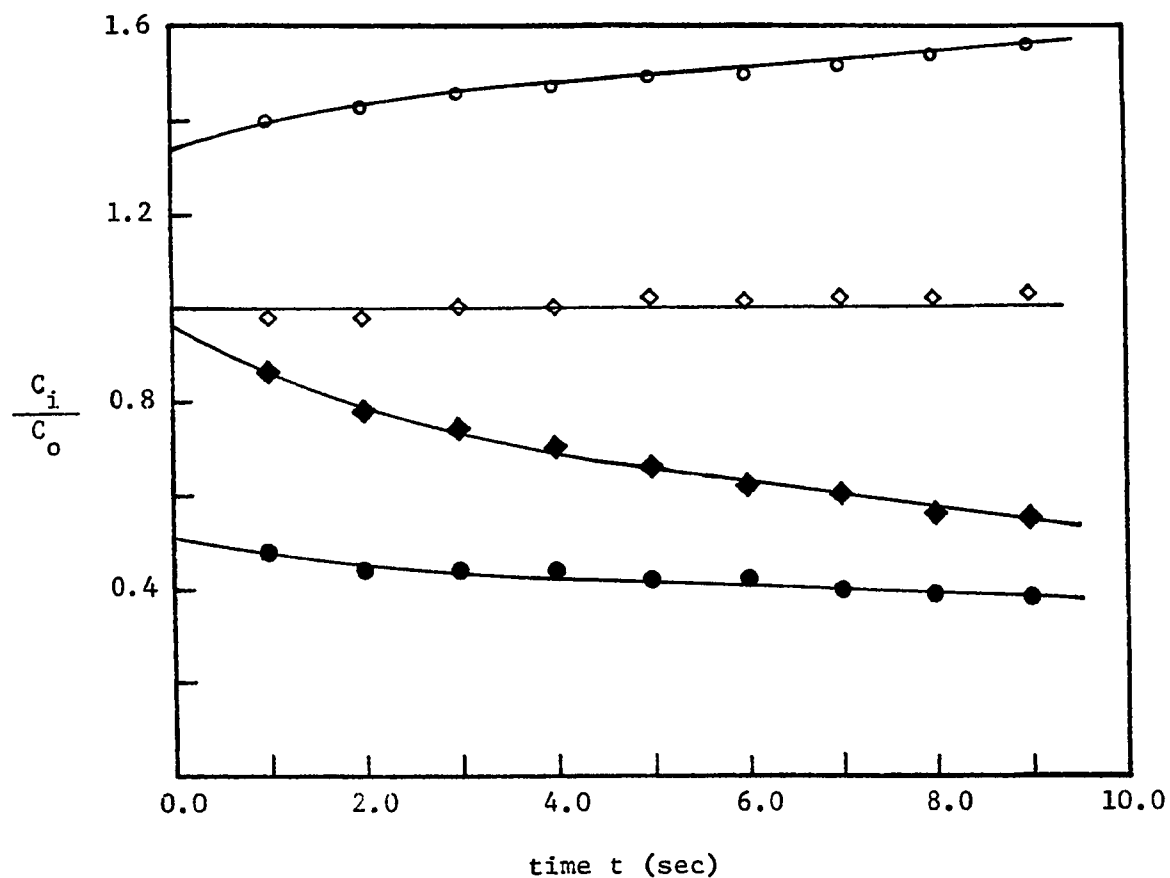


Fig. 5 B

Test for d.c. adsorption equilibrium on 6-dimethyladenosine in pH 8 fluoride buffer ( 0.5 M NaF plus 0.01 M  $\text{Na}_2\text{HPO}_4$  ).

0.03 mM (◆), 1.00 mM (●) at - 0.5 V ( vs. SCE )

0.03 mM (◇), 1.00 mM (○) at - 1.2 V

The time dependence of the capacitance ratio is especially noted in the 0.03 mM solution at - 0.5 V (◆) and 1.00 mM solution at -1.2 V (○). 6-methyladenosine exhibits similar time dependence of capacitance.

A computer program developed in this laboratory was used to integrate the capacitance data numerically to obtain surface charges, surface tensions and surface pressures (See Appendix).

Direct Surface Tension Measurements Using Capillary Electrometers

The apparatus utilized to measure interfacial tension directly with a capillary electrometer using a maximum bubble pressure technique<sup>125,126</sup> is shown schematically in Figure 6. This apparatus is similar to that used by Broadhead et al.<sup>122</sup> A Brinkman/Wenking Model LT73 potentiostat was utilized. The location of the mercury in the pyrex capillary was observed with a Gaertner 2206-A cathetometer through an optically-flat quartz window sealed in one side of the cell (Fig. 6). The cell was water-jacketed and maintained at a temperature of  $25.0 \pm 0.1^\circ\text{C}$ . The pressure at the mercury-test solution interface was varied by adjusting the pressure of the air above the mercury by means of a syringe and two microburets. The coarse-adjust utilized a 20.0 ml plastic syringe, while fine pressure adjustment was accomplished with two Gilmont 2.0 ml micrometer burets. A Mensor Corporation quartz manometer pressure gauge was used to measure the air pressure.

Two different types of capillary were employed. The first was a simple drawn-out pyrex capillary which dipped vertically into the test solution, i.e., the apparatus shown in Fig. 6 which is a classical Lippman capillary electrometer. For these capillaries interfacial tension was measured when the mercury column was adjusted to a reference point which is 1 mm above the tip of the capillary. At this point the internal radius was 0.00297 cm. The second capillary was an inverted J-shaped pyrex capillary; this capillary was siliconized in a manner analogous to that used for the DME in the a.c. polarographic capacitance measurements. With the latter capillary the pressure was adjusted in the apparatus shown in the Fig. 6 until mercury drops start to form

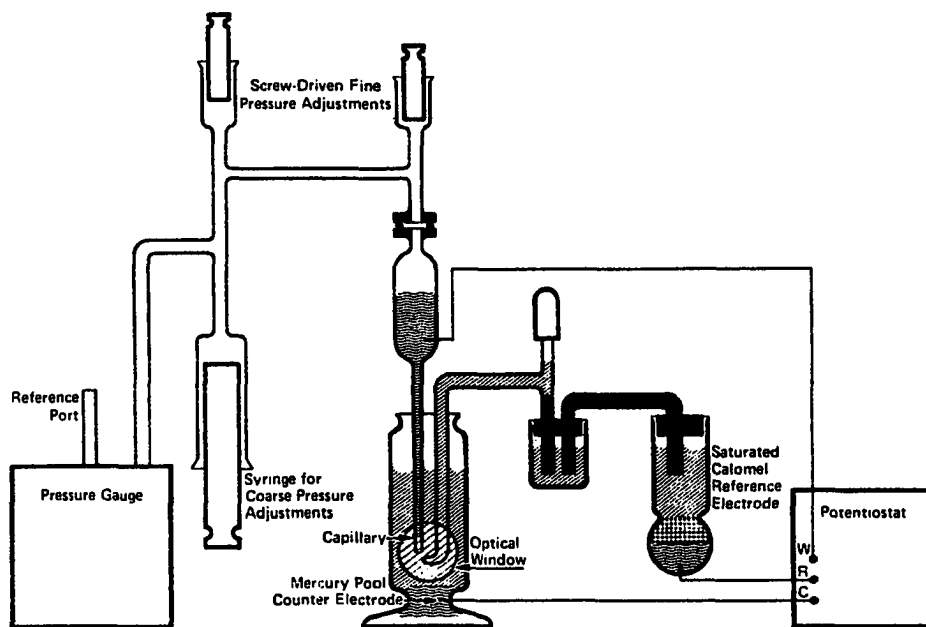


Fig. 6

Apparatus for direct measurement of interfacial ( or surface) tension at the mercury/solution interface.

at the capillary tip. This method is identical to a maximum bubble pressure experiment which is commonly used to measure surface tension at the air/liquid interface.<sup>123</sup> The internal radii of the pores at the tip of the two J-shaped capillaries used were 0.00118 cm and 0.00189 cm. The total pressure on the mercury-electrolyte interface was the value measured on the Mensor pressure gauge added to the mercury head over the capillary. The depth of immersion of the capillary into the solution was accurately (to  $\pm 0.01$  cm) measured with the cathetometer so that a small correction for the back hydrostatic pressure could be subtracted from the total pressure.

In the case of the conventional simple, drawn-out straight capillary the total measured pressure,  $\Delta P$ , is directly proportional to the interfacial tension,  $\gamma$ , and inversely proportional to the capillary radius by the relationship<sup>123</sup>

$$\Delta P = \frac{2\gamma}{r} \quad (32)$$

where  $r$  is the internal radius of the capillary at the predetermined reference point. The same equation applies in the maximum bubble pressure method except that  $r$  refers to the internal radius of capillary at its tip.

The values of radii,  $r$ , for both capillary were determined with a 0.100 M  $\text{HClO}_4$  solution where the interfacial tension at  $-0.500$  V at  $25^\circ\text{C}$  is 425.56 dyne/cm according to Hansen *et al.*<sup>122</sup> All potentials are referred to the saturated calomel electrode (SCE) at  $25^\circ\text{C}$ .

Data points were normally taken at 50 mV intervals between  $-0.2$  V and  $-1.8$  V. In the case of the vertical capillary, several

drops of mercury were expelled from the tip before the electrocapillary curve at each concentration was measured.

With the maximum bubble pressure (MBP) method it was found that once the pressure had been reached at which bubble formation occurred the flow of mercury could not be stopped unless the pressure within the system was drastically reduced. Schiffrin<sup>124</sup> has suggested that this effect is probably caused by the mechanical momentum associated with the moving liquid inside the capillary. Further information on the maximum bubble pressure technique can be found in the reports of Schiffrin<sup>124</sup> and Lawrence and Mohilner.<sup>125,126</sup>

In potassium fluoride (NaF) solution Lawrence et al.<sup>127</sup> and Schiffrin<sup>124</sup> noted that interfacial tension data obtained by measurements with a conventional capillary electrometer (i.e., with a straight capillary) were at variance with the integrated capacitance results, particularly at potentials at or more positive than the ECM potential. This effect is apparently due to variations of the wetting properties of the glass capillary at positive electrode polarizations leading to changes in the contact angle between mercury and glass.

This effect was investigated for the 0.5 M NaF plus 0.01 M Na<sub>2</sub>HPO<sub>4</sub> buffer solution (pH 8.0) used here by comparing interfacial tension vs. potential curves for the pure background electrolyte solution obtained with a conventional capillary electrometer (vertical capillary), with a maximum bubble pressure method (J-shaped capillary) and by double integration of capacitance vs. potential curves. Typical results are presented in Fig. 7 where it is seen that there is excellent agreement between the latter results and those obtained by use of the

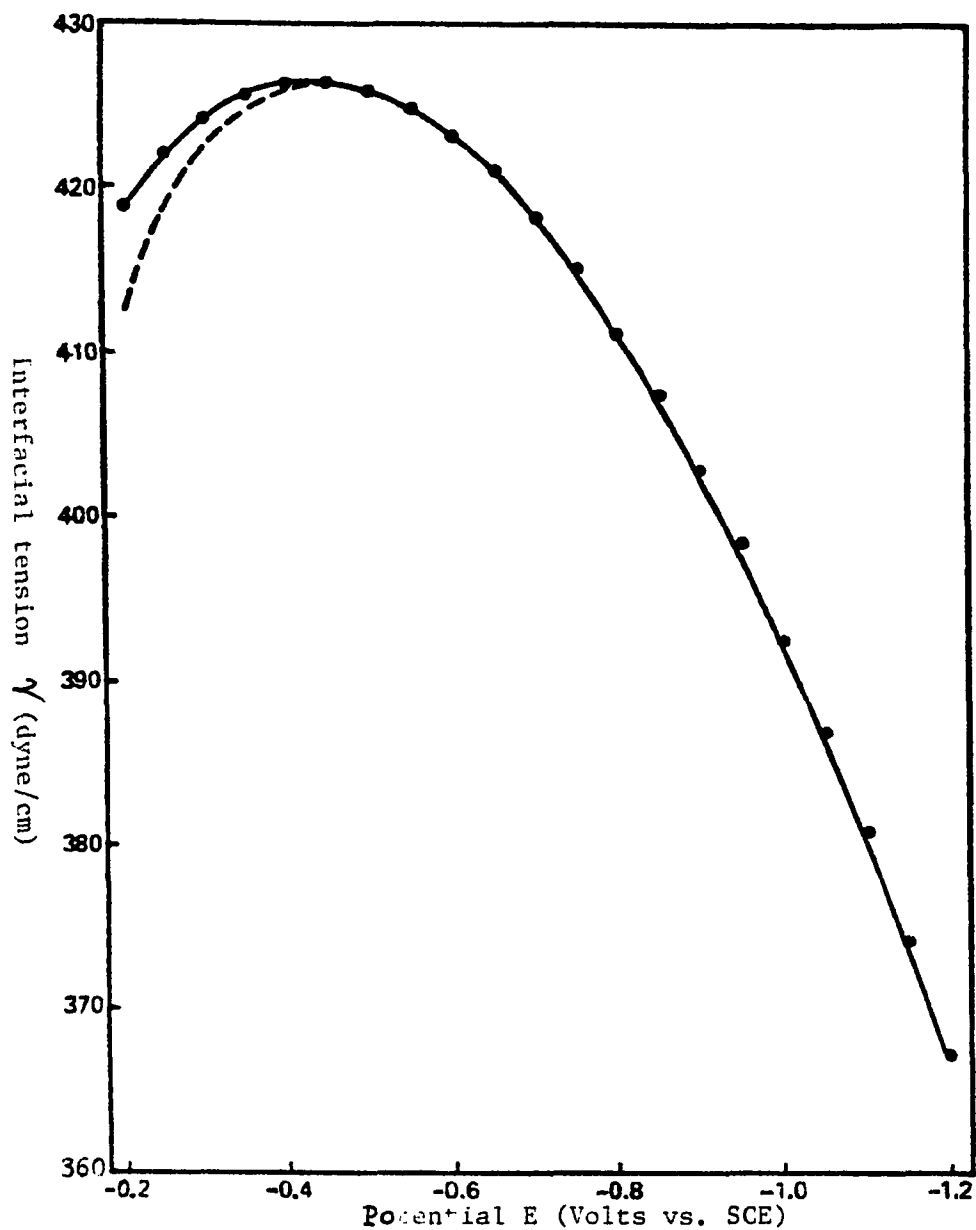


Fig. 7  
 Interfacial tension vs. potential curves for 0.5 M NaF plus 0.01 M  $\text{Na}_2\text{HPO}_4$  buffer pH 8. Solid line (—) is the curve measured by the maximum bubble pressure method (J-shaped capillary); dashed line (---) is the curve measured with the conventional capillary electrometer (vertical, straight capillary). The points (●) are values obtained by double integration of capacitance data.<sup>138</sup>

conventional vertical capillary electrometer, particularly at potentials close to and positive of the ECM. Indeed, the ECM potential measured by the maximum bubble pressure method (-0.433 V) differed significantly from that obtained by the use of the vertical capillary electrometer.

Similarly, comparison of charge vs. potential curves (Fig. 8) obtained by the differentiation of  $\gamma$  vs. potential curves, indicates that there is excellent agreement between data obtained from capacitance and the MBP method. Again, a pronounced deviation of charge data obtained from the vertical capillary electrometer results is noted at or positive of the ECM. Because of the discrepancy between the vertical capillary electrometer results and those obtained by capacitance and MBP method, only the latter two techniques were utilized extensively.

In order to obtain charge values from the electrocapillary data obtained with the MBP method, a set of surface tension data as a function of potential was first fitted to a sixth order polynomial of the type shown in eqn. (33).

$$\gamma = a_1(E-E_M)^2 + a_2(E-E_M)^3 + a_3(E-E_M)^4 + a_4(E-E_M)^5 + a_5(E-E_M)^6 \quad (33)$$

where  $E_M$  is the potential of the electrocapillary maximum (i.e., ECM).

A nonlinear least squares procedure was employed to obtain optimum values of all six parameters (namely,  $a_1$ ,  $a_2$ ,  $a_3$ ,  $a_4$ ,  $a_5$  and  $E_M$ ). The root mean square (RMS) deviation observed over all concentrations for each adsorbate was about  $\pm 0.2$  dyne/cm. The use of polynomials of higher degree did not improve the  $\gamma$  vs. E fit.

Charge (q) vs. potential (E) curves were then obtained by analytical differentiation of the  $\gamma$ , fitted to eqn. (33), with

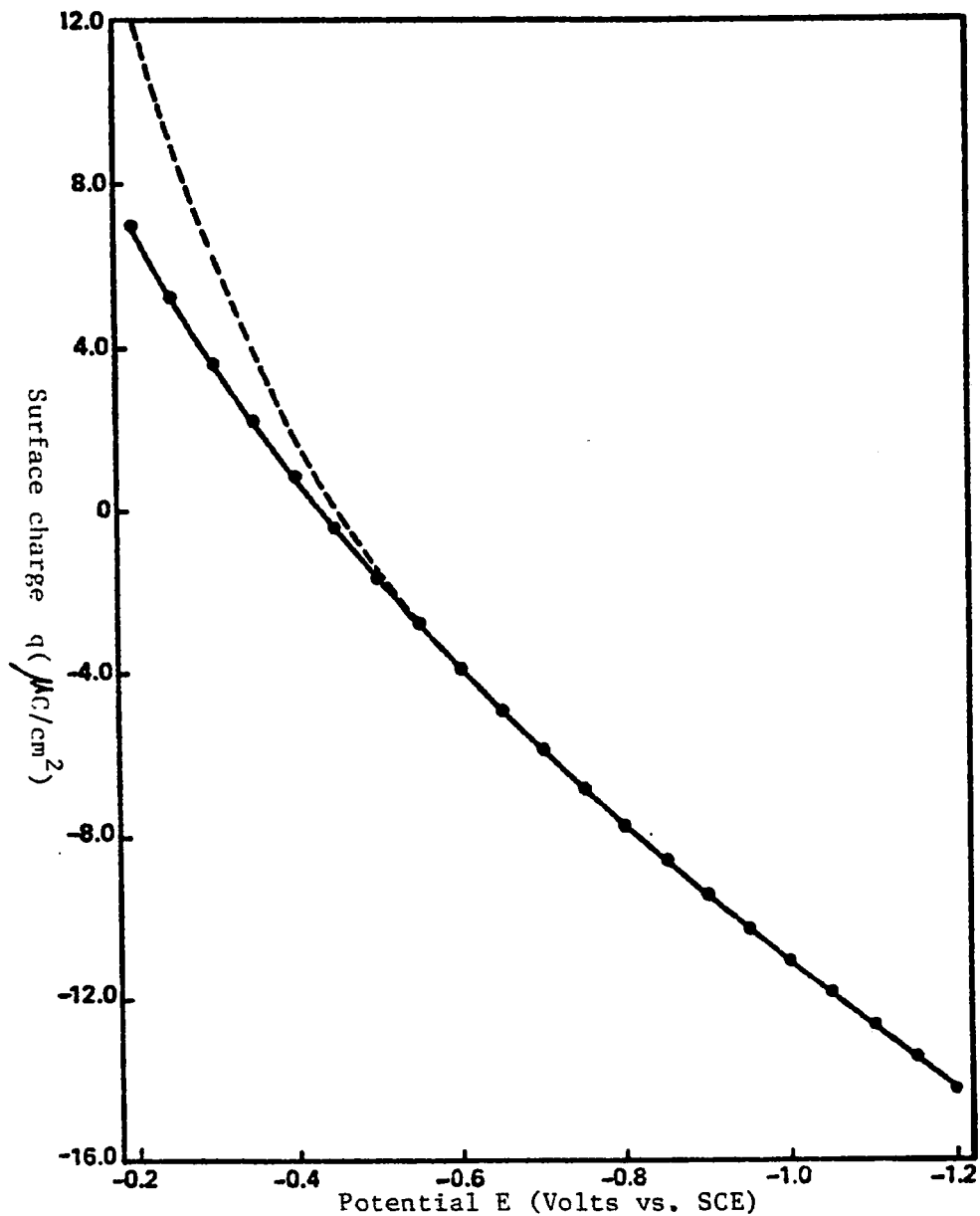


Fig. 8

Charge vs. potential curves for 0.5 M NaF plus 0.01 M Na<sub>2</sub>HPO<sub>4</sub> buffer pH 8. Solid line( — ) is the curve measured by the maximum bubble pressure method(J-shaped capillary); dashed line( --- ) is the curve measured with the conventional capillary electrometer(vertical capillary). The points (●) are values obtained by single integration of capacitance data.<sup>138</sup>

respect to potential, hence

$$q = 2a_1(E-E_M) + 3a_2(E-E_M)^2 + 4a_3(E-E_M)^3 + 5a_4(E-E_M)^4 + 6a_5(E-E_M)^5 \quad (34)$$

Capacitance can be also obtained from the electrocapillary interfacial tension curve by double differentiation of eqn. (33), namely, differentiating eqn. (34) with respect to potential yields eqn. (35).

$$C = \frac{dq}{dE} = 2a_1 + 6a_2(E-E_M) + 12a_3(E-E_M)^2 + 20a_4(E-E_M)^3 + 30a_5(E-E_M)^4 \quad (35)$$

All data treatment to calculate surface tension ( $\gamma$ ), surface charge ( $q$ ) and capacitance from the measured pressure was carried out by a computer program developed by the author in this laboratory (See Appendix).

In Fig. 9, the capacitance values obtained directly from the a.c. polarographic method and those obtained from the double differentiation (i.e., eqn. (35)) of the  $\gamma$  vs.  $E$  curve from the MBP method were compared. There is a good agreement between the two methods, particularly in the potential region of -0.5 V to -1.6 V. The discrepancy in the capacitance values from the two different methods in the extreme potentials is probably due to the inaccuracy in the algebraic expression of surface tension as function of potential, i.e., eqn. (33).

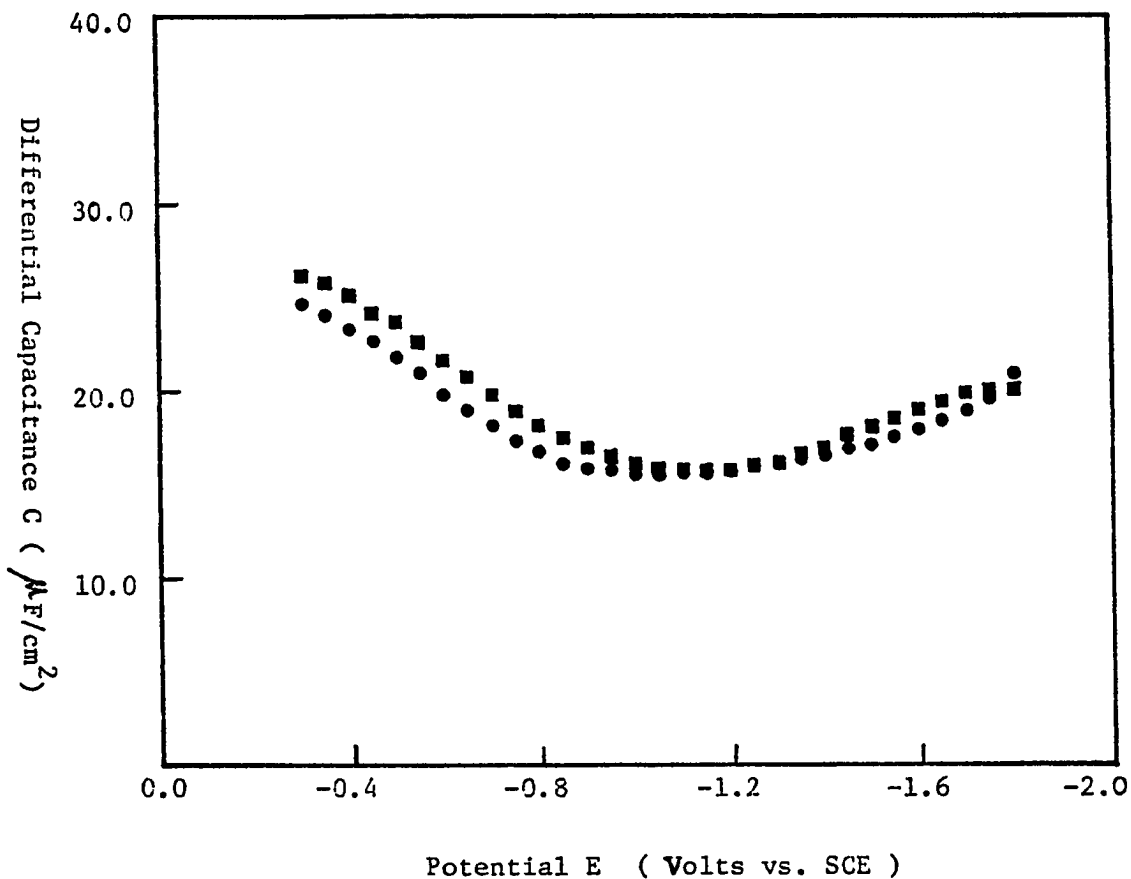


Fig. 9

Differential capacitance vs. potential curve for fluoride pH 8 buffer solution ( 0.5  $\text{M}$  NaF plus 0.01  $\text{M}$   $\text{Na}_2\text{HPO}_4$  ).

- obtained directly from the a.c. polarographic method.
- obtained indirectly by the double differentiation of interfacial tension vs. potential curve obtained from the maximum bubble pressure measurements.

## CHAPTER IV

### EFFECT OF pH ON THE INTERFACIAL BEHAVIOR OF URACIL

Recently, the adsorption behavior of uracil, various uracil derivatives, uridine, uridine-5'-monophosphate and uridine-3-5'-cyclic monophosphate was reported.<sup>138</sup> Basically, it was found that all these uracil derivatives exhibit an initial "dilute" adsorption region where the virtually flat uracil residue is adsorbed flat on the electrode surface, *i.e.*, with the plane of the ring atoms parallel to the electrode surface. However, uracil, 5-methyluracil (thymine) and 1,5-dimethyluracil exhibited a second adsorption region where they rearrange on the surface and adopt a perpendicular orientation. In the perpendicular surface orientation it was proposed that the uracils bind to the electrode surface through the N(3)-H or perhaps N(1)-H functions. However, only a limited number of methylated uracil derivatives were examined in the latter studies. In addition, such studies were restricted to a sodium fluoride (0.5 M), sodium phosphate (0.01 M Na<sub>2</sub>HPO<sub>4</sub>) pH 8.0 supporting electrolyte system.

This report is concerned with the electrosorption and related interfacial behavior of uracil over a wide range of pH. The pH range was selected to permit study of the behavior of the neutral uracil molecules and also the anionic species which forms at high pH.

### Results

Some typical differential capacitance versus potential (C versus E) curves for uracil at pH 3.0, 5.0, 8.0, and 11.0 are presented in Fig. 10. At pH 3, 5 and 8 and uracil concentrations up to about 20 mM there is a general depression of capacitance, compared to the pure background electrolyte solution, between about -0.1 V and -0.7 V followed by a broad adsorption/desorption peak at more negative potentials (Fig. 10A, B, C). At bulk solution uracil concentrations of about 22 mM and above a very sharply defined capacitance pit is noted at pH 3, 5 and 8 centered about -0.55 V. As the uracil concentration increases the depth of the capacitance pit remains unchanged although it systematically becomes wider.

At pH 11.0 the C versus E curves have a considerably altered appearance (Fig. 10D) compared to those observed at pH 8.0 and below. Between about -0.2 V and -0.9 V the capacitance first increases with increasing uracil concentration, then decreases with concomitant formation of a broad adsorption/desorption peak which shifts progressively toward negative potential. The anomalous capacitance pit does not form at pH 11.0 until the concentration of uracil reaches about 65 mM compared to ca. 24 mM at pH 8.0 and below.

The C versus E curves presented in Fig. 10 clearly support the view that there are two regions of adsorption. The "dilute" adsorption region corresponds to concentrations of uracil where a capacitance pit is not observed at any potential. The second, capacitance pit region, corresponds to potentials and concentrations where the capacitance pit is observed.

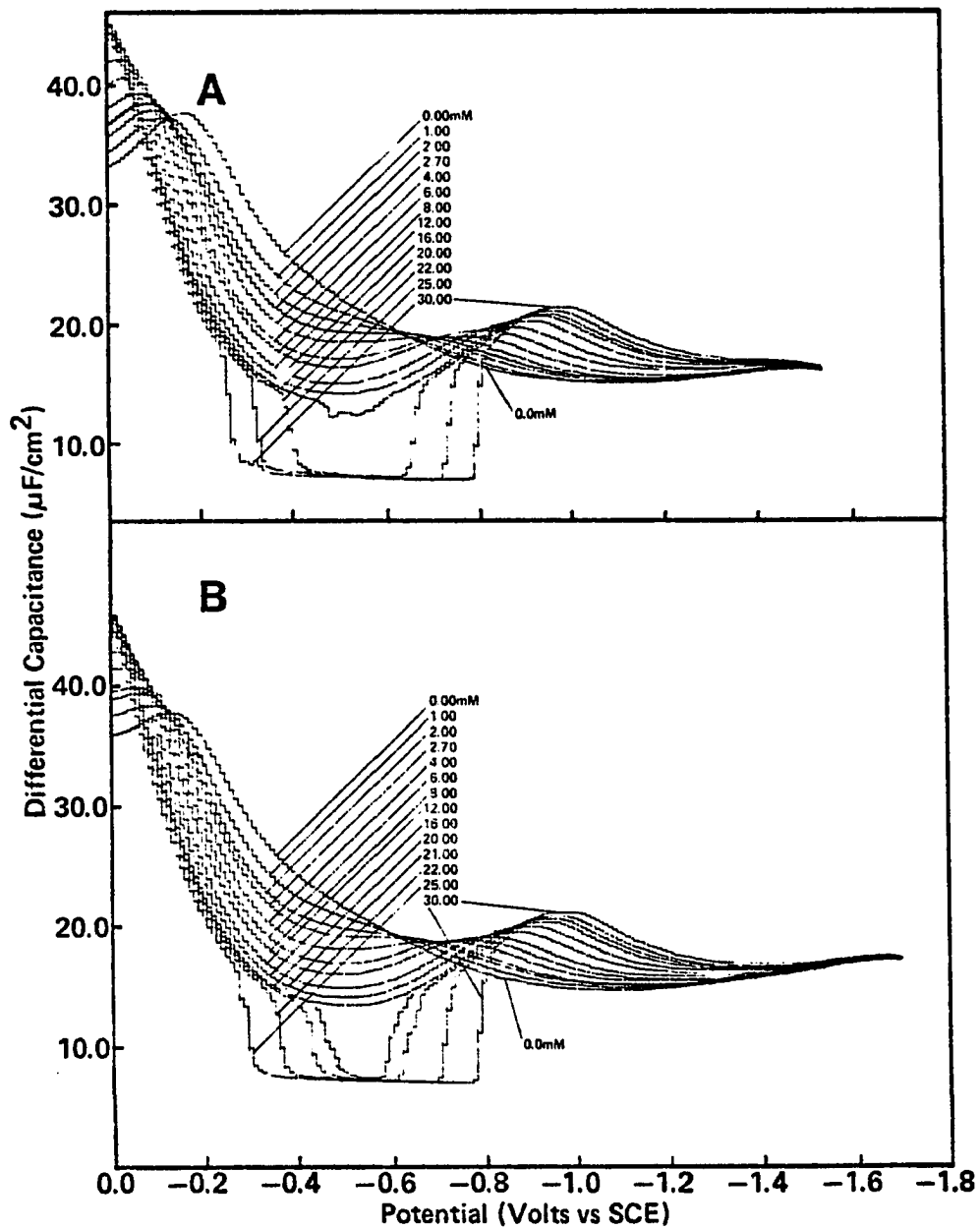
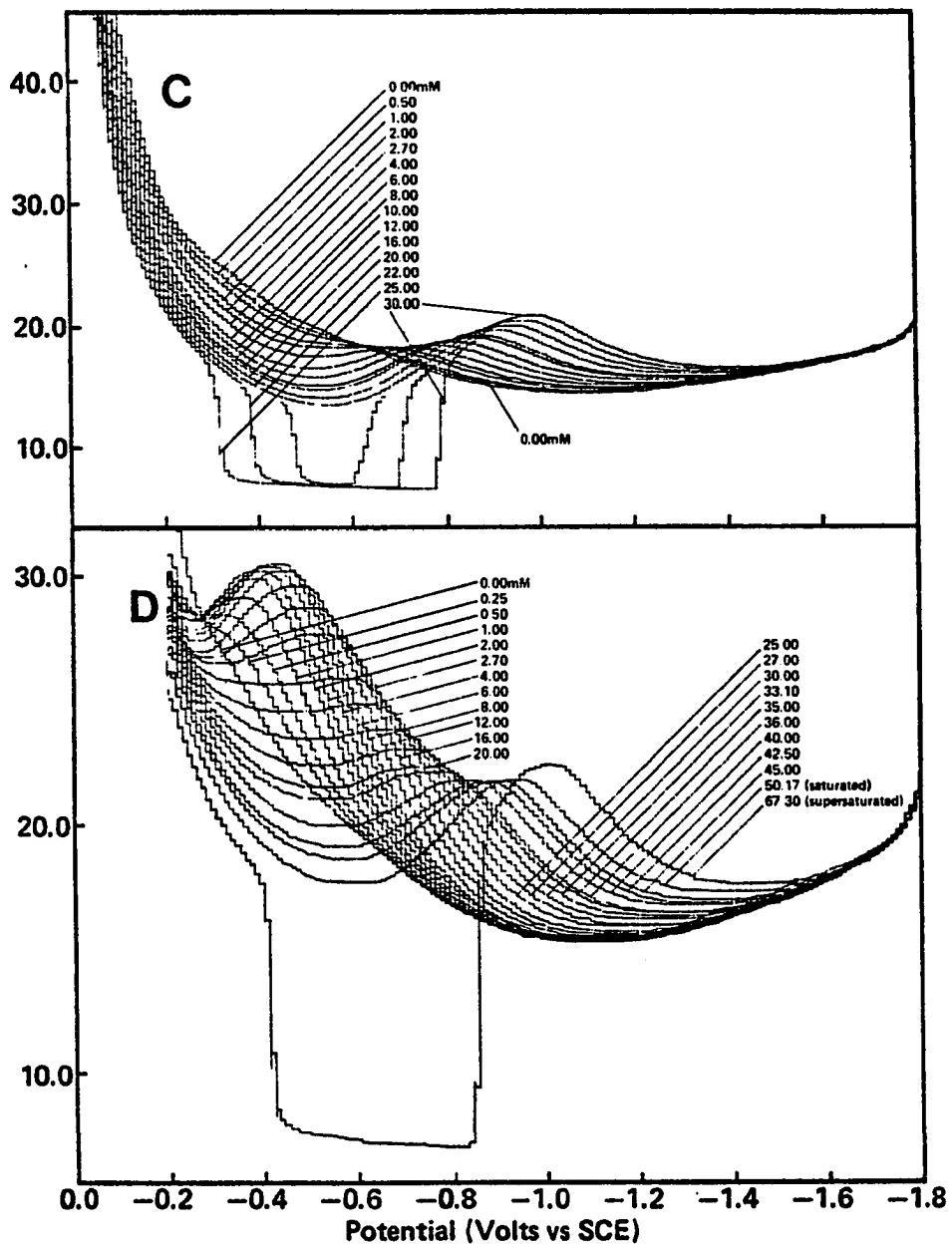


Fig. 10

Differential capacitance versus potential curves for uracil at (A) pH 3.0, (B) pH 5.0, (C) pH 8.0 and (D) pH 11.0 in phosphate buffers having an ionic strength of 0.5M. Curves were obtained at a frequency of 100Hz and an amplitude of 10mV peak-to-peak. Concentrations are shown in the figure.



It may be noted in Fig. 10A-D that all concentrations of uracil give C versus E curves which coincide with the pure background electrolyte curves at very negative potentials. Accordingly, for uracil concentrations corresponding to the dilute adsorption region, the back-integration method of Grahame et al.<sup>128</sup> was used to calculate the charge,  $q$ , and interfacial tension of the mercury-electrolyte interface. The detailed theory and procedures for such calculations are presented in Chapter II.

Interfacial tension data were also measured directly by means of the maximum bubble pressure technique, particularly at potentials and uracil concentrations where the anomalous capacitance pit appeared.

#### Dilute Adsorption Region at pH 3, 5 and 8

In the dilute adsorption region at pH 3, 5 and 8 the interfacial tension results were first used to calculate the surface spreading pressure,  $\pi$ , as a function of uracil activity,  $a$ , and electrode potential,  $E$ , using eqn. (36)

$$\pi(E) = \gamma_w(E) - \gamma(E) \quad (36)$$

where  $\gamma_w$  is the value of  $\gamma$  for the pure background electrolyte solution at  $a=0$ . Concentrations of uracil were taken as equal to activity throughout this study since the concentration was very low.

Plots of surface spreading pressure,  $\pi$ , versus the logarithm of activity of uracil at pH 3, 5 and 8 were superimposable by abscissa translation as shown in Fig. 11A, B, C. The continuous line in these figures represent the best fit of  $\pi$ ,  $a$  and  $E$  data to the empirical equation.

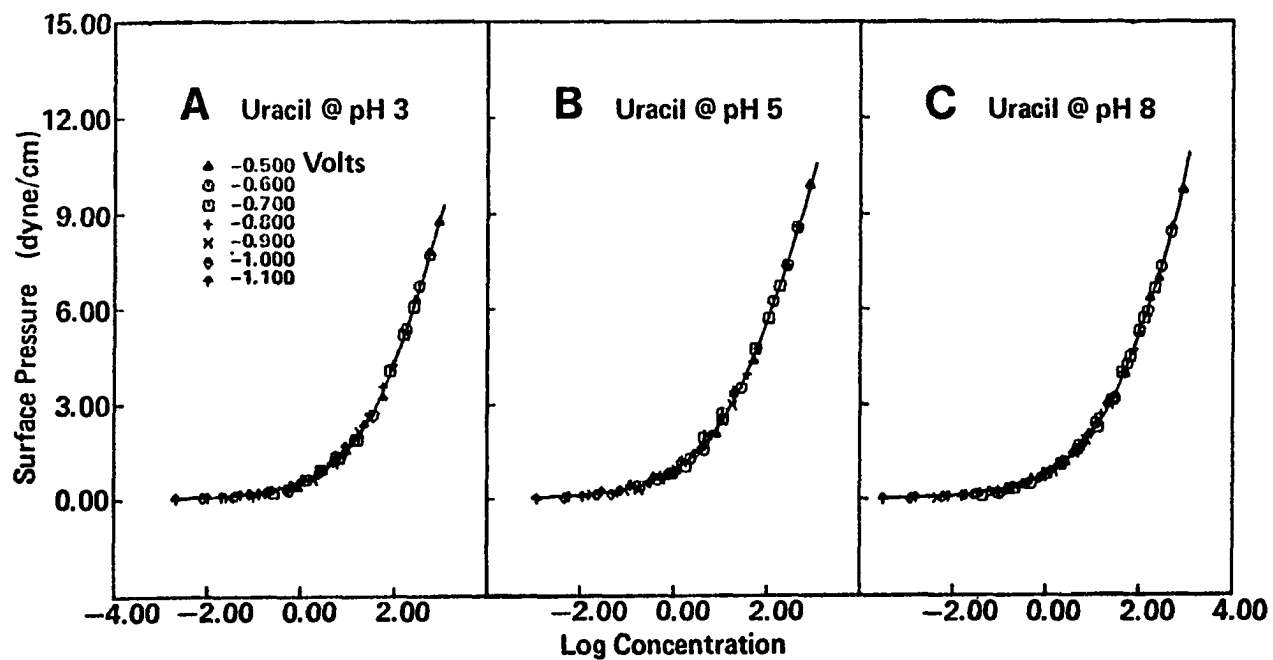


Fig. 11

Composite  $\pi$  versus  $\ln a$  plots for uracil at (A) pH 3.0, (B) pH 5.0 and (C) pH 8.0 in phosphate buffers having an ionic strength of 0.5M. The rms deviation in  $\pi$  from the calculated curve (continuous line) is for (A) 0.10, (B) 0.10, and (C) 0.07 dyne  $\text{cm}^{-1}$ . Data obtained from capacitance results.

$$\pi = A[\ln(1+Ba)] \left[ 1 + \frac{\alpha a}{(1+Ba)^2} + \frac{\beta a^2}{(1+Ba)^3} + \dots \right] \quad (37)$$

This equation is equivalent to the Langmuir equation at sufficiently low concentrations (or if  $\alpha = \beta \dots = 0$ ).  $A$  is equal to  $\Gamma_m RT$ , where  $\Gamma_m$  is the surface excess of uracil at  $\theta = 1$ . Regardless of the values which are determined for  $\alpha$ ,  $\beta$ , ... in eqn. (37),  $d\pi/d\ln a$  approaches  $\Gamma_m RT$  as  $a \rightarrow \infty$ . The parameter  $B$  is dependent on potential, and this adsorption coefficient  $B$  is related to the free energy of the adsorption at each potential by the relationship<sup>179</sup>

$$\Delta G = -RT \ln B \quad (38)$$

If data are to be fitted simultaneously at several different potentials, separate  $B$  values must be inferred at each potential. A non-linear least squares procedure was employed to obtain optimum values of all parameters. In practice, data were fitted initially by assuming  $\alpha = \beta = \dots = 0$ , and the least squares values of  $A$ ,  $B$ , and the root mean square deviation (rmsd) in  $\pi$  are determined. Then, the process is repeated with  $\alpha$  introduced as an additional parameter, and the least squares values of  $\alpha$ ,  $A$ ,  $B$  and rmsd are inferred. If the rmsd is significantly smaller than the rmsd for the previous fit, the process is repeated again, with  $\beta$  included as parameter. In the case of uracil at pH 3, 5 and 8, the composite fit of  $\pi$ ,  $a$  and  $E$  data was obtained with the equation

$$\pi = A \left[ \ln(1+Ba) \right] \left[ 1 + \frac{\alpha a}{(1+Ba)^2} \right] \quad (39)$$

Having obtained a composite fit for  $\pi$  and  $a$  at several different potentials, such as those shown in Fig. 11, the same functional

form of eqn. (37) was used to fit  $\pi$  and a data at individual potentials between -0.3 V and -1.2 V. In view of the fact that very good composite  $\pi$  versus  $\ln a$  plots were obtained (Fig. 11) it was concluded that at all potentials the value of  $\Gamma_m RT$  (A in eqn. (37)) was constant. This constant value of A was used in fitting  $\pi$  and a data at individual potentials. Analytical differentiation of the  $\pi$  versus  $\ln a$  fits of curves at individual potentials was used to calculate values of  $\Gamma RT$  at various concentrations and potentials using the Gibbs adsorption equation (eqn. (40)).

$$\Gamma RT = \frac{d\pi}{d \ln a} \quad (40)$$

Congruence of adsorption isotherms with respect to potential was tested by preparing plots of  $\Gamma RT$ , calculated by differentiation of fixed potential  $\pi$  versus  $\ln a$  curves, versus electrode charge,  $q$ . A representative plot of  $q$  versus  $\Gamma RT$  for uracil at pH 3 is presented in Fig. 12. Similar plots were obtained at pH 5 and 8. Clearly, linear  $q$  versus  $\Gamma RT$  plots are observed over a large range of potentials, which implies that the electrosorption isotherms for uracil between pH 3 and 8 are congruent with respect to potential. The latter condition of congruence prevailed at -0.3 V and at all more negative potentials until total desorption of uracil occurred.

Plots of electrode charge, obtained from a single integration of C versus E data, versus electrode potential for a range of uracil concentrations at pH 3, 5 and 8 exhibited a single, sharp crossing point. Such a plot, obtained for results at pH 3.0, is presented in Fig. 13. Almost identical plots were obtained at pH 5 and 8. At pH 3 the common crossing point occurs at -0.425 V and  $+0.19 \mu\text{C cm}^{-2}$ ,

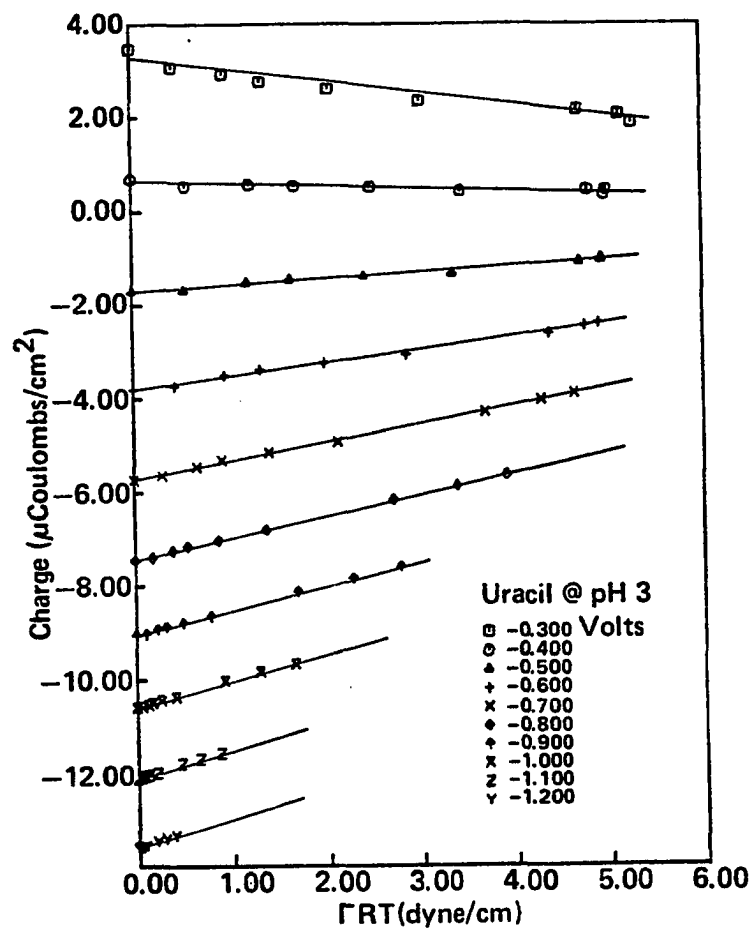


Fig. 12

Test of congruence of the electrosorption isotherms of uracil at pH 3.0 with respect to potential. Supporting electrolyte: phosphate buffer, ionic strength 0.5M. Potential values are indicated in the figure. Data obtained from capacitance results.

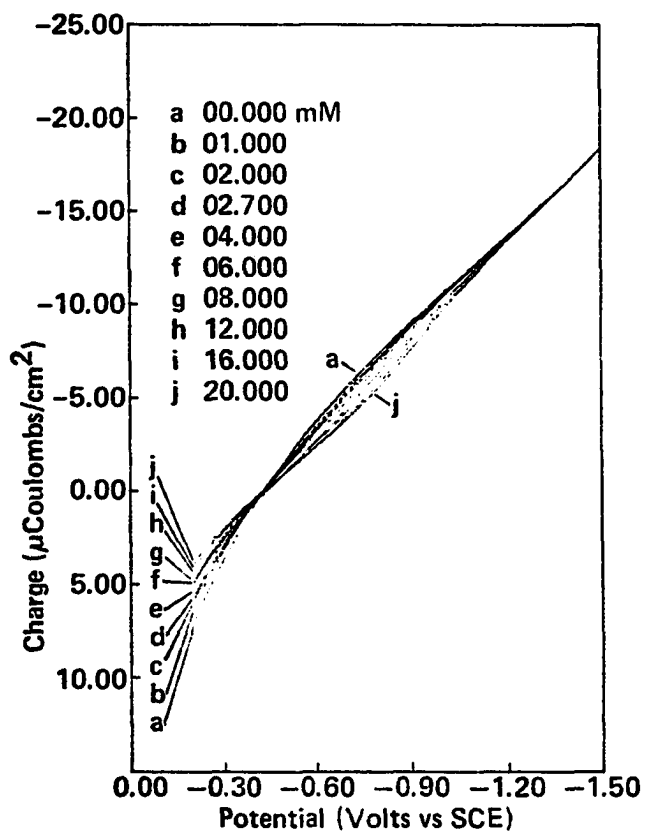


Fig. 13

Charge versus potential plots for uracil in phosphate buffer pH 3.0 having an ionic strength of 0.5M. Concentrations are shown in the figure.

these values corresponding to the potential and charge of maximum adsorption.<sup>89</sup> At pH 5 the potential of maximum adsorption was  $-0.404$  V and the corresponding electrode charge  $+0.83 \mu\text{c cm}^{-2}$ ; the values at pH 8 were  $-0.375$  V and  $+1.48 \mu\text{c cm}^{-2}$ .

In view of the fact that the adsorption isotherms of uracil between pH 3 and 8 were congruent with respect to potential, experimental  $\pi$ , E and  $a$  data were fitted to the generalized form of the Frumkin isotherm equation (eqn. (25)).

$$\frac{\theta}{1-\theta} = B_0 a \exp(2\alpha\theta) \exp\left(-\frac{1}{\Gamma_m RT} [\gamma_w(0) - \gamma_w(E)] + C' E E_N - \frac{C' E^2}{2}\right) \quad (25)$$

The non-linear least squares procedure which was described previously (See Chapter II) was used to fit experimental values of  $\pi$ ,  $a$  and E to equation (25) and to obtain the best values of the five unknown parameters, *i.e.*,  $\alpha$ ,  $B_0$ ,  $\Gamma_m$ ,  $E_N$  and  $C'$ .

The fact that the adsorption of uracil between pH 3 and 8 follows the Frumkin model was tested by preparing the reduced isotherms shown in Fig. 14. The experimental data in Fig. 14 were obtained by analytical differentiation of  $\pi$  versus  $\ln a$  plots. The continuous lines represent the best fits of all  $\pi$ , E and  $a$  data at potentials where the isotherms are congruent with respect to potential. Quite clearly, the experimental points, obtained without assuming any physical adsorption model, are in excellent agreement with the Frumkin isotherm (Fig. 14).

By detailed analysis of  $\pi$ , E and  $a$  data using the Frumkin adsorption equation (eqn. (25)) in the dilute adsorption region for uracil at pH 3, 5 and 8 the results shown in Table 2 were obtained.

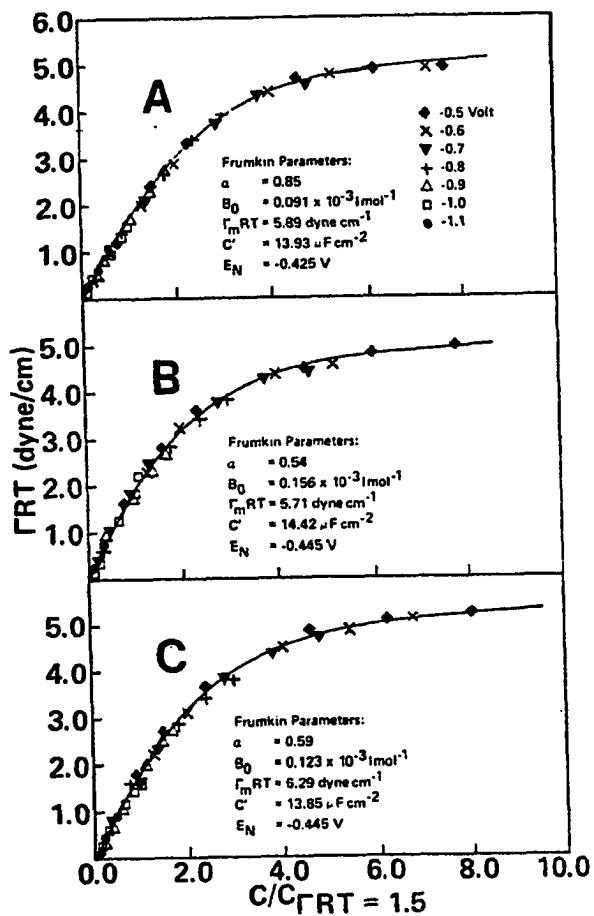


Fig. 14

Reduced adsorption isotherms for uracil at (A) pH 3.0, (B) pH 5.0 and (C) pH 8.0 in phosphate buffers, ionic strength 0.5 M. The solid line is the best fit of all  $\pi$ , E and a data to the generalized Frumkin equation with the values of  $\alpha$ ,  $B_0$ ,  $\Gamma_m RT$ ,  $C'$  and  $E_N$  being shown in the figure. Data obtained from capacitance results.

TABLE 2

Parameters of the generalized Frumkin isotherm for uracil determined from differential capacitance methods at various pH values in the dilute adsorption region.

pH <sup>a</sup>	$\alpha$	$B_0 \times 10^3$ (1 mol <sup>-1</sup> )	$\Delta G^\circ$ <sup>b</sup> (cal)	$C'$ <sup>c</sup> ( $\mu\text{F cm}^{-2}$ )	$E_N$ <sup>d</sup> (Volt vs. SCE)	$\Gamma_m$ (mole cm <sup>-2</sup> $\times 10^{10}$ )	Area per molecule ( $\text{\AA}^2$ )	rmsd <sup>e</sup> in $\pi$ (dyne cm <sup>-1</sup> )
3	0.85±0.06	0.091±0.004	-2673±28	13.93±0.48	-0.425±0.006	2.38±0.11	70±3	0.102
5	0.54±0.08	0.156±0.007	-2991±34	14.42±0.48	-0.445±0.005	2.30±0.13	72±4	0.095
8	0.59±0.05	0.123±0.004	-2851±14	13.85±0.35	-0.445±0.004	2.54±0.09	66±2	0.070
8 <sup>f</sup>	0.45±0.08	0.158±0.005	-2996±21	14.28±0.38	-0.474±0.003	2.60±0.12	64±3	0.156
11 <sup>g</sup>	1.72±0.03	0.007±0.001	-1159±82	12.11±0.54	-0.320±0.027	2.45±0.12	68±3	0.081

<sup>a</sup>Phosphate buffers having an ionic strength of 0.5 M unless otherwise stated.

<sup>b</sup> $\Delta G^\circ = Rt \ln B_0$  is the standard free energy of adsorption for uracil at the ECM potential for the pure supporting electrolyte (-0.430 V at pH 3, -0.429 V at pH 5, -0.427 V at pH 8 and -0.425 V at pH 11).

<sup>c</sup>Capacitance of a monolayer covered electrode.

<sup>d</sup>ECM potential when  $\theta = 1.0$ .

<sup>e</sup>Root mean square deviation.

<sup>f</sup>0.5 M NaF plus 0.01 M HPO<sub>4</sub> pH 8.0; data from reference 138.

<sup>g</sup>Isotherm analyzed as a function of charge rather than potential as at all lower pH values; see text for discussion.

Dilute Adsorption Region at pH 11

By double back-integration of experimental C versus E curves obtained for uracil at pH 11.0, it was possible to obtain interfacial tension,  $\gamma$ , and hence surface spreading pressure,  $\pi$ , data as a function of E and  $a$  as described earlier. However, it was found that plots of  $\pi$  versus  $\ln a$  at different potentials were not superimposable by abscissa translation as was the case at pH 8 and below. Consequently, as recommended by Parson et al.<sup>129,130</sup>  $\pi$  values were computed as a function of  $a$  at various values of electrode charge,  $q$ , rather than at various electrode potentials, i.e.,

$$\pi(q) = \pi_w(q) - \pi(q) \quad (40)$$

A composite fit of  $\pi$  as a function of  $a$  and  $q$  was then obtained using eqn. (37). It should be noted, however, that the term B in eqn. (37) now becomes dependent on  $q$  instead of E. Between electrode charge values of ca.  $-6$  to  $-12 \mu\text{c cm}^{-2}$ ,  $\pi$  versus  $\ln a$  curves were readily superimposable by abscissa translation as shown in Fig. 15. Such plots strongly suggest that the electrosorption isotherms for uracil at pH 11 are congruent with respect to electrode charge rather than with respect to electrode potential. This suggestion was further supported by the fact that plots of electrode potential versus FRT at values of constant charge were linear at electrode charge values of  $-6 \mu\text{c cm}^{-2}$  and more negative (Fig. 16).<sup>138</sup> The FRT values for the latter test were obtained by analytical differentiation of  $\pi$  vs.  $\ln a$  curves obtained at several individual  $q$  values.

It might also be noted that plots of  $q$  vs. E for various concentrations of uracil at pH 11 did not give a common crossing point as

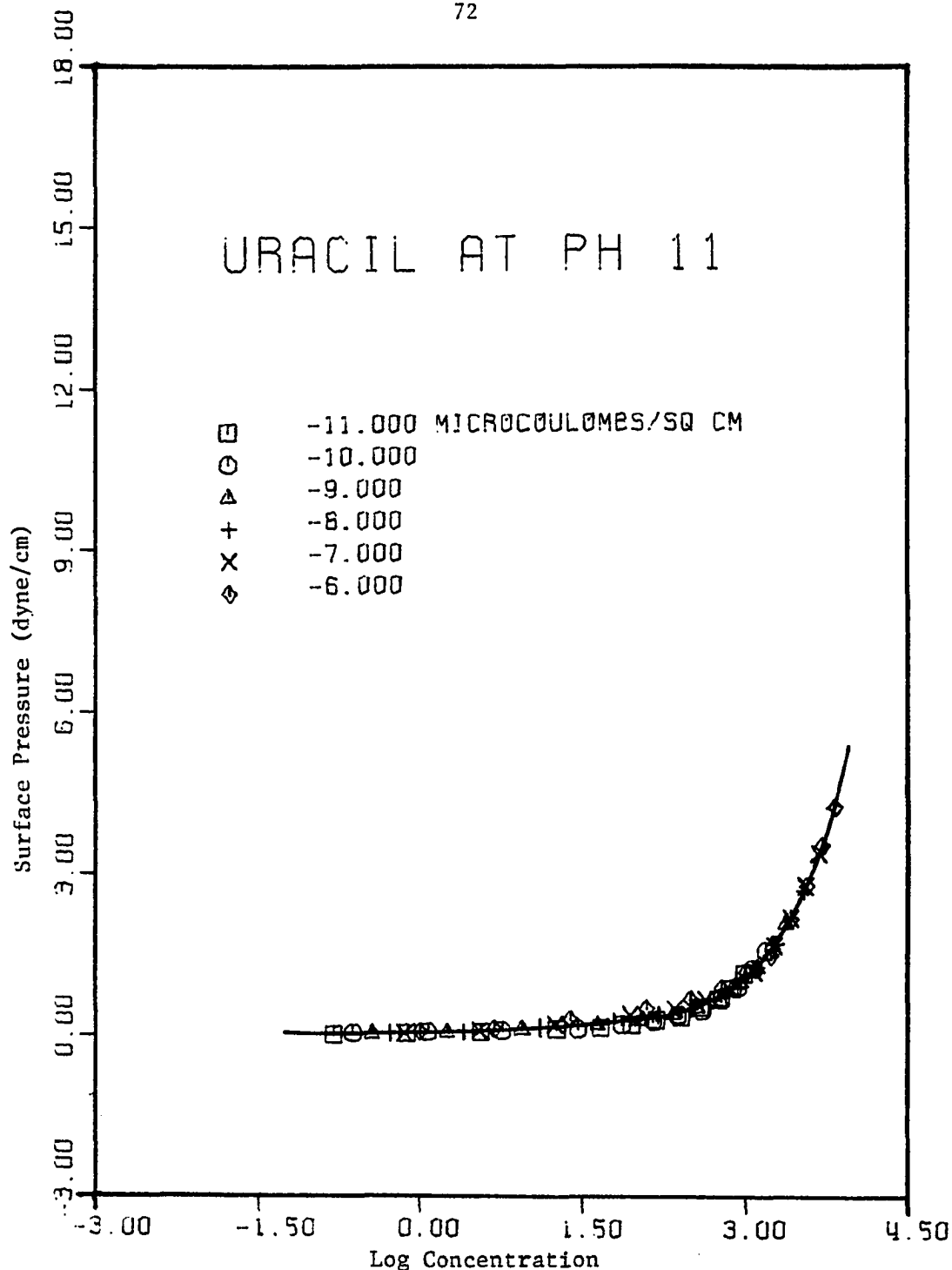


Fig. 15

Composite  $\pi$  versus  $\ln a$  plots for uracil at pH 11.0 in phosphate buffer, ionic strength 0.5 M at various charge values (indicated in the figure). The rms deviation in  $\pi$  from the calculated curve (continuous line) was 0.08 dyne  $\text{cm}^{-1}$ . Data obtained from capacitance results.

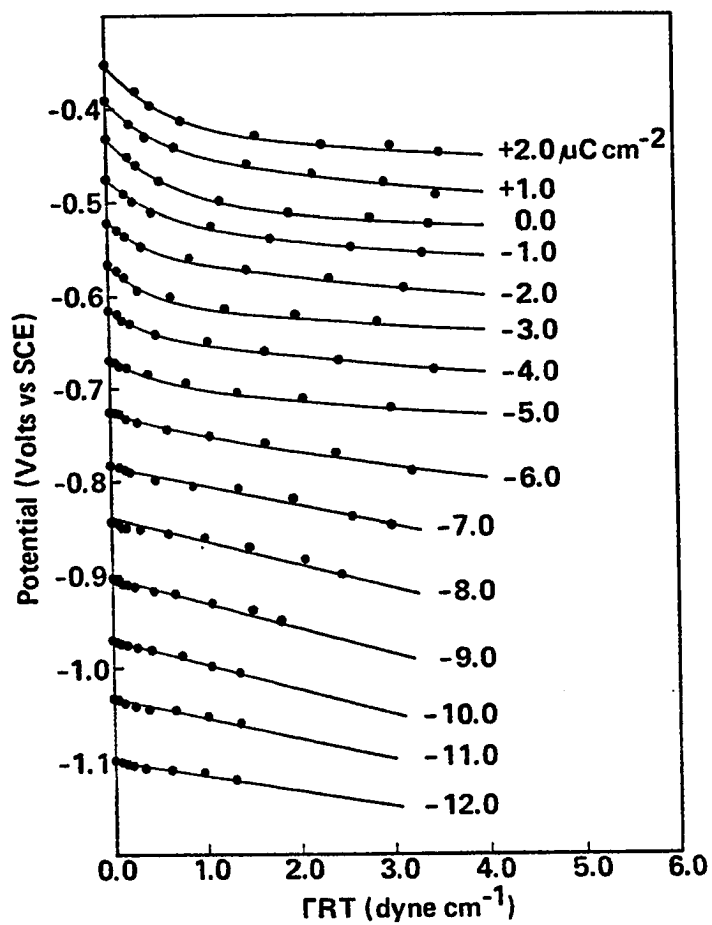


Fig. 16

Test of congruence of electrosorption isotherms with respect to charge for uracil in phosphate buffer pH 11.0, ionic strength 0.5 M. Charge values are indicated in the figure. Data obtained from capacitance results.

was noted at pH 3, 5 and 8 (see for example, Fig. 13). This could indicate that the value of the electrode potential and charge of maximum adsorption lie at potentials more positive than those accessible at the mercury electrode. Alternatively, such behavior could be indicative of a strong chemisorption effect or adsorbate reorientation process occurring at positive electrode potentials and charges.<sup>131</sup>

In view of the fact that the electrosorption of uracil at pH 11 appeared to be congruent with respect to electrode charge rather than electrode potential, analysis of  $\pi$  and a data was carried out as a function of electrode charge. It has been demonstrated<sup>132</sup> that if the adsorption coefficient B is a charge-dependent term that eqn. (41) is valid.

$$E = -\Gamma_m RT \left( \frac{d \ln B}{dq} \right) \theta + E_0 \quad (41)$$

where  $E_0$  is the potential corresponding to a given charge,  $q$ , where  $\theta=0$ . Accordingly,

$$\frac{d \ln B}{dq} = \frac{E_0 - E'}{\Gamma_m RT} \quad (42)$$

where  $E'$  is the value of  $E$  when  $\theta = 1.0$ . In addition,

$$E' = q/C' + E_N \quad (43)$$

if  $C'$  is a constant, independent of a charge.<sup>133</sup> Hence,

$$\frac{d \ln B}{dq} = \frac{E_0 + \left( \frac{q}{C'} - E_N \right)}{\Gamma_m RT} \quad (44)$$

Solving this equation gives eqn. (45):

$$B = B_0 \exp \left\{ \frac{1}{\Gamma_m RT} [(\gamma_w(q=0) - \gamma_w(q)) - \left( \frac{q}{2C'} + E_N \right) q] \right\} \quad (45)$$

where  $B_0$  is the adsorption coefficient at  $q=0$ .

Substituting eqn. (45) into the Frumkin equation (eqn. 6)

$$\frac{\theta}{1-\theta} = B_0 a \exp(2\alpha\theta) \quad (6)$$

gives a generalized form of the Frumkin equation (eqn. (44)) which differs from eqn. (25) principally because

$$\frac{\theta}{1-\theta} = B_0 a \exp(2\alpha\theta) \exp\left\{\frac{1}{\Gamma_m RT} [(\gamma_w(q=0) - \gamma_w(q)) - \left(\frac{q}{2C'} + E_N\right)q]\right\} \quad (46)$$

of the fact that  $B$  is the function of charge rather than potential. A non-linear least squares method very similar to that described previously to solve eqn. (25) was developed to fit  $\pi$ ,  $q$  and a data to obtain values of  $\alpha$ ,  $B_0$ ,  $\Gamma_m$ ,  $E_N$  and  $C'$ . Only  $\pi$  and a data obtained at  $q$  values where the congruence condition prevailed were used in this analysis. The results of such an analysis for the electrosorption of uracil at pH 11 are presented in Table 2. That the electrosorption of uracil at pH 11 is adequately described by the modified form of the Frumkin equation (eqn. (46)) can be seen by reference to Fig. 17. The experimental FRT data in this figure were obtained by analytical differentiation of  $\pi$  versus  $\ln a$  plots at individual charge values. The continuous line represents the best fit of all  $\pi$ ,  $q$  and a data to equation (46) at charge values where the isotherms are congruent with respect to charge. As noted previously, the individual experimental points are obtained without assuming a particular physical adsorption model, and are in reasonable agreement with the Frumkin isotherm.

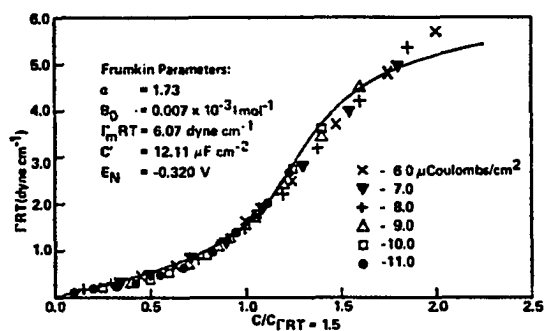


Fig. 17

Reduced adsorption isotherm for uracil in phosphate buffer pH 11.0, ionic strength 0.5 M. The solid line is the best fit of all  $\pi$ , E and a data to the generalized form of the Frumkin equation (eg. 12) with the values of  $\alpha$ ,  $B_0$ ,  $\Gamma_m RT$ ,  $C'$  and  $E_N$  being shown in the figure. Data obtained from capacitance results.

### Capacitance Pit Region

Since there is no simple way to integrate C versus E curves in the capacitance pit region to easily calculate interfacial tension data, it was necessary to measure such data directly using a maximum bubble pressure technique. Uracil solutions at pH 3, 5 and 8 first exhibit the capacitance pit at bulk solution concentrations of about 21 mM, significantly below the saturation limit of this compound, so that values of interfacial tension and hence  $\pi$  could be obtained over a relatively large range of concentrations where the capacitance pit occurs. However, at pH 11 the capacitance pit only appears at uracil concentrations of 65 mM which corresponds to a saturated solution. Accordingly, it was not possible to obtain  $\pi$  values over a sufficiently large range of uracil concentrations to allow determination of  $\Gamma_m$  values at pH 11.

Nevertheless, at pH 3, 5 and 8 plots of  $\pi$  versus  $\ln a$  for uracil at potentials where the capacitance pit could form exhibited a sharp change in slope at concentrations where the capacitance pit occurred (Fig. 18A, B, C). Since the limiting slope of the  $\pi$  versus  $\ln a$  plots in the dilute adsorption region is smaller than that in the capacitance pit region, it may be concluded, from eqn. (40), that the maximum surface excess of uracil in the capacitance pit region is significantly greater than in the dilute region. In other words, assuming monolayer coverage in both adsorption regions, the area occupied by one uracil molecule in the capacitance pit region is considerably less than in the dilute adsorption region, i.e., a more compact film is formed in the capacitance pit region. Values of  $\Gamma_m$  and the electrode

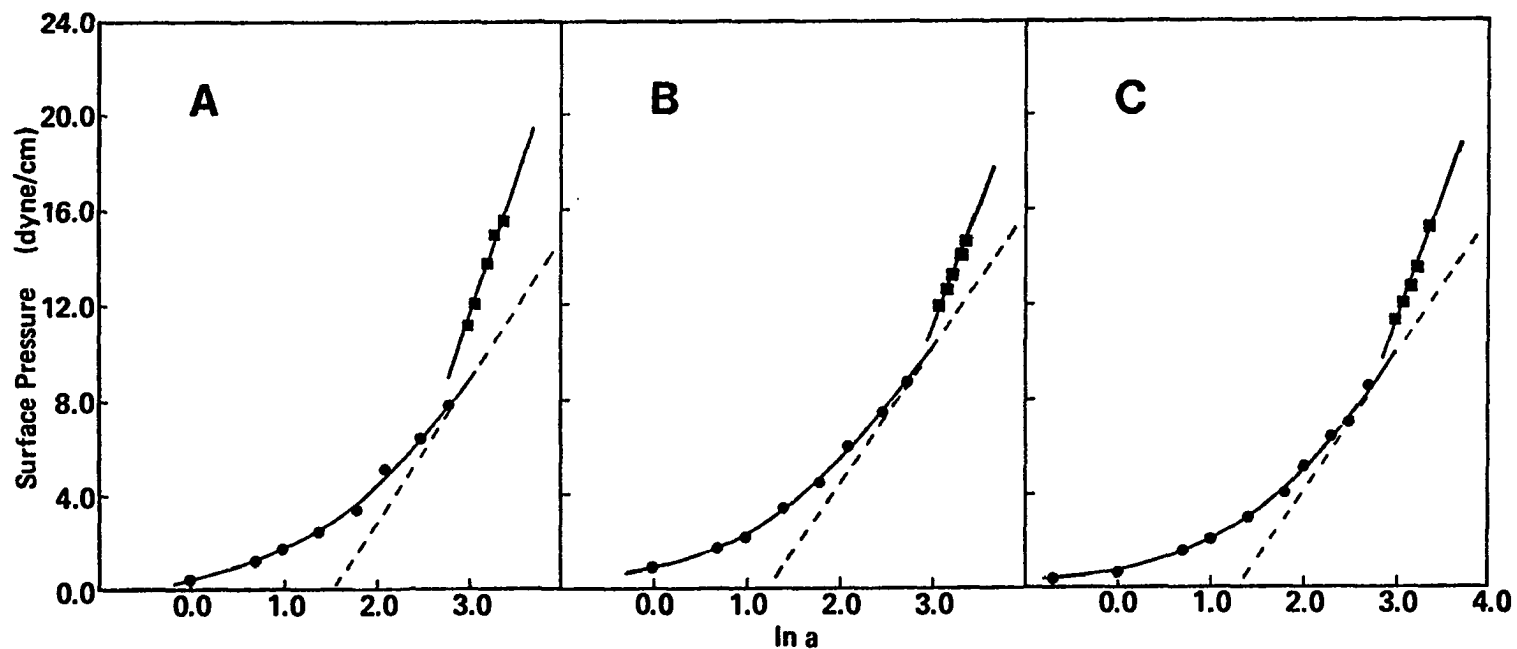


Fig. 18 Surface spreading pressure,  $\pi$ , versus  $\ln a$  plots for uracil at (A) pH 3.0, (B) pH 5.0 and (C) pH 8.0 in phosphate buffers, ionic strength 0.5 M. The solid circles (●) refer to experimental points obtained at -0.5V in the dilute adsorption region; the solid squares (■) refer to experimental points obtained at -0.5V in the capacitance pit region. The line through the solid circles is the best composite  $\pi$  vs.  $\ln a$  fit. Data obtained from the maximum bubble pressure method.

area occupied by a single uracil molecule in the two adsorption regions are presented in Table 3.

At each pH where measurements were possible it is noted that the electrode surface area occupied by uracil decreases by more than 40 per cent on passing from virtual surface saturation in the dilute region to surface saturation in the capacitance pit region.

TABLE 3

Area occupied by one uracil molecule at maximum surface coverage in the dilute and capacitance pit region between pH 3 and 8.

pH	$\Gamma_m$ (mole $\text{cm}^{-2} \times 10^{10}$ )		Area per molecule ( $\text{\AA}^2$ )	
	Dilute adsorption region	Capacitance pit region	Dilute adsorption region	Capacitance pit region
3	2.38±0.11	4.44±0.95	70±3	39±4
5	2.30±0.13	3.99±0.35	72±4	42±4
8	2.54±0.09	4.51±0.85	66±2	37±7
11	2.45±0.12	b	68±3	b

<sup>a</sup>Phosphate buffers, ionic strength 0.5 M.

<sup>b</sup>Insufficient  $\pi$  vs.  $\ln a$  data to allow calculation of  $\Gamma_m$  and an area.

### Discussion of Results

The results reported in Table 2 for the electrosorption of uracil reveal that in the dilute adsorption region the area occupied by one molecule at monolayer surface saturation is  $69 \pm 5 \text{ \AA}^2$  regardless of the pH of the solution and whether uracil exists as a neutral molecule or, at pH 11, as its monoanion ( $pK_a = 9.5$ ).<sup>134,135</sup> The results reported here were all obtained in phosphate buffers maintained at an ionic strength of 0.5 M. Such buffers were utilized because phosphate anions are apparently not specifically adsorbed on the mercury electrode surface in the range of potentials of interest in this study.<sup>136,137</sup> It might be noted that the parameters reported for the electrosorption of uracil at pH 8 in 0.5 M NaF plus 0.01 M  $\text{Na}_2\text{HPO}_4$  pH 8.0<sup>138</sup> (Table 2) are essentially indistinguishable from those observed in this study.

At pH 8 and below the lateral attraction coefficient,  $\alpha$ , is small but positive. Such values indicate, perhaps, a weak intermolecular interaction between adsorbed uracil molecules. However, the rather large, positive value of  $\alpha$  at pH 11, when uracil exists as its monoanion, indicates a relatively strong intermolecular attraction between the adsorbed species. The sigmoidal appearance of the electrosorption isotherm of uracil at pH 11 (Fig. 17) is also characteristic of a relatively strong lateral interaction between surface adsorbed molecules.<sup>139</sup> It is likely that in its anionic state enhanced hydrogen bonding between adjacent uracil molecules or uracil and bridging water molecules occurs hence influencing the value of  $\alpha$ .

The area occupied by one molecule of uracil at monolayer

surface saturation in the dilute adsorption region is essentially independent of pH at  $69 \pm 5 \text{ \AA}^2$  (Table 2). It was reported earlier that the area projected for one uracil molecule adsorbed on the surface in a flat surface orientation, *i.e.*, with the plane of the ring atoms parallel to the electrode surface, was  $53 \text{ \AA}^2$  (Fig. 19).<sup>138</sup> The present results, as well as those of the previous study, thus support the view that the uracil molecules do in fact adopt a flat orientation in the dilute adsorption region with the surface not covered with uracil being covered by water molecules.

Between pH 3 and 8 and at concentrations and potentials where uracil exhibits the anomalous capacitance pit the decrease in area occupied by each molecule to  $39 \pm 3 \text{ \AA}^2$  (Table 3) strongly supports the earlier suggestion<sup>137,138</sup> that the uracil molecules undergo a surface reorientation and adopt a perpendicular stance. It has been suggested that the binding of uracil occurs through the hydrogen at N(3), that is, an interaction resembling hydrogen bonding occurs between uracil and the electrode surface (Fig. 20). It was further suggested<sup>137</sup> that the hydrogen at N(1) could also participate to some extent in binding the perpendicularly adsorbed uracil to the electrode surface. However, the N(1)-H group was thought to be the weaker perpendicular binding site. This conclusion was based on results of studies of several uracil derivatives, in which it was found that if the N(3) position was methylated the uracil molecule could not adopt a perpendicular surface stance (*i.e.*, capacitance pit). However, certain N(1) substituted uracil derivatives could adopt a perpendicular

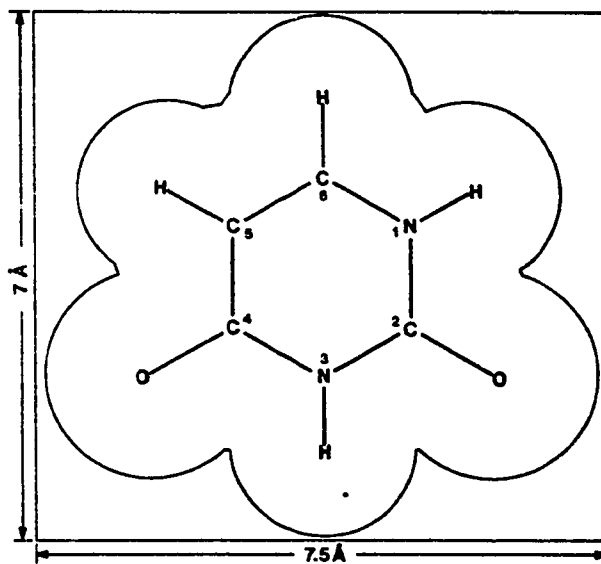


Fig. 19

Real and projected areas of uracil. Van der Waals radii for C, H, N and O used were 1.65 Å, 1.2 Å, 1.5 Å and 1.4 Å, respectively. The area enclosed within the van der Waals radii is  $34 \text{ Å}^2$ . The projected area is  $53 \text{ Å}^2$ .

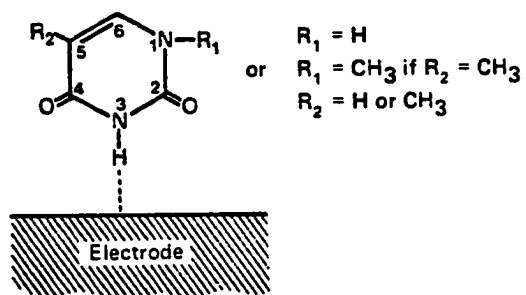
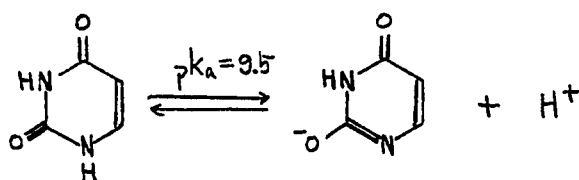


Fig. 20 Possible mode of binding of uracil and its derivatives to the electrode surface when in a perpendicular surface orientation .

surface orientation provided the N(3) position was not substituted. This finding is supported in the present study because, it will be recalled, at pH 11 uracil does exhibit a capacitance pit, albeit at significantly higher concentrations than at pH 8 and below. At pH 11 uracil is dissociated into its monoanionic form.<sup>134,135</sup> According to Shugar and Fox<sup>134</sup> the dissociation of uracil proceeds as shown in eqn. (47). In the monoanion of uracil the hydrogen at N(1) has clearly



been lost yet the capacitance pit still forms. Although it was not possible to quantitatively measure the area occupied by the monoanion of uracil in the capacitance pit region there is no reason to believe that it does not adopt the perpendicular surface orientation.

The standard free energy of adsorption of uracil at the ECM potential for the pure supporting electrolyte in the dilute adsorption region at pH 8 and below is essentially constant at ca. -2900 cal. (Table 2). However, at pH 11 the value of  $\Delta G^\circ$  is -1159 cal. which indicates that the monoanionic form of uracil is significantly less adsorbable.

According to Parsons<sup>140</sup> and Trasetti,<sup>97</sup> for example, the free energy of adsorption may be divided into chemical and electrical components (eqn. (48)).

$$\Delta G_{\text{ads}} = \Delta G_{\text{chem}} + \Delta G_{\text{el}} \quad (48)$$

The electrical component,  $\Delta G_{el}$ , in turn may be expressed as a power series of the electric field strength at the interface X, which can be varied by changing the electrode potential or charge, according to eqn. (49)

$$\Delta G_{el} = aX + bX^2 + \dots \quad (49)$$

hence

$$\Delta G_{ads} = \Delta G_{chem} + aX + bX^2 + \dots \quad (50)$$

The term  $\Delta G_{chem}$  represents the free energy of adsorption component which persists even when the electrical field becomes zero, i.e., at the ECM potential where  $q = 0$ . The term  $\Delta G_{el}$  is composed of a linear electrical field-dependent term which arises from the electrostatic interaction of the charge of an ion or permanent dipole with fixed orientation with the field. The quadratic term in eqn. (50) arises as a result of the interaction of the induced dipole (and hence polarizability) of an ion or molecule with the interfacial electrical field. The implication of eqn. (50), therefore, is that the adsorption of small inorganic ions exhibits  $\Delta G_{ads}$  values which are linearly related to charge or potential,<sup>141,142</sup> whereas larger molecules and organic ions tend to exhibit a quadratic dependence of  $\Delta G_{ads}$  on charge or potential owing to their greater polarizability.<sup>82,89,141,143</sup> Values of  $\Delta G_{ads}$  for the electrosorption of uracil at pH 3, 5 and 8 at various potentials were calculated from the values of B in eqn. (37) (where  $\Delta G_{ads} = -RT \ln B$ ).

Similarly, values of  $\Delta G_{ads}$  at various electrode charge values were obtained from the B values derived by fitting  $\pi$  versus  $\ln a$  data

to eqn. (35) at constant charge values. A curve of  $\Delta G_{\text{ads}}$  versus electrode potential at pH 3 is shown in Fig. 21A which exhibits an approximately quadratic form. Similar curves were observed at pH 5 and 8. Such curves strongly support the view that the electrical component of the interaction of adsorbed neutral uracil molecules is primarily due to the interaction of an induced dipole with the electrical field at the interface. At pH 11 the  $\Delta G_{\text{ads}}$  and electrode charge exhibit a more linear relationship (Fig. 21B) indicating a more pronounced interaction between the charge of the monoanionic uracil species and the interfacial field. The fact that the relationship between  $\Delta G_{\text{ads}}$  and  $q$  shown in Fig. 21B is not perfectly linear, however, supports the view that a contribution from the polarizability of the uracil monoanion and the electric field persists.

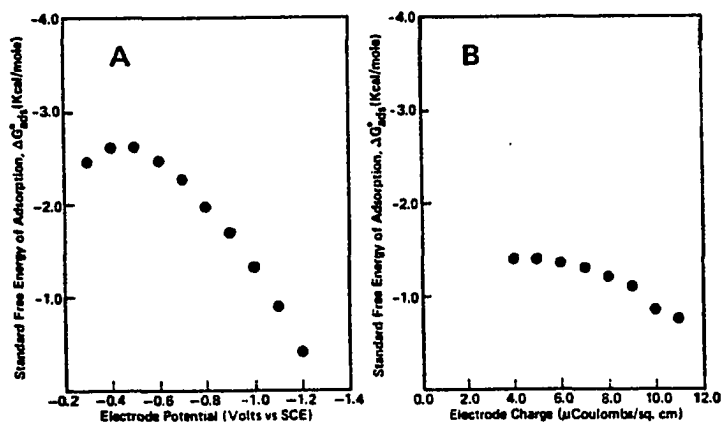


Fig. 21

(A) Free energy of adsorption versus potential curve for uracil in phosphate buffer pH 3.0 and (B) free energy versus electrode charge curve for uracil in phosphate buffer pH 11.0.

## CHAPTER V

### INTERFACIAL BEHAVIOR OF ADENINE AND ITS NUCLEOSIDES AND NUCLEOTIDES

In a recent report from this laboratory<sup>145</sup> the adsorption of adenine, deoxyadenosine and deoxyadenosine mononucleotides at a mercury electrode was described. This study utilized a pH 9.0 borate system and was based on the differential capacitance measurements at a dropping mercury electrode. It was concluded from this work that adenine exhibits two types of adsorption. At a low adenine concentration, over large ranges of potential, it was concluded that this purine base is adsorbed with its virtually planar ring system parallel to the electrode surface, i.e., in a flat surface orientation. This region of adsorption is referred to as the dilute region. At higher adenine concentrations very sharply defined and characteristic pits (namely, a sudden depression) were observed in the capacitance vs. potential (C vs. E) curves. Deoxyadenosine also exhibited a similar capacitance pit although at much more negative potentials than observed with adenine. The cause of these capacitance pits in the case of adenine and deoxyadenosine has not been previously investigated.

Subsequent reports from this laboratory on the interfacial behavior of other purine and pyrimidine derivatives which are important

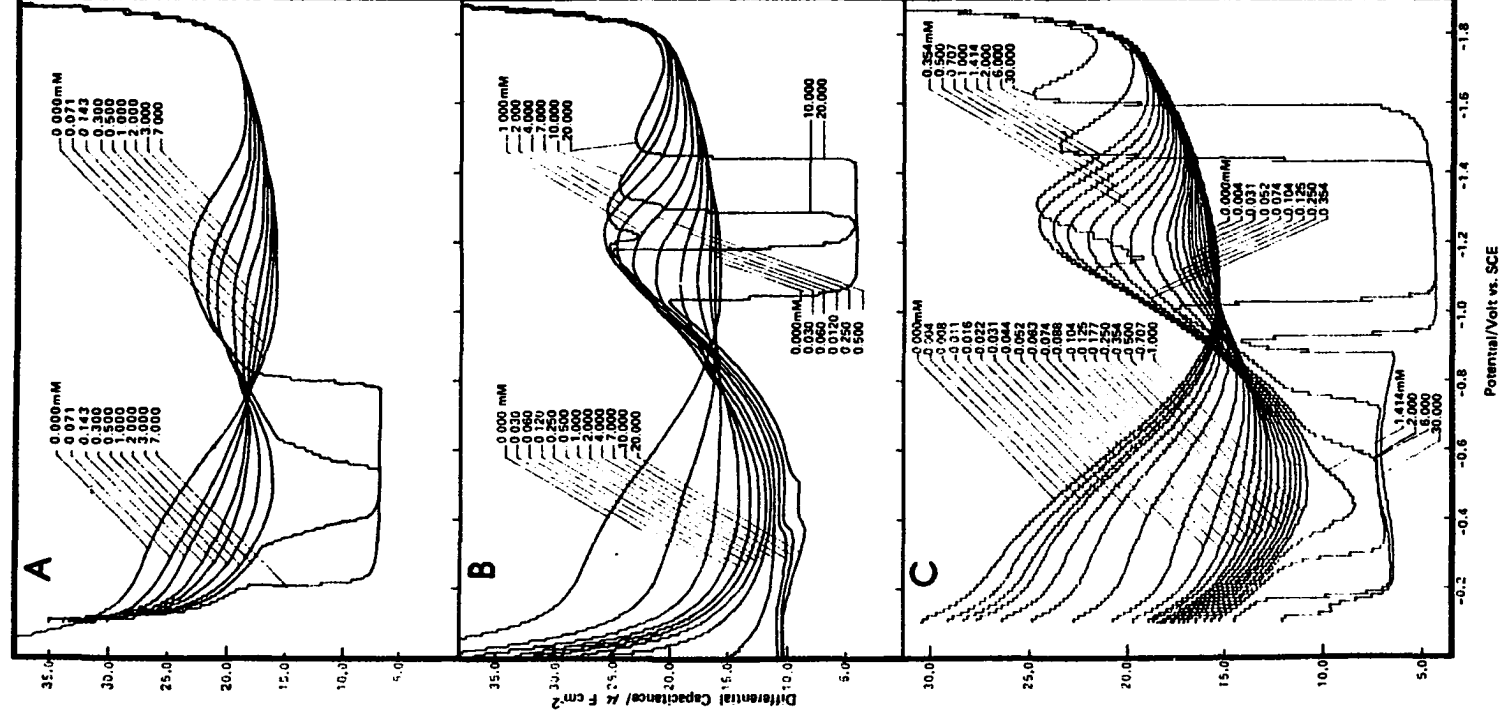
as constituents of nucleic acids such as thymine,<sup>146</sup> uracil<sup>138</sup> and methylated uracil derivatives<sup>138</sup> have utilized a fluoride/phosphate buffer system pH 8.0. The latter buffer system was adopted in such studies because it gives more reproducible and more readily interpretable capacitance results.

This report is concerned with an examination of the interfacial behavior of adenine in fluoride/phosphate buffer pH 8.0 and with the behavior of adenosine and adenosine-5'-monophosphate (AMP). The latter compounds have not previously been studied by quantitative surface electrochemical methods. In order to more clearly understand the nature of the interfacial processes responsible for the capacitance pits of adenine and adenosine, a number of methylated derivatives and AMP were studied by means of differential capacitance and capillary electrometer with the maximum bubble pressure methods.

### Results and Discussion

The methods used for analysis of capacitance results can be understood by reference to Fig. 22A which shows a set of  $C$  vs.  $E$  curves for adenine between  $-0.1$  V and  $-1.9$  V. At adenine concentrations up to about  $2$  mM a systematic decrease of capacitance, compared to that of the pure supporting electrolyte, occurs between about  $-0.15$  V and  $-0.75$  V followed by a broad adsorption/desorption peak at more negative potentials. At adenine concentrations between  $2$ - $3$  mM a very sharply defined capacitance pit occurs centered at  $-0.5$  V. With further increase in adenine concentration the minimum capacitance within the pit remains constant but the range of potentials over which the pit occurs increases.

In the case of adenosine (Fig. 22B) similar behavior is observed with the exception that two capacitance pits are observed. The capacitance pit observed at ca.  $-0.5$  V is rather poorly developed at pH 8.0. However, a recent report by Vetterl<sup>144</sup> using a fluoride/phosphate buffer system but a pH 7.0 shows a very well developed capacitance pit centered at  $-0.4$  to  $-0.5$  V. The second capacitance pit for adenosine is centered at  $-1.25$  V (Fig. 22B). 6-Methyladenosine gives  $C$  vs.  $E$  curves very similar to those of adenosine in that two capacitance pits are formed centered at  $-0.45$  V and  $-1.25$  V (Fig. 22C). However, 6-methyladenosine exhibits only the more positive capacitance pit centered at  $-0.37$  V (Fig. 22D).  $C$  vs.  $E$  curves for AMP gave no evidence of any capacitance pits (Fig. 22E). Thus, in the case of all the compounds except AMP there are quite clearly at least two



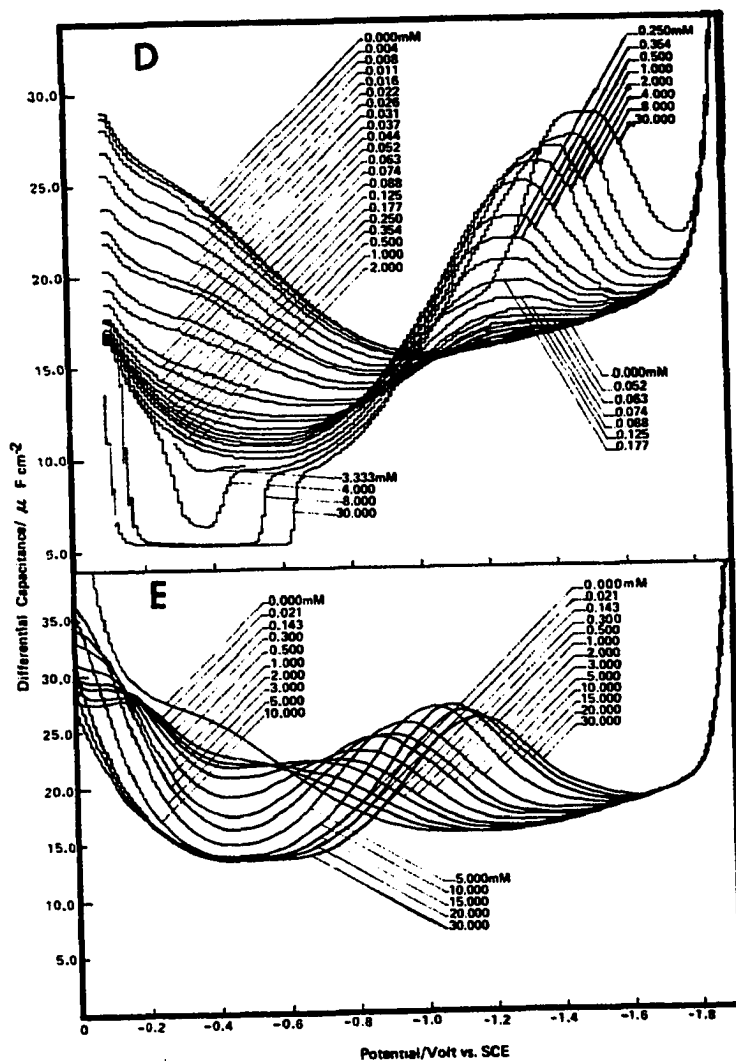


Fig. 22

Differential capacitance vs. potential curves for (A) adenine, (B) adenosine, (C) 6-methyladenosine, (D) 6-dimethyladenosine and (E) adenosine-5'-monophosphate in 0.5 M NaF plus 0.01 M Na<sub>2</sub>HPO<sub>4</sub> buffer pH 8.0. Curves were obtained at a frequency of 100 Hz and an amplitude of 10 mV peak-to-peak. Concentrations are shown in the figure.

regions or types of adsorption. The initial or dilute region corresponds to that range of concentrations and potentials where capacitance pits do not occur. The second or capacitance pit region corresponds to that range of concentrations and potentials where capacitance pits are observed. Quantitative interpretation of capacitance data could not be easily carried out in regions where capacitance pits occur<sup>138</sup> hence detailed analysis of capacitance data was restricted to the dilute adsorption region.

In the dilute adsorption region all adenine derivatives, in both the fluoride/phosphate buffer pH 8.0 and the borate buffer pH 9.0, gave C vs. E curves which were coincident with the curve for pure supporting electrolyte solution at about -1.7 V and more negative potentials. In addition, adenine, adenosine and AMP exhibited both d.c. and a.c. adsorption equilibrium under the experimental conditions used for capacitance measurements. Thus, in the case of the latter three compounds the double back-integration method of Grahame et al.<sup>128</sup> could be used to calculate the excess charge of the mercury electrode using eqn. (51)

$$q - q^* = \int_{E^*}^E C dE \quad (51)$$

where  $q$  is the charge relative to  $q^*$ , the charge at the potential,  $E^*$ , where the integration is commenced (typically  $E^*$  was -1.8 V). The value of the electrocapillary maximum (ECM) potential for the pure background electrolyte solution was measured by the maximum bubble pressure technique (Chapter II) and was found to be -0.433 V in the pH 8.0 NaF/Na<sub>2</sub>HPO<sub>4</sub> buffer and -0.495 V in the pH 9.0 borate buffer.

Since  $q = 0$  at the ECM potential for pure background electrolyte solution it is easy to calculate the absolute charge for the latter solutions at  $E^*$ . At  $E^*$  all  $C$  vs.  $E$  curves were coincident with the background curve; hence it may be concluded that the charge values,  $q^*$ , for all solutions at  $E^*$  are identical.

Thus, the values of  $(q - q^*)$  in eqn. (51) are readily converted to absolute charge values as a function of both potential,  $E$ , and the bulk solution concentration of the adenine derivative. In this study the bulk solution activity,  $a$ , of the adenine derivative was taken to be identical to its concentration. In order to obtain interfacial tension values a further integration was performed (eqn. (52)).

$$\gamma = \gamma_0 - \int_{E=0}^E q \, dE \quad (52)$$

The value of  $\gamma_0$  in eqn. (52), the interfacial tension for the pure background solution at the ECM potential, was obtained directly from maximum bubble pressure measurements. Equation (52) was thus employed to obtain interfacial tension data as a function of both  $E$  and  $a$ . In the case of the methylated adenosine derivatives neither a.c. nor d.c. adsorption equilibrium was established at the mercury electrode and hence the latter methods for calculation of surface charge or interfacial tension could not be used. The adsorption of various adenine derivatives was also studied by direct measurements of interfacial tension using a maximum bubble pressure technique. This technique was used to obtain interfacial tension data in both the dilute and capacitance pit regions of adsorption.

### Dilute Adsorption Region

Analysis of interfacial tension data, obtained by double back-integration of  $C$  vs.  $E$  curves or from maximum bubble pressure measurements, involved first, calculation of surface spreading pressure values,  $\pi$ , as a function of the adenine derivative activity and electrode potential using eqn. (36).

Over quite large ranges of potentials plots of  $\pi$  versus the logarithm of the bulk activity of each adenine derivative were superimposable by abscissa translation. Typical  $\pi$  vs.  $\ln a$  plots for various adenine derivatives are presented in Fig. 23. The calculated curves in Fig. 23 represent the best least squares fit of  $\pi$ ,  $a$  and  $E$  data to the empirical equation (39).

The same non-linear least squares method, which is described in detail in Chapter IV, was employed to obtain optimum values of all parameters in eqn. (39), namely  $A$ ,  $B$ , and  $\alpha$ . Having obtained a composite fit of  $\pi$  and  $a$  data at several different potentials (typically five or six potentials between  $-0.5$  V and  $-1.0$  V) for a particular adenine derivative, the same functional form of eqn. (39) was used to fit data at fixed potentials, typically between  $-0.3$  V and  $-1.2$  V. Because very good composite fits of  $\pi$  vs.  $\ln a$  data were obtained between ca.  $-0.5$  V and  $-1.0$  V (see Fig. 23) it was assumed that at all potentials the value of  $\Gamma_m RT$  ( $A$  in eqn. (39)) was constant. This constant value of  $A$  was used in fitting  $\pi$  and  $a$  data at individual potentials. Analytical differentiation of the  $\pi$  vs.  $\ln a$  fits of curves at individual potentials was used to calculate values of  $\Gamma RT$  at various

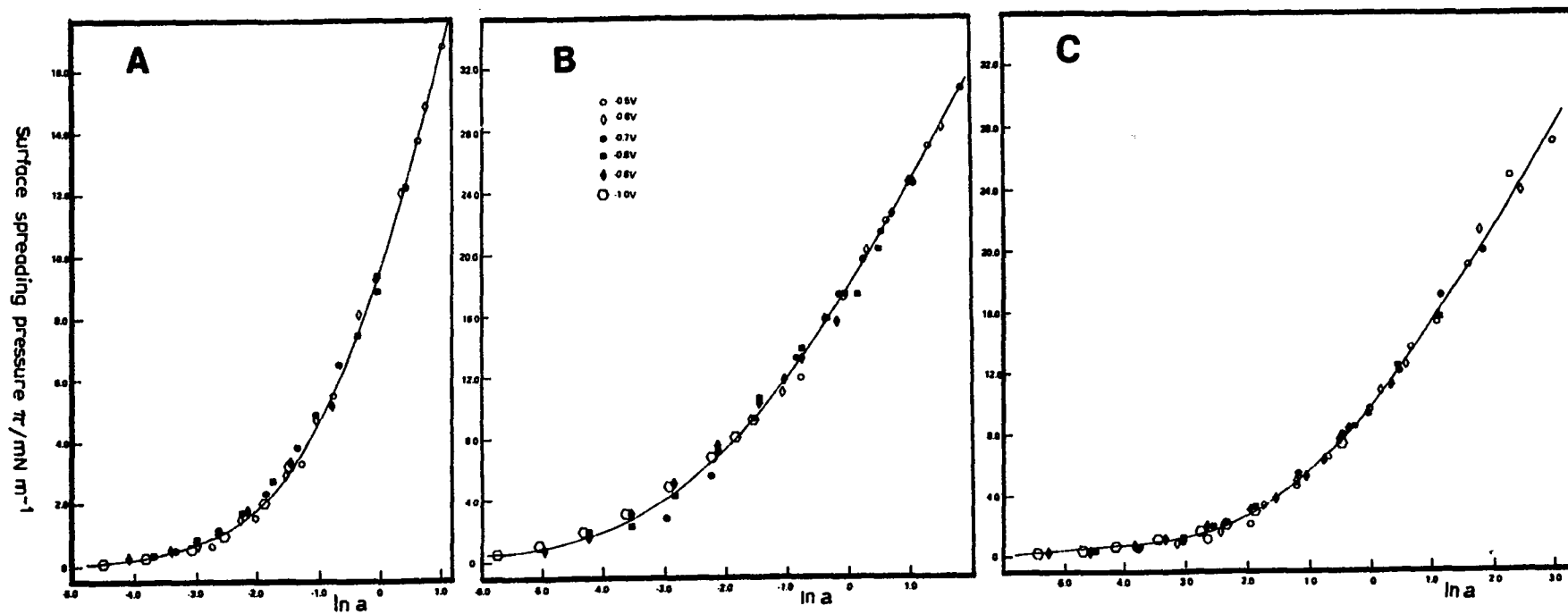


Fig. 23

Composite  $\pi$  vs.  $\ln a$  plots for (A) adenine, (B) adenosine and (C) adenosine 5'-monophosphate in 0.5M NaF plus 0.01M  $\text{Na}_2\text{HPO}_4$  pH 8.0. The root mean square deviation in  $\pi$  from the calculated curve (solid line) is for (A) 0.330, (B) 0.475 and (C) 0.358 dyne  $\text{cm}^{-1}$ . Data for these curves were obtained from capacitance results.

concentrations and potentials using the Gibbs adsorption equation (eqn. (40)). Congruence of electrosorption isotherms with respect to potential for adenine, adenosine and AMP was tested by preparing plots of  $\Gamma_{RT}$  (obtained by analytical differentiation of fixed potential  $\pi$  vs.  $\ln a$  curves) vs. electrode charge,  $q$ .<sup>138</sup> All three compounds gave linear  $q$  vs.  $\Gamma_{RT}$  plots at potentials of  $-0.4$  V and more negative. Such linear plots indicate that the electrosorption isotherms for adenine, adenosine and AMP are congruent with respect to potential over the latter range of potentials.

In view of the congruence of adsorption isotherms with respect to potential for the latter adenine derivatives  $\pi$ ,  $E$  and  $a$  data were fitted to the generalized form of the Frumkin equation (eqn. (25)). The non-linear least squares method, as described in Chapter II, has been used to fit  $\pi$ ,  $E$  and  $a$  data (at potentials where the congruence condition obtains) to eqns. (25) and (5) to obtain the optimum values for the parameters  $\alpha$ ,  $B_o$ ,  $\Gamma_m$ ,  $E_N$ , and  $C'$ . Some typical examples of reduced isotherms for various adenine derivatives are shown in Fig. 24. The experimental  $\Gamma_{RT}$  points in Fig. 24 were obtained by analytical differentiation of  $\pi$  vs.  $\ln a$  plots at individual potentials and hence are obtained without assuming any adsorption model. The solid curves represent the best fits of all  $\pi$ ,  $E$  and  $a$  data to the Frumkin model (eqn. (25)) over the range of potentials where the isotherms are congruent with respect to potential. Clearly the experimental points fit closely to the Frumkin model. The data used to prepare Figs. 23 and 24 were obtained from capacitance measurements. However, essentially identical data were obtained from maximum bubble pressure measurements.

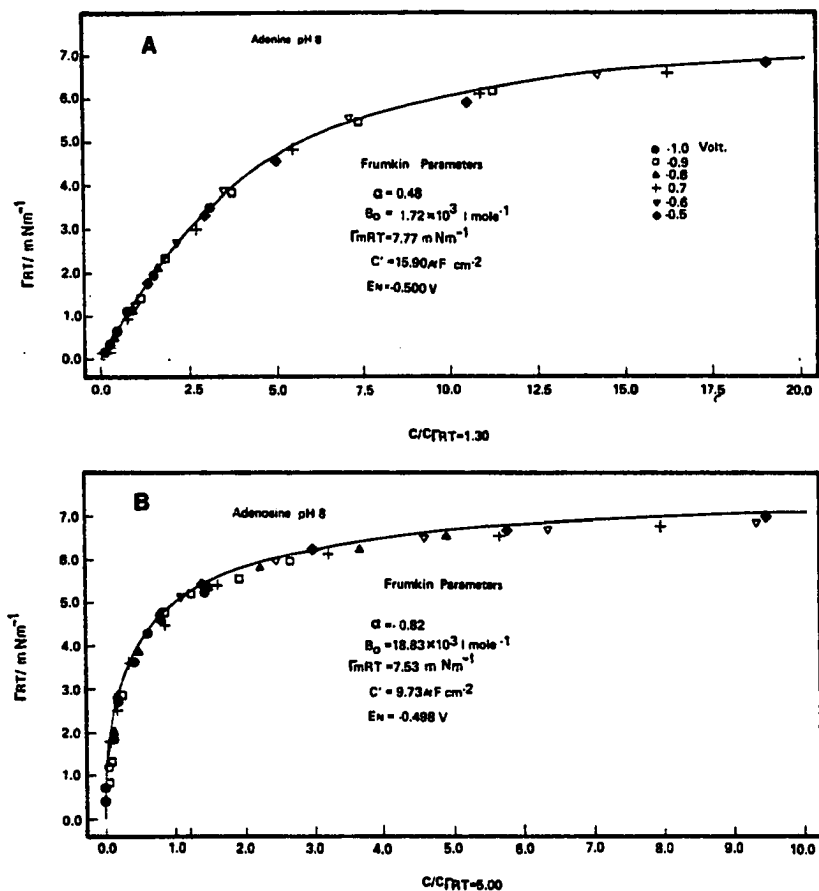


Fig. 24

Reduced electroadsorption isotherms for (A) adenine, (B) adenosine and (C) AMP in 0.5M NaF plus 0.01M  $\text{Na}_2\text{HPO}_4$  buffer pH 8.0. Isotherm (D) is for adenine in borate buffer pH 9.0. The solid line is the best fit of all  $\pi$ , E and a data to the generalized Frumkin equation with the values of  $\alpha$ ,  $B_0$ ,  $\Gamma_m RT$ ,  $C'$  and  $E_N$  being shown in the figure. Data obtained from capacitance results.

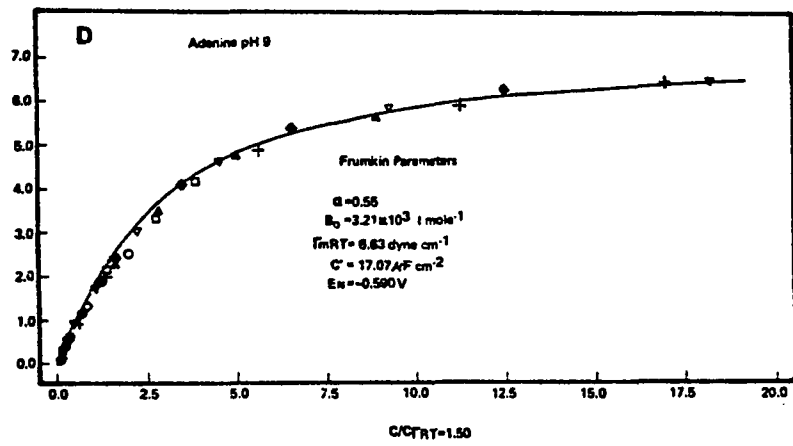
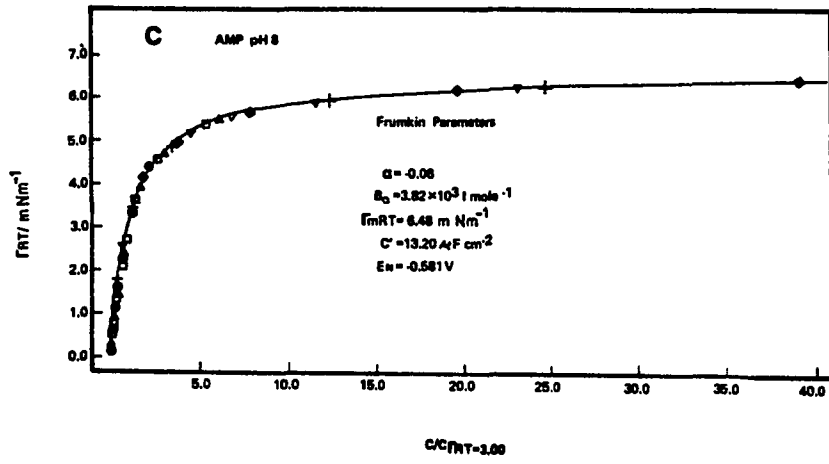


TABLE 4

Parameters of the generalized Frumkin equation for adenine, adenosine and AMP determined by analysis of capacitance and maximum bubble pressure data in the dilute adsorption region

Compound	Method <sup>a</sup>	$\alpha$	$10^{-3} \times B_0 /$ $l \text{ mol}^{-1}$	$\Delta G^{\circ b} /$ $\text{kJ mol}^{-1}$	$C' /$ $\mu\text{F cm}^{-2}$	$E_N^c / \text{V}$	$10^{-10} \Gamma_m /$ $\text{mol cm}^{-2}$	Area per molecule/ $\text{nm}^2$	RMSD <sup>d</sup> in $\pi/\text{Nm}^{-1}$
Adenine/ pH 8.0 <sup>e</sup>	C	$0.48 \pm 0.12$	1.72	-18.5	15.90 <sup>g</sup>	$-0.500 \pm 0.008$	3.14	$0.55 \pm 0.03$	0.33
	MBP	$0.39 \pm 0.20$	1.71	-18.4	15.62	$-0.518 \pm 0.012$	2.92	$0.57 \pm 0.06$	0.30
Adenine/ pH 9.0 <sup>f</sup>	C <sup>h</sup>	$0.54 \pm 0.21$	1.77	-18.5	16.92	$-0.560 \pm 0.10$	3.04	$0.55 \pm 0.04$	0.54
	MBP	$0.55 \pm 0.13$	3.21	-20.0	17.07	$-0.590 \pm 0.01$	2.66	$0.62 \pm 0.04$	0.28
Adenosine/ pH 8.0 <sup>e</sup>	C	$-0.82 \pm 0.23$	18.83	-24.4	9.73	$-0.498 \pm 0.018$	3.04	$0.55 \pm 0.03$	0.48
	MBP	$-0.59 \pm 0.26$	21.24	-24.7	12.56	$-0.504 \pm 0.032$	2.73	$0.61 \pm 0.04$	0.34
AMP/ pH 8.0 <sup>e</sup>	C	$-0.06 \pm 0.13$	3.82	-20.4	13.19	$-0.581 \pm 0.009$	2.62	$0.63 \pm 0.02$	0.36

<sup>a</sup> Results obtained by analysis of (C) capacitance data or (MBP) maximum bubble pressure data.

<sup>b</sup>  $\Delta G^{\circ} = -RT \ln B_0$ . The  $\Delta G^{\circ}$  values are those at the ECM potential for the pure supporting electrolyte.

<sup>c</sup> ECM potential when  $\theta = 1.0$ .

<sup>d</sup> Root mean square deviation.

<sup>e</sup> 0.5 M NaF plus 0.01 M Na<sub>2</sub>HPO<sub>4</sub> pH 8.0.

<sup>f</sup> Borate buffer pH 9.0.

<sup>g</sup>  $C'$  obtained by extrapolating a plot of  $1/C$  vs.  $1/c$  to  $1/c = 0$ , where  $C$  is the capacitance at the potential of maximum adsorption and  $c$  is the concentration.

<sup>h</sup> Capacitance results from ref. 145.

Analysis of  $\pi$ ,  $E$  and  $a$  data for each adenine derivative in the dilute adsorption region using the Frumkin adsorption model gave the results shown in Table 4. These results indicate that the attraction coefficient,  $\alpha$ , is generally small, suggesting that only relatively weak interactions occur between the adsorbed organic molecules. The standard free energy of adsorption values at the ECM potential for the pure supporting electrolyte solution,  $\Delta G^\circ$ , are quite large in magnitude for all adenine species which indicates that at the latter potential, which is quite close to the potential of maximum adsorption, these compounds are quite strongly adsorbed at the mercury electrode. There appears to be no significant difference between the adsorption behavior of adenine in fluoride/phosphate buffer pH 8.0 and borate buffer pH 9.0 (Table 4). The areas occupied by adenine and its nucleoside and nucleotide at complete monolayer coverage are very similar (Table 4). Averaging the results for adenine obtained at both pH 8.0 and pH 9.0, using both capacitance and maximum bubble pressure techniques, the area obtained was  $57 \text{ \AA}^2$ . Very similar values are obtained for adenosine and AMP. The results obtained here for adenine, and its nucleoside and nucleotide at pH 8.0 are in excellent agreement with those obtained for adenine and its deoxynucleoside and monodeoxynucleotide at pH 9.0.<sup>145</sup>

#### Capacitance Pit Region

Surface spreading pressure values,  $\pi$ , could be obtained in both the dilute and capacitance pit adsorption regions for adenine using the maximum bubble pressure technique. In the case of adenosine, 6-methyladenosine and 6-dimethyladenosine the mercury thread exhibited

very severe sticking and rather irreproducible behavior within the fine bore capillary of the maximum bubble pressure apparatus at concentrations and potentials where the capacitance pit occurred. This effect was least severe with adenosine at potentials corresponding to the more negative capacitance pit and some approximate surface spreading pressure results could be obtained in this region. In the case of the methylated adenosine derivatives the sticking effect was too severe to permit even approximate  $\pi$  values to be obtained.

In the case of adenine the capacitance pit is centered at  $-0.5$  V at pH 8.0. Accordingly,  $\pi$  values for increasing bulk solution concentrations of adenine were measured at a fixed potential of  $-0.5$  V. A plot of  $\pi$  vs.  $\ln a$  so obtained is presented in Fig. 25. Essentially identical plots were obtained at potentials between  $-0.4$  V and  $-0.7$  V. It is clear from Fig. 25 that such plots of  $\pi$  vs.  $\ln a$  exhibit a sharp change in slope at concentrations where the capacitance pit is first noted. At high values of  $\pi$  in the dilute adsorption region (Fig. 25) the plot of  $\pi$  vs.  $\ln a$  almost reaches the limiting straight line expected when  $\theta = 1.0$ , *i.e.*, complete monolayer coverage of the electrode. At slightly higher concentrations, where the capacitance pit is formed, a new, steeper straight line is formed. This must imply that the surface monolayer undergoes a rearrangement where the layer in the dilute region reorients to give a second layer also with  $\theta = 1.0$ . The steeper slope of the  $\pi$  vs.  $\ln a$  plot at concentrations where the capacitance pit is observed compared to that for  $\theta = 1.0$  in the dilute adsorption region indicates that  $\Gamma_m$  values are larger in

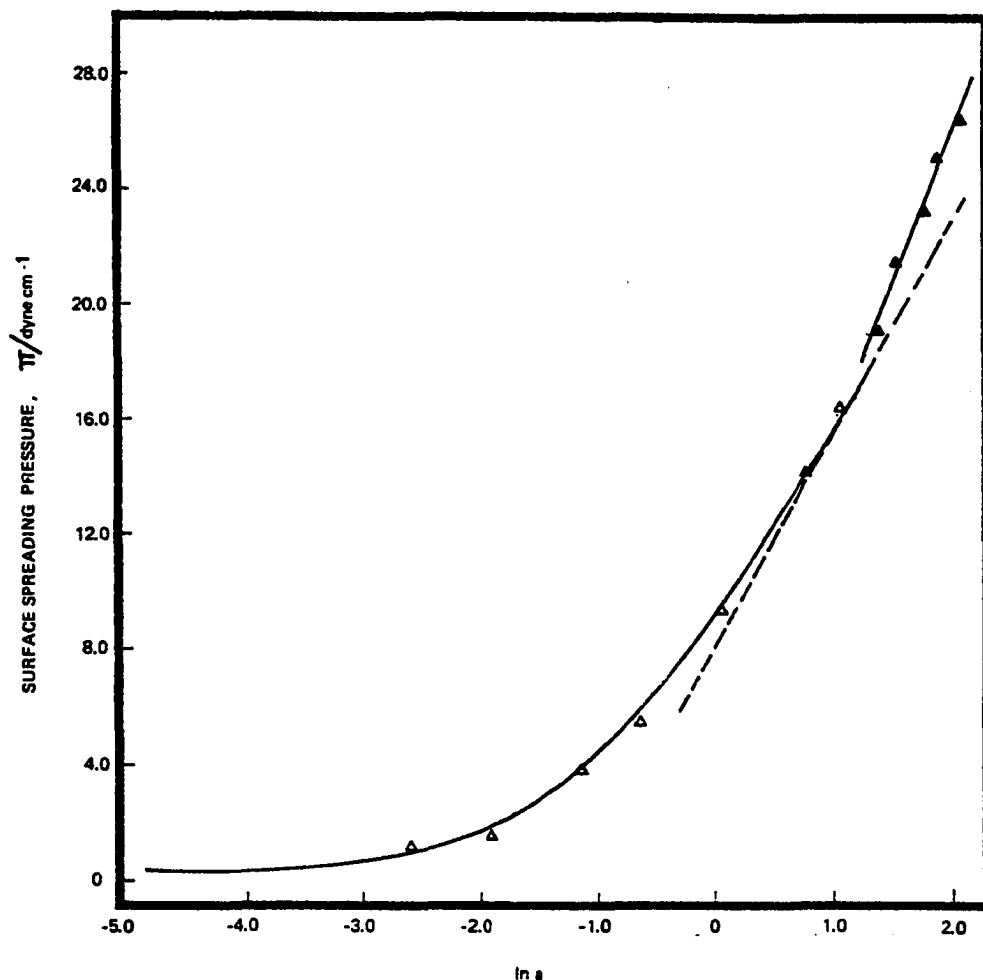


Fig. 25

Surface spreading pressure,  $\pi$ , vs.  $\ln a$  plots for adenine in 0.5M NaF plus 0.01M  $\text{Na}_2\text{HPO}_4$  pH 8.0. Open triangles ( $\Delta$ ) refer to experimental points obtained at -0.5V in the dilute adsorption region; solid triangles ( $\blacktriangle$ ) refer to experimental points obtained at -0.5V at concentrations where the capacitance pit is observed. The solid line through open triangles is the best least squares fit of all data in the dilute adsorption region at potentials where congruence with respect to potential obtains. The line through the solid triangles is the best straight line through points obtained at all potentials where the capacitance pit is observed.

the former region than in the dilute region. This in turn implies that in the capacitance pit region the area occupied by one molecule of adenine on the electrode surface is smaller than in the dilute region; i.e., a more compact monolayer is formed in the capacitance pit region. A summary of some typical results for adenine in both the dilute and capacitance pit adsorption regions at pH 8.0 and 9.0 are presented in Table 4. It can be observed that the area occupied by one adenine molecule on the electrode surface at monolayer saturation in the capacitance pit region is about 30 per cent less than in the dilute adsorption region. Thus, at bulk solution concentrations and potentials where the capacitance pit occurs, adenine must undergo a surface reorientation such that the area occupied per molecule decreases from about  $60 \text{ \AA}^2$  to about  $40 \text{ \AA}^2$ .

In the case of adenosine maximum bubble pressure readings at potentials corresponding to the ill-formed capacitance pit at around  $-0.5 \text{ V}$  were not possible due to severe and irreproducible sticking of the mercury thread in the fine bore capillary. At potentials corresponding to the more negative capacitance pit again rather irreproducible results were obtained. However, in the region of the latter pit sticking of the mercury thread was less severe with the result that some approximate  $\pi$  values could be obtained. The slope of the  $\pi$  vs.  $\ln$  a plot in the capacitance pit region appeared to be slightly steeper than the limiting slope observed in the dilute adsorption region. However, because of the uncertainty in the measured  $\pi$  values at concentrations and potentials corresponding to the capacitance pit region it was only possible to

approximate the area occupied by one adenosine molecule in the latter region at ca. 45-55 Å<sup>2</sup>.

Attempts to obtain  $\pi$  vs. ln a plots for 6-methyladenosine and 6-dimethyladenosine also could not be obtained because of very severe sticking of the mercury thread inside the capillary of the maximum bubble pressure apparatus.

Surface Orientations

## Adenine

The electrode surface area occupied by one adenine molecule in the dilute adsorption region is, on average,  $57 \text{ \AA}^2$ . Using data obtained for the crystal structure of adenine<sup>147</sup> we have calculated the areas which would be occupied by one adenine molecule in a variety of surface orientations using the ORTEP programs of Johnson.<sup>148</sup> Such calculations reveal that the largest area which adenine could occupy corresponds to that if it were to lie flat on the electrode surface, i.e., with the plane of the ring atoms parallel to the electrode surface. In the latter surface orientation the area enclosed within the van der Waals radii of the peripheral atoms of adenine is about  $52 \text{ \AA}^2$  (Fig. 26A). However, it would probably not be possible to pack the irregularly-shaped adenine molecules together in a surface monolayer such that they would each occupy only  $52 \text{ \AA}^2$ . Accordingly, the area expected to be occupied by one adenine molecule lying flat on the electrode surface is shown in Fig. 26A enclosed by the rectangular box, i.e.,  $62 \text{ \AA}^2$ . This projected area corresponds quite closely to that observed experimentally for adenine in the dilute adsorption region. Thus, it has been concluded that in the latter region adenine adopts a flat surface orientation on the electrode surface. Any electrode surface not covered with adenine molecules is probably covered with adsorbed water molecules.

As noted earlier, the fact that the area occupied by one adenine molecule decreases significantly on passing from the dilute to capacitance pit adsorption regions suggests that the molecule reorients to a more

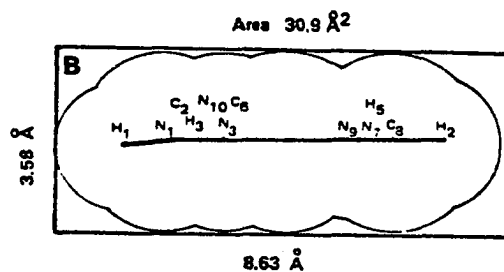
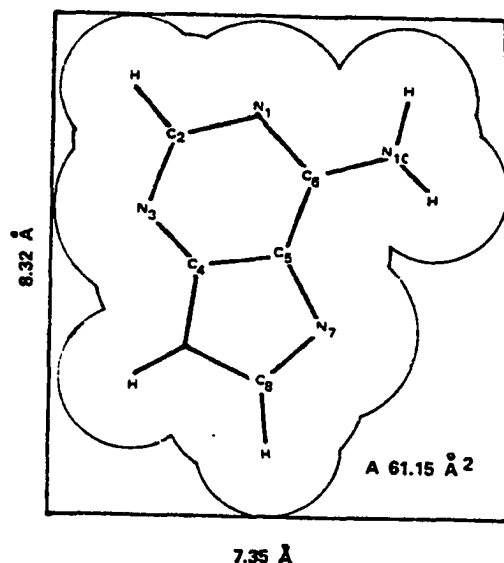


Fig. 26

Projected areas for adenine. (A) When average plane of ring atoms is parallel to the electrode surface, *i.e.*, in a flat surface orientation. Area within van der Waals radii is *ca.* 52Å; area within rectangle with sides 7.3Å and 8.32Å is 61.15Å<sup>2</sup>. (B) When plane of atoms is perpendicular to the electrode surface and surface binding is through the exocyclic amino group hydrogens. Area within rectangle of sides 3.58Å and 8.63Å is 30.9Å<sup>2</sup>. Van der Waals radii employed were C: 1.65Å, H: 1.2Å, N: 1.5Å.

compact surface stance. This may only be achieved if the adenine molecule adopts a perpendicular surface orientation. The actual surface orientation may be deduced from the fact that 6-methyl- and 6-dimethyladenine do not exhibit any capacitance pits, i.e., perpendicular orientation.<sup>110</sup> This implies, therefore, that unsubstituted adenine is bound to the electrode through its exocyclic amino group. The latter group of adenine is the site for Watson-Crick hydrogen bonding to uracil or thymine in RNA or DNA, respectively. It is proposed that a similar hydrogen bonding of adenine to the mercury electrode occurs when adenine adopts its perpendicular stance in the capacitance pit region. This perpendicular orientation is shown in Fig. 27A. Such an orientation is supported by the fact that the potential at which the capacitance pit is first observed, i.e., the optimum potential for formation of the perpendicular layer is -0.50 V. At this potential the electrode carries a small negative charge conducive to formation of a hydrogen bond with the exocyclic amino group of adenine. The projected area which should be occupied by adenine in the surface orientation shown in Fig. 27A is  $31 \text{ \AA}^2$  (Fig. 26B). This is in quite reasonable agreement with the experimentally measured area (Table 5). When in the perpendicular surface orientation of the type shown in Fig. 27A adjacent adenine bases would be sufficiently close together to undergo highly cooperative base-base stacking interactions much as such bases stack in double helical nucleic acids. In view of the fact that neither 6-methyladenine nor 6-dimethyladenine exhibit a capacitance pit, it may be concluded that both of the amino

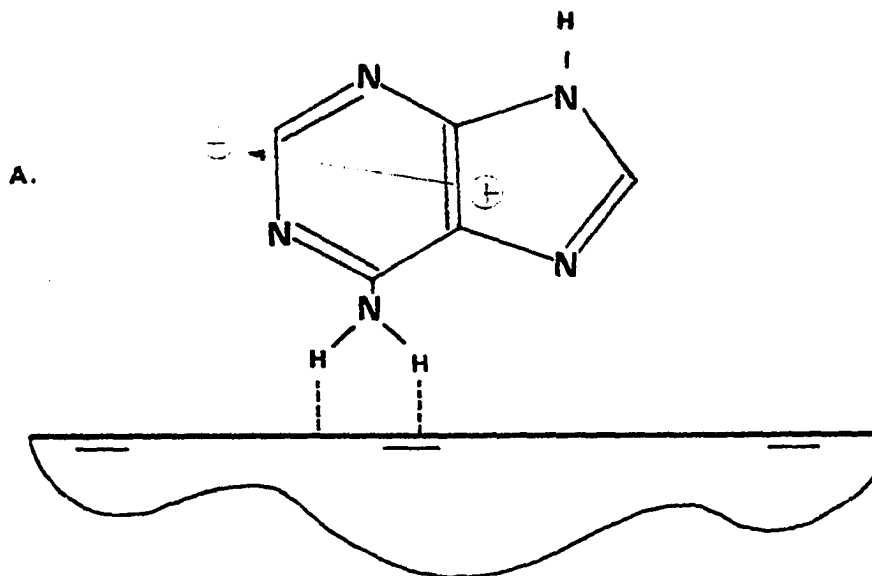
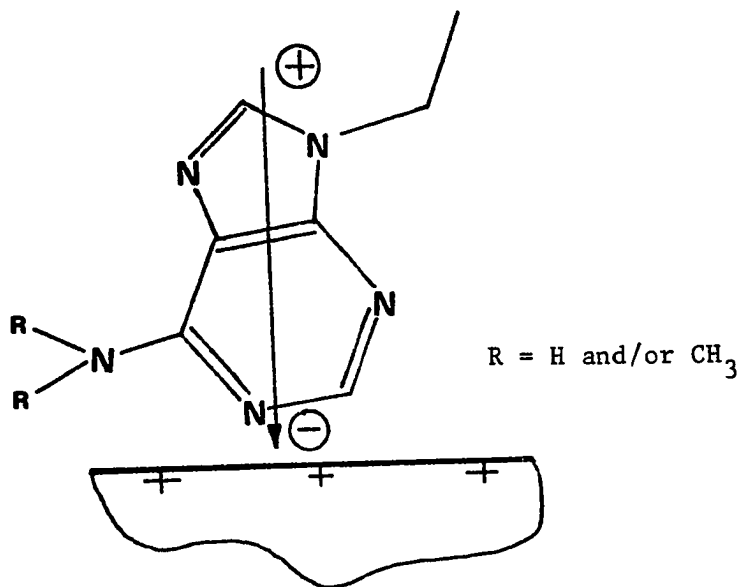


Fig. 27

Proposed surface orientations for (A) adenine in the capacitance pit centered at  $-0.5V$ , (B) adenosine, methyl- and dimethyladenosine in the capacitance pit centered at ca.  $-0.4V$  and (C) adenosine and methyladenosine in the capacitance pit centered at ca.  $-1.25V$ . Arrows indicate the direction and polarity of the permanent dipoles.

B.



C.

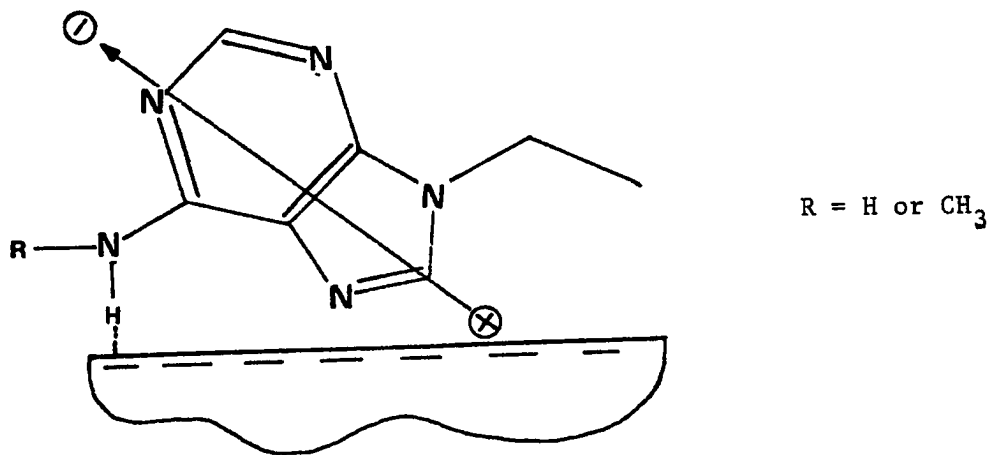


TABLE 5

Area occupied per molecule at maximum surface coverage in the dilute and capacitance pit adsorption regions for adenine and adenosine

Compound	pH	Area per molecule/ $\text{\AA}^2$	
		Dilute Adsorption Region	Capacitance Pit Region <sup>c</sup>
Adenine	8.0 <sup>a</sup>	57±6	40
Adenine	9.0 <sup>b</sup>	62±4	43
Adenosine	8.0 <sup>a</sup>	61±4	~45-55

<sup>a</sup>Fluoride/phosphate buffer pH 8.0.

<sup>b</sup>Borate buffer pH 9.0.

<sup>c</sup>Results from maximum bubble pressure measurements.

group hydrogen atoms are necessary to bind adenine to the electrode surface when it adopts the perpendicular surface stance.

At adenine concentrations where the capacitance pit is well defined (e.g., 7 mM in Fig. 22A) it may be noted, at potentials both more negative and positive than the optimum value for formation of the perpendicular layer (-0.5 V), that a very sharp decrease of capacitance occurs to values characteristic of the dilute adsorption layer. This implies that a very highly potential and concentration-dependent collapse of the perpendicular layer takes place. Although it is not possible to exactly specify the cause of this collapse, it is proposed that at sufficiently positive or negative potentials water dipoles can compete successfully with adenine molecules for electrode surface sites. Displacement of even a few adenine molecules from the electrode surface would result in collapse of the perpendicular surface layer because of its highly cooperative nature. In other words, disruption of only a few stacking interactions by replacing bases with water on the surface would cause the perpendicular array of adenine molecules to break down.

#### Adenosine

The area occupied by one adenosine molecule at monolayer surface coverage in the dilute adsorption region is very similar to that of adenine (Table 4). Since adenosine has a molecular weight which is almost double that of adenine it is clear that in order to explain the observed adsorption behavior of adenosine in the dilute region the surface conformation of the nucleoside must be considered.

Adenosine exists in the anti conformation in the solid state.<sup>149</sup> The anti and syn conformations and their relation to the torsion angle,  $\phi_{CN}$ , may be understood by reference to Fig. 28. Although adenosine exists preferentially in the anti conformation Haschemeyer and Rich<sup>150</sup> have shown that the steric barrier to interconversion between the anti and syn conformations is small. In addition, the energy difference between the two conformations is thought to be about  $1 \text{ kcal mol}^{-1}$ ,<sup>151</sup> i.e., very small. Accordingly, it should be energetically and sterically easy for adenosine to adopt either the syn or anti conformations.

In a recent report<sup>152</sup> it was shown that D-ribose adsorbs at a mercury electrode in a flat surface orientation, i.e., with the average plane of atoms in the sugar ring parallel to the electrode surface. However, D-ribose at  $-0.433 \text{ V}$  at pH 8.0 is  $-1657 \text{ cal}$ <sup>152</sup> compared to  $>4400 \text{ cal}$  for adenine (Table 4). This implies for adenosine, which consists of a strongly adsorbed adenine residue and a weakly adsorbed D-ribose residue, that in the dilute adsorption region the adenine residue will be preferentially adsorbed in a flat surface orientation. This in turn would result in the sugar residue adopting an orientation approximately perpendicular to the electrode surface. With the base adsorbed on the electrode surface and the sugar perpendicular it may be shown<sup>152</sup> that in the anti conformation the nucleoside should occupy significantly larger surface area than the base. On the other hand, in the syn conformation (see Fig. 28) with the base adsorbed flat on the electrode, the sugar residue is largely rotated out of the plane of the electrode surface. This allows the adenine residues to pack

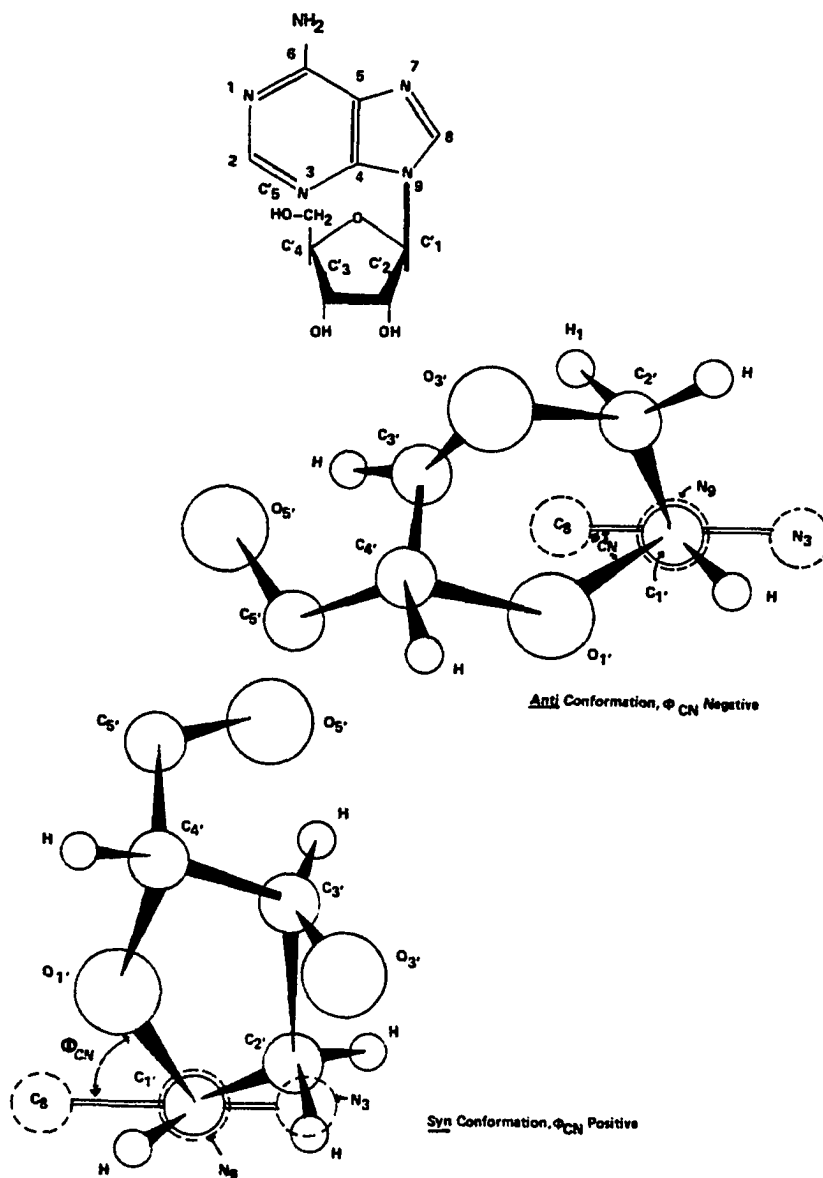


Fig. 28

Schematic illustration of the torsion angle,  $\phi_{CN}$ , in purine nucleosides. The plane of the base is viewed end-on with the glycosyl C'(1)-N(9) bond perpendicular to the plane of the paper. The torsion angle is the dihedral angle between the plane of the base and the plane formed by the C'(1) to O'(1) bond of the furanose ring and the C'(1) to N(9) bond. When O'(1) lies directly over C(8) then  $\phi_{CN}$  is zero. Positive angles are measured when C'(1)-O'(1) is rotated in a clockwise direction when viewing from C'(1) to N(9). (Adapted from reference 156).

together almost as closely as in the absence of the sugar moieties. Since, experimentally, the areas occupied by adenine and adenosine are very similar (Table 4) it may be concluded that in the dilute adsorption region adenosine is adsorbed with the base residue flat on the electrode surface with the molecule in the syn conformation.

Adenosine, at pH 8.0, exhibits a poorly formed positive capacitance pit at around  $-0.5$  V and a well-defined negative capacitance pit centered at  $-1.25$  V (Fig. 22B). The area occupied by adenosine in the positive capacitance pit could not be measured. However, at potentials and concentrations corresponding to the negative capacitance pit, maximum bubble pressure measurements indicate that the area occupied per adsorbed adenosine molecule ( $45-55 \text{ \AA}^2$ ) is a little smaller than in the dilute adsorption region ( $61 \text{ \AA}^2$ ). Of considerable significance is the fact that methylation of the amino group of adenosine does not cause the disappearance of all capacitance pits. Thus, 6-methyladenosine gives only the positive capacitance pit (Fig. 22D). These observations suggest that, unlike adenine, the amino group of adenosine is not of prime importance in binding the nucleoside to the electrode surface in the capacitance pit adsorption regions. Accordingly, it is proposed that interaction of the permanent dipole moment of adenosine and its methylated derivatives with the electrode surface is responsible for binding adenine residues to the electrode surface. Because the surface area occupied by adenosine at least in the negative capacitance pit region is apparently somewhat smaller than in the dilute region, and because in either capacitance pit region the molecules cannot be in a flat surface orientation, it has been

concluded that all capacitance pits must correspond to regions where adenine residues are adsorbed perpendicular to the surface.

The permanent dipole moments for adenine, adenosine and their methylated derivatives are presented in Fig. 29. The dipole moment of adenosine in the anti conformation (5.6 Debye) is significantly larger than for adenine (3.0 Debye) and for adenosine in the syn conformation (1.9 Debye). The effect of methylation of the amino group of the latter compounds on their dipole moments is small (Fig. 29). Dipole moments for the methylated compounds were calculated by a vectorial additive method.<sup>153</sup>

Adenosine, 6-methyl- and 6-dimethyladenosine all give a positive capacitance pit. It is not possible to measure the optimum potential for formation of this capacitance pit for adenosine because of its ill-defined nature. However, for 6-methyladenosine the optimum potential for formation of the positive capacitance pit is  $-0.42$  V, while for 6-dimethyladenosine the value is  $-0.37$  V. At the latter potentials the mercury electrode carries a small positive charge (ECM potential is  $-0.433$  V). It thus seems reasonable to conclude that the adenine residues of adenosine and its methyl derivatives are oriented with the negative end of their dipole directly toward the positively charged electrode. The dipole moments of the latter molecules are greatest when the usually more favored anti conformation is adopted. In this conformation the negative end of the dipole lies approximately between the N(1) and C(6) positions. Accordingly, it is proposed that the adenine residues of adenosine, methyl- and dimethyladenosine

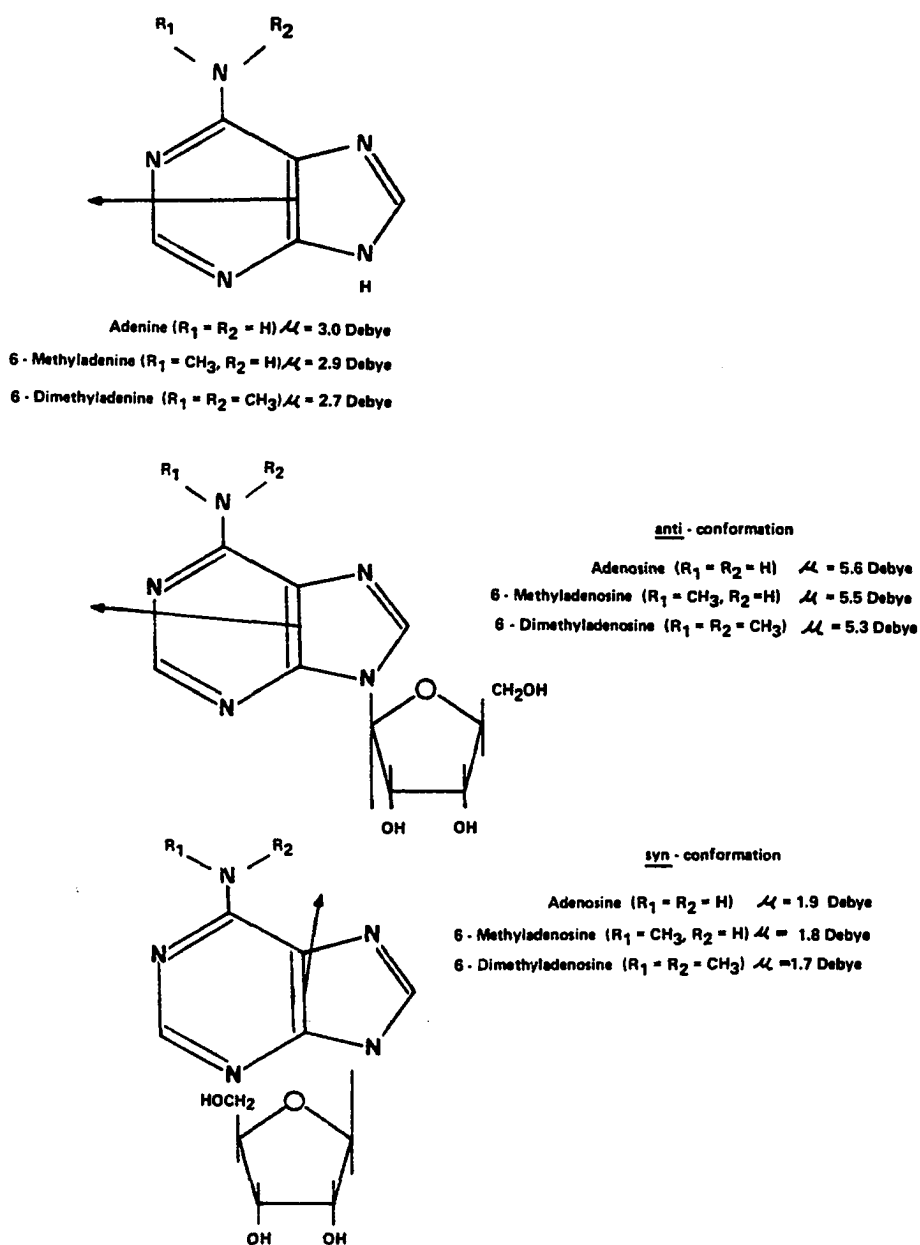


Fig. 29

Permanent dipole moments for adenine<sup>157,158</sup> adenosine<sup>159</sup> and their methylated derivatives. The arrow indicates the direction for the dipole with the head corresponding to the negative end.

are adsorbed at the electrode surface in a perpendicular orientation with the N(1)-C(6) group closest to the electrode surface (Fig. 27B). In the anti conformation molecular models reveal that adjacent perpendicular adenine residues can approach close enough to permit extensive intermolecular stacking interactions and hence stabilization of the perpendicular layer. This is not surprising because in natural, double helical nucleic acids the nucleotide residues adopt the anti conformation.<sup>154</sup> In the surface orientation shown in Fig. 27B for the positive capacitance pit the amino group appears to contribute little to the binding of the adenine residue to the electrode surface, since methylation of this group does not inhibit formation of the positive perpendicular layer.

It seems reasonable to conclude that collapse of the positive perpendicular layer is due to electrostatic repulsion of the negative dipole at negative potentials coupled with adsorption of water dipoles. At positive potentials competitive adsorption of solvent must become sufficiently strong to cause replacement of a few nucleoside molecules, with concomitant collapse of the highly associated perpendicular layer.

Adenosine and 6-methyladenosine also exhibit a negative capacitance pit (Fig. 22B,C) while 6-dimethyladenosine (Fig. 22D) does not. Assuming again that the adenine residues of the nucleosides are adsorbed perpendicular to the electrode surface, then this more negative pit must be caused by a different surface orientation to that in the positive capacitance pit. The shape of the negative capacitance pit, particularly the steep sides both negative and

positive of the optimum potential (-1.25 V) suggest catastrophic collapse of the surface layer, again indicative of a highly cooperative surface film, i.e., close approach and hence intermolecular stacking of base residues. The fact that 6-dimethyladenosine does not give rise to the negative capacitance pit, whereas adenosine and 6-methyladenosine do, suggests that at least one amino group hydrogen is necessary to allow the perpendicular orientation to take place. At the optimum potential for formation of the negative capacitance pit (-1.25 V) the mercury electrode carries a large negative charge. Thus, it would be expected that the positive end of the dipole would be oriented towards the electrode surface. Since adenine does not give a negative capacitance pit yet it has two unsubstituted amino hydrogen atoms it may be concluded that both hydrogen bonding via at least one of the amino hydrogen atoms and interaction of the positive end of a dipole are necessary for binding the perpendicular adenine residues of adenosine and 6-methyladenosine to the electrode surface. The fact that adenosine and methyladenosine give the negative perpendicular layer while adenine and methyladenine do not must be related to their dipole moments. Thus the anti conformations of adenosine and methyladenosine have relatively large dipole moments (Fig. 29) while adenine and methyladenine have much smaller dipole moments. Hence, the interaction between the positive end of the dipole of adenosine and methyladenosine and the negatively charged electrode must be much larger than in the case of adenine and methyladenine. Accordingly, it is proposed that in the negative capacitance pit region adenosine and methyladenosine adopt the perpendicular orientation shown in Fig. 27C where both

nucleosides are in their more favored anti conformation. In the latter conformation the nucleosides have dipole moments almost twice that of the bases and three times that in their syn conformation. In the negative capacitance pit region it is thus proposed that the adenine residue of adenosine or methyladenosine is anchored to the electrode surface by electrostatic interaction between the positive end of their dipole and the negatively charged electrode surface and a hydrogen bond between an amino hydrogen and the electrode surface. The dipole moment of adenine is apparently not large enough to allow this molecule to adopt a stable, perpendicular layer on the electrode surface.

If adenosine does in fact adopt the perpendicular orientation proposed in Fig. 27C then each molecule should occupy an area of about 52-58 Å<sup>2</sup>. This area is in reasonable agreement with that measured experimentally (45-55 Å<sup>2</sup>, Table 5). It must again be stressed that the experimental area is only an approximate value. Molecular models again reveal that adjacent base residues of adenosine in the perpendicular orientation shown in Fig. 27C could readily undergo strong intermolecular stacking interactions to stabilize the perpendicular film.

It might also be noted that the syn conformation of adenosine is absolutely excluded in the negative capacitance pit region because the dipole moment is not only very small (1.9 Debye) but also the positive end of the dipole is such (Fig. 29) that the weakly adsorbed sugar residue would be oriented towards the electrode surface, not

the base residue. Earlier work<sup>152</sup> has unequivocally demonstrated that the D-ribose is not adsorbed to any significant extent at -1.25 V.

#### Adenosine-5'-monophosphate

AMP exhibits only a dilute adsorption region (Fig. 22E) and the area occupied by one molecule at monolayer saturation ( $63 \text{ \AA}^2$ ) is only slightly larger than for adenine and adenosine. This behavior can be readily explained if AMP adopts the syn conformation on the electrode surface in an identical fashion to that proposed for adenosine. In this surface conformation with the base residues adsorbed flat on the electrode the sugar phosphate residue is largely rotated out of the plane of the electrode and adenine residues can pack together almost as closely as for the unsubstituted base.

AMP does not exhibit capacitance pits presumably because of significant electrostatic repulsions between adjacent, negatively charged phosphate groups.

### Conclusions

The results presented indicate that adenine, adenosine and AMP all exhibit an initial, dilute adsorption region where the base residues adsorb flat on the electrode surface. In this orientation the interaction between the adenine residue and the surface must be primarily between the  $\pi$ -electron cloud and, presumably, the conduction band of the electrode. In effect, a rather weak non-specific bond anchors the adenine residue to the electrode surface. Adenosine and AMP appear to adopt their syn conformations because only in this conformation are the sugar and sugar phosphate residues largely above the plane of the electrode surface so that adenine residues can pack almost as closely together as does the free base. The electrode surface areas occupied by adenine, adenosine and AMP at complete monolayer surface coverage in the dilute adsorption region (ca.  $60 \text{ \AA}^2$ ) have been measured by two independent and well established surface electrochemical methods. These areas differ considerably from those reported by Krznaric and coworkers<sup>155</sup> who found that at pH 3.4 and  $5^\circ\text{C}$  adenosine occupied an area of  $150 \text{ \AA}^2$  and AMP an area of  $153 \text{ \AA}^2$ .

Adenine exhibits a single capacitance pit, which has an optimum potential of formation of  $-0.5 \text{ V}$ , i.e., the electrode carries a small negative charge. At potentials and concentrations where this capacitance pit forms it is suggested that adenine reorients from a flat to a perpendicular surface orientation and is bound to the electrode through its two amino hydrogen atoms, i.e., a hydrogen bond of the type  $-\text{N} \begin{array}{l} \text{H}\cdots \\ \text{H}\cdots \end{array} \left( \begin{array}{l} \text{---} \\ \text{---} \\ \text{---} \\ \text{---} \\ \text{---} \\ \text{---} \end{array} \right) (-)$  electrode is formed. That this is so is shown

by the fact that methylation of one or both amino hydrogen atoms destroys the ability of adenine to form a perpendicular surface layer.

Adenosine and 6-methyladenosine exhibit two capacitance pits. Owing to experimental difficulties it has not been possible to accurately measure the electrode surface areas occupied by the latter molecules. However, by a systematic study of adenine, adenosine and their methylamino derivatives, it has been concluded that at potentials and concentrations where the positive capacitance pit is formed the adenine residues of adenosine and its methylated derivatives adopt a perpendicular stance with the negative end of the dipole oriented towards the slightly positively charged electrode. The anti conformation of adenosine has a much larger dipole moment than the syn conformation and in addition stacking interactions between adjacent base residues are more favorable in the anti conformation.

In the negative capacitance pit region it is again believed that adenosine and 6-methyladenosine are adsorbed with the adenine residues perpendicular to the electrode surface. However, in this region it is proposed that the positive end of the dipole is directed towards the negatively charged electrode. Because of the very large dipole moment of the anti form of adenosine the latter conformation is preferred.

A recent report by Vetterl<sup>144</sup> suggested that in the negative capacitance pit region adenosine is adsorbed with the base residue perpendicular to the electrode through the C(8) position with the nucleoside in the syn conformation. In view of the fact that adenine cannot exhibit a negative capacitance pit and that the dipole moment

for syn adenosine is so small and the positive end of the dipole is at C(5) it is believed that the syn conformation cannot be correct. It also appears, in the negative capacitance pit region, that at least one amino group hydrogen is hydrogen bonded to the electrode surface. This cannot occur with the surface orientation proposed by Vetterl.<sup>144</sup>

## CHAPTER IV

### A PRELIMINARY STUDY OF ELECTROCHEMICAL OXIDATION OF 5-METHYLTETRA- HYDROPTERIN AT THE PYROLYTIC GRAPHITE ELECTRODE

#### INTRODUCTION

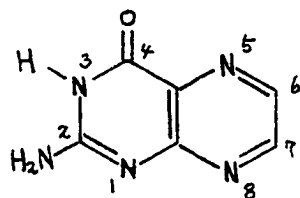
In recent years, electrochemistry has aided in the elucidation of the in vitro oxidation mechanism of some biologically important molecules such as purines and pyrimidines.<sup>180-184</sup> That the study of electrochemical reaction mechanisms can yield valuable information as to the nature of in vivo enzymatic reaction mechanisms is not surprising, because both types of reactions involve the transfer of electrons to molecules specifically oriented on a charged surface in the presence of a large excess of inert electrolytes. Accordingly, knowledge of the electrochemical reaction mechanism can increase one's understanding of the in vivo reaction mechanism but even more importantly, the electrochemical mechanism may suggest the existence of intermediate species, or the involvement of enzymes which previously were not suspected of being involved in a particular biological reaction.

Pteridines are widely distributed in living systems yet many of the biological roles of these molecules are either unknown or are very incompletely understood.<sup>187,188</sup> Certain reduced or unconjugated

forms of some pteridines are of metabolic importance as coenzymes in hydroxylation reactions,<sup>189</sup> and as intermediate in the photosynthetic electron transport process.<sup>190</sup> For example, the hydroxylation of phenylalanine to tyrosine requires not only the enzyme phenylalanine hydroxylase and oxygen, but also tetrahydrobiopterin as a cofactor. A number of studies have suggested that the reduced pterine undergoes a variety of redox and related chemical reactions as it functions as the cofactor. However, the actual nature of these reactions are not known, nor are the effects of pteridine structure solutions conditions and other solution reactants understood.

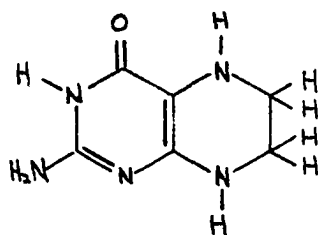
Electrochemical reduction of several pteridine derivatives have been reported in some detail.<sup>191-193</sup> The electrochemical oxidation of pteridines has not been investigated extensively as yet, although Dryhurst et al. studied several hydroxy derivatives of pteridine.<sup>194</sup>

This investigation is a part of the preliminary efforts to unravel the details of the complex redox chemistry of biologically important pteridines in terms of the electrical potentials required for the electron-transfer process to occur, the nature of the intermediates formed and the course and controlling conditions for their follow-up chemical and/or electrochemical reactions and the products formed. It is the objective of this work to understand the effect of methylation at the 5 position of tetrahydropterin (II) on the electrochemistry of this compound; namely, the electrochemical oxidation of 5-methyltetrahydropterin (III).



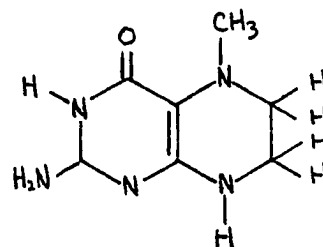
( I )

Pterin



( II )

Tetrahydropterin



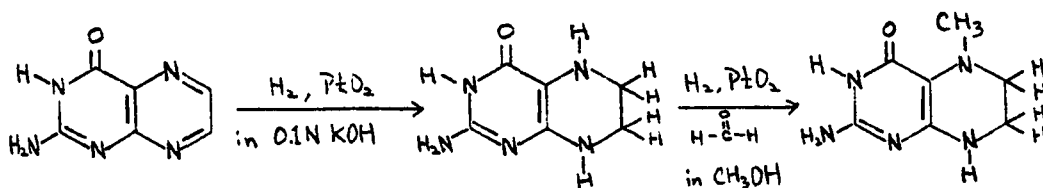
( III )

5-Methyltetrahydropterin

## EXPERIMENTAL

Chemicals

Pterine was obtained from Sigma, and 5-methyltetrahydropterine was synthesized by the reductive alklation method of Matsuura et al.<sup>195-196</sup> as follows:



Elemental analysis of the product found: C, 30.47%; H, 5.05%; N, 24.99%, and  $C_7H_{11}N_5O \cdot 2HCl \cdot 0.6H_2O$  (as reported by Matsuura et al.<sup>195</sup>) requires C, 31.75%; H, 5.40%; N, 26.44% and  $C_7H_{11}N_5O \cdot 2HCl \cdot 1H_2O$  requires C, 39.88%; H, 5.52%; N, 25.75%. Melting point range of the product is in between 235°C-242°C (237-239°C; reported).

Platinum oxide (Adam's catalyst) was obtained from Sargent-Welch Scientific Co. (Skokie, Ill.). Phosphate buffers are prepared as described in Chapter III.

Voltammetric Procedure

Linear sweep voltammetry and cyclic sweep voltammetry were performed with an instrument based on conventional operational amplifier design,<sup>197</sup> employing a function generator patterned after that of Myers and Shain.<sup>198-199</sup> Voltammograms were recorded on a Hewlett-Packard Model 7001 A X-Y Recorder or a Houston Omnigraphic Model 2000 X-Y recorder or a MFE Plotamatic Model Q15 X-Y recorder.

Fast sweep voltammograms were obtained with a Princeton Applied Research Corporation Model 175 Universal programmer and were recorded on a Tektronix Model 5031 Dual Beam Storage Oscilloscope, and photographed with a Tektronix Model C-70 camera.

A water-jacketed one-compartment cell (5 ml capacity) maintained at a known and constant temperature (usually  $25.0^{\circ}\pm 0.1^{\circ}\text{C}$ ), which is very similar to the polarographic cell used for the capacitance measurement, was used for the voltammetry. A pool of mercury inserted at the bottom of the cell served as the counter electrode. A reference electrode, namely the saturated calomel electrode (SCE) was positioned close to the PGE using a fine Luggin capillary. For convenience, all potentials are reported versus a saturated calomel electrode. Temperature of the voltammetric cell and the water-jacketed glass bubbling chamber was maintained by circulating water from a bath heated by an incandescent bulb in a circuit with  $25^{\circ}\text{C}$  or  $40^{\circ}\text{C}$  thermostats and a mercury relay (H-B Instrument Co.).

The pyrolytic graphite electrodes were machined from small rods of pyrolytic graphite (Pfizer Chemical, Inc., Ridgefield, New Jersey) to a square pillar shape (ca. 2 mm x 2mm x 10 mm), and were

sealed into 2.5 mm or 3.5 mm (ID) glass tubing (ca. 120 mm long) with an epoxy resin (Hysol Epoxi-Patch, Dexter Corporation, Olean, New York). The electrodes were ground flush with the end of the glass tube and were resurfaced prior to the running of each voltammogram with 600-grit silicon carbide paper (Buehler Ltd., Evanston, Ill.) mounted on a rotating disc. The electrode was then sprayed with a fine stream of doubly distilled water to remove the graphite powder from the surface, and dried by gently touching the surface with an absorbent paper tissue. Test solutions of 5-methyltetrahydropterin were prepared immediately prior to each study. These solutions were made by dissolving the solid compound in a solution of 1:1 phosphate buffer: doubly-distilled water, yielding an ionic strength of 0.5 M. Deaeration was accomplished by bubbling nitrogen through the solution for approximately 10 minutes before the experiment was run, and then passed in a stream over the solution during the run.

Coulometric Electrolysis Procedure

For controlled potential electrolysis a three-compartment cell was used with each compartment separated by a medium-porosity sintered glass disc: Salt bridge placed on the counter and reference sides of the discs were prepared by dissolving 4 grams agar (Difco Laboratories) in 90 ml of phosphate buffer (ionic strength 0.5 M) of the appropriate pH. A saturated calomel reference electrode (SCE) and a platinum foil counter electrode were utilized.

Controlled potential electrolysis was carried out using Princeton Applied Research Corporation Models 173 or 373 Potentiostat/Galvanostats. Current integration during electrolysis was performed with a Koslow Scientific Co. (North Bergen, New Jersey) Model 541 coulometer.

Controlled potential coulometry was performed at the pyrolytic graphite electrode (area ca. 10 cm<sup>2</sup>) with a working compartment volume of 25 ml. During electrolysis, solutions were stirred magnetically with a Teflon-coated bar.

15 ml of test solutions (concentration range 0.1-1.0 mM) of 5-methyltetrahydropterin in either pH 3 or pH 8 phosphate buffer was placed in the working electrode compartment of the electrolysis cell. During the electrolysis, the current was monitored and when it had decreased to a low, constant value, the counts per unit time produced by the coulometer were noted and the electrolysis stopped. Completion of oxidation was confirmed by the absence of the volt-ammetric oxidation peak of 5-methyltetrahydropterin.

Thin-Layer Spectroelectrochemistry Experiments

Thin-layer spectroelectrochemistry experiments utilized a Harrick Rapid Scan Spectrophotometer (RSS) Model B and a signal processing module (Harrick Scientific Co., Ossining, New York). Spectral sweeps and absorbance versus time curve were recorded on a Hewlett-Packard Model 7015 X-Y Recorder.

Optically transparent thin-layer electrochemical cells used were similar to those described by Norvell and Mamantov.<sup>200</sup> Reticulated vitreous carbon (Chemtronics International, Inc., Ann Arbor, Michigan) was used as the optically transparent electrode. Reticulated vitreous carbon (RVC) of 100 ppi (porosity grade) was sliced to a 0.5 mm thickness with a depth constructed cheese cutter. Using liquid organic silver (Electro Metallics, East Newark, New Jersey), a copper wire was bonded in flame to a 28 mm x 10 mm x 0.5 mm segment of sliced RVC. This was then positioned between two 25.4 mm x 50.8 mm x 1.6 mm quartz slides (Esco Products, Oak Ridge, New Jersey) with carbon extending slightly beyond the shorter sides of the quartz slides. Hysol-Epoxi Patch resin was used to position the RVC. The longer sides of the slides and a portion of the top adjacent to the carbon was sealed with epoxy resin. Part of the attached copper wire was left extending from the epoxy resin for electrical contact to the carbon electrode. This left an open ended assembly allowing for solution circulation and carbon surface reconditioning. A consistent carbon surface was obtained by the rapid circulation of an air/water mixture. This agitation was induced by suction and followed by a distilled

water wash to remove any trapped air. Controlled potentials applied to the electrode were maintained with a Princeton Applied Research Corporation Model 174A Polarographic Analyzer. The advantage of an optically transparent carbon electrode compared to a gold-minigrid electrode is the extended potential range that is available at the former electrode without oxidation of the electrode. This occurs with a gold electrode upon exceeding ca. +0.75 V vs. SCE.

#### Isolation of Electrolysis Products

After complete oxidation of 5-methyltetrahydropterin on the plateau of the major oxidation peak (+0.5 V vs. SCE) in pH 3 phosphate buffer, the yellow solution of products was lyophilized, yielding a yellow solid. A liquid chromatographic separation method utilizing a dual column was used for the separation of the oxidation products from the salts (phosphate and chloride). This system employed a 2.5 cm x 100 cm Pharmacia column containing 90 cm of Sephadex G-10 and 2.5 cm x 45 cm Pharmacia column containing 30 cm of Sephadex G-10. These columns were used in conjunction with a three-way valve for sample introduction and for switching to different solvent reservoirs. Doubly distilled water was used as an eluent with a flow rate of ca. 12 ml/hr.

The eluant from the columns was collected in 4.0 ml fractions with an ISCO Model 1200 Fraction Collector (ISCO, Lincoln, Nebraska). A wavelength was selected where all eluted compounds of interest gave significant absorbance values, and UV absorbance for each fraction was obtained on a Perkin-Elmer Hitachi Model 124 spectrophotometer

using 1.00 cm quartz cells.

Freeze drying was accomplished using a Virtis 12-port manifold containing an isopropanol/water mixture cooling trap. This cooling was maintained with a Neslab CryoCool Model CC-60. Mass spectra were obtained on a Hewlett-Packard 5985 Gas Chromatograph-Mass Spectrometer (GC/MS) system. The final identification of products will be based on trimethyl silyl derivatives which can be purified by gas chromatography and analyzed by mass spectrometry.

Closed tube silylations of 5-methyltetrahydropterin oxidation products were performed with bis(trimethylsilyl)trifluoroacetamide (BSTFA). Silylation results in the replacement of active hydrogen atoms present as hydroxyl and/or amine groups by a trimethyl silyl substituent. This reduces the polarity of the compound and correspondingly makes many compounds volatile and thermally stable, i.e., convert them to a form suitable for gas chromatographic analysis.

Approximately 0.5 mg of each oxidation product was silylated in a 3.0 ml Reacti-Vial (Pierce Chemical Co.) containing 50-75  $\mu$ l of reagent (BSTFA) and 50-75  $\mu$ l of solvent (acetonitrile). This mixture was continuously stirred for 20-30 min. during silylation at a temperature of 135°C. Then, using a Hamilton 701N-10  $\mu$ l syringe, 5.0  $\mu$ l of the product mixture was injected onto a 2.0 mm i.d. x 6.0 ft. chromatographic column (Supelco, Inc.) containing 3% SE-30 on Chromosorb W [HP] (Pierce Chemical Co.) of a Varian Model 2400 Gas Chromatograph. Chromatographic conditions were isothermal for 12 min. at 90°C followed by 6°C/min. temperature programming rate up to a 200°C maximum. The injector temperature was maintained at 225°C, and the flame ionization

detector temperature at 30 ml/min. The carrier gas (N<sub>2</sub>) flow rate was set at 30 ml/min.

Successfully silylated product mixtures were chromatographed on a Hewlett-Packard 5985 GC/MS system with all conditions set the same except for a 10 ml/min. carrier gas flow rate and detector voltages at 70 eV for electron impact.

## RESULTS

Stability of 5-Methyltetrahydropterin in Aqueous Media

The stability of 5-methyltetrahydropterin at several pH values was studied by observing the decrease in absorbance of the shortest wavelength (218 nm) UV absorption peak with time. Typical results are tabulated below in Table 6.

Initially colorless solutions of 5-methyltetrahydropterin at basic pH turned pale yellow after 3 hrs. of the exposure in the air. Because of the base catalyzed decomposition of 5-methyltetrahydropterin, a more extensive study was carried out at pH 3.0.

Linear and Cyclic Voltammetry at the PGE

Between pH 3-7 at the PGE, 5-methyltetrahydropterin exhibits two oxidation peaks (peaks  $P_O^I$  and  $P_O^{II}$  in Fig. 30, 31A) which shifts to more negative potential with increasing pH. At pH 3 peak  $P_O^I$  appeared at +0.33 V ( $E_p$ , the peak potential), and peak  $P_O^{II}$  appeared at ca. +1.24 which is burried under the background (Fig. 30). Upon

TABLE 6

UV spectrophotometric study of the stability of 5-methyltetrahydropterin in aqueous solution

Buffer	Ionic Strength	pH	Decrease in absorbance after 30 min. at $\lambda = 218$ nm
Phosphate	0.5	3.0	no detectable change
water	0.0	5.5	1%
phosphate	0.5	6.9	2%
phosphate	0.5	8.0	4%

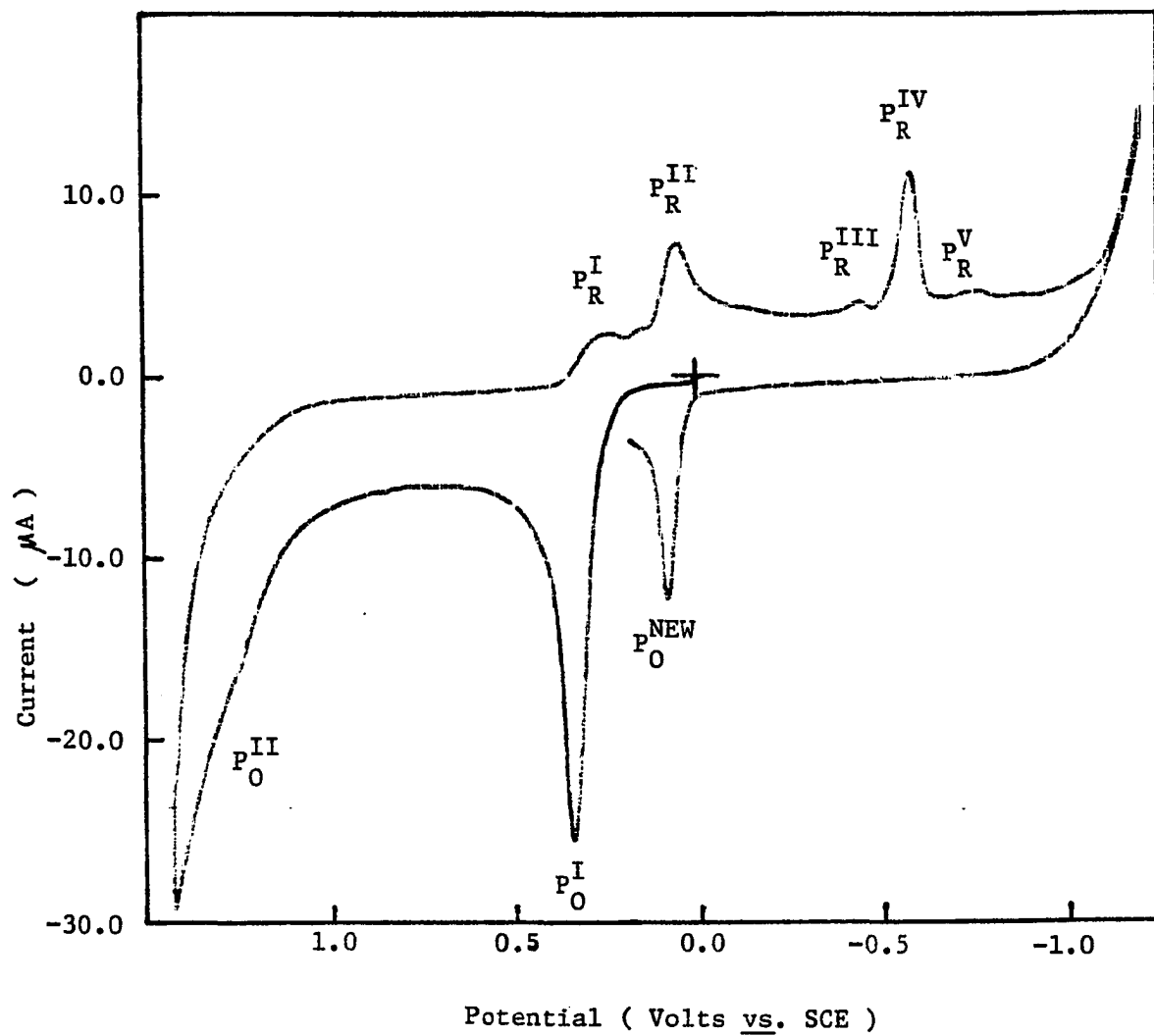


Fig. 30  
Cyclic voltammogram of 1.0 mM 5-methyltetrahydropterin in pH 3.0 phosphate buffer at the PGE. Voltage sweep pattern, 0.00V  $\rightarrow$  -1.42V  $\rightarrow$  1.20V  $\rightarrow$  0.20V. Scan rate, 200 mV/sec.

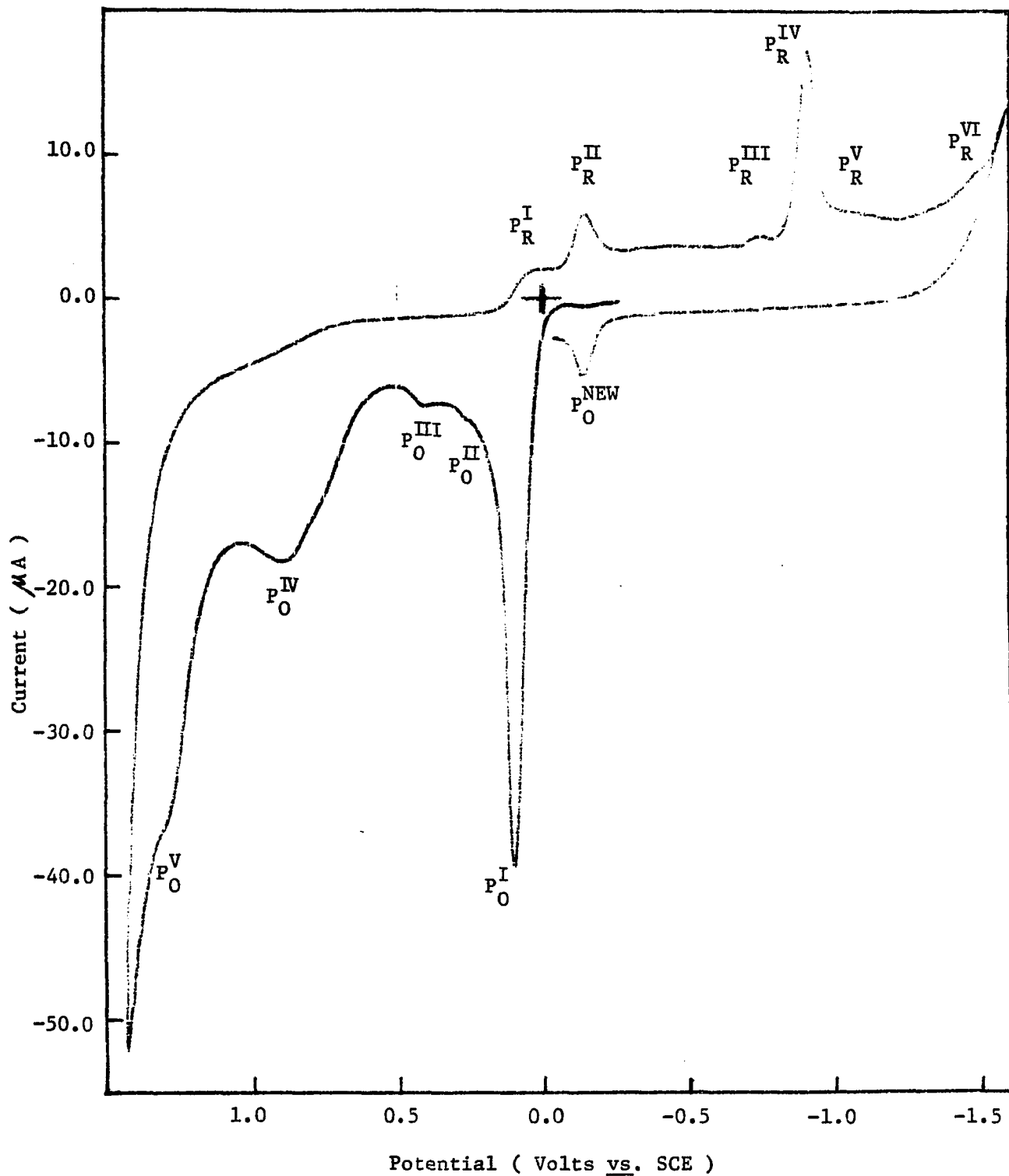


Fig. 31 A

Cyclic voltammogram of 1.00 mM 5-methyltetrahydropterin in pH 8.0 phosphate buffer at the PGE. Voltage sweep pattern,  $-0.25\text{ V} \rightarrow 1.42\text{ V} \rightarrow -1.60\text{ V} \rightarrow -0.05\text{ V}$ . Scan rate, 200mV/sec.

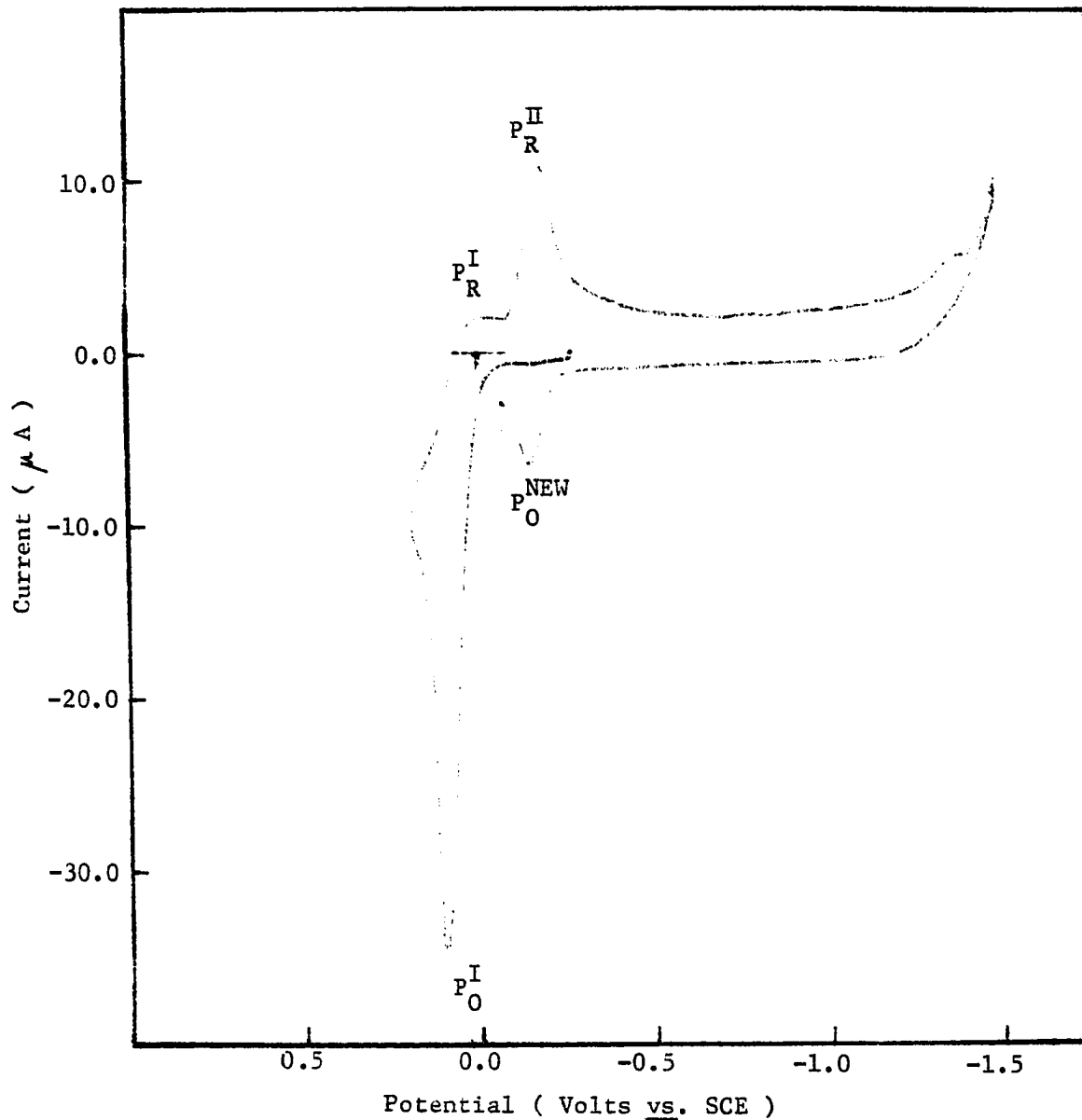


Fig. 31 B

Cyclic voltammogram of 1.00 mM 5-methyltetrahydropterin in pH 8.0 phosphate buffer at the PGE. Voltage sweep pattern,  $-0.25 \text{ V} \rightarrow 0.20 \text{ V} \rightarrow -1.48 \text{ V} \rightarrow -0.06 \text{ V}$ . Scan rate, 200 mV/sec.

It should be noted that peaks  $P_{R}^{III}$ ,  $P_{R}^{IV}$  and  $P_{R}^{V}$  are not present.

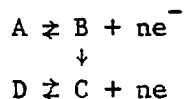
Cyclic voltammogram at pH 3.0 shows similar behavior.

reversing the scan at +1.5 V five reduction peaks appear at

- (1)  $E_p = +0.25$  V for  $P_R^I$ , (2)  $E_p = +0.05$  V for  $P_R^{II}$  (major),
- (3)  $E_p = -0.45$  V for  $P_R^{III}$ , (4)  $E_p = -0.69$  V for  $P_R^{IV}$  (major), and
- (5)  $-0.75$  V for  $P_R^V$ .

When the scan direction was switched again (at about -1.2 V) towards positive potentials, a new oxidation peak emerged at +0.08 V ( $P_O^{NEW}$ ) at pH 3. It should be noted that reduction peaks  $P_R^{III}$ ,  $P_R^{IV}$  and  $P_R^V$  are not present (Fig. 31B) when the scan direction is reversed at about +0.45 V (i.e., immediately after the first oxidation peak). This behavior strongly suggests that these three reduction processes are due to the reduction of the products formed in the  $P_O^{II}$  process.

The peak current ratio of the first two reduction peaks,  $i_{PR^I}/i_{PR^{II}}$ , become larger at higher scan rates, i.e., the peak height of  $P_R^I$  becomes relatively higher than that of  $P_R^{II}$  (Fig. 32). This suggests that the product (B) of the first oxidation process ( $P_O^I$ ) undergoes a chemical reaction to give another species (C) which is more difficult to reduce.



Upon assuming a cyclic voltammogram at the end of a controlled potential electrolysis at +0.45 V at pH 3,  $P_O^{II}$  still remains, and  $P_R^I$ ,  $P_R^{II}$ , and  $P_R^V$  are no longer observed.

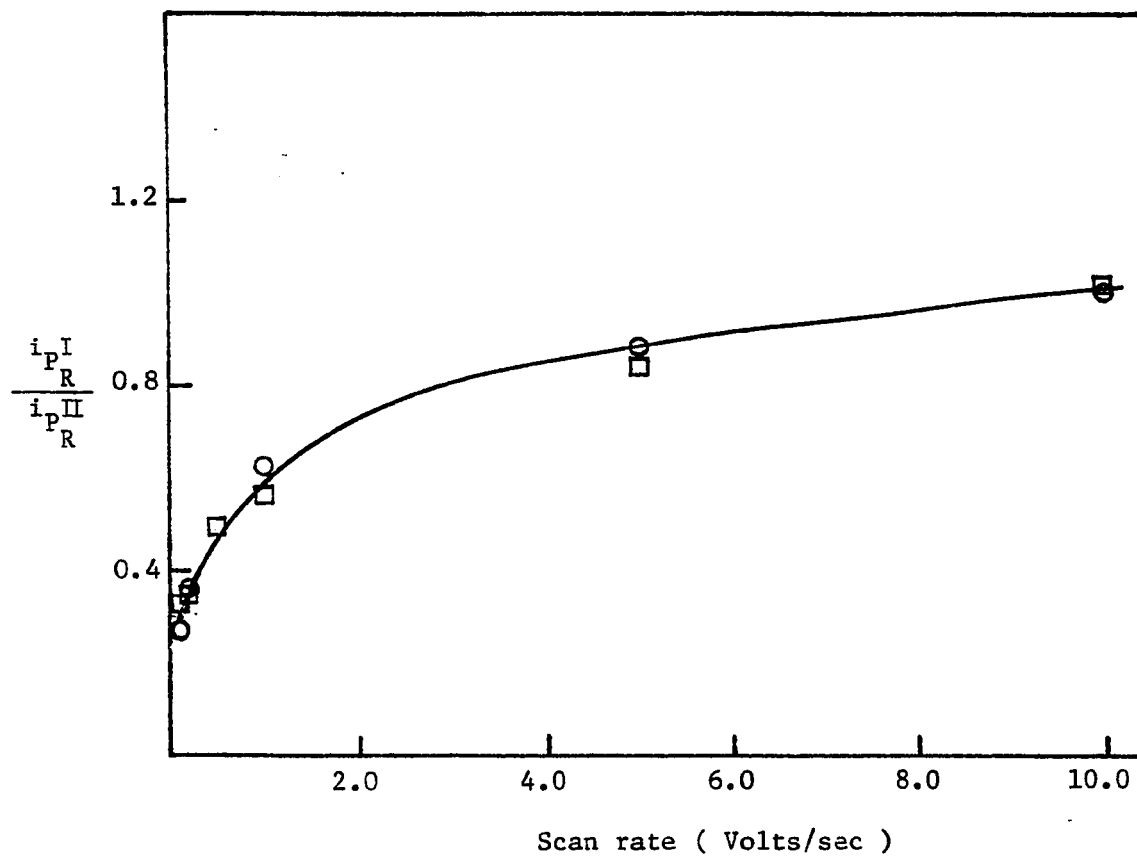


Fig. 32  
Variation of the peak current ratio,  $i_{pR}^I / i_{pR}^{II}$ , with the scan rate for 5-methyltetrahydropterin in pH 3.0(O) and in pH 8.0(□) phosphate buffer at the PGE.

pH Study

At higher pH the oxidation peaks are shifted towards more negative potentials, and the cyclic voltammogram essentially remains the same except (a) three additional minor oxidation peaks emerge and (b) one additional reduction peak emerges. For example, at pH 8 (Fig. 31A and 31B), the oxidation peaks appeared at (1)  $E_p = +0.10$  V for  $P_o^I$  (major), (2)  $E_p = +0.25$  V for  $P_o^{II}$  (new), (3)  $E_p = +0.42$  V for  $P_o^{III}$  (new), (4)  $E_p = +0.89$  for  $P_o^{IV}$  and (5)  $E_p = +1.30$  V for  $P_o^V$  (new), and reduction peaks appeared at (1)  $E_p = +0.02$  V for  $P_r^I$ , (2)  $E_p = -0.15$  V for  $P_r^{II}$ , (3)  $E_p = -0.75$  V for  $P_r^{III}$ , (4)  $E_p = -0.92$  V for  $P_r^{IV}$ , (5)  $E_p = -1.12$  V for  $P_r^V$ , and (6)  $E_p = -1.48$  V for  $P_r^I$  (new). When the scan direction was switched again (at about  $-1.6$  V) towards positive potential, a new oxidation peak ( $P_o^{NEW}$ ) emerged at  $E_p = -0.15$  V and this behavior is quite similar to that at pH 3.0.

Among the oxidation peaks, the first oxidation peak ( $P_o^I$ ), which is the largest and due to a major oxidation process, is the main object of this investigation.

 $E_p$  vs. pH Plot

A plot of peak potentials ( $E_p$  vs. pH (Fig. 33) gave a straight line with a slope of 0.065 (eqn. (53)) and 0.061 (eqn. (54)) for the  $P_o^I$  and  $P_o^{NEW}$ , respectively, which suggests that the same number of  $e^-$  (n) and  $H^+$  (p) are involved in the two oxidation processes.

$$E_p = (0.50 - 0.065 \text{ pH}) \text{ V for } P_o^I \quad (53)$$

$$E_p = (0.28 - 0.061 \text{ pH}) \text{ V for } P_o^{NEW} \quad (54)$$

Determination of p/n ratio for the minor oxidation peaks was very

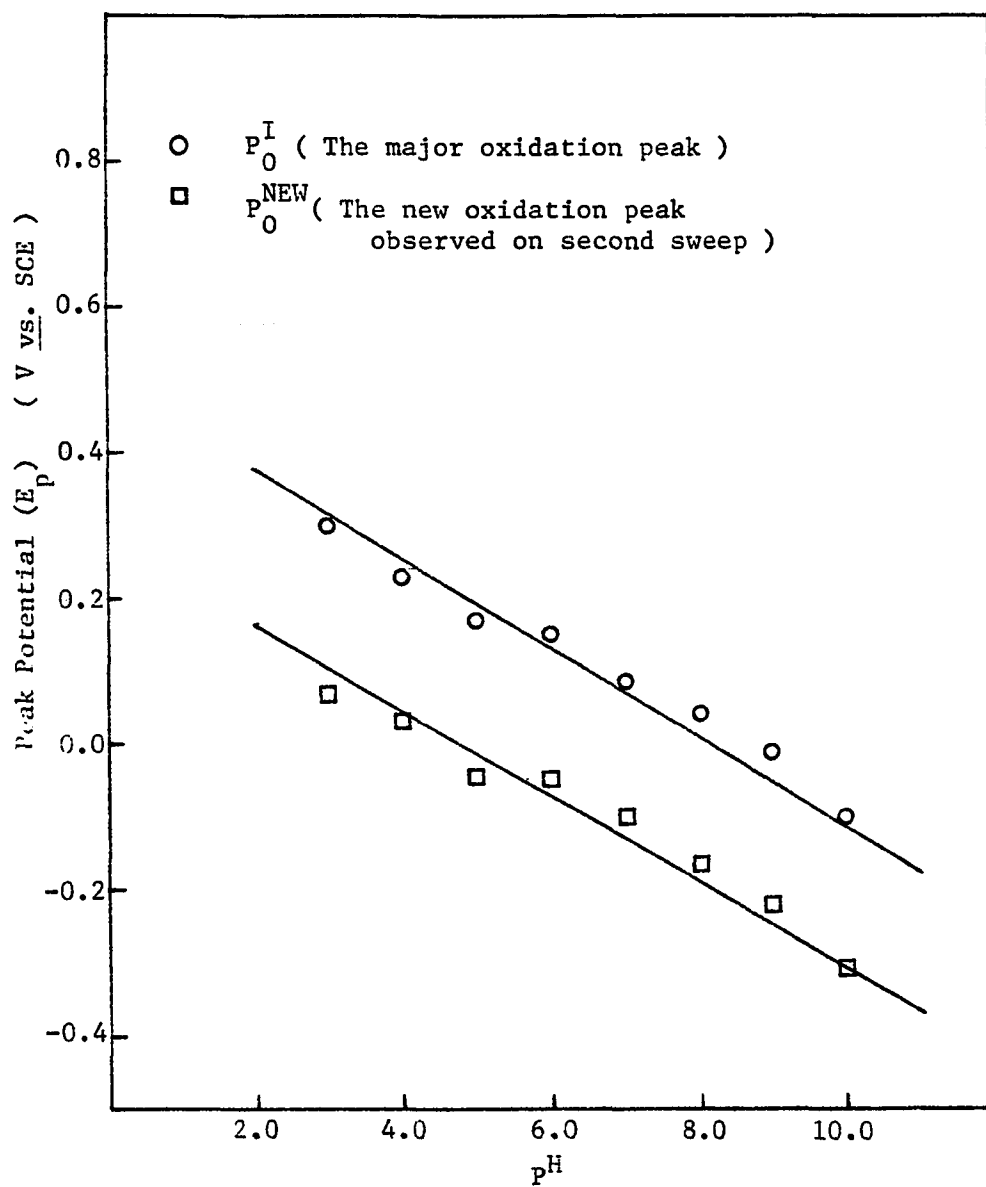


Fig. 33  
Variation of peak potentials( $E_p$ ) with pH for 1.00 mM 5-methyltetrahydropterin at the PGE. Scan rate 5 mV/sec.

difficult because of small peak currents which are sometimes irreproducible.

#### $i_p$ vs. pH Plot

A plot of peak current vs. pH for peak  $P_o^I$  is shown in Fig. 34, and clearly the peak currents are virtually independent of pH. This indicates that the protonated form of 5-methyltetrahydropterin can undergo oxidation electrochemically as readily as the neutral form can, since 5-methyltetrahydropterin ( $pK_a = 5.99$ ) exists as a protonated form at pH 3 and as a neutral form at pH 8.<sup>195</sup>

#### Scan Rate Study

Studies of the dependence of peak current upon potential scan rate revealed that for peak  $P_o^I$  an increase in peak current function,  $i_p/AC V^{1/2}$  (where  $i_p$  = peak current ( $\mu A$ ),  $A$  = electrode area ( $cm^2$ ),  $C$  = bulk concentration of electroactive species, ( $mM \ell^{-1}$ ), and  $V$  = voltage sweep rate ( $V \text{ sec}^{-1}$ ), with increasing scan rate  $V$  (Fig. 35). Such behavior is usually indicative of reactant adsorption at the electrode.<sup>201</sup> The steeper slope observed at pH 8 indicates that 5-methyltetrahydropterin is more strongly adsorbed at this pH than at pH 3.

#### Concentration Study

The involvement of adsorption was confirmed by studies of the dependence of peak height upon concentration. For a diffusion controlled peak, the height of the peak should vary directly as the concentration increases; therefore, a plot of  $i_p/C$  vs.  $C$  should

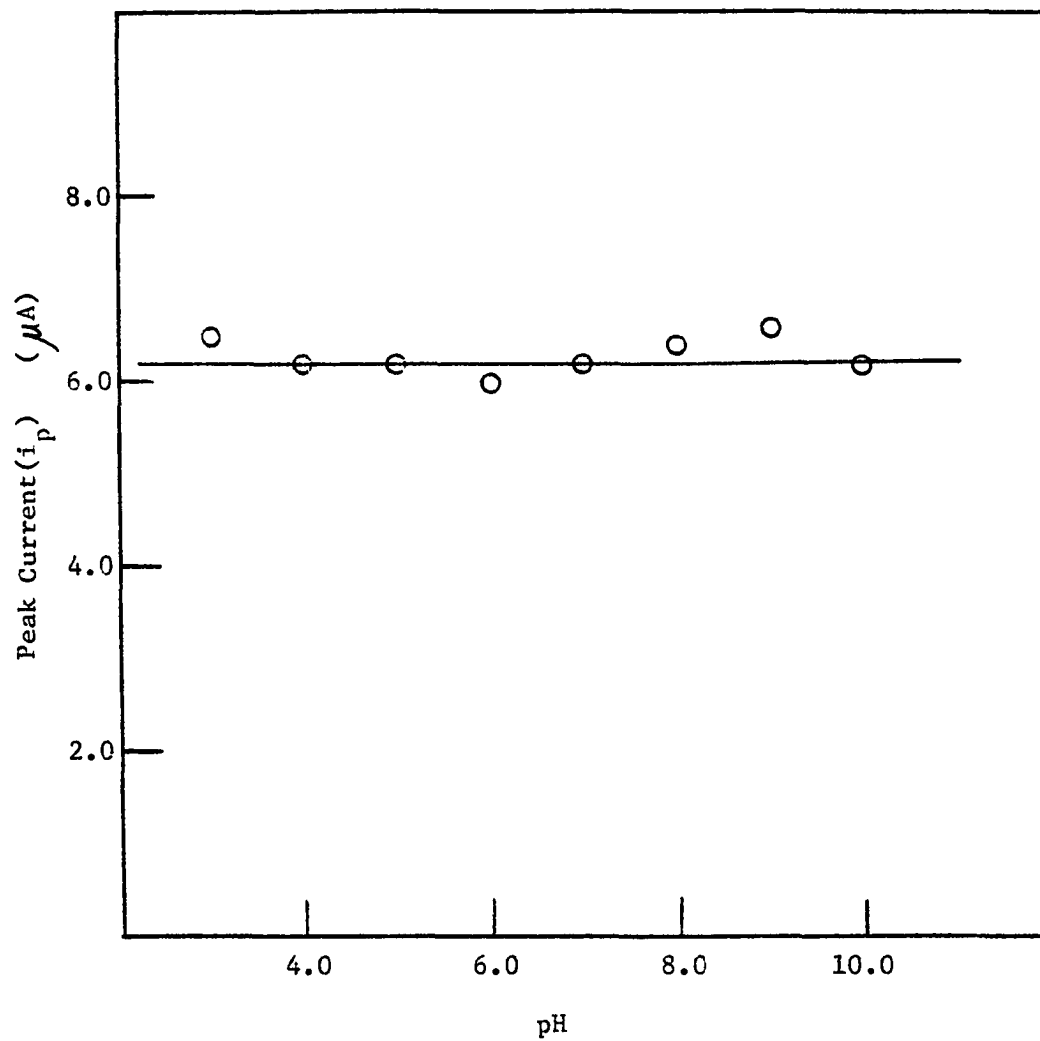


Fig. 34  
Variation of peak currents ( $i_p$ ) with pH for peak  $P_O^I$  of 1.00 mM  
5-methyltetrahydropterin at the PGE in phosphate buffers.  
Scan rate, 20 mV/sec.

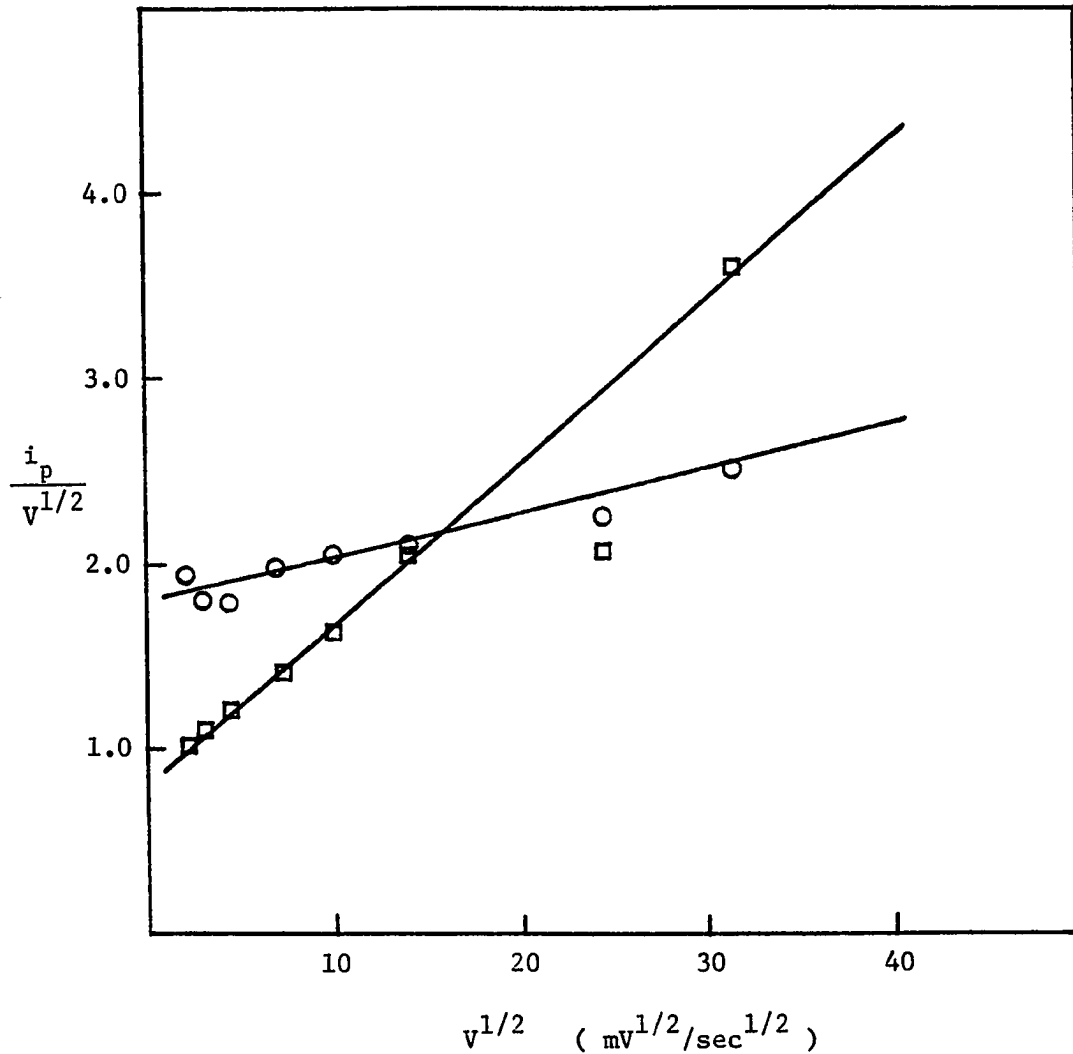


Fig. 35  
 Variation of  $i_p/v^{1/2}$  with the scan rate for 1.00 mM 5-methyl-tetrahydropterin at the PGE at pH 3.0(○) and pH 8.0(□) phosphate buffers.  $i_p/v^{1/2}$  was used instead of the peak current function ( $i_p/ACv^{1/2}$ ), since the electrode area(A) and the concentration(C) remained constant during the measurements.

yield a straight line parallel to the concentration axis. However, for a process in which adsorption is a factor,  $i_p/C$  decreases with increasing concentration.<sup>202</sup> It can be seen that the peak  $P_O^I$  exhibits behavior characteristic of adsorption from Fig. 36.

#### Controlled Potential Coulometry

At pH 3.0 and 8.0 at the appropriate controlled potentials, which were slightly (ca. 100 mV) more positive than the oxidation peak potentials, showed that 2 electrons per molecule are involved in the oxidation of the compound (Table 7). The colorless solution of 1.0 mM 5-methyltetrahydropterin turned yellow after about 1 1/2 hrs. of electrolysis, and it usually took 8-12 hrs. to reach completion of electrolysis. After complete oxidation at the above pH values, the solution showed decreased absorbance at the characteristic UV spectrum of 5-methyltetrahydropterin ( $\lambda_{max} = 265$  nm at pH 3.0), but instead showed a completely new UV absorption peak at 385 nm (Fig. 37).

TABLE 7

Coulometric determination of the number of electrons involved in the oxidation of 5-methyltetrahydropteridin

Buffer	Ionic Strength (M)	pH	Initial Concentration (mM)	Controlled Potential (V vs. SCE)	n-values (mean $\pm$ std. dev.)	number of runs
phosphate	0.5	3.0	0.1	+0.45	2.19 $\pm$ 0.29	3
phosphate	0.5	3.0	1.0	+0.45	2.12 $\pm$ 0.33	9
phosphate	0.5	8.0	0.1	+0.20	2.10 $\pm$ 0.24	3

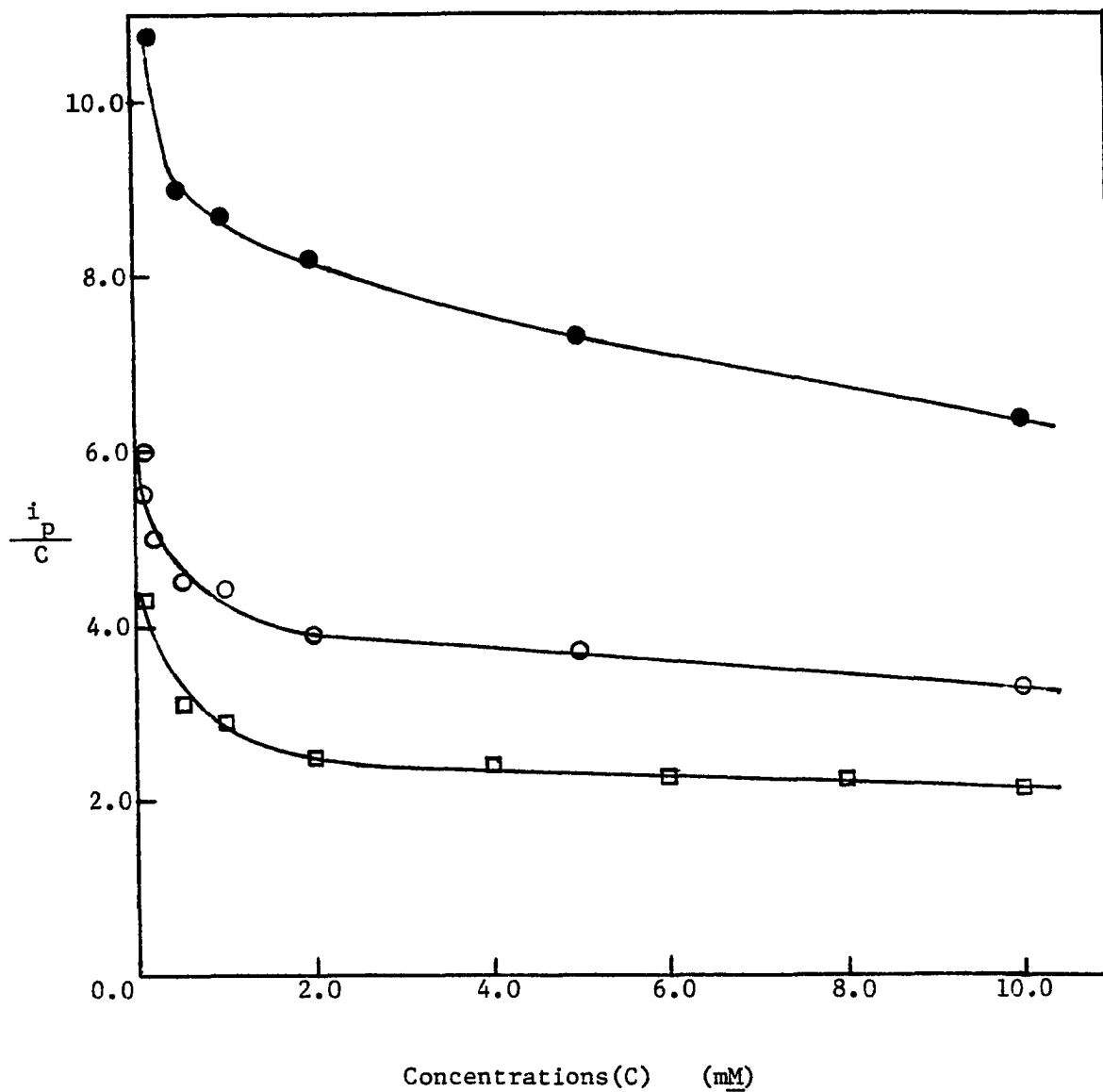


Fig. 36  
Variation of  $i_p/C$  with concentration(C) at the PGE for peak  $P_O^I$   
of 5-methyltetrahydropterin in pH 3.0 (○, 5 mV/sec; ●, 20 mV/sec)  
and in pH 8.0 (□, 5 mV/sec) phosphate buffer.

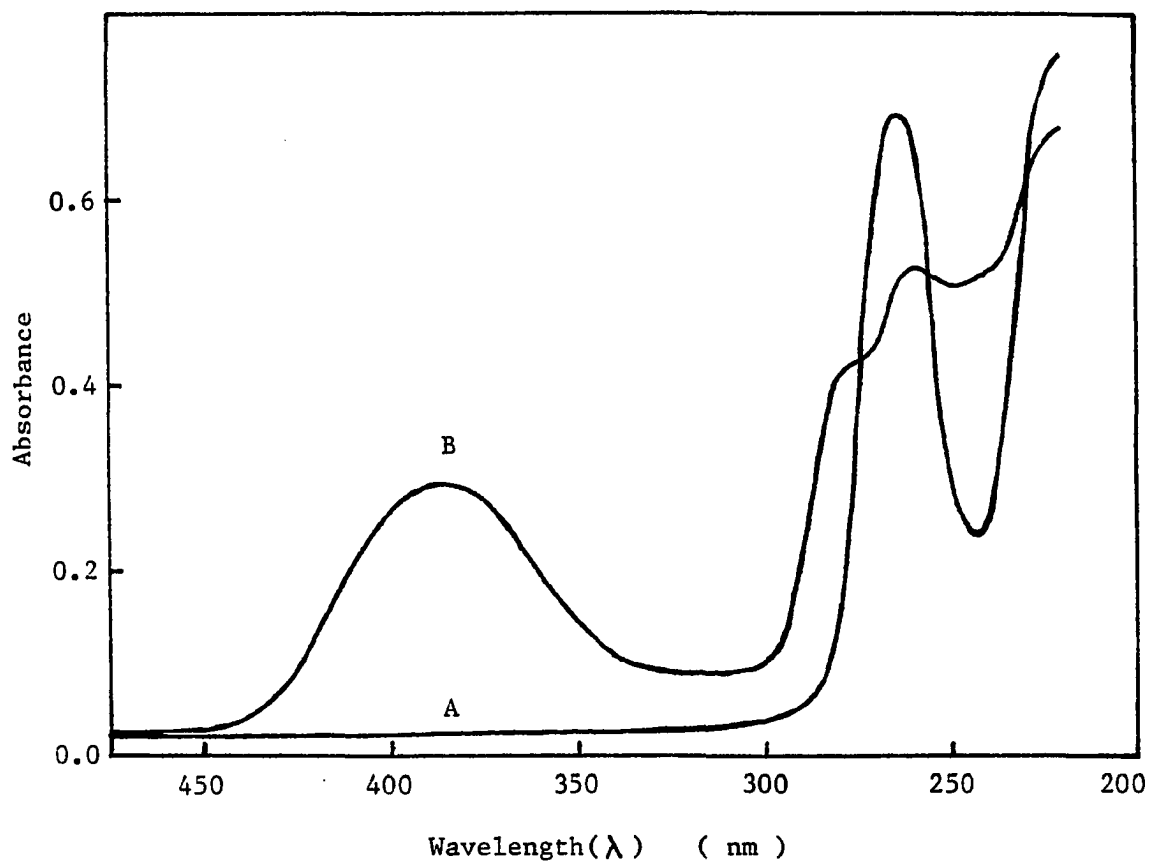


Fig. 37  
UV spectrum of 5-methyltetrahydropterin in pH 3.0 phosphate buffer before(A) and after(B) the controlled potential electrolysis at + 0.45 V.

Spectroelectrochemical Study for the Intermediate Detection

A typical u.v. spectrum obtained prior to electrolysis of 5-methyltetrahydropterin at pH 3.0 at RVC electrode in a thin-layer cell is shown in curve A of Fig. 38. The  $\lambda_{\text{max}}$  values occur at 218 nm and 266 nm. Upon application of a potential of +0.5 V the u.v. peak at 218 nm decreases with time and shifts towards a longer wavelength. Correspondingly, the UV peak at 266 nm increases with time and also shifts towards longer wavelengths.

The trace B in Fig. 38 represents the spectrum of an exhaustively electrolyzed 5-methyltetrahydropterin solution. When the potential was turned off the final trace barely changed with respect to time, and this strongly suggests that the lifetime of the possible intermediate is very short.

Most methyl derivatives of 5,6,7,8-tetrahydropterin exhibit two maximum absorption bands around (215-225)nm and (264-275)nm in acidic pH<sup>195</sup>, and the two  $\lambda_{\text{max}}$  for the corresponding dihydropterins generally shift towards longer wavelength<sup>203,204</sup>. This also suggests that the product of this short term electrolysis likely be a dihydropterin.

A u.v. spectrum obtained prior to electrolysis at pH 8.0 is shown in curve A of Fig. 39 where two absorption maxima are observed at 220 nm and 285 nm. As the electrolysis proceeds, the two peaks disappear, and correspondingly a new absorption band appears and grows ( $\lambda_{\text{max}} = 245$  nm). The latter peak reaches a maximum (trace B) and then it also decreases. This strongly supports the view that upon electrochemical oxidation of 5-methyltetrahydropterin in basic pH (pH 8), an unstable intermediate absorbing at 245 nm is formed.

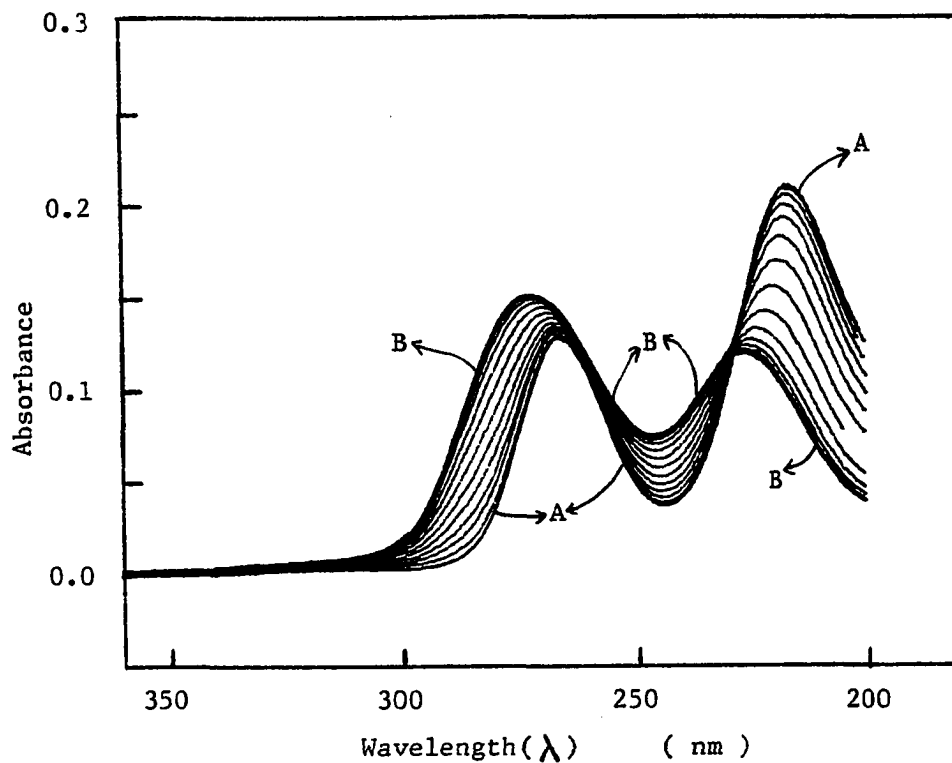


Fig. 38

UV spectrum of 10.0 mM 5-methyltetrahydropterin solution electrolyzing at +0.50 V in pH 3.0 phosphate buffer at a graphite electrode in a thin layer spectroelectrochemical cell. Trace A is the spectrum before the electrolysis and trace B is the spectrum of an exhaustively electrolyzed solution.

Repetitive scans are 5.0 seconds.

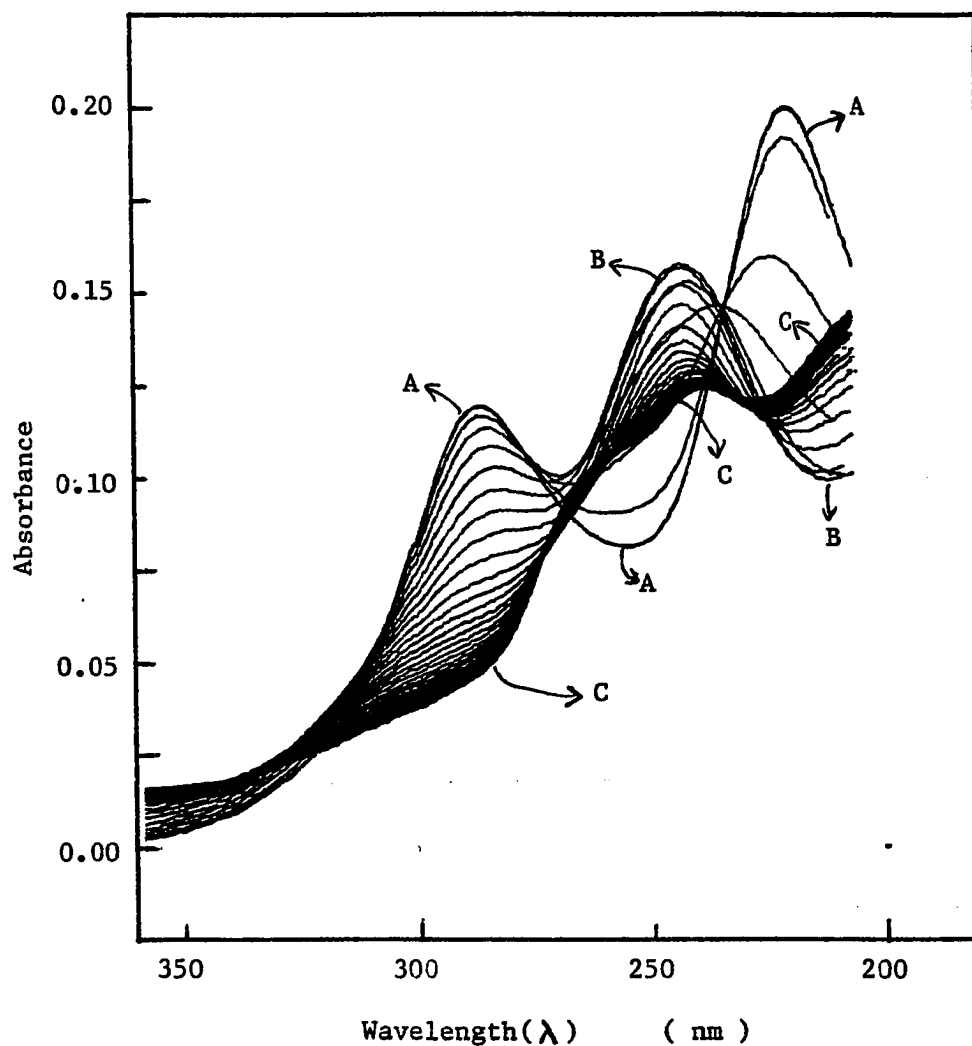


Fig. 39  
UV spectrum of 10.0 mM 5-methyltetrahydropterin solution electrolyzing at + 0.15 V in pH 8.0 phosphate buffer at a graphite electrode in a thin layer spectroelectrochemical cell. Trace A is the spectrum before the electrolysis, trace B is the spectrum of the intermediate, and trace C is that of the exhaustively electrolyzed solution. Repetitive scans are 5.0 seconds.

Curve C in Fig. 39 is the spectrum of an exhaustively electrolyzed 5-methyltetrahydropterin solution at a time when all of the u.v.-absorbing intermediate has disappeared. The first order rate constant ( $k_1$ ) for the decay of this intermediate is ca.  $1.9 \times 10^{-3} \text{ sec}^{-1}$ , which corresponds to the half life of ca. 364 sec.

#### Isolation of Products

The yellow solution of oxidation products of 5-methyltetrahydropterin in pH 3 phosphate buffer was lyophilized to give yellow solid, and a dual G-10 column was used to separate the products from the salts, namely phosphate and chloride (Fig. 40).

Complete removal of salts from the product was not yet possible with this separation method. However, a mass spectrum (direct insertion, detector voltages at 70 eV) of the impure yellowish brown solid, which was very hygroscopic, was obtained (Fig. 41) and it was quite reproducible. It is not very clear at present whether the 98 (m/e) peak is due to a molecular ion or a fragment ion, although a mass spectrum (Fig. 42) of GC/MS of silylated products seemingly suggest that the 98 (m/e) peak can be indeed due to the molecular ion which has three replaceable hydrogens. It is necessary to run MS at a lower energy (12 eV) to confirm the 98 (m/e) peak.

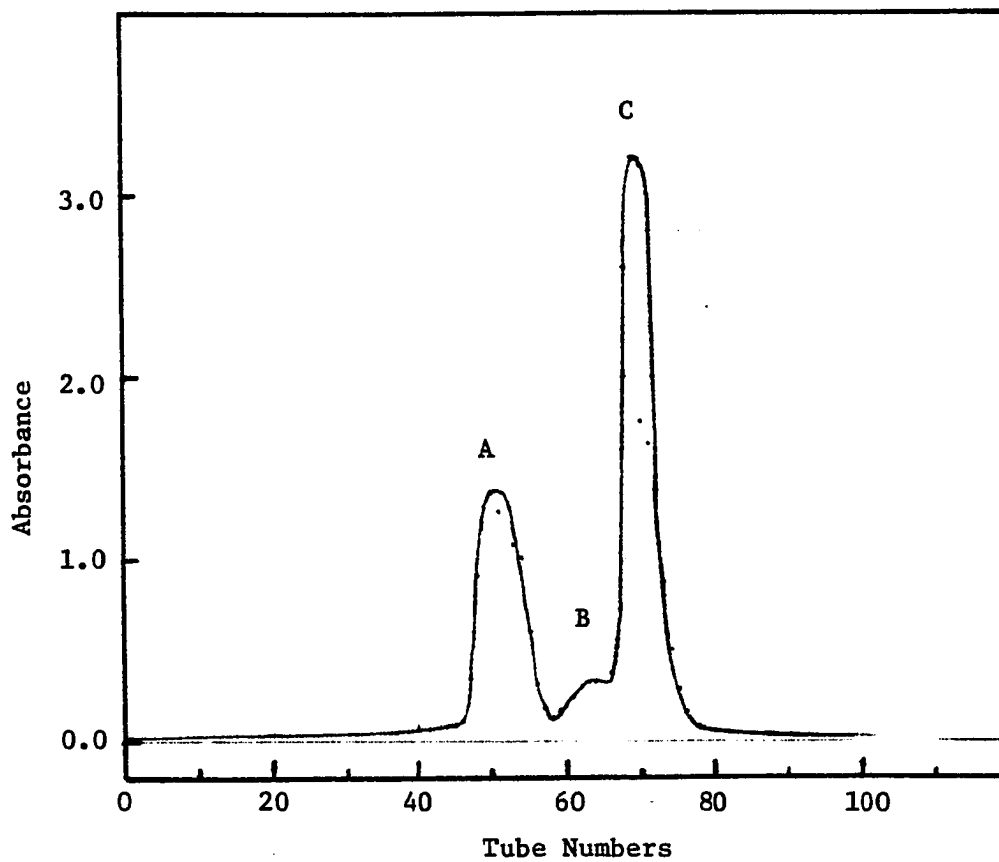


Fig. 40

Liquid chr matogram of the oxidation products of 10.0 mg of 5-methyl-tetrahydropterin in pH 3.0 phosphate buffer electrolyzing at + 0.45 V ( vs. SCE ) and seperated in a dual column, single system of Sephadex G-10 which was eluted with doubly distilled water. Flow rate was set at 20 ml/hr and the UV absorption was monitored at 200 nm. Peak A ; phosphate, Peak B ; chloride, Peak C ; yellow product.

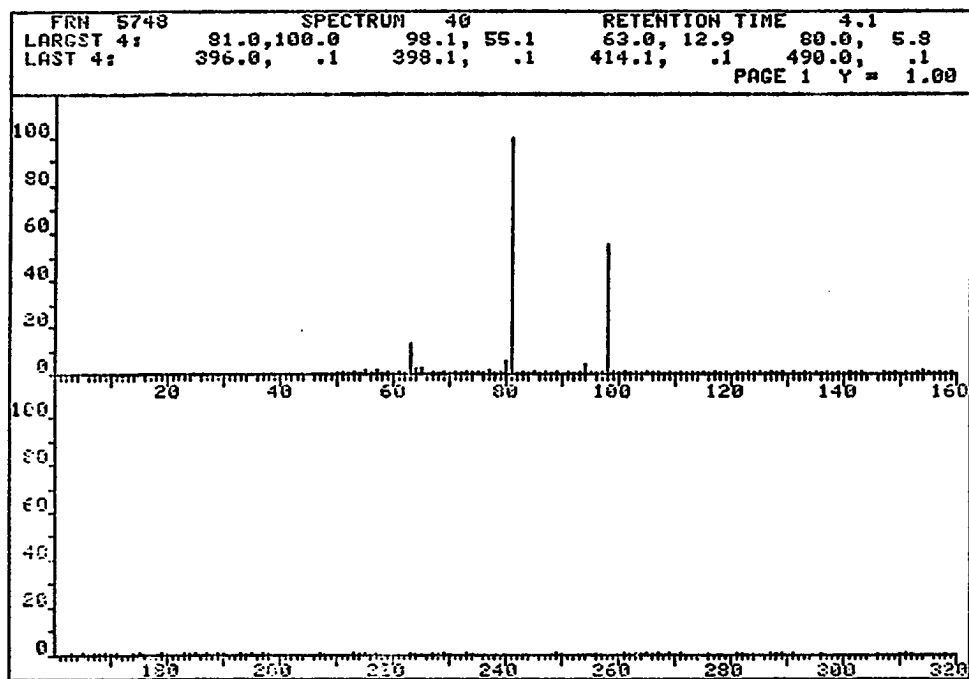


Fig. 41  
 Mass spectrum ( direct insertion, 70 eV ) of electrolysis product  
 of 5-methyltetrahydropterin in pH 3.0 phosphate buffer.

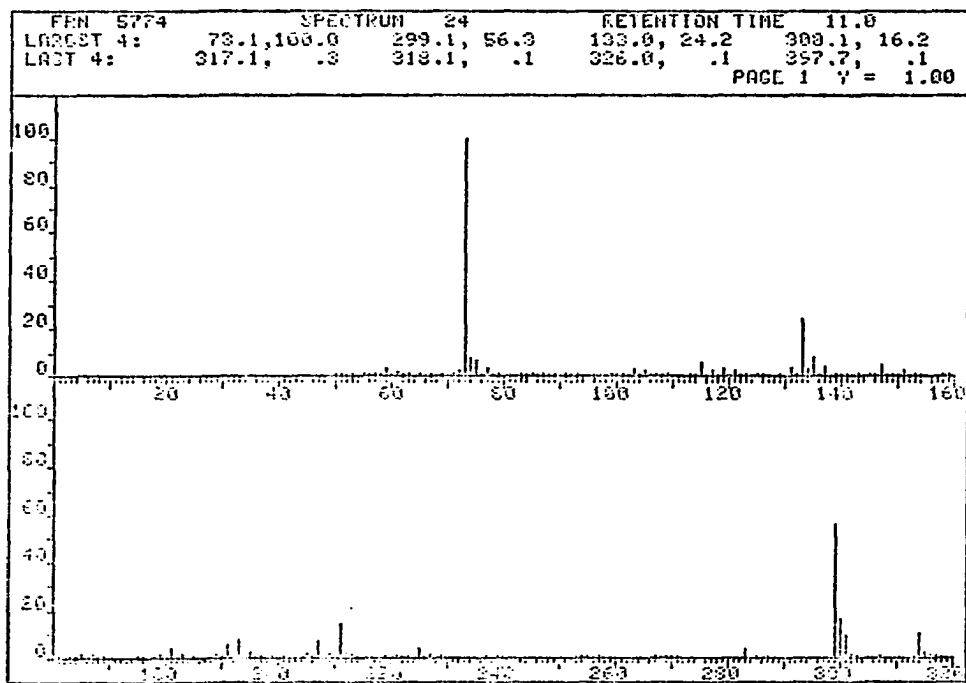
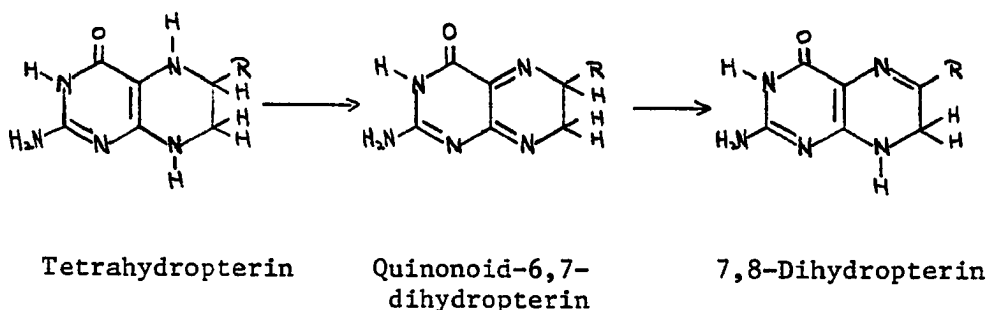


Fig. 42  
 Mass spectrum ( GC/MS ) of the silylated electrolysis product  
 of 5-methyltetrahydropterin in pH 3.0 phosphate buffer.

Possible Reaction Scheme

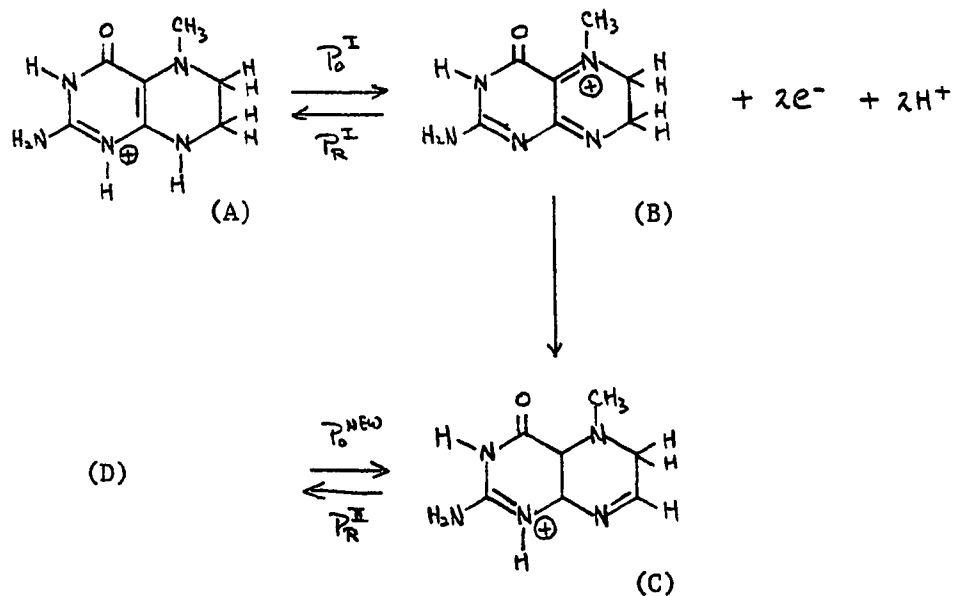
It has been suggested that quinonoid dihydropterins are the initial, unstable dihydro products of non-enzymatic oxidation of tetrahydropterins.<sup>205-209</sup> A substantial amount of evidence indicates that this labile intermediate rapidly rearranges to the more stable 7,8-dihydropterin.



Archer and Scrimgeour,<sup>206</sup> for example, oxidized 6,7-dimethyl-5,6,7,8-tetrahydropterin with ferricyanide and proposed that the corresponding quinonoid-dihydropterin, which rearranges to 7,8-dihydro compound, is formed. There is also evidence that 5-methyl-5,6,7,8-tetrahydrofolic acid<sup>210</sup> and 5-methyl-6,7-diphenyl-5,6,7,8-tetrahydropterin<sup>211</sup> undergo oxidation to give corresponding quinonoid ions which either hydrate to unstable 4 $\alpha$ -hydroxy-5-methyl-5,6-dihydropterin or rearrange to 5-methyl-5,6-dihydropterin.

Therefore, it is proposed that 5-methyltetrahydropterin (A) undergoes a two electron/two proton electrochemical oxidation at PGE in pH 3 phosphate buffer. Probably the immediate product is a

quinonoid ion (B) which rapidly undergoes rearrangement to 5-methyl-5,6-dihydro compound (C) and this 5,6-dihydro compound is more difficult to reduce to a product (D) than the quinonoid ion.



Although the product of a short term electrolysis in the thin layer spectroelectrochemical cell might be 5-methyl-5,6-dihydropteridine (C), the product of a long term electrolysis under controlled potential coulometric cell is quite different from C as evidenced by UV data and the structure is yet to be elucidated.

APPENDIX

## APPENDIX

## COMPUTER PROGRAMS

- A. Program INTGN2P ; Integration of capacitance data .
- B. CRVFIT ; Fitting of background  $\eta$  vs. E data to various polynomial equations .
- C. ELCAP ; Calculation of surface tension values from the electrocapillary pressure data .
- D. ECFP ; Fitting and differentiations of raw  $\eta$  vs. E data to calculate charges and capacitance, and plotting .
- E. SDC ; Fitting of  $\pi$  vs.  $\ln c$  data to the generalized Frumkin equation, and plotting.
- F. PIRICALC ; Fitting of  $\pi$  vs.  $\ln c$  data to the empirical equation( composite of potentials ).
- G. PIRICALI ; Fitting of  $\pi$  vs.  $\ln c$  data to the empirical equation( individual potentials )

## NOTE:

- 1) Programs A, E, F and G were originally developed by Dr. Sherril D. Christian in this Department.
- 2) Programs B, C and D were originally developed by the author.
- 3) Programs B, D, E, F and G utilize a subprogram NLLSQ. NLLSQ is a non-linear least squares subroutine which may be called by WATFIV or FORTRAN from the library of the Computing Center of the University of Oklahoma. The subroutine was developed by Dr. Eric Enwall in this Department,<sup>112</sup> and the version used here was updated in May, 1976.

A. Program INTGN2P

This is a program to calculate differential capacitance from the capacitive current vs. potential curves from the phase-selective a.c. polarographic measurement, namely, this program will carry out the following ;

- 1) Calculate the differential capacitance from the raw capacitive current
- 2) Calculate the charge values by numerical integration of C vs. E curve
- 3) Calculate the surface tension values by integrating the q vs. E curve
- 4) Calculate the surface pressure values
- 5) Plot (A) C vs. E, (B) q vs. E, (C)  $\chi$  vs. E, and (D)  $\pi$  vs.  $\ln(\text{concentration})$

```
C   A PROGRAM TO INTEGRATE DIFFERENTIAL CAPACITANCE DATA.
C   CARD 1 IS TITLE. CARD 2 IS NO. OF CONCENTRATIONS, NO. OF
C   POTENTIALS THE NUMBER OF THE ECM POTENTIAL FROM THE FINAL
C   POTENTIAL , AND EITHER A 0 OR A 1 DENOTING USE OF 1 CR MORE
C   CONVERSION FACTORS, RESPECTIVELY, ANOTHER 1 CR 0 DENOTING WHETHER
C   OR NOT YOU WANT A PRINT OUT OF RESULTS, AND A FINAL 1 CR 0
C   DENOTING USE OF PRINTER CF NCT. (EACH RESPECTIVELY) - 3 SPACES EACH
C   CARD 4 IS THE VALUE OF THE FINAL POTENTIAL, THEN THE POTENTIAL
C   INCREMENTS, AND THEN THE CONVERSION FACTOR, IF ONLY ONE IS USED.
C   IF MORE THAN ONE CONVERSION FACTOR IS USED, THEN THE NEXT CARDS
C   GIVE THE FACTOR'S VALUE AT EACH CONCENTRATION-10 SPACES EACH.
C   LEAVE THESE CARDS OUT IF ONLY ONE FACTOR IS USED. THE NEXT CARDS
C   ARE THE VARIOUS CONCENTRATIONS-10 SPACES EACH. FINALLY, THE
C   VOLTAGE READINGS ARE GIVEN, BEGINNING WITH THE FINAL POTENTIAL,
C   6 SPACES EACH, AND A NEW CARD FOR A NEW CONCENTRATION. THE
C   BACKGROUND MUST BE THE FIRST CONCENTRATION.
C
```

```
INTEGER TITLP
```

```
DIMENSION E(40), C(30), VLTG(30,40), CAP(30,40), QBKD(30,40), TITLE(20)
```

```
*, Q(30,40), GAM(30,40), GMAX(30), PI(30,40), GG(30,40), CCNV(30)
```

```
*, VLTR(30,40), RLNC(30), RLACS(30), SS(30,40), YP(30), YQ(30), YP(30)
```

```
*, DDQ(30,40), GDQ(30,40), TITLP(20)
```

```
REAL*8 CF(30)
```

```
READ(5,100)TITLE
```

```
READ(5,100)TITLP
```

```
100 FORMAT(20A4)
```

```
READ(5,101) LC,LE,NECM,MNCCNV,IPRINT,IPLCT
```

```
101 FORMAT(10I3)
```

```
READ(5,102)FNLPTOT,POTINC,SICNV, QIONE,GIONE
```

```
102 FORMAT(8F10.8)
```

```
C
```

```
*****
```

```
IPRINT=0
```

```
IPRINT=1
```

```
IPLCT=0
```

```
IPLCT=1
```

```
IPNCH=1
```

```
IPNCH=0
```

```
KR=1
```

```

C
*****
IF(MNCONV.EQ.0) GO TO 997
READ(5,996)(CCNV(I),I=1,LC)
996 FCRMAT(8F10.8,/,8F10.8,/,8F10.8)
GC TO 995
997 CCNTINUE
DO 994 I=1,LC
CCNV(I)=SICCNV
994 CONTINUE
995 CCNTINUE
READ(5,103) (C(I),I= 1,10), (CH(I),I= 1,10)
*, (C(I),I=11,20), (CH(I),I=11,20)
*, (C(I),I=21,30), (CH(I),I=21,30)
103 FCRMAT ( 10F7.3,T1,10A7 / 10F7.3,T1,10A7 / 10F7.3,T1,10A7 )
DC 105 I=1,LC
READ(5,104)(VLTR(I,J),J=1,LE)
104 FCRMAT(13F6.4,/,13F6.4,/,13F6.4)
105 CCNTINUE
DO 15 I= 1, LC
DO 15 J= 1, LE
KE = LE-J+1
VLTG(I, J) = VLTR(I,KE)
15 CONTINUE
RLNC(1)=-9.999
DC 16 I=2,LC
RLNC(I)=ALOG(C(I))
16 CCNTINUE
DC 106 J=1,LE
E(J)=FNLPCOT+POTINC*(J-1)
106 CCNTINUE
DC 107 I=1,LC
DC 107 J=1,LE
CAP(I, J)=VLTG(I, J)*CCNV(I)
107 CCNTINUE
QEKD(1,1)=0
DC 108 J=2,LE
DQEKD=(CAP(1,J)+CAP(1,J-1))*0.5*(E(J)-E(J-1))
QEKD(1, J)=QEKD(1, J-1)+DQEKD
108 CCNTINUE
DC 109 I=1,LC
Q(I,1)=-26.21239
Q(I,1)=-24.21
Q(I,1)= QIDNE
DC 109 J=2,LE
DQ=(CAP(I, J)+CAP(I, J-1))*0.5*(E(J)-E(J-1))
Q(I, J)=Q(I, J-1)+DQ
109 CCNTINUE
DC 110 I=1,LC
GAM(I,1)=0
DC 110 J=2,LE
DGAM=(Q(I, J)+Q(I, J-1))*5.0*(E(J)-E(J-1))
GAM(I, J)=GAM(I, J-1)+DGAM
IF(DGAM.LT.0) GMAX(I)=GAM(I, J-1)+DGAM
110 CCNTINUE

```

```

DC 111 I=1,LC
DC 111 J=1,LE
PI(I,J)=GAM(I,J)-GAM(1,J)
DDQ(I,J)= G(I,J) - Q(I,J)
111 CCNTINUE
DC 112 I=1,LC
DC 112 J=1,LE
GG(I,J)=GAM(I,J)-GMAX(I)
      GAM(I,J)= SIGNE-GAM(I,J)
112 CCNTINUE
IF(IPRINT.EQ.0) GO TO 1999
C ***** PRINT ROUTINE
C
C ***** GRAND OUTPUT
      WRITE(6,113) TITLE
113 FCRMAT(1H1,20A4)
      WRITE(6,114) LC,LE,FNLPCT,PCINC
114 FCRMAT(///,1X,' NUMBER OF CCNCENTRATIONS= ',I2,/,
*1X,' NUMBER OF PCTENTIALS= ',I2,/,1X,' PCTENTIAL OF CCINCIDENCE=
* ',F6.3,'V',///,' INTEGRATICN INCREMENTS= ',F6.3,'V',/)
899 CCNTINUE
DC 999 I=1,LC
      WRITE(6,113) TITLE
      WRITE(6,898) CCNV(I)
898 FCRMAT(/,1X,' CONVERSION FACTOR= ',F10.5)
      WRITE(6,115) C(I)
115 FCRMAT(///,26X,F7.3,1X,'MM')
      WRITE(6,116)
116 FCRMAT(//,1X,'POTENTIAL CURRENT CAPACITANCE CHARGE   PI      SRF TEN
*      G(E)      DDQ  LOG(DDQ)',/)
      DC 998 J=1,LE
      WRITE(6,117) E(J),VLTG(I,J),CAP(I,J),G(I,J),PI(I,J),GAM(I,J)
* ,GG(I,J)
117 FCRMAT( 10F9.3)
998 CCNTINUE
999 CONTINUE
C
C ***** PI      OUTPUT
C
      WRITE(6,113) TITLE
      WRITE(6,64)
64 FCRMAT( 46X,'SURFACE PRESSURE' )
      WRITE(6,60) (E(40-J), J= 9,31,2)
60 FCRMAT( // , ' VOLTAGE', 6X, 12F7.3 )
68 FCRMAT(' C (MM)', 1X, ' LN C' )
      PRINT 67,(GG(1,40-I),I= 9,31,2)
67 FCRMAT( ' G(E)', 9X, 12F7.3)
      PRINT 63
63 FCRMAT(F8.3, 9X, 10F7.2 )
      DD 600 I=1,LC
      WRITE(6,65) C(I),RLNC(I),(PI(I,40-J),J= 9,31,2)
65 FCRMAT( F8.3, F7.3, 12F7.3 )
600 CCNTINUE

```

```

WRITE(6,60) (E(J), J= 1,12 )
PRINT 67 ,(GG(1,I),I= 1,12 )
PRINT 68
DO 601 I=1,LC
WRITE(6,65 ) C(I),RLNC(I),(PI(I,J),J= 1,12 )
601 CONTINUE
WRITE(6,113) TITLE
WRITE(6,64)
WRITE(6,60) (E(J), J=19,30,1)
PRINT 67 ,(GG(1,I),I=19,30,1)
PRINT 68
DO 602 I=1,LC
WRITE(6,65 ) C(I),RLNC(I),(PI(I,J),J=19,30,1)
602 CONTINUE
C
1999 CONTINUE
C
C ***** PUNCH ROUTINE
IF(IPNCH.EQ.0) GOTO 799
71 FORMAT( 9F7.3)
WRITE(7,71) (E(32-J),J= 5,21,2)
WRITE(7,71) (GG(1,32-J), J= 5,21,2)
73 FORMAT( 9F7.3, 1X, F7.3, ' U DC ' )
DC 703 I= 1,LC
WRITE(7,73) (PI(I,32-J),J= 5,21,2), C(I)
703 CONTINUE
799 CONTINUE
C
IF(IPLCT.EQ.0) GO TO 2999
C **** PLCT ROUTINE
CALL SETMSG( 30, ' 29 INCH FLCTTER, PLEASE ' )
CALL SETMSG( 30, ' PREFER BLACK BALLPOINTED PEN ' )
C
C THE GRAND FLCT ROUTINE
DC 1133 J=1,LC
YP(I)= 4.2-0.2*(I-1.)
YR(I)= 7.5-0.2*(I-1.)
SS(I,J)= (PI(I,J) + 5.0) / 5.0
FLNCS(I)=(RLNC(I)+4.5)/1.5
1133 CONTINUE
C
CALL PLCT(0.0,- 6.0,-3)
CALL PLCT(0.0, 1.0,-3)
CALL PLCT(0.0, 4.0,-3)
CALL SYMBCL ( 0.0, -1.0, 0.49, '+' ,0.0, 1 )
CALL SYMBCL ( 8.5, -1.0, 0.49, '+' ,0.0, 1 )
CALL SYMBCL ( 17.0, -1.0, 0.49, '+' ,0.0, 1 )
CALL SYMBCL ( 17.0, 10.0, 0.49, '+' ,0.0, 1 )
CALL SYMBCL ( 8.5, 10.0, 0.49, '+' ,0.0, 1 )
CALL SYMBCL ( 0.0, 10.0, 0.49, '+' ,0.0, 1 )
CALL SYMBCL ( 0.0, 21.0, 0.49, '+' ,0.0, 1 )
CALL SYMBCL ( 8.5, 21.0, 0.49, '+' ,0.0, 1 )
CALL SYMBCL ( 17.0, 21.0, 0.49, '+' ,0.0, 1 )

```

```

C          ***** SURFACE TENSION VS. POTENTIAL
CALL OFFSET( 0.0,-0.3,280.0,20.0)
CALL PLCT( 1.50, 0.0, -3 )
DC 3331 K=1,KR
CALL AXIS(0.0,0.0,29H POTENTIAL ( VCLTS VS. SCE ) , -29.6,0.0,0.0,
*0.0,-0.3 )
CALL AXIS(0.0,0.0,26HSURFACE TENSICNS (DYNE/CM),26,9.0,90.0,
* 280.0,20.0 )
CALL PLCT ( 0.0, 9.0, 3 )
CALL PLCT ( 6.0, 9.0, 2 )
CALL PLCT ( 6.0, 0.0, 2 )
CALL PLCT ( 0.0, 0.0, 3 )
CALL SYMBOL (1.0,4.5, 0.1, 21H FROM TOP TO BOTTOM ,0.0, 21 )
CALL SYMBOL ( 1.0, YP(1), 0.1, ' MILLIMOLE ', 0.0, 18)
DC 2000 I=1,LC
CALL SYMBOL ( 1.0, YP(I), 0.1, CH(I), 0.0, 8 )
CALL PLCT(E(I),GAM(I,1),13)
DC 1500 J=2,LE
1500 CALL PLCT ( E(J),GAM(I,J),12)
2000 CONTINUE
XPT=1.0
YPT=5.0
HTT=0.15
CALL SYMBOL(XPT,YPT,HTT, TITLP , 0.0,18 )
3331 CONTINUE
C          ***** SURFACE PRESSURE VS. LN(CONC)
CALL PLCT(0.0,0.0, 3)
CALL PLOT( 8.5,0.0, -3)
DC 3332 K=1,KR

CALL AXIS(0.0,0.0,19H LN CCNTRATION , -19.6,0.0,0.0, -4.5,1.5 )
CALL AXIS(0.0,0.0,26HSURFACE PRESSURE (DYNE/CM),26,9.0,90.0,
*-5.0,5.0)
CALL PLCT ( 0.0, 9.0, 3 )
CALL PLCT ( 6.0, 9.0, 2 )
CALL PLCT ( 6.0, 0.0, 2 )
CALL PLCT ( 0.0, 0.0, 3 )
DO 1100 J=13,27,2
JS=(J/2)-6
JG=(J-3)/2
YQ(JG)= 7.0 - 0.2*(JG- 1)
CALL SYMBOL( 1.0, YQ(JG),0.1, JS, 0.0, -1 )
CALL NUMBER ( 1.5, YQ(JG), 0.1, E(J), 0.0, 3 )
CALL SYMBOL( RLNC(2),SS(2,J),0.1,JS,0.0,-1)
DC 2100 I=3,LC
2100 CALL SYMBOL( RLNC(I),SS(I,J),0.1,JS,0.0,-1)
1100 CONTINUE
CALL SYMBOL (1.2,YQ(1), 0.1, 17H VCLTS ,0.0, 17)
XPT=1.5
XPT=2.0
YPT=8.0
HTT=0.15
CALL SYMBOL(XPT,YPT,HTT, TITLP , 0.0,18 )
3332 CONTINUE
CALL PLCT(20.0, 3.0, 3)

```

```

C          ***** CHARGE DENSITY VS. PCTENTIAL
CALL CFFSET(0.0,-0.3,-26.0, 4.0)
CALL PLCT ( -8.5,11.5,-3)
DC 3333 K=1,KR
CALL AXIS(0.0,0.0,29H PCTENTIAL ( VOLTS VS. SCE ) ,-29.6.0.0.0.
*0.0,-0.3 )
CALL AXIS(0.0,0.0, 43H CHARGE DENSITY ( MICROCOULOMBS / SQ. CM ) ,
*43.9.0,90.0,-26.0, 4.0)
CALL PLCT ( 0.0, 9.0, 3 )
CALL PLCT ( 6.0, 9.0, 2 )
CALL PLCT ( 6.0, 0.0, 2 )
CALL SYMBOL ( 4.0, YR(1), 0.1, ' MILLIMCLE ', 0.0, 18)
DC 2200 I=1,LC
CALL SYMBOL ( 4.0, YR(I), 0.1, CH(I), 0.0, 8 )
CALL PLCT ( E(1), Q(I,1),13 )
DC 1200 J=2,LE
1200 CALL PLCT ( E(J), Q(I,J),12 )
2200 CONTINUE
XPT=1.5
YPT=8.0
HTT=0.21
CALL SYMBOL(XPT,YPT,HTT, TITLP , 0.0,18 )
3333 CONTINUE
C          ***** DIFFERENTIAL CAPACITANCE VS. PCT
C
CALL CFFSET(0.0,-0.3, 0.0, 8.0)
CALL PLCT ( 8.5, 0.0,-3)
DC 3334 K=1,KR
CALL AXIS(0.0,0.0,29H PCTENTIAL ( VOLTS VS. SCE ) ,-29.6.0.0.0.
*0.0,-0.3 )
CALL AXIS(0.0,0.0,45H DIFFERENTIAL CAPACITANCE ( MICROFARADS/SQ.CM)
*,45.9.0,90.0, 0.0, 8.0)
CALL PLCT ( 0.0, 9.0, 3 )

CALL PLCT ( 6.0, 9.0, 2 )
CALL PLCT ( 6.0, 0.0, 2 )
CALL SYMBOL ( 2.0, YR(1), 0.1, ' MILLIMCLE ', 0.0, 18)
DC 2300 I=1,LC
CALL SYMBOL ( 2.0, YR(I), 0.1, CH(I), 0.0, 8 )
CALL PLCT ( E(1),CAP(I,1),13 )
DC 1300 J=2,LE
1300 CALL PLOT ( E(J),CAP(I,J),12 )
2300 CONTINUE
XPT=1.0
YPT=8.0
HTT=0.21
CALL SYMBOL(XPT,YPT,HTT, TITLP , 0.0,18 )
3334 CONTINUE
CALL PLCT(0.0,0.0,999)
C
2999 CONTINUE
STCP
END

```

B. Program CRVFIT

This is the program to fit surface tension vs. potential data for the background electrolyte solutions to a various type of polynomial equation, and it will also calculate charge and capacitance values by single and double differentiation of the equation.

```

$JOB
1      IMPLICIT REAL*8 (A-H,C-U,W-Z)
2      DIMENSION X(200,10),Y(200),B(10),IB(10),TITLE(10),JJ(10)
3      1000 CONTINUE
4      DO 1 K=1,10
5          1 IB(K)=0
6          READ(5,102,END=999) TITLE
7          WRITE(6,103) TITLE
8          READ (5,100)NO,NP,NCM,M,ID,IP
9          WRITE(6,105)NC,NP,NCM,M,ID,IP
10         IF(NC.EQ.0 ) STOP
11         NNP=IABS(NP)
12         NNC=IABS(NC)
13         MM =IABS( M)
14         NPA=NNP-NCM
15         IF(NCM.LE.0 ) GOTC 3
16         READ (5,100) (JJ(K),K=1,NCM)
17         WRITE(6,104) (JJ(K),K=1,NOM)
18         DO 2 K=1,NCM
19             KK=JJ(K)
20             2 IB(KK)=1
21             3 IF(IP.EQ.0 ) READ (5,101) (B(K),K=1,NNP)
22             IF(IP.EQ.0 ) WRITE(6,106) (B(K),K=1,NNP)
23             IF(NC.LT.0 ) GOTC 9
24             DO 410 J=1,NNC
25                 X(J,1)=-0.2-0.05*(J-1)
26                 IF (X(1,1).NE.-0.2) WRITE(6,888)
27             410 CONTINUE
28             READ 51,(Y(J),J=1,NC)
29             51 F0FMAT( 23X ,6F6.2,/,F5.2,9F6.2,/,F5.2,9F6.2,/,F5.2,9F6.2 )
30             5 CONTINUE
C          END DATA MASSAGE
31             9 CONTINUE
32             Y(200)= NNP-NGM
33             CALL NLLSQ(X,Y,B,IB,NP,NNC,M,IRET)
34             GOTO 1000
35         999 STCP
36         100 F0FMAT (25I3)
37         101 F0FMAT(8F10.0)
38         102 F0FMAT(10A8)
39         103 F0FMAT('1',10A8,/)
40         104 F0FMAT(' INVARIANT PARAMETER SUBSCRIPTS ',10I3)
41         105 F0FMAT(' NC=',I3,' NP=',I3,' NCM=',I3,' M=',I3,' D=',I3,' IP=',I3)
42         106 F0FMAT(' INITIAL PARAMETER VALUES',/,2(2X,5(1PD11.3)),/)
43         888 F0FMAT(1H1,10X,'YOUR INITIAL POTENTIAL MAY BE IN ERROR')
44         END

```

```

45     SUBROUTINE YCALC(X,Y,B,YC,WDEL,I)
46     IMPLICIT REAL*8 (A-H,C-Z)
47     DIMENSION X(200,10),Y(200), B(10)
C       YCALC ROUTINE SPECIFIC TO RUN
48     NPA= Y(200)
49     YC=B(2)
50     X(I,2)=0.
51     X(I,3)=0.
52     DO 51 J=3,NPA
53     Z=J-1
54     CCEFF=Z*(Z-1.)
55     X(I,2)=X(I,2)+Z*B(J)*(X(I,1)-B(1))**(J-2)/(-10.)
56     X(I,3)=X(I,3)+CCEFF*B(J)*(X(I,1)-B(1))**(J-3)/(-10.)

```

```

57     51 YC = YC+ B(J)*(X(I,1)-B(1))**(J-1)
58     X(I,4)=B(2)-YC
59     WDEL=Y(I)-YC
60     RETURN
61     END

```

```

62     SUBROUTINE DCALC(X,Y,B,D,NP,I)
63     IMPLICIT REAL*8 (A-H,C-Z)
64     DIMENSION X(100,5),Y(100),B(10),D(10)
C     D CALC ROUTINE SPECIFIC TO RUN OR DUMMY
65     RETURN
66     END

```

\$EXEC        DATA CARDS FOLLOW THIS CARD TRAILED BY \$STCP

C. Program ELCAP

This is the program to calculate surface tension from the pressure data (obtained by the Mensor quartz manometer reading) at various potentials. It will calculate charge values by numerical differentiation and surface pressure by subtractions. It will also plot (A)  $\sigma$  vs. E, and (B)  $\pi$  vs.  $\ln(\text{concentration})$ .

```

C      PROGRAM ELCAP
C
C *****
C
C      THIS IS THE PROGRAM FOR THE CALCULATION OF THE SURFACE PRESSURE FROM
C      ELECTROCAPILLARY DATA AT VARIOUS CONCENTRATIONS OF ORGANIC COMPOUNDS.
C      IT ALSO GIVES THE G(E) VALUES,
C
C          THE CHARGE DENSITY BY DIFFERENTIATING THE SURFACE TENSIONS,
C          THE DIFFERENTIAL CAPACITANCE BY THE DOUBLE DIFFERENTIATION
C
C      THE SYMBOLS USED ARE ;
C      E (40)      ; THE          POTENTIALS
C      C (20)      ; THE CONCENTRATIONS
C      RLNC(20)   ; THE LN(C)
C      Q (20,40)  ; THE QUARTZ MENSOR PRESSURE READINGS
C      P (20,40)  ; THE CONVERSION OF THE QUARTZ MENSOR INTO TORR
C      G (20,40)  ; THE SURFACE TENSIONS
C      S (20,40)  ; THE SURFACE PRESSURES
C      HH(20)     ; THE MERCURY HEADS
C      HS(20)     ; THE SOLUTION HEADS( IE, THE BACK PRESSURE )
C
C *****
C
C      REAL*8 CH(20)
C      DIMENSION E(33),Q(20,33),P(20,33),G(20,33),S(20,33),H(20,33)
C      * , C(20), RLNC(20), GE(33)
C      * , SS(20,40),RLNCS(20)
C      * , TITLE( 20 )
C      * , TITLP( 20 )
C      * , YP(20), YU(20)
C      READ(5, 53)          TITLP
C 53 FORMAT( 20A4 )
C      READ(5,53)  TITLE
C      READ(5,54) DIA, FH, FSR, RF
C 54 FORMAT(8F10.3)
C      READ(5,52) (C(I),I= 1,10), (CH(I),I= 1,10)
C      * ,          (C(I),I=11,20), (CH(I),I=11,20)
C 52 FORMAT ( 10F7.3, T1, 10A7 / 10F7.3, T1, 10A7 )
C      LC=14
C      LC=19
C      LC=18
C      LC= 9

```

```

LE=29
  IPRNT=0
  IPRNT=1
    IPLCT=0
    IPLCT=1
      IPNCH=1
      IPNCH=J
  HS=HSF/13.6
  DC 510 I=1,LC
  READ 51. (G(1,J),J= 1,LE)
51 FORMAT( 35X ,4F6.2,/,F5.2,9F6.2,/,F5.2,9F6.2,/,F5.2,9F6.2 )
510 CONTINUE
C          *****
  RLE=LE
  RFV=RH/RLE
  DC 400 I= 1, LC
  DC 400 J= 1, LE
  H(I,J) = HF - RH*(I-1) - RFV*(J-1)
400 CONTINUE
  DC 410 J=1,LE
  ES=-0.15
  ES=-0.20
  ES=-0.30
  E(J)= ES -0.05*(J-1)
410 CONTINUE
  MC=LC- 1
  RLNC(1)=-9.999
  DO 420 I=2,LC
  RLNC(I)=ALCG(C(I))
420 CONTINUE
  DC 300 I=1,LC
  DC 300 J=1,LE
  P(I,J)=10.1e68*Q(I,J)+(5.0208*10**(-4))*Q(I,J)**2
  *-(4.32819*10**(-6))*Q(I,J)**3+H(I,J)-HS
  G(I,J)=(  DIA          )*(333.224)*P(I,J)
  S(I,J)=G(1,J)-G(I,J)
300 CONTINUE
  DC 310 J=1,LE
  GE(J)=G(1,6)-G(1,J)
  GE(J)=G(1,7)-G(1,J)
310 CONTINUE
  IF(IPRNT.EQ.0)  GOTD 899
C          *****
  DC 800 I=1,LC,2
  WRITE( 6, 90 )
  WRITE( 6, 91 ) TITLE
90 FORMAT(1H1)
91 FORMAT( 1X, 20A4, / )

```

```

PRINT 95, LC, LE, DIA, HH, RH, HS
95 FORMAT( /,2X,'LC=',I2,3X,'LE=',I2,3X,'DIA=',F9.6,3X
*, 'HH=',F6.2,3X,'RH=',F4.2,3X, 'HS=',F4.2, // )
WRITE( 6,92 ) C(I), C(I+1)
92 FORMAT( 18X,F7.3, 1X,'MM', 37X,F7.3,1X, 'MM')
WRITE(6,80)
80 FORMAT( 2(/),2( 2X,'VOLTAGE' , ' MENSOP',1X , ' PRESS',2X,
*'SRF TEN', 1X,' SF PRS',4X),//)
DC 700 J=1,LE
WRITE(6,70) E(J),Q(I,J),P(I,J),G(I,J),S(I,J)
* E(J),Q(I+1,J),P(I+1,J),G(I+1,J),S(I+1,J)
70 FORMAT( 2(F9.3,F8.3,2F9.3,F8.3,4X )
700 CONTINUE
800 CONTINUE
899 CONTINUE
C *****
WRITE( 6, 90 )
WRITE( 6, 91 ) TITLE
PRINT 95, LC, LE, DIA, HH, FH, HS
WRITE(6,61)
61 FORMAT( ' C (MM)',2X,' LN C',30X,'SURFACE TENSIONS',/
**/,20X,'-0.20V',2X,'-0.30V',2X,'-0.40V',2X,'-0.50V',2X,'-0.60V',
* 2X,'-0.70V',2X,'-0.80V',2X,'-0.90V',2X,'-1.00V',//)
DC 610 I=1,LC
WRITE(6,65 ) C(I),RLNC(I), (G(I,J),J=1,17,2)
610 CONTINUE
C *****
WRITE( 6, 90 )
WRITE( 6, 91 ) TITLE
PRINT 95, LC, LE, DIA, HH, RH, HS
WRITE(6,60)
60 FORMAT( 46X,'SURFACE PRESSURE', // , ' VOLTAGE', 11X,
* '-0.20V',2X,'-0.30V',2X,'-0.40V',2X,'-0.50V',2X,'-0.60V',
* 2X,'-0.70V',2X,'-0.80V',2X,'-0.90V',2X,'-1.00V',/ )
PRINT 62,( GE(I), I= 1,17,2)
62 FORMAT( ' GE',14X,9F8.3 )
PRINT 63
63 FORMAT(' C (MM)', 2X, ' LN C' )
DC 600 I=1,LC
WRITE(6,65 ) C(I),RLNC(I), (S(I,J),J= 1,17,2)
65 FORMAT( F8.3,F8.3,2X,9F8.3 )
600 CONTINUE
WRITE(6,66)
66 FORMAT( // , ' VOLTAGE', 11X,
* '-1.15V',2X,'-1.20V',2X,'-1.25V',2X,'-1.30V',2X,'-1.35V',
* 2X,'-1.40V',2X,'-1.45V',2X,'-1.50V',2X,'-1.55V',/ )
PRINT 62,( GE(I), I=20,28 )
PRINT 63
DC 601 I=1,LC
WRITE(6,65 ) C(I),RLNC(I), (S(I,J),J=20,28 )
601 CONTINUE

```

```

IF(IPNCH.EQ.0) GOTC 799
DO 707 I=1,LC
WRITE(7,67) (S(I,J),J=1,17.2), C(I)
67 FORMAT(9(1X,F6.3), 1X, F7.3,1X,' ')
707 CCNTINUE
799 CCNTINUE
C
IF(IPL0T.EQ.0) GOTU 2955
*****
CALL SETMSG( 30,' BLACK BALLPINTED PEN PLEASE ' )
CALL SETMSG( 30,' 29 INCH PLOTTER, PLEASE ' )
C
CO 1133 I=1,LC
YP(I)= 4.5-0.2*(I-1.)
DO 1133 J=1,LE
SS(I,J) = (S(I,J)+5.0) / 5.0
RLNCS(I)=(RLNC(I)+4.5)/1.5
1133 CCNTINUE
*****
CALL OFFSET( 0.0,-0.3,250.0,25.0)
CALL PLOT(0.0,- 6.0,-3)
CALL PLOT(0.0, 1.0,-3)
CALL SYMBCL ( 0.0, -1.0, 0.49, '+',0.0, 1 )
CALL SYMBCL ( 8.5, -1.0, 0.49, '+',0.0, 1 )
CALL SYMBCL ( 17.0, -1.0, 0.49, '+',0.0, 1 )
CALL SYMBCL ( 17.0, 10.0, 0.49, '+',0.0, 1 )
CALL SYMBCL ( 17.0, 10.0, 0.49, '+',0.0, 1 )
CALL SYMBCL ( 8.5, 10.0, 0.49, '+',0.0, 1 )
CALL SYMBCL ( 0.0, 10.0, 0.49, '+',0.0, 1 )
CALL SYMBCL ( 0.0, 21.0, 0.49, '+',0.0, 1 )
CALL SYMBCL ( 8.5, 21.0, 0.49, '+',0.0, 1 )
CALL SYMBCL ( 17.0, 21.0, 0.49, '+',0.0, 1 )
CALL PLOT( 1.50, 0.0, -3 )
CALL AXIS(0.0,0.0,29H PCTENTIAL ( VOLTS VS. SCE ) , -25.0,0.0,0.0,
*0.0,-0.3 )
CALL AXIS(0.0,0.0,0.0,26HSURFACE TENSIONS (DYNE/CM),26,9.0,90.0,
*250.0,25.0 )
CALL PLOT ( 0.0, 9.0, 3 )
CALL PLOT ( 6.0, 9.0, 2 )
CALL PLOT ( 6.0, 0.0, 2 )
CALL PLOT ( 0.0, 0.0, 3 )
CALL SYMBCL (1.0,5.0, 0.1, 21H FPCW TCP TC BOTTCW ,0.0, 21 )
CALL SYMBCL ( 1.0, YP(1), 0.1, ' MILLIMOLE ', 0.0, 18)
DC 2000 I=1,LC
CALL SYMBCL ( 1.0, YP(I), 0.1, CH(I), 0.0, 8 )
CALL PLOT(E(I),G(I,1),13)
DC 1000 J=2,LE
1000 CALL PLOT ( E(J), G(I,J),12 )
2000 CCNTINUE
XPT=1.0
YPT=8.0
HTT=0.21
CALL SYMBCL(XPT,YPT,HTT, TITLP ,0.0,18)
*****

```

```

CALL PLCT(0.0,0.0, 3)
CALL PLCT( 8.5,0.0, -3)
CALL AXIS(0.0,0.0,19F LN CONCENTRATION ,-19.6,0.0,0,-4.5,1.5 )
CALL AXIS(0.0,0.0,26HSURFACE PRESSURE (DYNE/CM),26.9,0.90,0.
*-5.0,5.0)
CALL PLCT ( 0.0, 9.0, 3 )
CALL PLCT ( 6.0, 9.0, 2 )
CALL PLCT ( 6.0, 0.0, 2 )
CALL PLCT ( 0.0, 0.0, 3 )
  LES= 5
  LET=17
DC 1100 J=LES,LET,2
  JS= J/2-LES/2
  JJ=(J-3)/2
  YQ(JJ)= 7.0 - 0.2*(JJ- 1)
CALL SYMBCL( 1.0, YQ(JJ),0.1, JS, 0.0, -1 )
CALL NUMBER ( 1.5, YQ(JJ), 0.1, E(J), 0.0, 3 )
CALL SYMBCL( RLNC(2),SS(2,J),0.1,JS,0.0,-1)
DC 2100 I=3,LC
2100 CALL SYMBCL( RLNC(I),SS(I,J),0.1,JS,0.0,-1)
1100 CONTINUE
  CALL SYMBOL (1.2,YQ(1), 0.1, 17H          VOLTS ,0.0, 17)

XPT=1.0
YPT=8.0
HTT=0.21
CALL SYMBCL(XPT,YPT,HTT,  TITLP          .0.0,18)
CALL PLCT ( 0.0, 0.0, 999 )
2999 CONTINUE
STCP
END

```

```

      MS = M
      NPS = NP
      NNOS = NNC
      NPA = NNP - NOM
      MM = IABS ( M )
      NNC = IABS ( NC )
      NNP = IABS ( NP )
      IF ( NO, 20, 0 ) STOP
      WRITE ( 6, 105 ) NO, NP, NOM, M, IO, IP
      READ ( 5, 100 ) NC, NP, NCM, M, IC, I, I
      WRITE ( 6, 103 ) TITL
      READ ( 5, 102 ) TITL
      IE ( K ) = 0
      DO 1 K = 1, 10
      IF ( L, GE, 2 ) GOTO 555
      DD 1000 L = 1, LC
      *****
      IPNCH = 1
      IPNCH = 0
      KR = 1
      KR = 2
      KR = 3
      IPLCT = 1
      IPLCT = 0
      IPRNT = 1
      IPRNT = 0
      LE = 27
      LE = 33
      LC = 1
      LC = 3
C *****
      COMMON LC, LE, CIA, HH, RT, HS
      COMMON E, C, QM, GM, H, CH
      * TITL ( 10 ), TITL ( 10 )
      * YP ( 20 ), YQ ( 20 ), YR ( 20 )
      * C ( 20 ), PLNC ( 20 ), H ( 20, 40 ), SS ( 20, 40 ), FLNCS ( 20 )
      * GE ( 20, 40 ), SP ( 20, 40 ), QQ ( 20, 40 ), CC ( 20, 40 ), GMF ( 20, 40 )
      * E ( 40 ), GM ( 20, 40 ), GF ( 20, 40 ), DL ( 20, 40 ), PR ( 20, 40 ), GM ( 20, 40 )
      DIMENSION X ( 200, 10 ), Y ( 200, 10 ), B ( 10 ), IG ( 10 ), JU ( 10 ), BS ( 10 ), IBS ( 10 )
      INTEGER TITL
      REAL*8 CH ( 20 )
      IMPLICIT REAL*8 ( A-H, C-U, W-Z )
      PFCGAM MAIN
C *****

```

This program is essentially same as the program ELGAP, but the important difference is that the raw  $\eta$  vs. E data is fitted to a polynomial eqn, and the charge and capacitance values are obtained by analytical differentiations (single and double, respectively) of the equation. It also plots (a)  $\eta$  vs. E, (b)  $\eta$  vs. ln c, (c) q vs. E, and (d) C vs. E.

D. Program ECFP

```

IF(NCM.LE.0 ) GOTO 3
READ (5,100) (JJ(K),K=1,NOM)
WRITE(6,104) (JJ(K),K=1,NOM)
DO 2 K=1,NOM
KK=JJ(K)
IB(KK)=1
    IBS(KK)= IB(KK)
2 CONTINUE
3 IF(IP.EQ.0 ) READ (5,101) (B(K),K=1,NNP)
IF(IP.EQ.0 ) WRITE(6,106) (B(K),K=1,NNP)
IF(NC.LT.0 ) GOTO 9
C ***** CALL ELCAP
CALL ELCAP
555 CONTINUE
    NNC =NNCS
    NP  =NPS
    M   =MS
    DO 5 K=1,NOM
    KK=JJ(K)
    IB(KK)=IBS(KK)
5 CONTINUE
    IF( L.EG. 1) GOTO 554
    WRITE(6,103) TITLE
    WRITE(6, 92) C(L)
    WRITE(6,105) NC,NF,NCM,M,IO,IP
    WRITE(6,104) (JJ(K),K=1,NOM)
    IF(IP.EG.0 ) WRITE(6,106) (B(K),K=1,NNP)
554 CONTINUE
C *****
DO 411 J=1,LE
X(J,1) = E(J)
411 CONTINUE
DO 510 J=1,LE
510 Y(J)= GM(L,J)
C END DATA MESSAGE
9 CONTINUE
Y(200)= NNP-NCM
C ***** CALL NLLSQ
CALL NLLSQ(X,Y,B,IB,NP,NNC,M,IRET)
DO 777 J=1,LE
GMF(L,J)=X(J,10)
    CG(L,J)=X(J,2)
    CC(L,J)=X(J,3)
    GE(L,J)=X(J,4)
    DL(L,J)=X(J,9)
777 CONTINUE
1000 CONTINUE
DO 300 I=1,LC
DO 300 J=1,LE
SP(I,J)= GMF(1,J) - GMF(I,J)
PR(I,J) = GMF(I,J)/0.002740/333.224
QF(I,J)=(PR(I,J)-H(I,J)+HS)/10.668
300 CONTINUE
RLNC(1)=-9.999

```

```

DO 420 I=2,LC
  RLNC(I)=DLOG(C(I))
420 CCNTINUE
C ***** PRINT ROUTINE
C ***** GAMMA OUTPUT
  WRITE( 6, 90 )
  WRITE( 6, 91 ) TITLE
  PRINT 95, LC, LE, DIA, HH, RH, HS
  WRITE(6,61)
61 FCRMAT( 30X, 'SURFACE TENSIONS ', // )
  WRITE(6,62) (C(I),I=1,10)
62 FORMAT( 1X, 'CONC', 12X, 10F7.3 )
96 FCRMAT( / )
  WRITE( 6, 96 )
DC 630 J=1,LE
  WRITE(6,63) E(J),(GMF(I,J),I= 1,10 )
63 FORMAT(F8.3, 9X, 10F7.2 )
630 CONTINUE
  IF(LC.LE.10.) GOTO 641
  WRITE( 6, 90 )
  WRITE( 6, 91 ) TITLE
  PRINT 95, LC, LE, DIA, HH, RH, HS
  WRITE(6,61)
  WRITE(6,62) (C(I),I=11,LC)
  WRITE( 6, 96 )
DC 640 J=1,LE
  WRITE(6,63) E(J),(GMF(I,J),I=11,LC )
640 CCNTINUE
641 CONTINUE
  IF(IPRNT.EQ.0) GOTO 899
C ***** GRAND OUTPUT
DC 800 I=1,LC
  WRITE( 6, 90 )
  WRITE( 6, 91 ) TITLE
90 FCRMAT(1H1)
91 FCRMAT( 1X, 20A4, // )
  PRINT 95, LC, LE, DIA, HH, RH, HS
95 FCRMAT( /,2X, 'LC=', I2,3X, 'LE=', I2,3X, 'DIA=', F9.6,3X
  *, 'HH=', F6.2,3X, 'RH=', F4.2,3X, 'HS=', F4.2 , // )
  WRITE( 6,92 ) C(I)
92 FCRMAT( 26X,F7.3, 1X,'MM' , / )
  WRITE(6,80)
80 FCRMAT( //, 2X, 'VOLTAGE', 6X, 'QM', 3X, 'QMF ', 5X, 'DEL', 3X,
  * 'PRESS', 6X, 'GM', 3X, 'GMFIT', 6X, 'GE', 1X, 'SRF PRS', 1X,
  * 'CHG DEN', 1X, 'DIF CAP' , / )
DC 700 J=1,LE
  WRITE(6 ,70) E(J),QM(I,J),GF(I,J),DL(I,J), PR(I,J)
  *,GM(I,J),GMF(I,J), GE(I,J), SP(I,J), QQ(I,J), CC(I,J)
70 FCRMAT( 1X, 12( 1X, F7.3 ) )
700 CONTINUE
800 CONTINUE

```

```

899 CONTINUE
C ***** PI OUTPUT
  WRITE( 6, 90 )
  WRITE( 6, 91 ) TITLE
  PRINT 95, LC, LE, DIA, HH, RH, HS
  WRITE(6,64)
64 FORMAT( 46X, 'SURFACE PRESSURE' )
  WRITE(6,60) (E(J), J= 1,23,2)

60 FORMAT( // , ' VOLTAGE', EX, 12F7.3 )
68 FORMAT( ' C (MM)', 1X, ' LN C' )
  PRINT 67,(GE(1,I),I= 1,23,2)
67 FORMAT( ' GE',11X, 12F7.3 )
  PRINT 63
  DC 600 I=1,LC
  WRITE(6,65) C(I),RLNC(I),(SP(I,J),J= 1,23,2)
65 FORMAT( F8.3, F7.3, 12F7.3 )
600 CCNTINUE
  WRITE(6,60) (E(J), J= 1,12 )
  PRINT 67 ,(GE(1,I),I= 1,12 )
  PRINT 68
  DC 601 I=1,LC
  WRITE(6,65) C(I),RLNC(I),(SP(I,J),J= 1,12 )
601 CCNTINUE
  WRITE( 6, 90 )
  WRITE( 6, 91 ) TITLE
  PRINT 95, LC, LE, DIA, HH, RH, HS
  WRITE(6,64)
  WRITE(6,60) (E(J), J=19,30,1)
  WRITE( 6, 96 )
  PRINT 67 ,(GE(1,I),I=19,30,1)
  PRINT 68
  DC 602 I=1,LC
  WRITE(6,65) C(I),RLNC(I),(SP(I,J),J=19,30,1)
602 CCNTINUE
100 FORMAT (25I3)
101 FORMAT(8F10.0)
102 FORMAT(10A4)
103 FORMAT('1',10A4,/)
104 FORMAT(' INVARIANT PARAMETER SUBSCRIPTS ',10I3)
105 FORMAT(' NC=',I3,' NP=',I3,' NOM=',I3,' M=',I3,' D=',I3,' IP=',I3)
106 FORMAT(' INITIAL PARAMETER VALUES',/,2(2X,5(1PD11.3)),/)
C ***** PUNCH ROUTINE
  IF(IPNCH.EQ.0) GOTO 799
71 FORMAT( 9F7.3)
  WRITE(7,71) (E(J),J= 5,21,2)
  WRITE(7,71) (GE(1,J), J= 5,21,2)
  DC 703 I= 1,LC
  WRITE(7,73) (SP(I,J),J= 5,21,2), C(I)
73 FORMAT( 9F7.3, 1X, F7.3, ' U PH 11 ' )
703 CCNTINUE

```

```

WRITE(7,71) (E(J),J= 4,12,1)
WRITE(7,71) (GE(1,J), J= 4,12,1)
DO 705 I= 1,LC
WRITE(7,73) (SP(1,J),J= 4,12,1), C(I)
705 CONTINUE
WRITE(7,71) (E(J),J=20,28,1)
WRITE(7,71) (GE(1,J), J=20,28,1)
DO 707 I= 1,LC
WRITE(7,73) (SP(1,J),J=20,28,1), C(I)
707 CONTINUE
799 CONTINUE
C
IF(IPLOT.EQ.0) GOTO 2999
C ***** PLCT ROUTINE
CALL SETMSG( 30, ' PREFER BLACK BALLPOINTED PEN ' )
DO 1133 I=1,LC
  YP(I)= 4.5-0.2*(I-1.)
  YR(I)= 7.5-0.2*(I-1.)
DC 1133 J=1,LE
SS(1,J)= (SP(1,J) + 4.0) / 4.0
RLNCS(I)=(RLNC(I)+4.5)/1.5
1133 CONTINUE
C
CALL PLOT(0.0,- 6.0,-3)
CALL PLOT(0.0, 1.0,-3)
CALL PLCT(0.0, 4.0,-3)
CALL SYMBOL ( 0.0, -1.0, 0.49, '+' ,0.0, 1 )
CALL SYMBCL ( 3.5, -1.0, 0.49, '+' ,0.0, 1 )
CALL SYMBOL ( 17.0, -1.0, 0.49, '+' ,0.0, 1 )
CALL SYMBCL ( 17.0, 10.0, 0.49, '+' ,0.0, 1 )
CALL SYMBCL ( 8.5, 10.0, 0.49, '+' ,0.0, 1 )
CALL SYMBOL ( 0.0, 10.0, 0.49, '+' ,0.0, 1 )
CALL SYMBCL ( 0.0, 21.0, 0.49, '+' ,0.0, 1 )
CALL SYMBOL ( 8.5, 21.0, 0.49, '+' ,0.0, 1 )
CALL SYMBCL ( 17.0, 21.0, 0.49, '+' ,0.0, 1 )
C ***** SURFACE TENSION VS. POTENTIAL
CALL OFFSET( 0.0,-0.3,250.0,20.0)
CALL PLCT( 1.50, 0.0, -3 )
DC 3331 K=1,KR
CALL AXIS(0.0,0.0,29H POTENTIAL ( VOLTS VS. SCE ) ,-29,6.0,0.0,
*0.0,-0.3 )
CALL AXIS(0.0,0.0,26HSURFACE TENSIONS (DYNE/CM),26,9.0,90.0,
*250.0,20.0 )
CALL PLCT ( 0.0, 9.0, 3 )
CALL PLOT ( 6.0, 9.0, 2 )
CALL PLCT ( 6.0, 0.0, 2 )
CALL PLOT ( 0.0, 0.0, 3 )
CALL SYMBOL (1.0,4.8, 0.1, 21H FROM TOP TO BOTTOM ,0.0, 21 )
CALL SYMBOL ( 1.0, YP(I), 0.1, ' MILLIMCLE ', 0.0, 18)
DC 2000 I=1,LC
CALL SYMBCL ( 1.0, YP(I), 0.1, CH(I), 0.0, 8 )
CALL PLOT(E(1),GMF(1,1),13)

```

```

DC 1500 J=2,LE
1500 CALL PLCT ( E(J),GMF(I,J),12)
2000 CCNTINUE
XPT=1.0
YPT=5.5
HTT=0.14
CALL SYMBCL(XPT,YPT,HTT, TITLP , 0.0,18 )
3331 CCNTINUE
C ***** SURFACE PRESSURE VS. LN(CONC)
CALL PLCT(0.0,0.0, 3)
CALL PLCT( 2.5,0.0, -3)
DC 3332 K=1,KR
CALL AXIS(0.0,0.0,19H LOG CONCENTRATION ,-19.6.0,0.0,-4.5,1.5 )
CALL AXIS(0.0,0.0,26HSURFACE PRESSURE (DYNE/CM),26.9.0,90.0,
*-4.0,4.0)
CALL PLOT ( 0.0, 9.0, 3 )
CALL PLCT ( 6.0, 9.0, 2 )
CALL PLCT ( 6.0, 0.0, 2 )
CALL PLCT ( 0.0, 0.0, 3 )
LES= 5
LET=17
DC 1100 J=LES,LET,2
JS= J/2-LES/2
JG=(J-3)/2
YQ(JG)= 7.0 - 0.2*(JG- 1)
CALL SYMBCL( 1.0, YQ(JG),0.1, JS, 0.0, -1 )
CALL NUMBER ( 1.5, YQ(JG), 0.1, E(J), 0.0, 3 )
CALL SYMBGL ( RLNC(2),SS(2,J),0.1,JS,0.0,-1)
DC 2100 I=3,LC
2100 CALL SYMBCL( RLNC(1),SS(1,J),0.1,JS,0.0,-1)
1100 CCNTINUE
CALL SYMBCL (1.2,YQ(1), 0.1, 17H VOLTS ,0.0, 17)
XPT=1.0
YPT=8.0
HTT=0.21
CALL SYMBCL(XPT,YPT,HTT, TITLP , 0.0,18 )
CALL SYMBCL(1,0,8.0,0.21, 18H ,0.0,18)
3332 CCNTINUE
C ***** CHARGE DENSITY VS. PCTENTIAL
CALL OFFSET(0.0,-0.3,-26.0, 4.0)
CALL PLCT ( -8.5,11.5,-3)
DC 3333 K=1,KR
CALL AXIS(0.0,0.0,29H PCTENTIAL ( VOLTS VS. SCE ) ,-29.6.0,0.0,
*0.0,-0.3 )
CALL AXIS(0.0,0.0, 43H CHARGE DENSITY ( MICROCOULCMBS / SQ. CM ) ,
*43.9.0,90.0,-26.0, 4.0)
CALL PLOT ( 0.0, 9.0, 3 )
CALL PLCT ( 6.0, 9.0, 2 )
CALL PLCT ( 6.0, 0.0, 2 )
CALL SYMBCL ( 4.0, YR(1), 0.1, ' MILLIMOLE ', 0.0, 18)

```

```

DC 2200 I=1,LC
CALL SYMBOL ( 4.0, YR(I), 0.1, CH(I), 0.0, 8 )
CALL PLCT ( E(I),QQ(I,1),13 )
DC 1200 J=2,LE
1200 CALL PLCT ( E(J),QQ(I,J),12 )
2200 CONTINUE
XPT=1.0
XPT=1.5
YPT=8.0
HTT=0.21
CALL SYMBCL(XPT,YPT,HTT, TITLP , 0.0,18 )
3333 CONTINUE
C ***** DIFFERENTIAL CAPACITANCE VS. PCT
CALL OFFSET(0.0,-0.3, 0.0,10.0)
CALL PLOT ( 8.5, 0.0,-3)
DC 3334 K=1,KR
CALL AXIS(0.0,0.0,29H POTENTIAL ( VOLTS VS. SCE ) ,-29.6.0,0.0,
*0.0,-0.3 )
CALL AXIS(0.0,0.0,45H DIFFERENTIAL CAPACITANCE (MICROFARADS/SQ.CM)
*.45,9.0,90.0, 0.0, 10.0)
CALL PLCT ( 0.0, 9.0, 3 )
CALL PLCT ( 6.0, 9.0, 2 )
CALL PLCT ( 6.0, 0.0, 2 )
CALL SYMBOL ( 2.0, YR(I), 0.1, ' MILLIMOLE ', 0.0, 18)
DO 2300 I=1,LC
CALL SYMBOL ( 2.0, YR(I), 0.1, CH(I), 0.0, 8 )
CALL PLCT ( E(I),CC(I,1),13 )
DO 1300 J=2,LE
1300 CALL PLOT ( E(J),CC(I,J),12 )
2300 CONTINUE
XPT=1.0
YPT=8.0
HTT=0.21
CALL SYMBOL(XPT,YPT,HTT, TITLP , 0.0,18 )
3334 CONTINUE
CALL PLCT ( 0.0, 0.0, 999 )
2999 CONTINUE
STOP
END

```

```

SUBROUTINE YCALC(X,Y,B,YC,NDEL,I)
IMPLICIT REAL*8 (A-H,C-Z)
DIMENSION X(200,10),Y(200), B(10)
C YCALC ROUTINE SPECIFIC TO RUN
NPA= Y(200)
YC=B(2)
X(I,2)=0.
X(I,3)=0.
DO 51 J=3,NPA
Z=J-1
COEFF=Z*(Z-1.)
X(I,2)=X(I,2)+Z*B(J)*(X(I,1)-B(1))**(J-2)/(-10.)

```

```

X(I,3)=X(I,3)+CDEFF*B(J)*(X(I,1)-B(1))**(J-3)/(-10.)
51 YC = YC+ B(J)*(X(I,1)-B(1))**(J-1)
X(I,4)=B(2)-YC
X(I,10)=YC
WDEL=Y(I)-YC
X(I, 9)=WDEL
RETURN
END

```

```

C *****
SUBROUTINE DCALC(X,Y,B,D,NP,I)
IMPLICIT REAL*8 (A-H,C-Z)
DIMENSION X(100,5),Y(100),B(10),D(10)
C CALC ROUTINE SPECIFIC TO RUN OR DUMMY
RETURN
END

SUBROUTINE ELCAP
IMPLICIT REAL*8 (A-H,C-U,W-Z)
REAL*8 CH(20)
DIMENSION E(40),GM(20,40), P(20,40),GM(20,40)
*, C(20), H (20,40),TITLE(20)
COMMON E,C,GM,GM,H ,CH
COMMON LC, LE, DIA, HH, RH, HS
READ(5,53) TITLE
53 FORMAT( 20A4 )
READ(5,54) DIA, HH, HSR, RH
54 FORMAT(8F10.3)
READ(5,52) (C(I),I= 1,10), (CH(I),I= 1,10)
*, (C(I),I=11,20), (CH(I),I=11,20)
52 FORMAT ( 10F7.3, T1, 10A7 / 10F7.3, T1, 10A7 )
HS=HSR/13.6
DC 510 I=1,LC
READ 51,(GM(I,J),J= 1,LE)
51 FORMAT( 23X ,6F6.2,/,F5.2,9F6.2,/,F5.2,9F6.2,/,F5.2,9F6.2 )
510 CCNTINUE
RLE=LE
RFV=RH/RLE
DC 400 I= 1, LC
DC 400 J= 1, LE
F(I,J) = HH - RH*(I-1) - RFV*(J-1)
400 CCNTINUE
DC 410 J=1,LE
E(J)=-0.2-0.05*(J-1)
410 CCNTINUE
DC 300 I=1,LC
DC 300 J=1,LE
P(I,J)=10.1668*GM(I,J)+(0.00050208)*(GM(I,J)**2)
* -0.00000432819*(GM(I,J)**3) +H(I,J) -HS
GM(I,J)=( DIA )*(333.224)*P(I,J)
300 CCNTINUE
RETURN
END

```

E. Program SDC

This is the program to fit  $\pi$  vs.  $\ln c$  at various potentials to the generalized Frumkin isothermal equation in order to obtain  $\Theta, \alpha, B_0, \Gamma_{MRT}, C'$  and  $E_N$ .

```

C      PROGRAM MAIN
      IMPLICIT REAL*8 (A-H,C-U,W-Z)
      DIMENSION P(20,10),C(20),E(10),G(10),PN(20,10),PNS(20,10)
      *, RN(20,10),RNS(20,10), YP(20), TITLP(10)
      *, X(200,10),Y(200), E(10),IE(10),TITLE(10),JJ(10)
      COMMON RNECM
      LC=12
      LC=13
      LC=4
      LC=11
      LE=7
      LE=8
      IPLCT=0
      IPLOT=1
      L=1
1000  CONTINUE
      DC 1 K=1,10
      1  IB(K)=0
      READ(5,102,END=999) TITLE
      READ(5,102) TITLP
      WRITE(6,103) TITLE
      READ(5,100)NC,NP,NOM,M,IO,IP
      WRITE(6,105)NC,NP,NOM,M,IO,IP
      IF(NOM.EQ.0) STOP
      NNP=IABS(NP)
      NNC=IABS(NC)
      MM =IABS( M)
      NPA=NNP-NCM
      IF(NOM.LE.0) GOTO 3
      READ(5,100)(JJ(K),K=1,NCM)
      WRITE(6,104)(JJ(K),K=1,NCM)
      DC 2 K=1,NCM
      KK=JJ(K)
      2  IB(KK)=1
      3  IF(IP.EQ.0) READ(5,101)(B(K),K=1,NNP)
      IF(IP.EQ.0) WRITE(6,106)(B(K),K=1,NNP)
      IF(NC.LT.0) GOTO 9
      READ 80, RNECM
      80  FORMAT( F10.3 )
      81  FORMAT( 8F7.3, EX, F7.3 )
      READ 81, (E(I),I=1,LE)
      READ 81, (G(I),I=1,LE)
      DC 250 I= 1,LC
      READ 81,(P(I,J),J=1,LE) ,C(I)

```

```

250 CCNTINUE
  WRITE(6,21) (C(I),I= 1,LC)
21  FORMAT( / ,1X , 'CCNC(MM); ', 15F6.2, / . 11X, 15F6.2 )
  WRITE(6,22) (E(I),I= 1,LE)
22  FORMAT(1X,'VOLT( V); ', 10F6.2,/)
  DC 260 I=1,NNC
  J=(I-1)/LC+1
  K=I-(J-1)*LC
  Y(I)=P(K,J)
  X(I,1)=C(K)
  X(I,3)=E(J)
  X(I,4)=G(J)
  X(I,2)=0.5
260 CCNTINUE
C   BEGIN DATA MESSAGE THESE CARDS SPECIFIC TO GIVEN EXAMPLE
  B(6)=B(6)**.5
C   END DATA MESSAGE
  9   CCNTINUE
  CALLNLLSG(X,Y,B,IB,NP,NNC,M,IRET)
  L=L+1
  GCTC 1000
999 CCNTINUE
  DC 270 IT=1,NNC
  I=IT
  JT=(IT-1)/LC+1
  KT=IT-(JT-1)*LC
  PN(KT,JT)=X(I,9)
  RN(KT,JT)=X(I,5)
270 CCNTINUE
  DC 88 J=1,LE
  WRITE(6,120) (PN(I,J),           I=1,LC)
  88 CCNTINUE
  DC 87 J=1,LE
  WRITE(6,120) (RN(I,J),           I=1,LC)
  87 CCNTINUE
120 FORMAT(          20(1X,F5.2))
100 FORMAT (25I3)
101  FORMAT(8F10.0)
102  FORMAT(10A8)
103  FORMAT('1',10A8)
104  FORMAT(' INVARIANT PARAMETER SUBSCRIPTS ',10I3)
105  FORMAT(' NC=',I3,' NP=',I3,' NUM=',I3,' M=',I3,' D=',I3,' IP=',I3)
106  FORMAT(' INITIAL PARAMETER VALUES',/,2(5X,5(1PD15.7)),//)
  IF(IPLCT.EG.) GOTO 2999
C ***** PLCT ROUTINE
  CALL SETMSG( 30,' BLACK BALLPOINTED PEN PLEASE ' )
C ***** PI VS. LN(C) FLCT FCF HI PI  CCMPS
  NNCL=NNC-1
  DC 1233 J=1,NNC
  DC 1233 I=1,NNCL
  IF(X(I,9).LT.X(I+1,9)) GCTC 1233
  XP=X(I,9)
  X(I,9)=X(I+1,9)
  X( I+1,9)=XP
1233 CCNTINUE

```

```

DC 1234 J=1,NNO
DC 1234 I=1,NACL

IF(X(I,5).LT.X(I+1,5)) GOTC 1234
XC=X(I,5)
X(I,5)=X(I+1,5)
X(I+1,5)=XC
1234 CCNTINUE
DC 1235 I=1,NNO
  X(I,9) = (X(I,9)+5.0)/5.0
  X(I,5) = (X(I,5)+6.0)/2.0
1235 CCNTINUE
DO 1133 I=1,LC
DC 1133 J=1,LE
PNS(I,J)=( F (I,J)+5.0)/5.0
RNS(I,J)=(RN(I,J)+6.0)/2.0
1133 CCNTINUE
CALL PLCT(0.0,- 6.0,-3)
CALL PLCT(0.0, 1.0,-3)
CALL SYMBCL ( 0.0, -1.0, 0.49, '+' ,0.0, 1 )
CALL SYMBCL ( 8.5, -1.0, 0.49, '+' ,0.0, 1 )
CALL SYMBCL ( 17.0, -1.0, 0.49, '+' ,0.0, 1 )
CALL SYMBCL ( 17.0, 10.0, 0.49, '+' ,0.0, 1 )
CALL SYMBCL ( 8.5, 10.0, 0.49, '+' ,0.0, 1 )
CALL SYMBCL ( 0.0, 10.0, 0.49, '+' ,0.0, 1 )
CALL PLOT( 1.50, 0.5, -3 )
CALL AXIS(0.0,0.0,19H LN CONCENTRATION ,-19,6.0,0.0,-6.0,2.0 )
CALL AXIS(0.0,0.0,26HSURFACE PRESSURE (DYNE/CM),26,9.0,90.0,
*-5.0,5.0)
CALL PLCT ( 0.0, 9.0, 3 )
CALL PLCT ( 6.0, 9.0, 2 )
CALL PLCT ( 6.0, 0.0, 2 )
CALL PLOT ( 0.0, 0.0, 3 )
DC 1100 J=1,LE
  YP(J)= 7.0 - 0.2*(J-1)
  IF( J.EQ.1) JS=0
  IF( J.EQ.2) JS=2
  IF( J.EQ.3) JS=4
  IF( J.EQ.4) JS=1
  IF( J.EQ.5) JS=3
  IF( J.EQ.6) JS=5
  IF( J.EQ.7) JS=9
  CALL SYMBCL( 1.0, YP(J), 0.1, JS, 0.0, -1 )
  CALL NUMBER ( 1.5, YP(J) , 0.1, E(J), 0.0, 3 )
  CALL SYMBCL(RNS(I,J),PNS(I,J), 0.1, JS, 0.0, -1 )
DO 2100 I=2,LC
2100 CALL SYMBCL(RNS(I,J),PNS(I,J), 0.1, JS, 0.0, -1 )
1100 CCNTINUE
  CALL PLCT ( X(I,5),X(I,9), 3 )
  DC 3100 I=2,NNO
  CALL PLOT ( X(I,5),X(I,9), 2 )
3100 CCNTINUE

```

```

CALL SYMBCL (1.2,YP(1), 0.1, 17H          VCLTS ,0.0, 17)
XPT=0.5
YPT=5.3
HTT=0.14
CALL SYMBCL(XPT,YPT,HTT,  TITLP          ,C.0,18)
CALL PLCT ( 0.0, 0.0, 999 )
2999 CONTINUE
STOP
END

```

```

SUBROUTINEYCALC(X,Y,B,YC,WDEL,I)
IMPLICITREAL*8(4-H,C-Z)
DIMENSIONX(200,10),Y(200),E(10)
CCMMCN FNECM
C YCALC ROUTINE SPECIFIC TO RLN
CM=X(I,1)
A1=B(6)**2
IF(A1.LT.1.E-10) GO TO 600
CK=A1/1000.
AQ=X(I,1)*CK*CK
BQ=-2.*CK*X(I,1)-1.
CQ=X(I,1)
CM=-BQ-(BQ*EQ-4.*AG*CQ)**.5
CM=CM/2./AG
600 CONTINUE
CACLD=X(I,2)
CCUNT=49.
TEST=X(I,3)**2
IF(TEST.LT.0.0001)GO TO 399
XXX=X(I,3)+RNECM
ENE=10.*E(4)*XXX*(2(5)+RNECM)
EEE=9.*E(4)*XXX*XXX
PHI=(X(I,4)+ENE-EEE)/B(3)
2B=B(2)*DEXP(-PHI)
GO TO 398
399 BB=DABS(B(2))
398 CONTINUE
BB=DABS(4B)
300 R=BB*CM*DEXP(2.*E(1)*CACLD)
CCUNT=CCUNT-1.
FCTN=CACLD-R/(1.+R)
FP=1.-R*2.*E(1)/(1.+R)/(1.+F)
CANEW=CACLD-FCTN/FP
DEL=DABS(CANEW-CACLD)
CACLD=CANEW
IF(CCUNT.LT.0.) GO TO 301
IF(DEL.GT..000000001)GO TO 300
X(I,2)=CACLD
301 F=-B(3)*((DLGG(1.-CANEW)+B(1)*CANEW*CANEW)

```

```

YC=F
RES=Y(I)-F
AAA=BB*CM/B(2)
AAA=DAES(AAA)
X(I,5)=DLOG(AAA)
BBBB=DABS(B(2))
X(1,6)=-1.987*298.16*DLOG(BBBB)
X(2,6)=B(3)/(8.314*10.**7*298.16)
X(3,6)=1./(8.314*10.**7*X(2,6))
WDEL=RES
X(I,9)=YC
X(I,7)=B(3)*X(I,2)
RETURN
END

```

```

SUBROUTINE DCALC(X,Y,B,D,NP,I)
IMPLICIT REAL*8(A-H,J-Z)
DIMENSION X(100,5),Y(100),E(10),D(10)
COMMON RNECM
C CALC ROUTINE SPECIFIC TO RUN OR DUMMY
RETURN
END

```

F. Program PIRICALC

This is the program to fit  $\pi$  vs.  $\ln c$  to the model free empirical equation (eq(35)) with all potentials (composite) to evaluate  $\frac{V}{RT}$ ,  $\theta$ ,  $\alpha$ ,  $\beta$ , ... .

```

C      PROGRAM MAIN
C
C      SAMPLE MAINLINE FOR NLLSQ FIVPAK COMPRESSED
C      PIRICAL FITS PI EMPIRICALLY TO CONCENTRATION, USING LANGMUIR PLUS
C      AN ADDITIONAL TERM.  THUS, PI = B2*DLG(1.+B1*C)**RR, WHERE
C      RR=(1.+B3*C/(1.+B4*C)**2).  RIGHT NOW, B4 IS FORCED TO EQUAL
C      B1, SO A MAXIMUM OF THREE PARAMETERS SHOULD BE USED IN THE
C      FITTING EQUATION PI(C).  THIS PROGRAM CAN HANDLE DATA AT ONE POTENTIAL
C      ALONE, OR SEVERAL SIMULTANEOUSLY.  IF SEVERAL ARE FITTED, B(I)
C      VALUES (I=5,6, 10) ARE NEEDED TO "SLIDE" CONCENTRATIONS.
C      INITIAL GUESSES OF THESE MUST BE PROVIDED.  THEY WILL BE OPTIMIZED
C      IF REQUIRED, ALTHOUGH THE VERY LAST B(I) MUST BE FIXED.
C      WITH PRESENT FORMATS, THE NUMBER OF PARAMETERS MUST NOT EXCEED
C      8, BUT B(9) AND B(10) ARE FIRST SET=1 BY THE PROGRAM.  NP IS
C      CHANGED TO -9 AND NNP TO 9.  THUS, B(10) IS FIXED AT 1.0 BUT B(9)
C      WILL VARY (UNLESS IT IS ONE OF THE OMITTED PARAMETERS).
C
      IMPLICIT REAL*8(A-H,C-U,W-Z)
      DIMENSION P(20,10),C(20),E(10),G(10),PN(20,10),PNS(20,10)
      *, RN(20,10),RNS(20,10), YP(20)
      *, SA(100), SB(100)
      DIMENSION PCT(20),QW(20),CW(20),GE(20),PECM(20)
      DIMENSION X(200,10),Y(200),B(10),IB(10),TITL
      *E(10),JJ(10);1000:CONTINUE;DC1K=1,10;1:IB(K)=0;READ(5,102,END=999)
      *TITLE;WRITE(6,103)TITLE;READ(5,100)NC,NP,NCM,M,ID,IP;WRITE(6,105)N
      *C,NP,NCM,M,ID,IP;IF(NC.EQ.0)STOP;NNP=IABS(NP);NND=IABS(NC);MM=IABS
      *(M);IF(NCM.LE.0)GOTO3;READ(5,100)(JJ(K),K=1,NCM);WRITE(6,104)(JJ(K
      *),K=1,NCM);DC2K=1,NOM;KK=JJ(K);2:IB(KK)=1;3:IF(IP.EQ.0)READ(5,101)
      *(B(K),K=1,NNP);IF(IP.EQ.0)WRITE(6,106)(B(K),K=1,NNP);IF(NC.LT.0)GO
      *TO9;
C
      LC=10
      LC=15
      LE=5
C
      READ 81, (E(J),J=1,LE)
      81 FORMAT( 25X, SF7.3, 1X, F7.3 )
      DO 250 I= 1,LC
      READ 81,(P(I,J),J=1,LE) ,C(I)
      250 CONTINUE
C
      DC 246 J= 1,LE
      SA(J)= E(J)
      246 CONTINUE
      DC 247 J= 1,LE
      JI=LE-J+1
      E(JI)=SA(J)

```

```

247 CONTINUE
  DC 240 I= 1,LC
  DO 241 J= 1,LE
  SB(J)=P(I,J)
241 CONTINUE
  DO 242 J= 1,LE
  JI=LE-J+1
  P(I,JI)=SB(J)
242 CONTINUE
240 CONTINUE
C
  WRITE(6,21) (C(I),I= 1,LC)
  21 FCFMAT( / ,1X , 'CCNC(MM); ', 15F6.2, / , 11X, 15F6.2 )
  WRITE(6,22) (E(I),I= 1,LE)
  22 FCFMAT(1X,'VCLT( V); ', 10F6.2,/ )
  DO 260 I=1,NNC
  J=(I-1)/LC+1
  K=I-(J-1)*LC
  Y(I)=P(K,J)
  X(I,1)=C(K)
  X(I,2)=E(J)
260 CONTINUE
C
C BEGIN DATA MESSAGE THESE CARDS SPECIFIC TO GIVEN EXAMPLE
  IF(NNP.LT.5)GO TO 209
  NNP=9
  NP=-9
209 CONTINUE
  DC109 J=5,10
109 IF(B(J).LT..000001)B(J)=1.
  Y(101)=5,
  DC112 I=1,NNC
  II=I+100
  IF(I.LT.2)GO TO 112
  IF(X(I,1).GT.X(I-1,1))Y(II)=Y(II-1)
  IF(X(I,1).LT.X(I-1,1))Y(II)=Y(II-1) + 1.
112 CONTINUE
110 CONTINUE
C END DATA MESSAGE
  9 CONTINUE
C
  CALLNLLSG(X,Y,B,IE,NP,NNC,M,IRET);GC TO 1000;999:STCP
100 FORMAT (25I3)
101 FCFMAT(8F10.0)
102 FCFMAT(10A8)
103 FCFMAT('1',10A8)
104 FORMAT(' INVARIANT PARAMETER SUBSCRIPTS ',10I3)
105 FORMAT(' NC=',I3,' NP=',I3,' NCM=',I3,' M=',I3,' C=',I3,' IP=',I3)
106 FCFMAT(' INITIAL PARAMETER VALUES',/ ,2(5X,5(1PD15.7)))
  STCP

  END

```

```

SUBROUTINE YCALC(X,Y,B,YC,MODEL,I):IMPLICIT REAL*8(A-H,C-Z)
DIMENSION X(200,10),Y(200),B(10)
YC=DCALC FCUTLINE SPECIFIC TC RUN
I1=100+I
J=Y(I1)+.00001
B(J)=DABS(B(J))
BB=B(J)
B(1)=DABS(B(1))
E1=DABS(B(1))
B2=DABS(B(2))
C=X(1,1)*BB
C=DABS(C)
X(1,5)=DLGC(C)
F=B2*DLGC(1.+B1*C)
BG=DABS(B(3))
IF(BG.LT..000001)FF=1.
IF(BG.LT..0001)GD TC 999
RR=1.+B(3)*C/(1.+E1*C)**2
FR=RR+B(4)*C/(1.+B1*C)**3
F=FF*RR
999 C=C*1.001
FF=B2*DLGC(1.+B1*C)
BG=DABS(B(3))
IF(BG.LT..000001)GG TC 888
IF(EG.LT..0000)GG TC 888
RR=1.+B(3)*C/(1.+B1*C)**2+B(4)*C/(1.+B1*C)**3
IF(BG.LT..0000)GG TC 888
988 FF=FF*RR
X(1,4)=(FF-F)/.001
X(1,3)=X(1,4)/R(2)
YC=F
RES=Y(1)-F
WDEL=RES
RETURN;END

SUBROUTINE DCALC(X,Y,B,D,NP,I):IMPLICIT REAL*8(A-H,C-Z)
DIMENSION X(100,5),Y(100),B(10),D(10)
DCALC FCUTLINE SPECIFIC TC RUN CR DUMMY
RETURN;END

```

C

C

C

G. Program PIRICALI

This is the program to fit  $\pi$  vs.  $\ln c$  at individual potentials to the model free empirical equation (eqn(35)) in order to obtain  $\theta$ ,  $\pi$ ,  $RT$ ,  $\alpha$ , and  $\beta$ .

```

C
C PROGRAM MAIN
C
C SAMPLE MAINLINE FOR NLLSQ FIVPAK COMPRESSED
C PIRICAL FITS PI EMPIRICALLY TO CONCENTRATION, USING LANGMUIR PLUS
C AN ADDITIONAL TERM.  THUS, PI = B2*DLOG(1.+B1*C)*RR, WHERE
C RF=(1.+B3*C/(1.+B4*C)**2),  RIGHT NOW, B4 IS FORCED TO EQUAL
C B1, SO A MAXIMUM OF THREE PARAMETERS SHOULD BE USED IN THE
C FITTING EQUATION PI(C).  THIS PROGRAM CAN HANDLE DATA AT ONE POTENTIAL
C ALONE, OR SEVERAL SIMULTANEOUSLY.  IF SEVERAL ARE FITTED, B(I)
C VALUES (I=5,6, 10) ARE NEEDED TO "SLIDE" CONCENTRATIONS.
C INITIAL GUESSES OF THESE MUST BE PROVIDED.  THEY WILL BE OPTIMIZED
C IF REQUIRED, ALTHOUGH THE VERY LAST B(I) MUST BE FIXED.
C WITH PRESENT FORMATS, THE NUMBER OF PARAMETERS MUST NOT EXCEED
C 8, BUT B(9) AND B(10) ARE FIRST SET=1 BY THE PROGRAM.  NP IS
C CHANGED TO -9 AND NNP TO 9.  THUS, B(10) IS FIXED AT 1.0 BUT B(9)
C WILL VARY (UNLESS IT IS ONE OF THE OMITTED PARAMETERS).
C
C IMPLICIT REAL*8(A-H,C-U,N-Z)
C DIMENSION P(20,10),C(20),E(10),G(10),PN(20,10),PNS(20,10)
C *, RN(20,10),RNS(20,10), YP(20)
C DIMENSION X(200,10),Y(200),B(10),IB(10),TITLE(10),JJ(10)
C *, ES(10),IBS(10)
C
C LC=6
C LC=10
C LC=15
C LE=8
C LE=9
C
81 FORMAT( 9F7.3, 1X, F7.3 )
DC 1000 L= 1,LE
IF( L.GE. 2) GOTC 555
DC 1 K=1,10
1 IB(K)=0
READ(5,102) TITLE
WRITE(6,103) TITLE
READ (5,100) NC,NP,NOM,M,IO,IP
WRITE(6,105) NC,NP,NCM,M,IO,IP
IF(NC.EQ.0 ) STOP
NNP=IABS(NP)
NNC=IABS(NC)
MM =IABS( M)
NPA=NNP-NCM
NACS=NNC
NPS =NP
MS =M

```

```

IF(NCM.LE.0 ) GOTO 3
READ (5,100) (JJ(K),K=1,NCM)
WRITE(6,104) (JJ(K),K=1,NCM)
DO 2 K=1,NCM
KK=JJ(K)
IB(KK)=1
  IBS(KK)= IB(KK)
2 CONTINUE
3 IF(IP.EQ.0 ) READ (5,101) (B(K),K=1,NNP)
IF(IP.EQ.0 ) WRITE(6,106) (B(K),K=1,NNP)
IF(NC.LT.0 ) GOTO 9
C
READ 81, (E(J),J=1,LE)
DO 250 I= 1,LC
READ 81,(P(I,J),J=1,LE) ,C(I)
250 CONTINUE
C
LEF=LE/2
DO 246 J= 1,LEH
JI=LE-J+1
XE = E(J)
E(J)=E(JI)
E(JI)=XE
246 CONTINUE
DO 247 I= 1,LC
DO 247 J= 1,LEH
JI=LE-J+1
XP =P(I,J)
P(I,J)=P(I,JI)
P(I,JI)=XP
247 CONTINUE
C
555 CONTINUE
C
NMC =NACS
NP =NPS
M =MS
IF(NCM.LE.0 ) GOTO 6
DO 5 K=1,NCM
KK=JJ(K)
IB(KK)=IBS(KK)
5 CONTINUE
6 CONTINUE
IF( L.EQ. 1) GOTO 554
WRITE(6,103) TITLE
WRITE(6, 92) E(L)
WRITE(6,105) NC,NP,NCM,M,IC,IP
WRITE(6,104) (JJ(K),K=1,NCM)
IF(IP.EQ.0 ) WRITE(6,106) (B(K),K=1,NNP)
554 CONTINUE
C *****
C

```

```

C
  WRITE(6,21) (C(I),I= 1,LC)
21  FORMAT( / ,1X , 'CCNC(MM); ', 15F6.2, / , 11X, 15F6.2 )
  WRITE(6,22) (E(I),I= 1,LE)
22  FCRMAT(1X,'VCLT( V); ', 10F6.2,/)
  DO 260 I=1,NND
  J=(I-1)/LC+1
  K=I-(J-1)*LC

  Y(I)=P(K,L)
  X(I,1)=C(K)
  X(I,2)=E(L)
260  CONTINUE
C
C BEGIN DATA MESSAGE THESE CARDS SPECIFIC TO GIVEN EXAMPLE
  IF(NNP.LT.5)GO TO 209
  NNP=9
  NP=-9
209  CONTINUE
  DC109 J=5,10
109  IF(B(J).LT..000001)B(J)=1.
  Y(101)=5.
  DC112 I=1,NND
  II=I+100
  IF(I.LT.2)GO TO 112
  IF(X(I,1).GT.X(I-1,1))Y(II)=Y(II-1)
  IF(X(I,1).LT.X(I-1,1))Y(II)=Y(II-1) + 1.
112  CONTINUE
110  CCNTINUE
C END DATA MESSAGE
  9  CONTINUE
C
  CALLNLLSG(X,Y,B,IB,NP,NND,M,IRET)
  92  FORMAT( / , 26X,F7.3, 1X,'VOLTS' / )
  100  FORMAT (25I3)
  101  FORMAT(8F10.0)
  102  FCRMAT(10A8)
  103  FORMAT('1',10A8)
  104  FCRMAT(' INVARIANT PARAMETER SUBSCRIPTS ',10I3)
  105  FCRMAT(' NO=',I3,' NP=',I3,' NCM=',I3,' M=',I3,' C=',I3,' IP=',I3)
  106  FCRMAT(' INITIAL PARAMETER VALUES',/,2(5X,5(1P015.7)))
1000  CCNTINUE
  STCP
  END

```

```

      SUBROUTINEYCALC(X,Y,B,YC,WDEL,I);IMPLICITREAL*8(A-H,C-Z)
DIMENSIONX(200,10),Y(200),B(10)
C   YCALC ROUTINE SPECIFIC TO RUN
      II=100+I
      J=Y(II)+.00001
      B(J)=DABS(B(J))
      BB=B(J)
      B(1)=DAES(B(1))
      B1=DABS(B(1))
      B2=DABS(B(2))
      C=X(I,1)*BB
      C=DABS(C)
      X(I,5)=DLCG(C)
      F=B2*DLCG(1.+B1*C)
      BQ=DABS(B(3))
      IF(BQ.LT..000001)RR=1.
      IF(BQ.LT..0001)GO TO 999
      RR=1.+B(3)*C/(1.+B1*C)**2
      RR=RR+B(4)*C*C/(1.+B1*C)**3
999  F=F*RR
      C=C*1.001
      FF=B2*DLCG(1.+B1*C)
      BQ=DABS(B(3))
      IF(BQ.LT..000001)GO TO 888

      IF(BQ.LT..0000)GO TO 888
      RR=1.+B(3)*C/(1.+B1*C)**2+B(4)*C*C/(1.+B1*C)**3
      IF(BQ.LT..0000)GO TO 888
888  FF=FF*RR
      X(I,4)=(FF-F)/.001
      X(I,3)=X(I,4)/B(2)
      YC=F
      RES=Y(I)-F
      WDEL=RES
      RETURN;END

SUBROUTINEDCALC(X,Y,B,D,NP,I);IMPLICITREAL*8(A-H,C-Z)
DIMENSION X(100,5),Y(100),B(10),D(10)
C   D CALC ROUTINE SPECIFIC TO RUN OF DUMMY
      RETURN;END

```

## REFERENCES

1. P. C. Heimenz, Principles of Colloid and Surface Chemistry, Marcel Dekker, New York, p. 3, 1977.
2. G. M. Barrow, Physical Chemistry, 2nd ed., McGraw-Hill, p. 769, 1961.
3. D. M. Considine (ed.), Van Nostrand's Scientific Encyclopedia, 5th ed., Van Nostrand Co., New York, 1976.
4. D. M. Drazic, Electrochemistry in Biology, in Electrochemistry, J. O'M. Bockris (ed.), MTP International Review of Science, Physical Chemistry Series, Vol. 6, Butterworth, London, p. 287, 1973.
5. E. W. Salzman, Surface Effects in Hemostasis and Thrombosis, in Chemistry of Biosurfaces, Vol. 2, M. L. Hair (ed.), Marcel Dekker, New York, p. 489, 1972.
6. L. Lorand and K. C. Robbins, Clotting and Lysis in Blood Plasma, in Physiological and Pharmacological Biochemistry, MTP International Review of Science, Biochemistry Series One, Vol. 12, p. 77, 1975.
7. E. W. Davie, K. Fujikawa, K. Kurachi and W. Kisiel, Advances in Enzymology, A. Meister (ed.), 48, 277 (1979).
8. L. Vroman, Blood Clotting Enzymology, W. H. Heager (ed.), Academic Press, New York, p. 279 (1967).
9. A. L. Bloom, J. Clin. Pathol., 15, 508 (1962).
10. P. N. Sawyer and S. Srinivasan, J. Biomed. Mater. Res., 1, 83 (1967); Am. J. Surg., 113, 42 (1967).
11. J. L. Brash and D. J. Lyman, Chemistry of Biosurfaces, M. L. Hair (ed.), Vol. 1, Marcel Dekker, p. 177, 1971.
12. T. L. Hill, J. Am. Chem. Soc., 80, 2142 (1958).
13. C. T. O'Conski and A. Katchalsky, Biophys. J., 5, 667 (1965).
14. E. Neumann and A. Katchalsky, Proc. Nat. Acad. Sci., U.S.A., 69, 993 (1972); E. Neumann, Bioelectrochem. Bioenergetics, 5, 313 (1978).

15. B. Katz, in *Biophysical Science - A Study Program*, J. L. Oncley (ed.), p. 466, 1959.
16. A. T. Genesan and L. Lederberg, *Biochem. Biophys. Res. Commun.*, 18, 824 (1965).
17. A. Ryter, *Bact. Rev.*, 32, 39 (1968).
18. D. E. Comings, *Ann. J. Human Genetics*, 20, 440 (1968).
19. R. L. O'Brian, A. B. Sanyal and R. H. Stanton, *Exp. Cell. Res.*, 76, 106 (1972).
20. F. Jacob, S. Brenner and F. Cuzin, *Cold Spr. Harb. Symp. Quant. Biol.*, 28, 329 (1963); *Journal of Cell Biology*, 72, 86 (1977)
21. R. O. Becker, *J. Bone Joint Surg.*, 43A, 643 (1961).
22. R. O. Becker and D. G. Murray, *Clin. Orthop.*, 75, 1969 (1970).
23. R. O. Becker, *Nature*, 235, 109 (1972).
24. R. O. Becker and J. A. Spadaro, *Bull. N. Y. Acad. Med.*, 48, 627 (1972).
25. M. Rose, *Bioelectrochem. Bioenergetics*, 5, 88 (1978).
26. R. O. Becker and D. G. Murray, *Clin. Orthop.*, 73, 169 (1970).
27. C. A. L. Basset, A. A. Pilla and R. J. Pawluk, *Clin. Orthop.*, 124, 128 (1977).
28. S. Eisenberg, S. Ben-or and S. Doljanski, *Exptl. Cell. Res.*, 26, 451 (1962).
29. E. Mayhew and L. Weiss, *Exptl. Cell. Res.*, 50, 441 (1968).
30. E. Mayhew, *J. Gen. Physiol.*, 49, 717 (1966).
31. T. P. Brent and J. A. Forrester, *Nature*, 215, 92 (1958).
32. L. Purdon, E. J. Ambrose and G. Klein, *Nature*, 181, 1586 (1958).
33. E. J. Ambrose, *Proc. 7th Canadian Cancer Res. Cont.*, Pergamon, Toronto, p. 247, 1967.
34. L. Weiss and T. S. Hauscha, *Int. J. Cancer*, 6, 270 (1970).
35. A. V. Field, A. A. Tytell, P. G. Lampson and M. R. Hilleman, *Proc. Nat. Acad. Sci., U.S.A.*, 58, 1004 (1967).

36. P. L. Schell, *Biochim. Biophys. Acta*, 240, 472 (1971).
37. B. Janik and R. G. Sommer, *Biopolymers*, 12, 2803 (1973).
38. J. O'M. Bockris, M. A. V. Devanathan and K. Muller, *Proc. Roy. Soc.*, A 274, 55 (1963).
39. P. J. Debye, *Polar Molecules*, Dover, New York, 1929.
40. D. M. Mohilner, in *Electroanalytical Chemistry*, A. J. Bard (ed.), Vol. 1, Marcel Dekker, New York, p. 241, 1966.
41. R. Reeves, in *Modern Aspects of Electrochemistry*, B. E. Conway and J. O'M. Bockris (eds.), Vol. 9, Plenum Press, New York, 1973.
42. L. Weiss, *Electrically Charged Groups at Cell Surfaces*, in *Proceedings of a Workshop in Bioelectrochemistry*, Princeton, New Jersey, Oct. 10-14, NSF, U.S.A., p. 173, 1971.
43. A. A. Pilla, *Bioelectrochem. Bioenergetics*, 1, 227, 1974.
44. F. Cope, *Biological Interfaces Behave Like Electrode Surfaces*, in *Proceedings of a Workshop in Bioelectrochemistry*, Princeton, New Jersey, Oct. 10-14, NSF, U.S.A., p. 72, 1971.
45. H. B. Brown, *Membrane Surface Charge; Discrete and Uniform Modelling*, in *Progress in Biophysics and Molecular Biology*, J. A. V. Butler and D. Noble (eds.), Vol. 28, 344, 1974.
46. F. W. Cope, *Bull. Math. Biophys.*, 25, 165 (1963).
47. F. W. Cope, *Arch. Biochem. Biophys.*, 103, 352 (1963).
48. F. W. Cope, *J. Chem. Phys.*, 40, 2653 (1964).
49. F. W. Cope, *Bull. Math. Biophys.*, 27, 237 (1965).
50. F. W. Cope, *Experientia. Suppl.*, 18, 223 (1971).
51. F. W. Cope, in *Oxidase and Related Systems*, T. E. King, H. S. Mason and M. Morrison (eds.), Wiley, New York, 1965.
52. F. W. Cope and K. D. Straub, *Bull. Math. Biophys.*, 31, 761 (1969).
53. F. W. Cope, *Adv. Biol. Med. Phys.*, 13, 1 (1970).
54. G. Dryhurst, A Private Communication .
55. B. Janik and P. J. Elving, *J. Amer. Chem. Soc.*, 92, 235 (1970).

56. B. Janik and P. J. Elving, *Chem. Rev.*, 68, 295 (1968).
57. G. Dryhurst and P. J. Elving, *Talanta*, 16, 855 (1969).
58. V. Vetterl, *Coll. Czech. Chem. Commun.*, 31, 2105 (1966).
59. V. Vetterl, *Coll. Czech. Chem. Commun.*, 34, 673 (1969).
60. V. Vetterl, *J. Electroanal. Chem.*, 19, 169 (1968).
61. V. Vetterl, *Biophysik*, 5, 255 (1968).
62. W. Lorenz, *Z. Elektrochem.*, 62, 192 (1958).
63. V. Vetterl, *Coll. Czech. Chem. Commun.*, 31, 2105 (1966); *ibid.*, 34, 673 (1969); *J. Electroanal. Chem.*, 19, 169 (1968); *Biophysik*, 5, 255 (1968).
64. W. Lorenz, *Z. Elektrochem.*, 62, 192 (1958).
65. J. W. Webb, P. Janik and P. J. Elving, *J. Amer. Chem. Soc.*, 95, 991 (1973).
66. G. Dryhurst, *Electrochemistry of Biological Molecules*, Academic Press, New York, p. 25, 98, 209 and 284, 1977.
67. D. L. McAllister and G. Dryhurst, *J. Electroanal. Chem.*, 47, 479 (1973).
68. B. Janik and R. G. Sommer, *Biopolymers*, 12, 2803 (1973).
69. I. R. Miller, *J. Mol. Biol.*, 3, 229 (1961).
70. J. Flemming, *Stud. Biophys.*, 8, 209 (1968).
71. E. Palecek, in *Progress in Nucleic Acid Research and Molecular Biology*, J. N. Davidson and W. E. Cohn (eds.), Academic Press, New York, Vol. 9, p. 31, 1969.
72. E. Palecek, in *Methods in Enzymology*, S. P. Colowick and N. D. Kaplan (eds.), Academic Press, New York, Vol. 21, Part D, p. 3, 1971.
73. M. Vorlickova, G. Jezkova, V. Brabec, Z. Pechan and E. Palecek, *Stud. Biophys.*, 24-25, 131 (1970).
74. P. Valenta and P. Grahmann, *J. Electroanal. Chem.*, 49, 41 (1974).
75. A. Silberberg, *J. Phys. Chem.*, 48, 2835 (1968); *J. Polymer Sci.*, Part C, 30, 393 (1970).

76. F. R. Eirich, *Croat. Chem. Acta*, 42, 372 (1970).
77. G. Gouy, *Ann. Chim. Phys.*, 29, 145 (1903); 8, 291 (1906); 9, 75 (1906).
78. A. N. Frumkin, *Z. Phys. Chem.*, 116, 466 (1925).
79. A. N. Frumkin, *Z. Phys.*, 35, 792 (1926).
80. A. N. Frumkin and B. B. Damaskin, in *Modern Aspects of Electrochemistry*, J. O'M. Bockris and B. E. Conway (eds.), Vol. 3, Butterworths, London, p. 149, 1964.
81. B. B. Damaskin, O. A. Petrii and V. V. Batrakov, *Adsorption of Organic Compounds at Electrodes*, Plenum Press, New York, 1971.
82. J. A. V. Butler, *Proc. Roy. Soc. Ser. A*, 122, 399 (1929).
83. J. O'M. Bockris, M. A. V. Devanathan and K. Muller, *Proc. Roy. Soc. Ser. A*, 274, 55 (1963).
84. J. O'M. Bockris, E. Gileadi and K. Muller, *Electrochim. Acta*, 12, 1301 (1967).
85. R. S. Hansen, D. J. Kelsh and D. H. Grautham, *J. Phys. Chem.*, 67, 2316 (1963).
86. R. Parsons, *J. Electroanal. Chem.*, 7, 136 (1964).
87. R. Parsons, *Rev. Pure Appl. Chem.*, 7, 91 (1968).
88. B. B. Damaskin, *J. Electroanal. Chem.*, 7, 155 (1964).
89. A. N. Frumkin, B. B. Damaskin and A. A. Survila, *J. Electroanal. Chem.*, 16, 493 (1968).
90. E. Dutkiewicz, J. D. Garnish and R. Parsons, *J. Electroanal. Chem.*, 16, 505 (1968).
91. B. B. Damaskin, *Elektrokhimiya*, 5, 771 (1969).
92. B. B. Damaskin, A. N. Frumkin and A. Chizhov, *J. Electroanal. Chem.*, 28, 93 (1970).
93. P. Delahay, *Double Layer and Electrode Kinetics*, Interscience, New York, 1965.
94. D. A. Mohilner, in *Electroanalytical Chemistry*, A. J. Bard (ed.), Vol. 1, Marcel Dekker, New York, p. 241, 1966.

95. R. Payne, *J. Electroanal. Chem.*, 41, 277 (1973).
96. R. Payne, *Progress in Surface and Membrane Science*, J. F. Danielli, M. D. Rosenberg and D. A. Cadenhead (eds.), Vol. 6, Academic Press, New York, p. 51, 1973.
97. S. Trasatti, *J. Electroanal. Chem.*, 53, 335 (1974).
98. R. Parsons, *Modern Aspects of Electrochemistry*, J. O'M. Bockris (ed.), Vol. 1, Butterworths, London, p. 103, 1954.
99. B. J. Piersma, *Electrosorption*, E. Gileadi (ed.), p. 19, 1967.
100. D. Schumann, *J. Chim. Phys.*, 64, 1399 (1967).
101. R. Parsons, *Proc. Roy. Soc. Ser. A.*, 261, 79 (1961).
102. R. Parsons, *Soviet Electrochemistry*, Vol. 1, Consultants Bureau, New York, p. 81, 1961.
103. I. Langmuir, *J. Am. Chem. Soc.*, 40, 1369 (1918).
104. J. W. Gibbs, *The Collected Works of J. W. Gibbs*, Longmans Green, New York, Vol. 1, p. 219, 1931.
105. A. W. Adamson, *Physical Chemistry of Surfaces*, 2nd ed., Interscience, New York, p. 82, 231, 1967.
106. *Ibid.*, p. 81, 87, 351, 1967.
107. Reference (93), p. 17.
108. E. Gileadi (ed.), *Electrosorption*, Plenum Press, p. 87, 3, 1967.
109. Reference (93), p. 21.
110. H. Kinoshita, S. D. Christian, M. H. Kim, J. G. Baker and G. Dryhurst, *Electrochemical Studies of Biochemical Systems*, ACS Symposium Series No. 38, D. T. Sawyer (ed.), ACS, Washington, D.C., p. 113, 1977.
111. D. E. Broadhead, K. G. Baikerikar and R. S. Hanson, *J. Phys. Chem.*, 80, 370 (1976).
112. Our computational program employs an optimizing program written by Dr. E. Enwall and incorporating an algorithm given by D. W. Marquardt, *J. Soc. Indust. Appl. Math.*, II, 431 (1963).
113. D. C. Grahame, *J. Am. Chem. Soc.*, 68, 301 (1946).
114. H. Jehring, *J. Electroanal. Chem.*, 20, 33 (1969).

115. H. Jehring, *J. Electroanal. Chem.*, 21, 77 (1969).
116. H. Bauer, *Electrodics*, John Wiley & Sons, New York - Toronto, p. 109, 1972.
117. G. Dryhurst, *Electrochemistry of Biological Molecules*, Academic Press, New York, p. 20, 1977.
118. G. Dryhurst and P. J. Elving, *Talanta*, 16, 855 (1969).
119. Reference (81), p. 16, 15, 18.
120. Reference (116), p. 118.
121. Reference (81), p. 15.
122. D. E. Broadhead, R. S. Hansen and G. W. Potter, *J. Colloid. Interface, Sco.*, 31, 61 (1969).
123. Reference (105), p. 10.
124. D. J. Schiffrin, *J. Electroanal. Chem.*, 23, 168 (1969).
125. J. Lawrence and D. M. Mohilner, *J. Electrochem. Soc.*, 118, 259 (1971).
126. *Ibid.*, 1597 (1971).
127. J. Lawrence, R. Parsons and R. Payne, *J. Electroanal. Chem.*, 16, 193 (1968).
128. D. G. Grahame, E. M. Coffin, J. P. Cummings and M. A. Poth, *J. Am. Chem. Soc.*, 74, 1207 (1952).
129. J. M. Parry and R. Parsons, *Trans. Faraday Soc.*, 59, 241 (1963).
130. R. Parsons, *Proc. Roy Soc.*, 261A, 79 (1961).
131. R. Parsons and P. C. Symons, *Trans. Faraday Soc.*, 64, 1077 (1968).
132. Reference (81), p. 72, 113.
133. Reference (81), p. 112.
134. D. Shugar and J. J. Fox, *Biochim. Biophys, Acta*, 9, 199 (1952).
135. P. A. Levene, L. W. Bass and H. S. Simms, *J. Biol. Chem.*, 70, 299 (1926).
136. R. Parsons and F. G. R. Zobel, *J. Electroanal. Chem. Interfac. Electrochem.*, 9, 333 (1965).

137. R. G. Barradas and G. J. Donaldson, *J. Electroanal. Chem. Interfac. Electrochem.*, 48, 239 (1973).
138. V. Brabec, S. D. Christian and G. Dryhurst, *J. Electroanal. Chem. Interfac. Electrochem.*, 85, 389 (1977); V. Brabec, S. D. Christian and G. Dryhurst, *Biophys. Chem.*, 7, 253 (1978).
139. Reference (81), p. 90.
140. R. Parsons, *J. Electroanal. Chem. Interfac. Electrochem.*, 5, 397 (1963).
141. Reference (93), p. 28, 89, 91, 116.
142. R. Parsons, *Trans. Faraday Soc.*, 55, 999 (1959).
143. Reference (81), p. 77.
144. V. Vetterl, *Bioelectrochem. Bioenerg.*, 3, 338 (1976).
145. H. Kinoshita, S. D. Christian and G. Dryhurst, *J. Electroanal. Chem. Interfac. Electrochem.*, 83, 151 (1977).
146. H. Kinoshita, S. D. Christian and G. Dryhurst, *J. Electroanal. Chem. Interfac. Electrochem.*, 85, 377 (1977).
147. J. Donohue, *Arch. Biochem. Biophys.*, 128, 591 (1968).
148. C. K. Johnson, ORNC Publication No. 3794 (1966).
149. A. E. V. Haschemeyer and H. M. Sobell, *Acta Cryst.*, 18, 525 (1965).
150. A. E. V. Haschemeyer and A. Rich, *J. Mol. Biol.*, 27, 369 (1968).
151. J. Jordan and B. Pullman, *Theor. Chim. Acta.*, 9, 242 (1968).
152. V. Brabec, S. D. Christian and G. Dryhurst, *J. Electrochem. Soc.*, 125, 1236 (1978).
153. V. I. Minkin and O. A. Ahadanov, *Dipole Moments in Organic Chemistry*, Plenum, New York, 1970.
154. L. D. Hamilton, *Nature*, 218, 653 (1968).
155. D. Krznaric, P. Valenta, H. W. Nurnberg and M. Branics, *J. Electroanal. Chem. Interfac. Electrochem.*, 93, 41 (1978).
156. P. O. P. T'so, in *Basic Principles in Nucleic Acid Chemistry*, P. O. P. T'so (ed.), Vol. 1, Academic Press, New York, p. 482, 1974.

157. H. DeVoe and I. Tinoco, *J. Mol. Biol.*, 4, 500 (1962).
158. E. Clementi, J. M. Andre, M. C. Andre, D. Klint and D. Hahn, *Acta Phys.*, 27, 493 (1969).
159. H. Berthod and B. Pullman, *Biochem. Biophys. Res. Commun.*, 46, 125 (1972).
160. M. A. Jensen and P. J. Elving, *Bioelectrochem. Bioenerg.*, 5, 526 (1978).
161. C. O. Schmamel, M. A. Jensen and P. J. Elving, *Bioelectrochem. Bioenerg.*, 5, 625 (1978).
162. J. Moiroux and P. J. Elving, *J. Electroanal. Chem.*, 102, 93 (1979).
163. V. Brabec and E. Palecek, *Biophys. Chem.*, 4, 79 (1976).
164. V. Brabec and E. Palecek, *J. Electroanal. Chem.*, 88, 373 (1978).
165. B. Malfoy, J. M. Sequaris, P. Valenta and H. W. Nürnberg, *J. Electroanal. Chem.*, 75, 455 (1977); J. M. Sequaris, P. Valenta, H. W. Nürnberg and B. Malfoy, *Bioelectrochem. Bioenerg.*, 5, 483 (1978).
166. H. W. Nürnberg, *Bioelectrochem. Bioenerg.*, 5, 314 (1978).
167. V. Brabec and G. Dryhurst, *J. Electroanal. Chem.*, 91, 219 (1978); V. Brabec and G. Dryhurst, *J. Electroanal. Chem.*, 89, 161 (1978).
168. V. Brabec, *Biophys. Chem.*, 9, 289 (1979).
169. D. Krznaric, P. Valenta and H. W. Nürnberg, *J. Electroanal. Chem.*, 65, 863 (1975).
170. P. Valenta and D. Krznaric, *J. Electroanal. Chem.*, 75, 437 (1977).
171. V. Vetterl, E. Kovarikova and R. Zaludova, *Bioelectrochem. Bioenerg.*, 4, 389 (1977).
172. E. Dutkiewicz and R. Parsons, *J. Electroanal. Chem.*, 11, 196 (1966).
173. R. Parsons, *J. Electroanal. Chem.*, 8, 93 (1964).
174. R. Parsons and F. G. R. Zobel, *Trans. Farad. Soc.*, 62, 4511 (1966).
175. R. S. Hansen, D. J. Klesh and D. H. Grantham, *J. Phys. Chem.*, 67, 2346 (1963).
176. R. Parsons, *Trans. Faraday Soc.*, 55, 999 (1959).

177. K. Koblhofer and D. M. Mohilner, *J. Phys. Chem.*, 75, 1698 (1975).
178. B. B. Damaskin, O. A. Petrii, V. Batrakov, *Adsorption of Organic Compounds on Electrodes*, Plenum, New York, p. 112, 1971.
179. Reference (81), p. 76.
180. W. A. Struck and P. J. Elving, *Biochemistry*, 4, 1343 (1965).
181. G. Dryhurst, *Topics in Current Chemistry*, 34, 47 (1972).
182. G. Dryhurst, *Electrochemistry of Biological Molecules*, Academic Press, New York, 1977.
183. G. Dryhurst, "Electrochemical Oxidation of Some Biologically Important Purines. Relationship to Biochemistry of Purines," in *Electrochemical Bioscience and Bioengineering*, H. T. Silverman, I. F. Miller and A. J. Salkind (eds.), the Electrochemical Society, New York, p. 228, 1973; *Bioelectrochemistry and Bioenergetics*, 1, 49 (1974).
184. B. M. Visinski and G. Dryhurst, "Mechanism of electrochemical oxidation of 5,6-diamino uracil at the pyrolytic graphite electrode, *J. Electroanal. Chem.*, 70, 199 (1976).
185. J. L. Owens, H. A. Marsh and G. Dryhurst, *J. Electroanal. Chem.*, 91, 231 (1978).
186. H. A. Marsh, Jr. and G. Dryhurst, *J. Electroanal. Chem.*, 95, 81 (1979).
187. W. Pfleiderer, *Angew. Chem.*, 75, 993 (1963); *Int. Ed.*, 3, 144 (1964).
188. S. H. Hutner, H. A. Nathan and H. Baker, *Vitam. and Horm.*, 17, 1 (1959).
189. S. Kaufman, *J. Biol. Chem.*, 242, 3934 (1967).
190. R. C. Fuller and N. A. Nugent, *Proc. Natl. Acad. Sci. U.S.*, 63, 1311 (1969).
191. J. Komenda and D. A. Laskafeld, *Collet. Czech. Chem. Commun.*, 27, 199 (1962).
192. Y. Asahi, *Yakugaku Zasshi*, 79, 1548 (1959); 79, 1559 (1959).
193. D. L. McAllister and G. Dryhurst, 47, 479 (1973).
194. D. L. McAllister and G. Dryhurst, 55, 69 (1974).

195. S. Matsuura and T. Sugimoto, Synthesis of 5-alkyl tetrahydropterins, in "Chemistry and Biology of Pteridines," K. Iwai, M. Akino, M. Goto and Y. Iwanami (eds.), International Academic Printing Co., Ltd., Tokyo, p. 35, 1970.
196. T. Sugimoto and S. Matsuura, Research Bulletin (Dept. General Educ., Nagoya University), 12, 124 (1968); S. Matsuura and T. Sugimoto, Research Bulletin (Dept. General Educ., Nagoya University), 13, 9 (1969).
197. G. Dryhurst, M. Rosen, and P. J. Elving, Anal. Chim. Acta, 42, 143 (1968).
198. R. L. Myers and I. Sahin, Chem. Instr., 2, 203 (1969).
199. D. L. McAllister and G. Dryhurst, Anal. Chim. Acta, 64, 121 (1973).
200. J. E. Norvell and G. Mamotov, Anal. Chem., 49, 1470 (1972).
201. R. N. Wopshall and I. Shain, Anal. Chem., 39, 1514 (1967).
202. R. S. Nicholson and I. Shain, Anal. Chem., 36, 706 (1964).
203. R. L. Blakley, The Biochemistry of Folic Acid and Related Pteridines, in Frontiers of Biology, A Neuberger and E. L. Tatum (eds.), North-Holland Publishing Co., Amsterdam London, p58, (1969)
204. S. Kaufman, J. Biol. Chem., 239, 332 (1964).
205. P. Hemmerich in Pteridine Chemistry, W. Pfleiderer and E. C. Taylor (eds.), Pergamon, London, pp. 143 and 323, 1964.
206. M. C. Archer and K. G. Scrimgeour, Can. J. Biochem., 48, 278 (1970).
207. S. Kwee and H. Lund, Biochim. Biophys. Acta, 297, 285 (1973).
208. S. Kaufman, J. Biol. Chem., 236, 804 (1961).
209. D. J. Vonderschmitt and K. G. Scrimgeour, Biochem. Biophys. Res. Commun., 28, 302 (1967).
210. J. A. Blair, A. J. Pearson and A. J. Robb, J. Chem. Soc., Perkin II, 18 (1975).
211. M. Viscontini and T. Okada, Helv. Chim. Acta, 50, 1845 (1967).